STP-PT-066

DESIGN GUIDELINES FOR CORROSION, EROSION AND STEAM OXIDATION OF BOILER TUBES IN PULVERIZED COAL-FIRED BOILERS

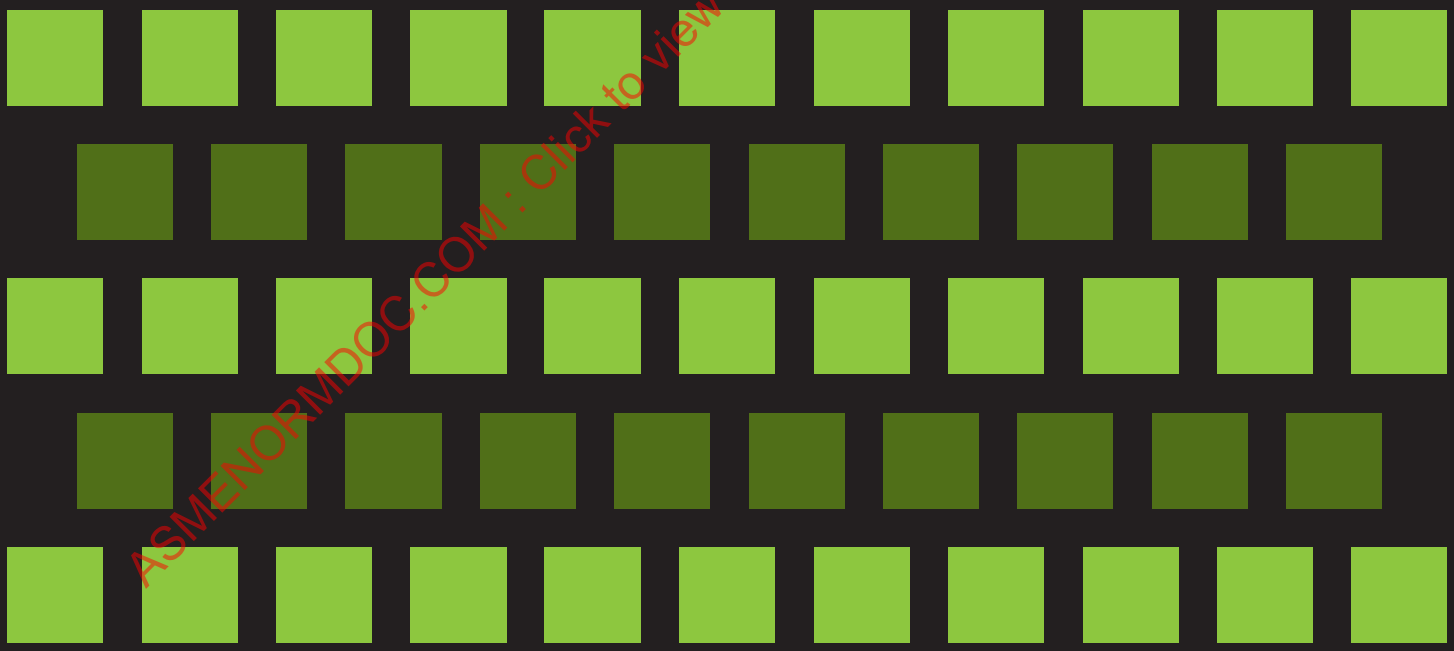

ASME STANDARDS TECHNOLOGY, LLC

STP-PT-066

DESIGN GUIDELINES FOR CORROSION, EROSION AND STEAM OXIDATION OF BOILER TUBES IN PULVERIZED COAL-FIRED BOILERS

Prepared by:

W. R. Livingston
Doosan Babcock Ltd.

Colin Davis
E.ON New Build & Tehnology Ltd.

Tony Fry
The National Physical Laboratory (NPL)

Ian Wright
WrightHT, Inc.

ASME STANDARDS TECHNOLOGY, LLC

Date of Issuance: March 26, 2014

ASME Standards Technology, LLC
Two Park Avenue, New York, NY 10016-5990

ISBN No. 978-0-7918-6936-9

TABLE OF CONTENTS

LIST OF FIGURES

PART ONE

PART TWO

FOREWORD

This report provides a development of design rules for advanced power plant boilers that pertain to fireside corrosion, erosion and steam oxidation of boiler tubes. These boilers will operate at advanced steam conditions, include discussion of CO_2 capture and contain co-firing of biomass or waste materials.

The authors acknowledge, with deep appreciation, the activities of ASME ST-LLC and ASME staff and volunteers who have provided valuable technical input, advice and assistance with review of, commenting on, and editing of, this document.

Established in 1880, the American Society of Mechanical Engineers (ASME) is a professional not-for-profit organization with more than 135000 members and volunteers promoting the art, science and practice of mechanical and multidisciplinary engineering and allied sciences. ASME develops codes and standards that enhance public safety, and provides lifelong learning and technical exchange opportunities benefiting the engineering and technology community. Visit www.asme.org for more information.

The ASME Standards Technology, LLC (ASME ST-LLC) is a not-for-profit Limited Liability Company, with ASME as the sole member, formed in 2004 to carry out work related to new and developing technology. The ASME ST-LLC mission includes meeting the needs of industry and government by providing new standards-related products and services, which advance the application of emerging and newly commercialized science and technology and providing the research and technology development needed to establish and maintain the technical relevance of codes and standards. Visit www.stllc.asme.org for more information.

PART ONE - DESIGN GUIDELINES FOR PULVERIZED COAL BOILERS

1 GENERAL OVERVIEW

The purpose of this document is to provide a set of Design Guidelines for boiler design engineers and others aimed at the minimization of the effects of fireside corrosion, particle impact erosion and steam-side oxidation on boiler tubing and other components of large, pulverized coal-fired boilers. Particular emphasis is placed on the boiler components considered to be at highest risk in advanced supercritical and ultra-supercritical boilers, i.e. the superheater and reheater tubing operating at metal surface temperatures up to approximately 1350°F (730°C).

Modern coal-fired steam power plants are required to incorporate the relevant advances in technology to improve efficiency and maximize power generated per unit of coal burned, and hence reduce the overall emissions of CO_2. They should also be fitted with advanced combustion technologies and environmental control equipment to comply with mandated limits on the release levels of the prescribed pollutant species to air, land and water.

The pressure part materials are required to have the relevant high-temperature strength capabilities, and the heat transfer surfaces are exposed to increasingly aggressive hot flue gases. The available alloys are increasingly required to operate near to the limits of their capabilities. The boilers are also expected to have the capability of cyclic operation, and pressure parts are required to have the minimum possible wall thickness, to minimize thermal fatigue.

It is increasingly important, therefore, that the minimum tube dimensions, calculated according to the ASME Boiler & Pressure Vessel Code, are not overly conservative. This has implications for the accuracy of the input data used in the calculations and, for the first time, there is a requirement to provide estimates of the alloy thickness losses expected over the lifetime of the component, due to environmental factors, both on the fluid side and the fire side of the tubes.

In this report, the knowledge currently available on the modes of environmental degradation expected for pressure parts in advanced coal-fired boilers, and the expected metal loss rates have been examined. The available approaches for the quantification and mitigation of the associated metal loss have been analyzed to provide a set of guidelines for incorporation into ASME B&PV Code calculations.

The major factors considered are:

- Increasing final steam temperatures lead to increased rates of oxide growth on the internal surfaces of the pressure parts, and this can result in increased risks of premature component failure. The modes of failure include delamination and blistering of the oxide layers, and/or exfoliation with loss of oxide fragments capable of causing tube blockage. These can result in rapid local overheating. More generally, the increases in tube metal temperatures, associated with oxide growth, can have a significant effect on the overall rate of steam-side oxidation, and a negative impact on plant integrity.
- Fireside corrosion of the furnace wall tubes, superheater and reheater tubes, and other high-temperature components can be responsible for excessive rates of metal wastage and premature failure of boiler components. Conditions leading to acceleration of such wastage are directly related to the increased operating temperatures and to the changes to the fuels and combustion conditions and hence to the flue gas chemistry, which can combine to create increasingly corrosive environments.
- Erosive wear from ash particle impact wear of the fireside surfaces of the boiler tubes and other components can be a significant cause of metal loss. In addition to direct removal of metal, the erosion process may act to modify or accelerate fireside corrosion by removing ash deposit layers

and protective oxide scales, exposing fresh metal surfaces to the aggressive fireside conditions and higher heat fluxes.

It is considered that the effects of these sources of metal loss on the overall thickness change due to environmental degradation, over the proposed lifetime of the components considered, can be aggregated into a single environmental loss factor, d_{env}, with the dimensions of mils, such that:

$$d_{env} = d_{st} + (d_{fw} \text{ or } d_{sh}) + d_{er} \quad (1)$$

where:
d_{st} = metal thickness loss due to steam-side oxidation;
d_{fw} = metal thickness loss due to furnace wall corrosion;
d_{sh} = metal thickness loss due to superheater/reheater corrosion;
d_{er} = metal thickness loss due to erosive wear.

2 CORROSION - FIRESIDE OF BOILER TUBES

2.1 Technical Background

The incidence of significant metal wastage due to accelerated fireside corrosion of boiler tubes has been a practical issue of some importance in coal-fired utility boilers for many years. The boiler design rules and design features that were introduced in the 1950's and 1960's, in response to corrosion problems associated with increases in boiler capacity and final steam temperatures at that time, have proved to be reasonably successful in containing the incidence of excessive corrosion losses. However, a number of current and future developments, associated principally with improvement of the environmental performance of coal-fired power plants, and the imperative to reduce the CO_2 emission levels, are changing this position somewhat, viz:

- The introduction of primary NO_x emission control technologies to large coal-fired boilers, which has involved the installation of air-staged, low-NO_x burners and the operation of a portion of the furnace volume under reducing conditions, has led to an increase in the incidence of excessive rates of furnace wall tube wastage. This has been associated with increases in the incidence of flame impingement and the presence of the gaseous and solid products of sub-stoichiometric coal combustion local to the furnace walls.
- The operation of boilers at minimum excess air levels for NO_x emission control also tends to increase the flue gas temperatures at the furnace exit and hence to increase the superheater metal temperatures, and can alter the balance of heat absorption through the boiler.
- The interest within the industry in the design of coal-fired utility boiler plants capable of producing steam at increasingly-higher temperatures and pressures, and hence generating electricity at higher efficiency levels, has led to an interest in new materials for high-temperature components that can operate at these advanced conditions.
- The co-firing of non-conventional fuels in boilers designed for coal firing has resulted in significant changes in the chemistry of the ash deposits on the heat exchanger surfaces in the furnace and the convective section, commonly with increased levels of alkali metal sulfates and chlorides. This has led to a number of instances where excessive corrosion rates have been reported.
- Current developments in the oxy-fuel firing of coal-fired boilers, to facilitate CO_2 capture and sequestration, has resulted in an increasing interest in the operation of boiler plants with advanced steam conditions, and with relatively high flue gas concentrations of CO_2 and H_2O and of the more important acid gas species, principally SO_2/SO_3 and HCl. These flue gas compositions are significantly outside the ranges for which there is relevant plant experience, and there are risks of excessive corrosion rates.

2.2 Furnace Wall Corrosion

Extensive plant experience over many decades has indicated that good combustion control and the maintenance of oxidizing conditions at the furnace walls tend to promote the growth of a thin, protective oxide scale on the fireside surface of furnace wall tubing that will tend to limit further corrosion. On the other hand, poor combustion conditions, i.e. reducing conditions and fluctuating oxidizing-reducing atmospheres local to the walls, have been implicated in the incidence of accelerated furnace wall tube corrosion, particularly when firing coals with high sulfur contents. In general terms, it has been found that operation with localized CO concentrations at the furnace wall in excess of 2-3% is considered to be undesirable. The effects of the furnace soot blowers and water cannons in removing ash deposits and exposing the furnace surfaces to higher temperatures and to particle impact erosion, in addition to the corrosive attack, also may act to increase the metal wastage rates.

At the boiler design stage, it is clear that ensuring that the furnace has sufficient volume to contain the flames or the fireball, and that the wing burner-side wall clearances in wall-fired plants are sufficient, will help prevent flame impingement. The use of curtain air supplies to protect certain vulnerable areas of the furnace wall surface in the burner region is also considered by some designers to be of benefit, but this inevitably involves the introduction of additional air to the furnace, and this may be incompatible with the optimization of low-NO_x firing systems.

There is no evidence to date to suggest that furnace wall wastage rates are higher under oxy-fuel firing conditions which are, in some cases, associated with significantly higher levels of acid gases in the recirculated flue gas streams, than are present from air firing. It should be noted, however, that plant experience of oxy-fuel firing is limited.

2.2.1 Predictive Methods for Furnace Wall Corrosion

A number of methods for the prediction of the rates of corrosion of furnace wall tubes have been proposed. These are based principally on the results of laboratory corrosion experiments or of measurements of metal loss rates on plant. While satisfactory predictions of corrosion rates for combustion conditions where low-NO_x firing is not practiced have been made, models for corrosion under low-NO_x firing conditions commonly incorporate parameters that are not readily available, such as the CO or H_2S levels in the combustion gas near the furnace walls. As a result, it is fair to say that, at the present time, there is no general consensus within the industry as to which of the available models provides the most reliable approach.

A number of corrosion models have been incorporated into Computation Fluid Dynamics (CFD) codes in an attempt to provide predictions of the localized metal wastage rates. EPRI, for instance, has made use of both pyrite deposition and chloride corrosion models with CFD models to provide predictions of the metal wastage distributions within several power plant boilers burning coals containing a range of sulfur and chlorine concentrations. Models of this type differ principally in the way that they attempt to quantify heat flux variations in the boiler and the severity of reducing conditions that apply at the furnace walls.

Clearly, there are important differences in the technical basis of the available predictive models of the corrosion process, and in the approach to validation of the models. It is difficult at the present time to recommend a preferred predictive method with any confidence.

2.2.2 Remedial Measures for Furnace Wall Corrosion

The remedial measures available for the control of furnace wall corrosion are based either on operational changes or on materials solutions. The implementation of remedial measures based on operational changes may include the following activities:

- There may, in some cases, be scope for the improvement of the coal mill performance, of the pulverized coal and air distributions to the burners, or for the modification of the burner settings to alter the flame conditions. These actions may help to move the flames away from the furnace side or rear walls, and reduce the impact of flame impingement on the furnace surfaces. Diagnostic techniques, such as the use of sniffer ports to permit sampling and analysis of the combustion gases (including CO, O_2, H_2S, etc.) local to the walls, or the use of corrosion probes inserted through the furnace wall membrane to provide an estimate of the corrosion rates at the conditions that apply at the walls, can be of assistance in this context.
- In some cases, where there is localized corrosion of furnace wall surfaces due to reducing conditions, it may also be appropriate to retrofit the boiler with a curtain air supply, which is injected local to the furnace wall, and which can be effective in reducing the extent of the localized reducing conditions. It should be noted, however, that the use of curtain air or of deliberately

opening up the furnace wall membranes to allow increased air ingress to help reduce sidewall corrosion is the subject of some controversy. Most boiler manufacturers and combustion equipment suppliers prefer to maximize the proportion of the combustion air that is delivered with the pulverized coal through the burners. This approach is considered to be preferable to increasing the level of tramp air ingress into the boiler, since there may be significant combustion, NO_x emission control and boiler efficiency implications.

- The use of CFD modeling of the coal flames and gas distribution in the furnace may be of some value as a means of determining the scope for flame shape alteration, prior to embarking on modification of the burners, or site test work may be justified to inform decisions about combustion modifications, and to analyze the results of boiler testing.
- It may be possible to reduce the corrosiveness of the ash deposits in some circumstances, by switching to fuels with lower sulfur or chlorine contents, or by restricting the application of certain primary NOx-control techniques when firing high-sulfur or high-chlorine coals.
- The use of fireside additives to modify the chemistry of the ash deposits may be of some benefit in some cases.
- Where the action of the on-line cleaning systems such as furnace wall steam soot blowers or water cannons has a significant role in the wall tube corrosion process, it may be possible to modify the operation of the installed equipment, e.g. change the nozzles, reduce the steam or water pressure, or reduce the usage level of the on-line cleaning systems.

In most cases, the traditional materials-related response to accelerated metal wastage of furnace wall tubes due to fireside corrosion has involved the application of simple repair or materials solutions, viz:

- Historically, the most common response to furnace wall tube wastage has been to carry out fireside inspections and tube thickness surveys during planned outages in areas suspected of damage, and to repair the affected tubes in the furnace and convective sections with tubing manufactured from the same material. This practice has been fairly widespread, but it may not always be the most cost-effective approach, particularly when the metal wastage rates are high and the remedial action is required on a regular basis, or where the metal wastage is widespread and replacement of very large areas of the affected furnace surface is required.
- The installation of facetted tubing, manufactured from carbon steel or from a higher-grade alloy, but with increased wall thickness on the fireside has been applied with some success.
- The installation of co-extruded tubing can offer up to a ten-fold reduction in corrosion rates under the most severe conditions, but has not found widespread application in large, membrane wall, coal-fired utility boiler furnaces for economic reasons.
- The use of coatings or weld overlays, with more corrosion-resistant materials, has been more widely practiced in recent years for the protection of furnace wall tubing.

Recently, there have been significant advances in the development of on-line and in-service diagnostic techniques, particularly for the assessment of furnace wall corrosion to help identify the areas most affected or to monitor the effectiveness of remedial measures. In general terms, furnace wall corrosion probes are of two types, viz:

- on-line electrochemical probes, and
- metal wastage probes.

The use of metal wastage probes is now fairly common practice, not only for development purposes but also for more routine corrosion monitoring, and a number of suitable systems are available. The use of on-line electrochemical probes is less well established technically, but there is experience of their use. Several such systems are under development and commercial systems are available.

2.2.3 Summary

In general, the risks of accelerated furnace wall tube corrosion have increased with the introduction of primary NO_x-control technologies into large pulverized coal-fired boilers. Overall, it is clear that, under most circumstances, the approach to the control of furnace wall corrosion should be focused in the first instance on combustion-related issues, i.e. on the root causes of the problem. However, until such control measures provide reliable data on, for instance, levels of CO near the walls that can be used to validate corrosion models, there are no acceptable means of predicting values of d_{fw} in Equation 1.

Where equipment or operational constraints act to reduce the scope for this approach, it may be appropriate to consider materials solutions, i.e. the employment of facetted tubes, or of coatings using more corrosion-resistant materials, depending on the severity of the problem. In the US the increasing application of staged combustion for NO_x control and switching to coals with S and Cl levels different from the design levels, due to economic pressures, have led to the widespread acceptance of the inevitability of severe furnace wall corrosion. The remedial measure being adopted almost universally is the use of weld-overlay coatings (typically of high-Ni alloys). While such coatings appear to reduce the rate of general corrosion satisfactorily, it is not unusual for severe corrosion to occur on any adjacent uncoated tubes, which prompts extension of the weld overlay.

However, where protective coatings such as weld overlays are used to combat furnace wall corrosion, the rate of general corrosion (of the coatings) typically is very low, and actual thinning of the load-bearing tube alloy ceases. For the scenario where furnace wall tubes are protected by such coatings, and there is expected to be no thinning of the pressure boundary tube walls for the intended lifetime of the tubes, then $d_{fw} = 0$. In the absence of such coatings, the rate of general corrosion of furnace wall tubes is very dependent on the prevailing local combustion environment, and can be very rapid. In those cases, at present the most expedient route for obtaining values of d_{fw} is to use some form of corrosion probe or to take tube samples to allow measurements of the corrosion rate to be made.

2.3 Fireside Corrosion of Superheater and Reheater Tubes

2.3.1 Technical Background

The traditional response within the industry to the increasingly aggressive corrosion conditions associated with higher steam temperatures has been to upgrade the materials of construction of the cooled and uncooled components of the superheater and reheater sections of the boiler.

The high-temperature corrosion resistance of alloys employed for this application can be roughly grouped by alloy type, viz:

- Low-alloy ferritic materials have the lowest corrosion resistance of the available tubing alloys.
- High-chromium martensitic alloys and low chromium-content austenitic alloys (12-15%) offer a significant improvement relative to the low-alloy ferritic alloys.
- The 300-series austenitic steels (18-20% chromium) offer slightly better corrosion resistance than the low-alloy steels.
- Further improvement in fireside corrosion resistance of the 300-series austenitic steels has been achieved by special thermo-mechanical processing to produce a fine-grained material (e.g., TP347HFG, Super304H), which are generally suitable for low-S coal and relatively mild corrosive conditions.
- Significantly improved fireside corrosion resistance when burning higher-S coals and in more aggressive environments is offered by the TP310-based steels having approximately 20-25% chromium content.

- Further significant improvements in corrosion resistance beyond that offered by the TP310 steels can be obtained by using Ni-based alloys with relatively high Cr contents.

It should be noted that the Ni-based alloys are significantly more expensive than the austenitic steels and can be difficult to process and fabricate. In practice, these materials are unlikely to be used except in applications where very high creep strengths are required, i.e. for the more advanced ultra-supercritical boilers. Currently, the higher-alloy materials are most frequently used to combat known aggressive conditions in the form of claddings, weld overlays, or sprayed coatings.

The general technical consensus is that accelerated corrosion of the superheater and reheater tubes is caused by the deposition of alkali metal (K and Na) sulfates on the tube surfaces. The mixed sulfate deposits become partially molten at tube surface metal temperatures above approximately 1075°F (580°C) and form a thin layer of highly-corrosive liquid next to the protective oxide scale initially formed on the tube surface. Dissolution by the molten salt is effectively a continuous process, with sulfur and oxygen diffusing down into the metal, and iron, chromium and nickel diffusing outward through the sulfate layer. At the hotter outer surface of the deposit, iron/chromium oxides are re-precipitated within the ash in a discontinuous form and no longer constitute a protective layer. This mode of attack results in a roughly linear corrosion-time curve, i.e. the corrosion rate does not decrease significantly with time.

The rate of this continuous transport process is highly dependent upon the metal surface temperature and on the heat flux through the tube. At metal surface temperatures above about 1075°F (580°C), the corrosion rate increases in a roughly exponential fashion. Above a peak temperature, which is commonly in the range 1200-1380°F (650-750°C) depending on the alloy, the molten sulfate compounds tend to become thermodynamically unstable and decompose to form less damaging solid species. This change causes the corrosion reaction rate to decrease at higher temperatures, and the result is the classical 'bell-shaped' corrosion rate-temperature curve.

The role of chlorine in superheater and reheater corrosion has been considered by a number of workers. By the mid-1980s, operational experience in the UK had shown that there was a good correlation between the chlorine content of the coal and the rate of corrosion of austenitic steel tubes [1]. As indicated below, this relationship was specific to the UK coals in use, for which the sulfur content was within a specific range, and the chlorine content could be related to the total amount of alkali metals (K + Na) that were available to participate in the corrosion process under the coal ash deposits.

2.3.2 Predictive Modeling

While several attempts have been made to develop a predictive model to relate the fireside corrosion of superheater and reheater tubes to key boiler operating parameters including the composition of the coal burned, success has been achieved only for special cases involving a limited range of parameters. At present, a universally-applicable analytical route for determining a value for d_{sh} in Equation 1 is not readily available.

Curve fitting of a database of operational data and data from probe trials in pulverized coal-fired boilers by the former Central Electricity Generating Board in the UK resulted in the development of a corrosion rate equation for austenitic SH tube materials [1]. This was known as the 'modified PE8' equation, which took the form:

$$r = A \times B \left(\frac{T_g}{G} \right)^m \left(\frac{T_m - C}{M} \right)^n (\%Cl - D) \qquad (2)$$

where r = corrosion rate in nanometers per hour, $nm.h^{-1}$;

T_g = flue gas temperature, ºC;
T_m = surface metal temperature, ºC;
Cl = coal chlorine content, %;
A = tube position factor (dimensionless);
B = material factor (dimensionless); and
C, G, M, D, m, n are constants.

The constant A accounted for the different propensities for corrosion attack within a tube bank, and has a higher value for leading tubes than for non-leading. This reflects the fact that the leading tubes in a bank tend to corrode at a significantly faster rate than the more sheltered non-leading tubes.

The constant B takes account of the relative performances of the different austenitic steels, and has a higher value for the 15-19%Cr steels, e.g. TP316, TP321, TP347, Esshete 1250, etc., and a lower value for TP310 steels with 23-27%Cr.

The limits of the data set from which the equation was derived are:

T_m = 1120-1256°F (605-680°C);
T_g = 1600-2192°F (871-1200°C); and
Cl in coal = 0.12-0.58 wt%.

The fairly narrow sulfur range found for UK coals meant that it was unnecessary to include, and indeed impossible to derive, a term related to the sulfur content of the fuel in the predictive equation.

The modified PE8 equation has been employed for the prediction of the corrosion rates of superheater and reheater tubes in coal-fired boilers in the UK for many years, and continues to be regarded as one of the more reliable methods. Research work to examine the application of correlations of this type to world-traded coals still continues [2].

Another predictive model for the corrosion of superheater and reheater tubing attempts to express a corrosion index in terms of acid-soluble oxides of the alkali metals, i.e. sodium and potassium in the corrosion deposits [4]. This expression takes the form:

$$Metal\_loss = f\left(\frac{Na_2O}{K_2O}\right)_{as} .f(CaO)_{as}.f(MgO)_{as}.f(SO_2).t.(-0.08+(Na_2O+K_2O)_{as}) \quad (3)$$

This relationship is useful in that it incorporates a factor for the effect of fuel sulfur content on the corrosion rate, but it has the disadvantage that the empirically-derived corrosion parameters were obtained from isothermal corrosion tests performed on one material (TP347) at a single test temperature and using synthetic ashes. The applicability to plant and to other alloy materials may be limited, although the general form of the equation may be valid.

2.3.3 Remedial Measures

For superheater and reheater corrosion, the scope for remedial measures based on boiler operational changes is limited, and these have generally been associated with attempts to control the fuel diet or the relevant metal temperatures in the boiler convective section.

Overall, the most popular responses to problems with accelerated metal wastage rates in this area largely have been based on materials solutions, i.e.

- replacement of the affected tubes using more corrosion-resistant materials; and
- the use of protective systems for the superheater and reheater surfaces considered to be at risk.

It is well established that the use of higher-grade, more corrosion-resistant materials, generally with higher chromium contents, can provide significant reductions in the rate of metal wastage of superheater and reheater tubes subject to high-temperature corrosion under coal ash deposits.

There is some experience in the use of higher-grade materials in the form of co-extruded tubing, particularly in cyclone-fired boilers burning eastern US, high sulfur bituminous coals. These materials have successfully extended the lifetime of tubes, such that the increased cost of the tubing was justified.

In addition to cladding, there have been trials with different forms of protective coatings including weld overlays, and with chromizing treatments to increase corrosion resistance, but none have achieved wide use. Interest in these approaches has been revived recently in the context of increasing the service temperatures of ferritic-martensitic steels for use under advanced, ultra-supercritical steam conditions. It should be noted, however, that in general the use of coatings on superheater and reheater tubes is not yet well-established practice for coal-fired boilers within the power industry.

As in the case of weld overlay coatings applied to furnace wall tubes, where a coating or cladding has sufficient integrity that fireside corrosion does not penetrate to the subjacent pressure boundary during the intended tube lifetime, even where severe corrosion of the cladding occurs, then the value of d_{sh} in Equation 1 can be taken as zero. Coatings in this category include cladding by co-extrusion, and weld overlay. It is important to note that this would not be the case where the mode of corrosion of the coating involved penetration of the full coating thickness and exposure of the tube surface beneath to the corrosive environment.

Clearly, a detailed knowledge of the potential modes of coating degradation is an important factor in determining how to incorporate the effect of a coating on tube lifetime considerations.

3 EROSION - ASH PARTICLE IMPACT EROSION

3.1 Technical Background

Erosive wear due to the impact of ash particles with the components of the heat exchange banks in the hot gas path of pulverized coal-fired boilers can have a significant effect on the lifetime of those components, resulting in increased plant maintenance costs and, in some cases, premature failure.

In general terms, the key areas of concern for erosion damage in coal-fired power plant are:

- the internal surfaces in coal mills;
- the pulverized coal pipework, particularly at and near bends;
- the internal components of burners;
- the gas-side surfaces of heat exchange tubes and other surfaces in the convective section of the boiler; and
- the internal surfaces of pneumatic ash conveying equipment.

The precise mechanism of material removal from a surface by particle impact erosion is relatively complex, and is very dependent on the details of the nature of the erodent, the aerodynamics of the system, the angle of impact, the properties of the target material, etc.

One of the key factors in determining the severity of the damage caused is the transfer of kinetic energy from the particle to the target material during the impact and rebound of the particle. It has normally been found that the rate of erosive wear (w), expressed, for instance, as the mass loss per unit mass of erodent, is strongly dependent on the velocity of the erodent particles on impact (v), and is usually found to vary according to the equation:

$$w = k\, v^n \tag{4}$$

where:

k is a constant, and n is the velocity exponent.

For most systems, the value of n is between 2 and 3, i.e. it is generally found that wear rates increase sharply with increasing particle impact velocity.

The key properties of the ash particles that influence their erosivity include:

- the hardness and mechanical strength of the particles;
- the particle size distribution, i.e. larger particles tend to be more erosive than the same mass of smaller ones; and
- the particle shape, i.e. particles with sharp edges have a greater erosive effect, particularly in terms of their cutting action on ductile materials, than do rounded particles.

Fly ash erosion of boiler tube surfaces causes metal wastage in two ways, viz:

- by direct removal of the tube material, and
- by removal of the fireside oxide scales or corrosion product layers, which acts to increase the fireside oxidation/corrosion rate.

In general terms, in the absence of corrosion, the wear rate of most metallic materials decreases linearly with increasing hardness. However, corrosion product/oxide removal can be the dominant effect at metal

surface temperatures above about 800°F (427°C). The combination of erosive wear with corrosive attack can lead to very high rates of metal loss.

The boiler operating variables that influence erosive wear are relatively well understood, and can be listed as follows:

- particle velocity, which in most cases is related to the local gas velocity,
- particle loading locally in the gas stream,
- angle of incidence of the particle impact on the component; and
- relative concentration of erosive particles in the fly ash (in particular, silica in the form of quartz).

During the design stage, boiler engineers generally place upper limits on the average flue gas velocities within the convective tube banks, depending on the ash contents of the coals to be fired and the erosion potential of the ashes. This is considered to be the first stage of the process of providing protection against excessive rates of erosive wear of the boiler components, before the more specific design rules and design features for the erosion protection of particular boiler components are considered.

The erosive wear of boiler tubes by fly ash can, however, be very localized in nature. While the average gas velocity and ash loading across a convective section tube bank are generally well understood, in practice the ash particle flow can become concentrated in certain areas, and there can be areas of locally-increased gas velocities. These factors can have significant impacts on the local tube erosion rates.

The angle of impact of the fly ash particles on the metal component has a large influence on the rate of erosion. For impacts in the curved surfaces of tubes, for instance, the different angles presented to the gas stream may mean that the maximum erosive wear rate may be on the sides of the lead tubes rather than the crowns. Even where there is significant ash deposition on the crown, erosive wear of the bare metal on the sides of the same tube is commonly observed.

While coals contain a wide variety of mineral species, principally oxides, sulfides, carbonates, phosphates and clay minerals, only those minerals that are harder than steel contribute significantly to the abrasive and erosive behavior of the coal particles. On this basis the minerals principally considered to contribute to the erosivity of most coals are quartz and iron pyrite particles, the coal substance and the clays being too soft. In fly ashes, the majority of the particles are glassy and rounded in nature, i.e. the erosion potential is different from that of the parent coal mineral material.

3.2 Predictive Modeling

One of the key requirements is for a methodology that can be used to characterize the erosion potential of coals and ashes based on information normally available during the proposal or early design stage of a boiler project, or during initial considerations of coals to be used, i.e.

- a design method that can provide a ranking of the erosion potential of a coal, based on the basic fuel specification, and/or
- laboratory methods for the characterization and testing of small samples of coal or of fly ash when available, for design and investigative purposes.

To a first approximation the erosion potentials of a coal and the associated fly ash will be related to the ash content of the as-received coal, particularly the levels of silica present as quartz, and pyrites. The erosion rate for a particular coal will generally be a linear function of the size and flux of those particles approaching the target material. For fly ashes, the proportion of the quartz particles that have passed through the

combustion process without being completely fused and have retained sharp, angular features is a key factor, which depends on the combustion conditions in the boiler.

The importance of the quartz content in determining the erosivity of fly ash leads to the need for sophisticated particle characterization methods, such as computer-controlled scanning electron microscopic techniques, for accurate quantification of the size, shape, and volume fraction of the quartz particles and other species.

The relative coarseness of fly ash materials can be graded roughly into three categories:

- fine fly ash with 15% of the fly ash greater than 1.8 mils (45 μm);
- coarse fly ash having 30% >1.8 mils (45 μm); and
- exceptionally coarse fly ash having 50% >1.8 mils (45 μm) fraction.

A simple fly ash erosion index, in fairly wide use within the industry, is based on the assumption that erosive wear of boiler pressure parts is primarily due to the fly ash particle size fraction greater than 1.8 mils (45 μm) in diameter. This fly ash erosion index (I_a) is presented below:

$$I_a = 0.44\, x_1\, (SiO_2 - 1.5\, Al_2O_3) + 0.18\, (SiO_2 - 1.5\, Al_2O_3) + 0.35\, x_1 + 0.14 \qquad (5)$$

where x_1 is the fly ash fraction > 1.8 mils (45 μm)

The associated fly ash erosion potential classification is as follows:

Ia <0.2	marginally erosive
0.2-0.4	moderately erosive
0.3-0.5	highly erosive
Ia >0.4	exceptionally erosive

This index is based on calculation of the silica content of the fly ash from the coal ash composition, using the assumption that the clay minerals in the coal have a SiO_2:Al_2O_3 mass ratio of 1.5, that all of the alumina content is in the form of clay mineral matter, and that the balance of the SiO_2 is in the form of quartz. Also contained in this index is the assumption that 50% or so of the quartz in the parent coal survives the flame as liberated particles, without fully melting or coalescing with the alumino-silicate and other ash particles.

In the absence of specific information about the size distribution of the fly ashes, a very simple erosion index based solely on the total quartz content of the coal also can be applied, with the quartz content of the ash being estimated using the simple method described above. The erosion potential classification applied in this case would be:

< 2% quartz in coal	low
2-3% quartz in coal	medium
3-5% quartz in coal	high
>5% quartz in coal	severe

This type of index is employed fairly widely within the industry to provide a relatively crude assessment or ranking of the erosion potential of the coal ash based on data available in most fuel specifications. Rankings of this type can be used to define the allowable average flue gas velocities, and the heat exchange tube cross pitches throughout the heat transfer banks in the boiler convective pass required to avoid excessive erosion. In general terms, during the boiler design process, the average flue gas velocities for the convective pass tube banks are selected to maintain the erosion wear rates of the boiler to tubes at acceptable levels, i.e. less

than 7 mils/year (20 nm/h) or so, which is equivalent to a metal loss of around 79 mils (2 mm) over 100,000 hours of operation.

In most cases, except for very low ash, benign coals, the average flue gas velocities will be less than 66 ft/s (20 m/s). For the majority of bituminous steam coals that have normal ash levels and moderate erosion index values, average flue gas velocities less than around 49 ft/s (15 m/s) commonly are applied. For coals with higher ash contents and more erosive ashes, more conservative average flue gas velocities of less than approximately 33 ft/s (10 m/s) may be required to avoid excessive erosion rates.

It should be recognized that significant distortion of the tube banks and other components can occur with time, and the formation of ash fouling deposits on the surfaces of the convective bank tubes, can influence the local flue gas velocity and fly ash flow patterns.

The tubes in convective section tube banks can also be subject to erosive wear due to action of the soot blowers. These devices normally employ high-velocity jets of steam, air or water to break up and dislodge ash deposits, but there is a tendency for significant levels of flue gas and ash particles to become entrained in the jets and accelerated towards the boiler surfaces, particularly the lead tubes in a bank. In most cases, instances of erosive wear due to soot blowers are associated with overuse, particularly when there are severe ash deposition problems, or with poor soot blower operation and maintenance.

It is clear that the indices described above do not provide a quantitative measure of the rate of erosive wear that could be used as a basis for providing a value for d_{er} in Equation 1 above, though a nominal/design value could be based on a metal loss of 79 mils in 100,000h. For boilers with known, persistent erosion problems, values of d_{er} would be based on actual plant or test measurements.

3.3 Remedial Measures

The relatively wide variability of flue gas velocities and fly ash particle fluxes resulting from the various sources discussed means that local erosion rates can vary dramatically in a given boiler design. As a result, measures often are needed to protect some regions of the convective pass from erosion. Various devices are available, such as baffles, vanes, and flow screens with a range of levels of flow resistance that can be used effectively to redirect the flue gas flow and reduce high, localized velocities and particle fluxes.

Some protective features commonly are applied to specific items of plant at the design stage. These include:

- sacrificial erosion shields to provide protection of the lead vertical and horizontal tubes in a convective bank, in regions where excessive gas velocities are expected;
- sacrificial erosion shields to protect the boiler tubes from the installed convective section soot blowers; or
- sacrificial barrier plates or inclined perforated plates to divert or even out the flue gas flow, or to protect the tube bends.

The use of sacrificial shields can involve significant maintenance in order to ensure that misalignment with time does not lead to new localization of gas velocities and particle loadings. Other protective features can be introduced after erosion problems have become persistent.

One very promising development in recent years is the use of analytical techniques, including CFD modeling, to guide the selection and placement of flow screens and baffles. Information of this type can be used to tailor the flow resistance provided by these devices to correct imbalances in gas and particulate flow rates, and reduce the erosion wear rates to acceptable levels.

4 OXIDATION - STEAM-SIDE OXIDATION

4.1 Technical Background

At elevated steam temperatures, the rate of oxide growth on the steam-touched surfaces of boiler tubes and steam pipework can become appreciable. The key parameters that control the rate of steam-side oxidation, and the tendency of oxide layers to delaminate and exfoliate are as follows:

- The rate of oxidation of the boiler tube material increases in a roughly exponential manner with increasing metal temperature.
- The rate of oxidation may also increase with increasing steam pressure, although this is commonly considered to be a secondary effect.
- The rate of steam oxidation of boiler steels generally decreases with increasing chromium content.
- For boiler tubes, the presence of a heat flux across the metal/oxide layer is considered to have significant effects both on the metal temperatures under the internal oxide, and on the growth rate and the physical nature of the oxide layer. For steam pipework, heat flux effects are obviously of much less importance.
- Any significant temperature variations or temperature cycling will have an impact on the physical properties of the growing oxide layer, and therefore on the oxide growth rates. Oxide layers that grow to significant thicknesses, i.e. above about 1-2 mils (25-50 μm) in thickness for austenitic steels typically used in boilers, have a tendency to delaminate, and to blister and/or exfoliate. The impacts on heat transfer and on the integrity of the system can be dramatic. Exposure to rapid temperature changes is a key factor in causing exfoliation of the oxide.

Under isothermal conditions and with a well-developed oxide layer of low porosity, the oxide layer thickness increases in a roughly parabolic fashion with time, i.e. the growing oxide layer has a significant protective effect. This may apply particularly to steam pipework for boiler plant operating under constant load conditions.

For boiler tubing, where there is a significant heat flux across the tube metal and the oxide layer, the insulating effect of the growing oxide layer will tend to result in a significant increase in the metal temperatures with time. This will result in a continual increase in the oxidation rates and will have an impact on the creep life of the tubes. The protective effect of the oxide layer in practice will, therefore, tend to be less than that which applies under isothermal conditions.

In practical situations, the effect of thermal cycling will have significant effects on the physical properties and integrity of the oxide layer, and the tendency for delamination, and this also has a significant impact on oxide growth rates.

The tendency of the oxide layers to delaminate can result in blistering and/or exfoliation, principally of the outer layer of the oxide scale. This can have a significant impact on the thermal conductivity of the scale. The resulting increases in metal temperature can be highly localized and dramatic, and can lead to premature boiler tube failures.

Exfoliation and loss of the scale can also result in particles or flakes of oxide being released into the steam. Depending on their size and shape, these particles can accumulate in locations such as bends in superheater and reheater tubes, and this can result in flow restrictions and metal temperature increases. There can also be carryover of particulate material in the steam to the turbine, resulting in significant increases in the erosive wear rates of turbine components.

4.2 Predictive Methods

The mechanistic understanding of the evolution of oxide scales growing on boiler tube alloys in steam indicates that, for the alloy classes usually used in steam boilers, the scales consist predominantly of two main layers of oxide, with the interface between these layers located at the original alloy surface. The usual practice is to use the thickness of the inner oxide layer as the best estimate of the thickness of alloy lost, and this is the approach that has been used in the current document.

A number of predictive models of the rate of oxide growth on metal surfaces in contact with steam at elevated temperatures have been developed. The models based on the results of laboratory or test rig experiments have helped to quantify the influences of variables that cannot be changed or measured readily in operating boilers. These tests, however, were normally carried out at ambient pressures and under isothermal conditions.

In the current work, these models have been used to calculate the thickness of the inner oxide layers as a measure of metal thickness loss, to provide values of d_{st} in Equation 1. In this case, the input data were taken solely from steam loop or steam oxidation probe experiments in large boilers, so that the results are as representative of realistic boiler operating conditions as is possible.

In a recent state of knowledge report on oxide growth and exfoliation on alloys exposed to steam, [5] the oxide thickness measurements from a wide range of sources were collated. The results indicated that the majority of the predictive models of steam oxidation then in use represented the oxidation kinetics with a parabolic rate law. The test data collated were for the following categories of boiler tube alloys:

- Ferritic steels, i.e. data for 2.25 % Cr, 9 % Cr and 12 % Cr alloys,
- Austenitic alloys, i.e. a limited set of data for the 300 series alloys, 304, 347, 310 etc., and
- Nickel-based alloys, i.e. data were available for a very limited range of alloys.

Recent developments in artificial neural networks lend themselves to the modeling of complex situations such as accounting for the multiple variables which have an influence on alloy oxidation [3]. For the current work, a new artificial neural network algorithm was generated to predict the inner layer thickness of oxide scales formed in steam (i.e., d_{st}) as a function of the key input parameters. The data generated from plant measurements for a range of temperatures, steam pressures, alloys and exposure times were used to generate the predictions. Additional short-term (up to 5,000 hours) laboratory-generated steam oxidation data were used to supplement the longer-term plant data, for neural network training purposes.

In the training process, the number of neurons used in the network was varied until a compromise between the best fit to the data and the use of as few neurons as possible, was achieved. The number of input parameters was refined to identify the most influential parameters, which were found to be:

- Metal temperature, °C
- Steam pressure, bar
- Exposure time, h
- Alloy Cr content wt%
- Alloy Mo content, wt%
- Alloy Fe content, wt%
- Alloy Si content, wt%
- Alloy S content, wt%
- Alloy Ni content, wt%

The final model had five neurons, which produced a very good fit to the measured data, with an r^2 value of 0.91. The results of testing of the model indicated that this type of approach appears to be eminently suitable for the analysis of steam oxidation test data, and for the development of predictive models of oxide growth. The trained model was used to generate oxidation kinetic curves to provide reference values of d_{st} for the alloys of interest.

These plots are presented in Appendix C, and an example of the results of the application of the model to data for Super 304H at 1202°F (650°C) is reproduced in Figure 4-1. These plots are intended to be used to look up values of the inner oxide thickness (d_{st} in Equation 1), associated with specific service conditions of time, temperature, and steam pressure.

The uncertainty level associated with the predicted value increases with time, for predictions of oxide thickness values for long exposure times. In some instances, the model is no longer valid at long exposure times and the predicted values begin to fall with increasing time. Generally, predictions for exposure times up to around 100,000 hours can be considered to be within the applicable range of the predictive capability of the model.

Figure 4-1: A Comparison of the Predicted Values of Inner Oxide Layer Thickness for Alloy Super 304H at 1202°F (650°C) Over a range of Pressures: 725, 2175, 2900, and 3610 psi (50, 150, 200, and 250 bar)

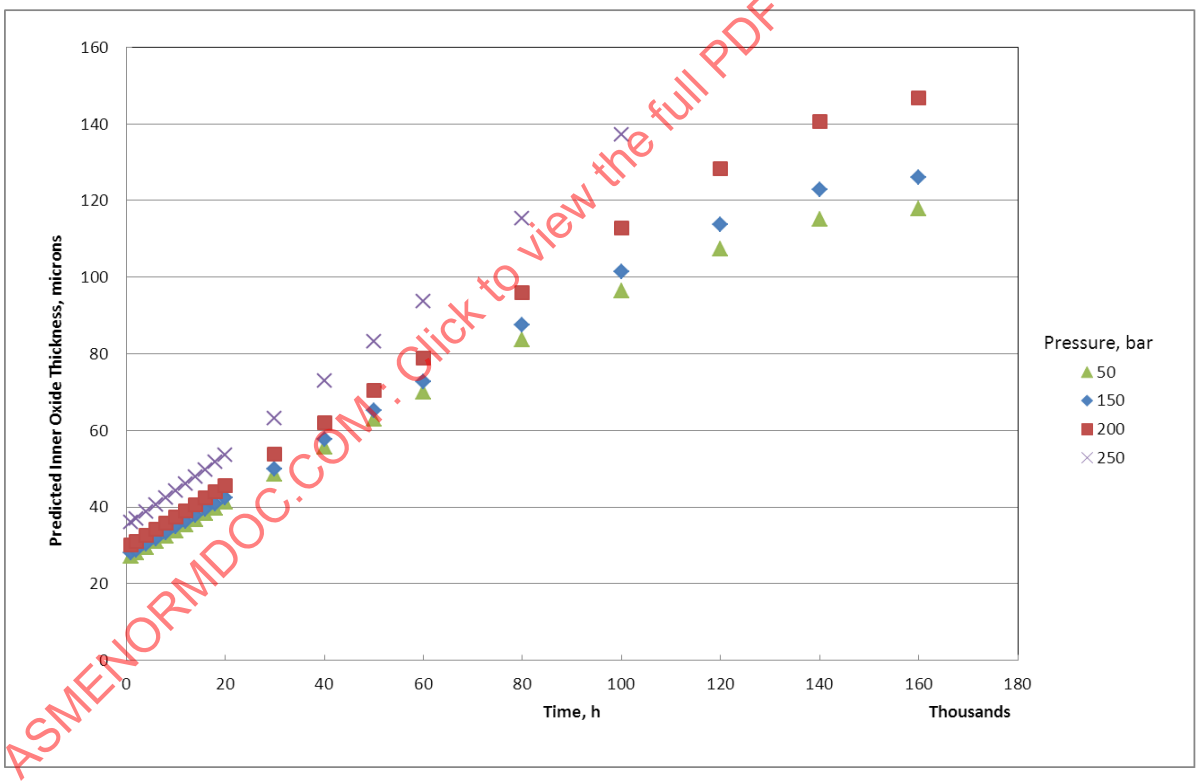

4.3 Remedial Measures

There are no significant boiler operational or process measures that can help reduce the rate of steam-side oxide growth, beyond general good boiler operational practice and the avoidance of overheating of the superheater and reheater tubes. The key to the avoidance of excessive oxide growth rates is the correct material selection for the particular duty.

It is considered in some quarters that it may be possible to minimize the extent of the delamination of the oxide layers by avoiding rapid boiler shutdowns, however the evidence for this in practice is limited and is largely anecdotal in nature.

The shot peening of some austenitic alloys has been shown to provide a significant protective effect, reducing the rate of oxide growth in steam for exposure times up to around 10,000 hours. The practical experience with this technique in operating boiler plants, to date, although growing, is limited.

5 CONCLUDING REMARKS

Of the three major sources of metal thickness loss from pressure parts in the fireside circuit of coal-fired steam boilers due to environmental degradation, two, i.e. fireside corrosion and particle impact erosion are related directly to the composition of the coal and the characteristics of the combustion process and one, steam-side oxidation, is affected by differences in the coal burned only to the extent of variations in heat flux and temperature distribution throughout the hot gas path.

The process of steam-side oxidation is relatively well understood, and sufficient data are available to allow the projection of accurate values of metal thickness loss (d_{st} in Equation 1) as a function of the major variables of temperature, time, and alloy type for use in ASME B&PV Code calculations.

Corrosion of the fireside surfaces of furnace-wall tubes typically involves sulfidation attack and the rate of metal loss can vary widely from rates similar to those for simple oxidation to catastrophic rates of associated with rapid corrosion-erosion, depending on the furnace conditions.

In areas subject to high levels of corrosive attack, the use of a protective coating or cladding may be appropriate. For those situations where the cladding/coating provides a continuous barrier for the intended lifetime of the tubes, there is expected to be no general corrosion loss of the tube walls so that the value of d_{fw} in Equation 1 can be taken as zero.

In other cases, where there is direct access of the fireside environment to the tube surface, values for d_{fw} will require specific measurements of the corrosion rate to be made using methodologies well known to the boiler manufacturers, since at present there is no proven analytical model to provide predictions. The areas of the furnace walls where the most aggressive corrosive environments are likely to occur are relatively well understood from previous experience, and this knowledge can be employed to guide efforts to measure corrosion rates in the appropriate locations and ensure that appropriate protective measures are in place.

The fireside corrosion conditions associated with oxy-firing technologies are less well understood, and there is insufficient experience at present to provide a basis for generating quantitative data on expected rates of metal thickness loss.

Superheaters and reheaters experience the highest tube metal temperatures in the boiler, and since both creep and corrosion are temperature-driven processes, it becomes increasingly important to be able to quantify factors affecting the thickness of the tube walls.

Fireside corrosion of superheater and reheater tubes involves the formation of complex, low-melting sulfates beneath deposits of fly ash. Good results have been obtained with analytical models of these processes that incorporate parameters related to the coal composition, the gas and tube surface temperature and the physical location in the tube bank, and further development work on these models is in progress.

Typically, the most practical approach to excessive metal loss rates of superheater and reheater surfaces is to change to a more corrosion-resistant tube material. The occurrence of corrosive attack is commonly far from uniform, and the estimation of rates of corrosion from careful measurements of tubes from service and from the results of corrosion testing has limitations.

Where this form of corrosion persists at an unacceptable rate, coextruded tubes with an outer cladding of a high-Cr alloy intended solely to provide corrosion protection have been used successfully. If a cladding can prevent access of the corrosive environment to the load-bearing tube wall for the intended lifetime of the component, then a value of zero could be assigned to d_{sh} in Equation 1. For all other scenarios, the

accurate prediction of the rate of metal thickness loss from superheater and reheater tubes remains a work in progress.

All the tubes surfaces exposed to the fireside environment of the boiler are susceptible to some form of erosive wear from the components of the coal fly ash, with the tubes in the convection sections being most at risk. Wear rates can be high where design features or ash deposits contribute to localized increases in gas velocity and concentration of ash particles in the gas. It is possible to minimize the risks of excessive erosive wear at the boiler design stage, but the current design methods cannot account for localized effects or from changes in combustion conditions.

Where erosive wear is a persistent problem, analytical techniques such as CFD modeling can be used to guide the design and placement of flow screens and baffles in order to reduce flow velocities and ash loadings to the design levels. There are some empirical approaches that can provide an indication of the potential of a coal to cause erosive wear from its composition, and measurements can be made using standard procedures to determine the expected rates of metal loss from individual alloys as part of the decision process for purchasing coals.

Overall, perhaps the only reasonable approaches available at present for obtaining values for d_{er} in Equation 1 are:

- The performance of specific measurements for each specific coal, using erosion test rigs to provide comparative data under relevant test conditions.
- Where flow-control screens and baffles have been installed based on measurement and analysis of actual gas velocities and particle loadings, it may be possible to use the value of the rate of metal loss used at the boiler design stage.

6 REFERENCES

[1] James, P.J., and L.W. Pinder, "Effect of coal chlorine on the fireside corrosion of boiler furnace wall and superheater/reheater tubing," Proc. *2nd Int. Workshop on Corrosion in Advanced Power Plants*, W.T. Bakker, J.F. Norton, and I.G. Wright, Eds., Tampa, Florida, 3-5 March, 1997. Also, *Materials at High Temperatures*, 14, 117 (1997).

[2] Lant, T., C. Keefe, C.J. Davies, B. McGhee, N.J. Simms, and A.T. Fry, "Modeling fireside corrosion of heat exchanger materials in advanced energy systems," pp. 255-267 in *Proceedings to the EPRI Sixth International Conference on Advances in Materials Technology for Fossil Power Plants (Santa Fe, NM, Aug. 31- Sep. 3, 2010),* D. Gandy, J. Shingledecker, and R. Viswanathan, Eds., ASM International (2011).

[3] Osgerby, S. and A.T. Fry, "The use of neural networks in understanding and predicting oxidation and corrosion behavior in advanced energy conversion systems," Materials at High Temperatures, 24 (4), 259-263 (2007).

[4] Shigeta, J., Y. Hamao, H. Aoki, and I. Kajigaya, "Development of a coal ash corrosivity index for high-temperature corrosion," Trans. ASME J. Eng. Mater. Technol., 109 (4), 299-305 (1987).

[5] Wright, I.G., P. F. Tortorelli, and M. Schütze, *Oxide Growth and Exfoliation on Alloys Exposed to Steam*, EPRI report No. 1013666 (2007).

PART TWO - INVESTIGATION OF CURRENT STATE-OF-THE-ART METHODS FOR CORROSION, EROSION AND STEAM OXIDATION OF BOILER TUBES IN PULVERIZED COAL-FIRED BOILERS

1 INTRODUCTION

There is an imperative to improve the electricity generation efficiency of fossil fuel fired power plants, for environmental and other reasons. In most cases, this will involve increasing the steam temperatures and/or steam pressures in both the superheater and reheater circuits of the boiler plants, and this is the subject of major programs of development and demonstration in a number of countries. This document is concerned with the impacts of increased steam conditions on the design and operation of coal-fired boilers, with the technical emphasis firmly on the large pulverized coal boilers.

As the temperatures and pressures of the steam are increased, both the fireside and the steam-side surfaces of the furnace walls, the superheater and reheater tubes, and the internal surfaces of the steam pipework will be progressively subjected to more aggressive conditions, which may lead to increased metal wastage rates and other related problems.

The principal processes that are most commonly responsible for the wastage and wear of boiler tubes in coal-fired boilers include:

- The fireside corrosion of the boiler tubes and other high temperature components, which can be responsible for increased and, in some cases, excessive rates of metal wastage.
- The erosion wear of the fireside surfaces of the tubes and other components by ash particles, which can be a significant cause of metal loss, and may act to further accelerate the impact of corrosion by removing ash deposit layers and protective oxide scales, exposing fresh metal surfaces to the aggressive fireside conditions.
- The steam-side oxidation processes, which can result in appreciable rates of oxide growth on the internal surfaces of the boiler tubing and other components. This can result in increased risks of exfoliation, blistering and spalling of the oxide layers, and can have a major impact on the heat transfer between the tube and the steam. By leading to further increases in both the internal metal surface and mid-wall temperatures, and to accelerate creep degradation, this can have a negative impact on plant integrity.

It is instructive in the current context to consider briefly the key technical aspects of each of these processes in turn.

1.1 Fireside Corrosion

The incidence of appreciable metal wastage due to the fireside corrosion of boiler tubes has been a significant issue in coal-fired utility boilers for many years. The boiler design rules and design features introduced in the 1950's and 1960's in response to corrosion problems, associated with the increases in boiler capacity and final steam temperatures at that time, have proved to be reasonably successful, and the incidence of accelerated corrosion damage was much reduced.

More recently, however, it has become apparent that a number of current and future developments, associated principally with improvement of the environmental performance of coal-fired power plants, and the imperative to reduce the CO_2 emission levels from power plants, have begun to change this position somewhat, viz:

- The introduction of primary NO_x emission control technologies to large coal-fired boilers, which has involved the installation of air-staged, low NO_x burners and the operation of a portion of the furnace volume under reducing conditions, has led to an increase in the incidence of excessive rates of furnace wall tube wastage. This has been associated with increases in the incidence of flame

impingement and the presence of the gaseous and solid products of sub-stoichiometric coal combustion local to the furnace walls.

- The operation of boilers at minimum excess air levels for NO_x emission control also tends to increase the flue gas temperatures at the furnace exit and can have an impact on the balance of the heat absorption throughout the boiler.
- The co-firing of non-conventional fuels in boiler plants designed for coal firing has resulted in significant changes in the chemistry of the ash deposits on the heat exchanger surfaces in the furnace and the convective section. In general this has led to increased levels of alkali metal sulphates and chlorides in the ash and, in a number of instances, excessive corrosion rates have been reported.
- There is current interest in the design of coal-fired utility boiler plants capable of producing steam at ever higher steam temperatures and pressures, and hence generating electricity at higher efficiency levels. This has led to a requirement for new materials for high temperature components that can operate at these advanced conditions. The resistance to fireside corrosion at elevated temperatures is clearly a key property of the candidate materials, and this needs to be demonstrated under plant conditions. There is also some indication from recent experience that a number of the newer materials can be less tolerant of temperature excursions than are the more traditional materials.
- The current developments in the oxyfuel firing of coal-fired boilers, to facilitate CO_2 capture and sequestration, has resulted in an increasing interest in the operation of boiler plants with advanced steam conditions, and with relatively high flue gas concentrations of CO_2 and H_2O and of the more important acid gas species, principally SO_2/SO_3 and HCl. The flue gas compositions that apply in these systems can be significantly outside the ranges for which there is relevant plant experience. This is considered to be one of the major risk areas associated with the development and deployment of this potentially important carbon dioxide emission abatement technology, and has been the subject of significant recent research work.

Overall, therefore, it is clearly understood within the industry that the ability to understand the corrosion processes, i.e. to predict the rate of fireside corrosion of boiler gas-side surfaces, and to control these to acceptable levels, is a major prerequisite of the successful development of advanced coal-fired boilers.

This is particularly the case for plants operating at advanced steam temperatures, with primary NO_x control and oxyfuel firing, and of boilers with the capability to co-fire biomass materials at high co-firing ratios. These developments are likely to be increasingly important elements of future coal-fired power plants with CO_2 emission abatement capabilities, and operating to the highest environmental standards.

1.2 Particle Impact Erosion

Erosive wear is associated principally with the impact of hard particles, carried in a fluid at significant impact velocities, on metallic and other surfaces. In general terms, the key areas of risk in thermal power plants are:

- internal surfaces of coal mills,
- internal surfaces of the pulverized coal pipework, and the burner internals, where erosive wear due to the impact of pulverized coal particles can have an effect on the equipment performance and can increase plant maintenance costs, and
- erosive wear of boiler tubes and other surfaces in the convective section, either by fly ash impact erosion or due to the action of the steam or air soot blowers.

In the context of the current project, the concern is exclusively with the erosive wear of high temperature boiler components due to the impact of coal fly ash particles carried in the flue gas stream.

Knowledge of the relative erosion wear rates for particular coals and ashes, and of specific target materials, is necessary to allow equipment suppliers to design for the intended fuel diet and to allow power plant operators to plan their maintenance schedules. Experienced suppliers of boiler plants and other equipment have the appropriate design rules and features that are effective in minimizing the impacts of erosive wear.

This is relevant to all coal-fired power plants, but is particularly important in the case of power plants that utilize fuels with high ash contents, such as those in the Indian subcontinent or in Southern Africa, where the engineering impacts and costs of the abrasive and erosive wear of boiler heat exchangers and other components can be very significant.

1.3 Steam Oxidation

At elevated steam temperatures, the rate of oxide growth on the steam-touched internal surfaces of boiler tubes and steam pipework can become appreciable. It is generally agreed, based on the knowledge gained from cumulative plant experience, and from the results of laboratory tests and test loop experiments in boilers, that the key parameters that control the rate of steam-side oxidation, and the tendency of oxide layers to delaminate and exfoliate are as follows:

- The rate of oxidation of any given boiler tube material increases exponentially with increasing metal surface temperature.
- The rate of oxidation may also increase with increasing steam pressure, although this is commonly considered to be a secondary effect.
- The rate of steam oxidation of boiler steels generally decreases with increasing chromium content.
- For boiler tubes, the presence of a heat flux across the metal/oxide layer has significant effects both on the metal temperatures under the internal oxide, and on the growth rate and the physical nature of the oxide layer. For steam pipework, the heat flux effects are obviously of much less importance.
- Any significant temperature variations or temperature cycling will also have an impact on the physical properties of the growing oxide layer, and therefore on the oxide growth rates. Exposure to thermal transients and steam pressure cycles are key factors in causing exfoliation of the oxide.
- Oxide layers that grow to significant thicknesses have a tendency to delaminate, and to blister and exfoliate. This can cause local hotspots and blockages, and oxide particles can be carried over with the steam to the turbine. The impacts of oxide growth on heat transfer and metal temperatures, and hence on the integrity of the system can be dramatic.

These are clearly important and fairly complex phenomena, and they are not, as yet, fully understood. These are the subjects of continuing research work in a number of boilermakers, power utility companies and research organizations, worldwide.

Under isothermal conditions and with a well-developed oxide layer of low porosity, the oxide layer thickness increases in a roughly parabolic fashion with time, i.e. the growing oxide layer has a significant protective effect. This may apply, particularly, to steam pipework for boiler plant operating under constant load conditions.

For boiler tubing, where there is a significant heat flux across the tube metal and the oxide layer, the insulating effect of the growing oxide layer will tend to result in a significant increase in the metal temperatures with time, and hence a further increase in the oxidation rates. Metal temperature increases will have an impact on the creep life of the tube.

There are, therefore, two competing effects which will influence the rate of oxide growth in boiler tubes with time, and the protective effect of the oxide layer in practice will tend to be less than that which applies

under isothermal conditions. In practical situations, the effect of thermal cycling will also have significant effects on the physical properties and integrity of the oxide layer, and the tendency for exfoliation. This also has a significant impact on oxide growth rates.

This behavior means that the oxide growth rates measured in isothermal laboratory tests will normally tend to underestimate those that apply in operating boiler plants under comparable conditions. These differences are a significant cause of concern when trying to relate the results of laboratory tests to those of plant exposures. This comparison is also affected by the relative loss of control over the test conditions that are an inevitable feature of plant tests.

The tendency of the oxide layers to delaminate can result in blistering and/or exfoliation of part of the oxide layer. Both types of behavior can have a significant effect on the thermal conductivity of the overall oxide layer. The resulting increases in metal temperature can be fairly dramatic and localized, and can lead to premature boiler tube failures.

Exfoliation and loss of the scale can also result in particles or flakes of oxide being released into the steam. Depending on their size and shape, these particles can accumulate in locations such as superheater/reheater tube bends, and can lead to blockages, with resultant flow restrictions and metal temperature increases. There can also be carryover of particulate material in the steam to the turbine, resulting in significant increases in wear rates of the surfaces of turbine components and valves from particle impact erosion.

It is clear that the steam-side oxide growth and exfoliation processes are relatively complex, and can be difficult and expensive to study. These processes occur at high temperatures in a flowing steam atmosphere, and occur over relatively long periods of time, of the order of several thousands of hours. These processes are also strongly influenced by a number of specific boiler operating parameters, such as the incident heat flux and the effects of thermal cycling, which can be difficult to reproduce in laboratory tests. The delamination, blistering and spalling behavior of the steam-side scales is particularly difficult to study systematically, since the phenomena involved occur at elevated temperatures over prolonged periods of time, and can depend on the tube geometry and other physical factors, as well as the thickness and structure of the oxide layer.

1.4 Materials and Temperatures

The materials of interest cover a fairly wide range of the current and potential candidate alloys employed for boiler tubes, thick-walled boiler components and steam pipework, e.g.

- ferritic alloys of relatively low chromium content, principally used for furnace wall tubes,
- ferritic/bainitic alloys of medium chromium content, for the furnace wall tubes and lower temperature elements of the superheater and reheater, and for steam pipework,
- austenitic alloys, for the higher temperature elements of the superheater and reheater banks, and
- nickel-based alloys, as potential candidate materials for the upper furnace wall tubes and for the highest temperature elements of the superheater and reheater banks of advanced boilers.

There is also increasing technical interest in the application of both conventional and novel surface treatments, coatings and claddings for the protection of both the fireside and steam side surfaces of boiler tubes and for the protection of the steam-side surfaces of steam pipework.

Looking first at the fireside corrosion of the furnace wall tubing, it is clear that historically the furnace tube metal temperatures have been relatively low, generally less than 450°C (842°F), and despite the relatively high heat fluxes in the furnace, there have been few problems with excessive rates of metal loss from corrosion or steam oxidation of the low alloy materials employed for this application. The main exceptions

to this have been in boiler plants which had problems with flame impingement on the walls due to poor design, faulty or poorly-maintained combustion equipment, or poor operation.

More recently, the introduction of low NO_x burners, staged combustion systems with over-fire air and other primary NO_x control technologies has led to changes in the composition of the flue gas in some parts of the furnace, and this has resulted, in some cases, in increased incidences of excessive rates of corrosion of furnace wall tubes, particularly within and just above the burner belt.

This has been the principal location to date for the application of protective surface coatings in large coal-fired utility boilers, although historically such coatings have been applied fairly widely in the furnaces in waste incineration plants. The approach has involved principally of the use of higher-grade materials applied to the affected tubes as co-extruded layers, weld overlay or spray coatings. Co-extruded tubes and sprayed coatings were successfully used in Britain during the 1980s and 1990s to overcome problems associated with poor combustion of British coals with relatively high sulphur and chlorine contents.

More recent experience of the application of these techniques, and principally the application of coatings and claddings, has been in North America, initially in supercritical boilers, but latterly also in sub-critical boilers. They were employed principally where there have been significant problems with excessive corrosion rates in pulverized coal-fired boiler plants retrofitted over the past couple of decades with primary NO_x reduction systems.

The substantial increases in final steam temperatures that are currently being proposed for the more advanced supercritical coal-fired boilers will result in significant increases in the furnace tube metal temperatures, particularly in the upper furnace sections, perhaps to maximum values of around 600°C (1112°F). This change has prompted a review of the materials that can be applied under these conditions, with creep strength enhanced ferritic (CSEF) alloys and nickel-based materials being considered in particular. There may also be increased interest in the application of coatings or other surface treatments to provide additional protection against excessive rates of fireside corrosion, and steam-side oxidation, in the more vulnerable locations.

The current generation of pulverized coal-fired utility boilers is being specified and constructed with final superheater and reheater steam temperatures up to around 600/620°C (1112/1148°F), respectively. These steam temperatures imply an absolute maximum fireside surface metal temperature for the superheater/reheater tubes of up to around 680-700°C (1256-1292°F). The current range of creep-resistant austenitic alloys can generally provide adequate tube lives in this application.

The more advanced boiler plants being proposed for the medium to long-term future, may operate at final steam temperatures in excess of 700°C (1292°F), and this would imply maximum metal temperatures in the superheater and reheater sections of up to perhaps 750-780°C (1382-1436°F). These temperature ranges can be considered to represent the upper limits of the range from which predictive modelling or test work will be required for fireside corrosion and steam oxidation behavior relevant to the working tubes in boiler plants likely to be built in the foreseeable future. The highest temperature superheater and reheater stages in these plants may require the use of nickel-based alloys with very high creep strengths, and high resistance to corrosion and steam oxidation.

For steam pipework, there is no corrosive fireside environment and no ash particle erosion, and the pipework is very well insulated. As a result, the heat fluxes that will apply across the oxide layers and tube walls are very low, and the pipework operates at close to isothermal conditions. The principal concern is the increased risk of excessive rates of steam-side oxidation at the elevated steam temperatures proposed for advanced coal-fired boilers. The metal surface temperatures of interest for the steam pipework would be in the range up to approximately 730°C (1346°F) or perhaps as high as 760°C (1400°F).

1.5 Content and Scope of the Design Guidelines

The scope of this document, is to review the current state of the art methods of designing for and assessing the effects of fireside corrosion, particle impact erosion and steam-side oxidation on boiler tube components, particularly superheater and reheater tubing, employed in the design of new supercritical and ultra-supercritical boilers. The upper metal temperature limit of interest is of the order of 730°C (1350°F).

As described above, the materials include:

- existing, commonly-used alloys that can be applied to the intended operating conditions;
- newer ferritic alloys, such as the creep-strength-enhanced ferritic (CSEF) steels;
- advanced creep resistance austenitic steels; and
- relevant nickel-based alloys.

For these materials, the following areas of concern are addressed:

- impact of local environmental conditions on fireside corrosion, erosion and steam oxidation,
- recommended temperature limitations for the alloy families, based on steam oxidation and other effects,
- approaches to fabrication of the boiler components that will influence corrosion, erosion and oxidation issues, if relevant, and
- effects of cyclic service on the fireside corrosion, erosion and steam oxidation processes.

The body of technical material reviewed as part of this investigation has included the existing work that has been performed as part of the advanced boiler cycle research performed by the relevant industrial and academic research organizations worldwide. Much of this work has been sponsored by organizations such as the EC, US DOE, the industry research organizations EPRI, VGB etc. and other national governments and funding bodies. The key areas of materials research from the technical literature have been identified and reviewed.

2 CORROSION- FIRESIDE

2.1 Introduction

Fireside corrosion has been an intermittent, but occasionally severe, problem for some large scale utility boiler operators over many decades. It is a complex process that is still not completely understood, or entirely predictable, even after many years of research by numerous organizations worldwide and, as such, is still the subject of further research. Whilst some plants have been operated for many years without suffering significant attack, others have suffered from furnace wall and/or superheater/reheater corrosion that, in the worst cases, has resulted in tube failures after less than one year of operation.

Boiler tubes operate at high temperatures and are exposed to variable heat fluxes and complex combustion-derived environments, with variable gas compositions and ash deposit chemistries. Boiler furnace sections and the superheater/reheater sections may be affected by different corrosion mechanisms. With good combustion conditions and benign fuels, boiler tubes will suffer only low rates of metal loss due to simple oxidation processes and, as a result, will operate with low metal wastage rates and extended tube lives. In some cases, however, the demands for high outputs with low emissions, sometimes in conjunction with poor quality fuels, can lead to accelerated wastage rates and reduced tube operating lives.

The drive to reduce the environmental impact of the operation of fossil fuel-fired boilers in recent years has led to increased steam temperatures, the co-firing of biomass and waste fuels and the development of oxyfuel firing technologies, all of which have the potential to influence the fireside corrosion wastage rates.

The predictions of the metal wastage rates for boiler tubing are based either on empirical experience and/or the results of corrosion tests in the laboratory or in combustion test rigs. The data are used to develop corrosion rate models that help determine new boiler design requirements, to define maintenance strategies for existing plant, or to predict the effects of altering fuel and operating conditions.

There are no standard or prescriptive test methods for high temperature corrosion measurement and testing, and a number of different approaches are employed at laboratory, test rig and plant scale. Laboratory scale studies are popular because they are relatively simple technically and are relatively inexpensive [6][7][8][9][10][11]. They provide precise control of the exposure conditions including the temperature, gas and deposit chemistry and exposure time.

Laboratory test work has a number of important disadvantages, however. It is only possible to employ simulated test environments, most often with un-cooled metal coupons without heat flux. The simulated ash deposits may become saturated with corrosion products over time, necessitating periodic interruptions to the test for ash deposit re-application. The simulated combustion gases are most frequently derived from bottled gas sources, and this has limitations in accurately simulating the full complexity of the combustion flue gases.

Testing in full scale, operating boilers with test pieces or corrosion probes has the advantage of long-term exposure to a real operating environment [12][13][14]. The test materials will be in the furnace or the flue gas pass with a dynamic gaseous environment, the continuous deposition and removal of fuel-derived ash, and a significant heat flux.

The principal disadvantage of plant testing is the reduction in the level of control over the test conditions. The test sections may be subjected to considerable variations in exposure conditions as a result of changes in boiler load, start-up and shutdown of the boiler and changes in fuel composition. It is also necessary to provide some form of cooling in order to control specimen metal temperatures.

Test materials in tube form can be inserted into the water or steam circuit of the boiler where they operate under normal boiler conditions and temperatures. In this case, access for insertion and removal of test pieces for examination is difficult and usually limited to periods of planned plant shutdowns.

To obtain elevated exposure temperatures it is possible to insert a test loop which draws cooling steam from the boiler circuit. This requires considerable design and planning, together with very close cooperation from the host site. This type of test loop will be expensive to construct and will still be subject to the operational constraints imposed by plant operation.

The alternative is to insert independently cooled probes with test pieces into the flue gases new or existing boiler openings. These probes and their control and cooling systems need to be rugged and reliable in order to have a reasonable chance of surviving in an operational boiler. This type of corrosion probe has the advantage of ease of installation and removal, often done whilst the boiler is operating. They also permit the test coupons to be exposed at temperatures not normally encountered within the boiler water/steam circuit.

Pilot scale testing using small scale combustion rigs can provide an intermediate position between laboratory and full scale plant testing [15][16][17][18]. The level of control over the exposure conditions is less precise than under laboratory conditions, but much better than can be achieved in an operational boiler. The corrosion coupons are exposed to real combustion gases, with the continual deposition of fuel derived ash and a significant heat flux. As in full scale plant, cooled corrosion probes are required to enable coupon exposures at set temperatures.

Pilot scale testing offers the ability to exercise control over the combustion environment by selecting or co-firing alternative fuels, by altering the combustion conditions e.g. under staged combustion, or changing the firing method e.g. under air or oxy-fuel combustion, or by the deliberate introduction of poor combustion conditions. Working at pilot scale also offers the possibility using test fuels that are not readily available in the tonnage quantities that would be required to conduct full scale plant trials.

Pilot scale testing has distinct disadvantages in terms of the limited test duration in most cases, as a result of ash handling or manpower. This is a major drawback where there are significant initial surface effects or corrosion process initiation periods. Very accurate metal loss measurements are also normally needed when the test pieces are exposed for short periods of time. Depending on the scale and arrangement of the test rig, there may also be significant constraints on the number of test sections that can be deployed.

After exposure in the laboratory, test rig or boiler plant, there are a number of options for determining the corrosion rate. Coupon weight gain or weight loss after ash and scale removal is frequently utilized to give an average rate of attack, although this method may not account for internal or sub-surface attack and will be affected by the delamination and spalling of the corrosion scales. Simple caliper measurements similarly yield an average metal loss, but again cannot account for internal attack.

The use of post exposure metallography is generally preferable. The corrosion coupons are sectioned and examined using optical or electron microscopy, in some cases with digital image analysis. These techniques enable metal loss and internal attack to be assessed, with multiple metal loss measurements enabling the nature of the corrosive attack to be fully characterized. Mounting the test specimens in cold curing resins and using non-aqueous cutting and polishing lubricants it is also possible to examine the microstructure and chemistry of the ash deposits and their interaction with corroded coupons to provide detailed information on the corrosion mechanisms.

In-boiler measurement of tubing thickness using ultrasonic techniques at routine plant outages remains one of the best methods of determining long term wastage rates. It should be noted, however, that there are significant measurement uncertainties with these techniques.

A number of on-line corrosion probes are available which use either resistance change or electrochemical techniques to determine the rates of wastage. The results derived from these probes can be very difficult to interpret and, at best, probably show only trends in wastage rates, rather than enabling accurate metal loss measurement or wastage rate predictions.

Overall, therefore, it is clear that the study of the high temperature corrosion processes that occur in boiler plants is technically very challenging, and is time consuming and expensive. All of the experimental approaches currently employed have distinct disadvantages, and no single method is capable of providing truly authoritative and reliable data.

2.2 Acid Dewpoint Corrosion

The effects of dewpoint corrosion have long been understood in fossil fuel-fired boilers, and the desire to avoid excessive corrosion of the internal surfaces of the flue gas ductwork and chimney has historically determined the selection of the boiler exhaust gas temperatures.

The sulfuric acid dewpoint temperature is normally in the range 90-160˚C (195-320˚F) dependent upon the fuel being fired. This is determined by the SO_3 and water concentration in the flue gas. Predictions of the sulfuric acid dewpoint temperature can be made using relationships developed by Verhoff and Banchero, or more recently by ZareNezhad [19][20].

Oxy-fuel firing with recycling of combustion gases to the furnace could significantly increase the partial pressures of both the SO_3 and water vapor in comparison to conventional air-fuel fired boilers. This has been observed after testing in the Schwarze Pumpe pilot plant, and may become important when oxyfuel firing is applied as a retrofit to existing coal-fired boilers [21].

Figure 2-1: Sulfuric Acid Dewpoint Temperature Variation Due to Combustion Gas Water Vapor and SO_3 Variation According to the Equation Defined by Verhoff and Banchero

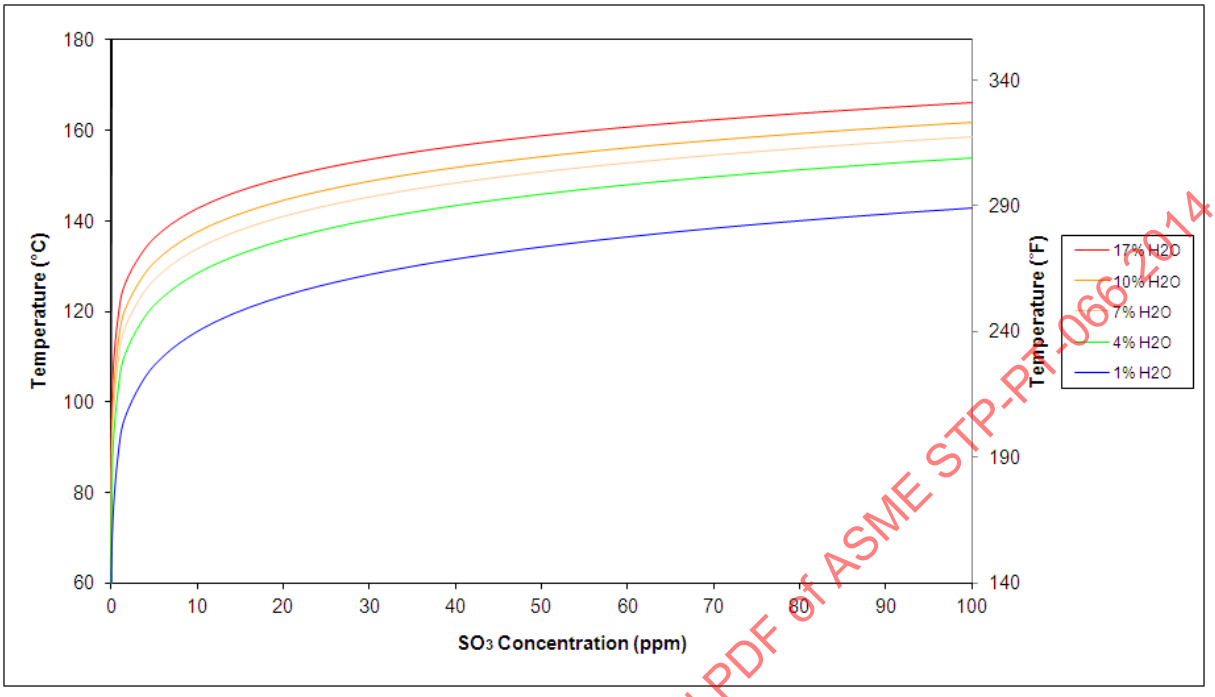

Figure 2-2: Hydrochloric Acid Dewpoint Temperature Variation Due to Combustion Gas Water Vapor and HCl Variation According to the Equation Defined by Kiang [17].

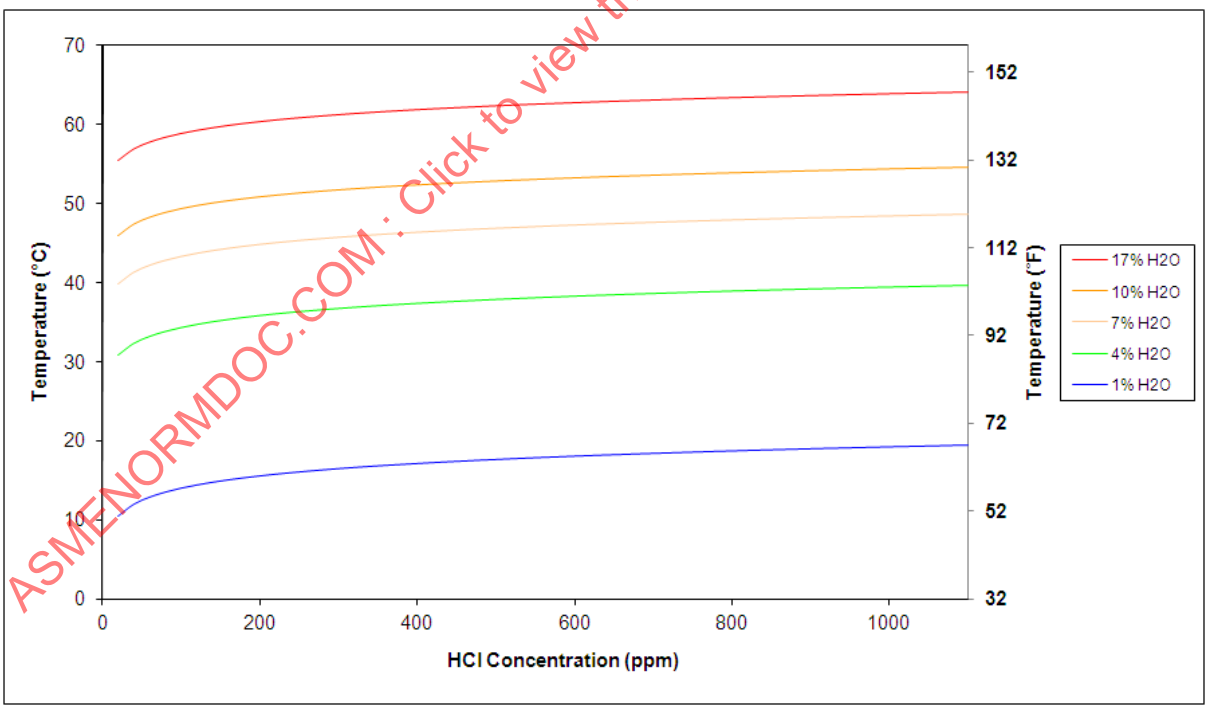

Dewpoint corrosion due to hydrochloric acid condensation is generally a lesser concern as, at all expected HCl vapor concentrations, the calculated dewpoint temperature would be significantly lower than that expected for SO_3 condensation.

2.3 Furnace Wall Corrosion

2.3.1 Introduction

The corrosion rates of boiler furnace wall tubes vary considerably and can be placed in the following categories:

- Low, i.e. up to around 10nm h^{-1} or 3 mil p.a.
- Moderate, i.e. in the range 10-100 nm h^{-1} or 3-35 mil p.a.
- Severe or catastrophic, i.e. in excess of 100 nm h^{-1}, or >35 mil p.a.

Corrosion rates within boiler furnaces can vary significantly. It is often the case that the vast majority of the wall tube surfaces will have suffered very little damage, and the worst affected areas are restricted to a few square meters of the surface.

Good corrosion resistance and low wastage rates in a boiler furnace depend upon the formation of a protective oxide scale that acts as a barrier limiting the diffusion rates of metal ions and corrodents.

Under oxidizing conditions where the combustion environment has a high oxygen content and is essentially free of carbon monoxide, the plain carbon or low alloy steels used to fabricate the furnace walls form a dense, duplex, predominantly oxide scale that thickens slowly with time. This type of scale is relatively defect free and is an effective diffusion barrier, leading to very low parabolic wastage rates and tube operating lives of many years.

Under more reducing conditions, where the furnace gases local to the wall have low oxygen concentrations and high carbon monoxide and hydrogen sulfide concentrations, the low alloy steel tubing forms relatively defective and less protective mixed oxide and sulfide corrosion scales. Under these conditions greatly increased metal loss rates can occur, with furnace wall tube operating life being reduced one or two years in extreme cases.

Furnace wall corrosion in coal fired boilers occurs most commonly near the burners and below any over-fire air injection ports. It is uncommon where the combustion conditions are well controlled, where flame and pulverized coal particle impingement is minimal, where benign coals are burnt, and where the geometry and aerodynamics of the furnace chamber make it more difficult for reducing conditions to occur in the vicinity of the furnace walls.

The combustion of pulverized coal is a dynamic process, subject to considerable variations between the burners, and the following fault conditions can lead to poor combustion:

- Unsatisfactory fuel and/or air distribution,
- Faulty burners,
- Insufficient combustion air, and
- Poor coal grinding performance.

These conditions can be encountered when the boilers are being operated at peak load, when the deficiencies in the plant can be exaggerated. Under these conditions, the flame envelope is expanded to its greatest extent, increasing the possibility of flame impingement on to the furnace walls. This can create reducing

conditions at the furnace walls, as characterized by having CO concentrations in excess of 2% and the absence of oxygen in the combustion gases. The ash deposits occurring under reducing conditions may contain significant levels of unburned material.

Flame impingement also exposes localized sections of the furnace wall to greater and more variable incident heat fluxes. This can exacerbate the reducing potential of the local environment. Flame impingement will also cause an increase in the amount of unburned or partially burned fuel particles arriving at the wall and adhering to the tube surface. Combustion of these particles will be retarded due to the relatively cooler tube surface, favoring a smoldering action and creating a highly localized reducing environment on the tube surface.

2.3.2 Furnace Wall Corrosion Rate Prediction

The quantification of a 'flame proximity factor' for front fired pulverized coal boilers and its effect on furnace wall fireside corrosion rates, in association with the coal chlorine content, was attempted in the late 1970s, and was summarized by James et al [23]. A regression analysis based on fifteen available data points from ten coal-fired power stations achieved a relatively good fit, with a correlation coefficient of 0.95, to an equation of the form:

Tube wastage rate = (A x %Coal Cl) + (B*HF) + (C x DF) - D

Where A, B, C & D are constants and;
HF is the 'heat flux factor' defined as:

$$HF = \left[\frac{[coal\_input\_at\_MCR] \times [proportion\_of\_time\_above\_70\%\_MCR]}{[area\_of\_heat\_transfer\_surface\_within\_the\_burnerbelt]} \right]$$

Where MCR = Maximum Continuous Rating of the boiler.

And;

DF is the 'deposition factor' defined as:

$$DF = \left[\frac{[prob.\_of\_3\_wing\_burners\_operating\_at\_MCR] \times [pf\_coarseness\_factor(>200mesh]}{[burner\_to\_side\_wall\_separation]} \right]$$

This multivariable equation identified an almost identical linear correlation between the corrosion rate and the fuel chlorine content to that derived in the Lees correlation, which is described below. Using this equation to predict the maximum rate of furnace wall corrosion yielded a closer correspondence with actual values than those based on coal chlorine content alone. However, difficulties in obtaining certain input values, and the relatively poor predictions obtained at several stations, meant that this relationship was not adopted as readily as the somewhat simpler correlation developed by Lees [24]. The conclusion is that the boiler furnace section needs to be sufficiently large to contain flame without impingement on the boiler walls.

The coal chemistry also has a significant influence on the furnace wall corrosion rates. Of greatest importance are the sulfur and chlorine contents, with increasing levels of both elements being detrimental. Coal sulfur contents are generally up to around 6%, with chlorine contents up to around 0.6%.

The effects of these coal constituents on furnace wall corrosion have been investigated by a number of research groups, and the conclusions of this work are summarized below.

Under oxidizing conditions, the sulfur is present predominantly as SO_2, with a minor quantity, normally less than 1%, which is further oxidized to SO_3. It has been proposed that SO_3 in the furnace can react with alkali metal sulfates within the ash deposits in order to form alkali pyrosulfates ($(Na, K)_2S_2O_7$). These species may be molten or partially molten at furnace wall tube metal temperatures enabling them to react with the protective oxide scales, and increase metal wastage rates. Although this proposal is compelling, no conclusive evidence for this mechanism being active in operational plant has been found [25].

In the presence of flame impingement and reducing conditions, reduced sulfur species can be detected by furnace wall gas sampling. The most easily measured in the combustion environment is H_2S, but using techniques such as Fourier Transform Infra-red (FTIR) spectroscopy, other species such as carbon disulfide (CS_2), methyl mercaptan (CH_3SH), carbonyl sulfide (COS) and elemental sulfur can be identified [26][27].

It has also been proposed that the presence of un-burnt carbon and iron pyrite (FeS_2) and/or pyrrhotite ($Fe_{(1-x)}S$) deposited with the ash under reducing conditions can lead to reducing conditions at the ash deposit/corrosion scale interface. The presence of these reduced sulfur species enhances the sulfide content in the corrosion scales rendering them defective or less protective and thereby enhancing the corrosion rates.

Bakker & Kung [8] observed that, under sub-stoichiometric conditions, the following reactions become possible:

$$FeS_2 + CO + H_2O \rightarrow FeS + H_2S + CO_2$$

$$S_{(\text{organicly bound})} + H_2 \rightarrow H_2S$$

When H_2S is present in flue gas, it will preferentially react with iron in the waterwall tubes to form FeS:

$$Fe + H_2S \rightarrow FeS + H_2$$

Existing magnetite (Fe_3O_4) corrosion scales present on furnace wall tube surfaces may also be disrupted and transformed to FeS:

$$Fe_3O_4 + 3H_2S + CO \rightarrow 3FeS + 3H_2O + CO_2$$

In this way, the scale formed on the steel may consist of iron oxide (Fe_3O_4), mixtures of Fe_3O_4 and FeS, or nearly pure FeS. The strength and adherence of the scale decreases with increasing FeS content, while its growth rate and permeability increase significantly. The result is increased diffusion and corrosion rates. The weak, sulfur-rich scale is also more easily removed by sootblowing or thermal cycling, which may further increase the rate of metal wastage.

An attempt has been made to model these processes by Kung [28] is based on the assumption that under reducing conditions the corrosion rates of iron-based alloys are assumed to be controlled by three variables, viz.

- H_2S concentration in the flue gas,
- Cr content in the alloy, and
- Metal temperature.

These variables are considered to be independent of each other, and the corrosion rate can be expressed as:

$$r = f(T) \times f(H_2S) \times f(Cr)$$

The temperature function f(T) can be represented by an Arrhenius-type relationship, viz:

$$f(T) = A \times e^{-\left(\frac{E_a}{RT}\right)}$$

where
A = constant
E_a = activation energy of the corrosion process
R = gas constant
T = absolute metal temperature

In general, the corrosion rates of alloys are considered to increase with increasing H_2S concentration in the flue gas. Where the order of the corrosion reaction involving H_2S is not known, a generic expression for $f(H_2S)$ can be written as:

$$f(H_2S) = B \times [H_2S]^{\beta}$$

where B and β are constants.

The corrosion rates of alloys typically decrease with increasing Cr concentration. Where the exact relationship between the corrosion rate and Cr concentration in the alloy is not known, a generic expression can be written as:

$$f(Cr\%) = \left(\frac{C}{(Cr\% + \gamma)^{\delta}}\right)$$

where C, γ, and δ are constants. Pure iron has a finite corrosion rate in reducing/sulfidizing gases: the constant γ therefore is introduced to prevent the value of f(Cr%) reaching infinity.)

The overall equation for corrosion rate expressed as mils.y^{-1} becomes:

$$rate = \alpha \times e^{-\left(\frac{E_a}{RT}\right)} \times [H_2S]^{\beta} \times \frac{1}{(Cr\% + \gamma)^{\delta}}$$

where α is a constant with the value $A \times B \times C$.

In simulated laboratory combustion environments the low and high chromium content alloys exhibited very different corrosion behaviors, and Kung divided the experimental data into two groups based on the Cr contents of the alloys, viz:

- group I consisted of the carbon and low-alloy steels ($0 \le Cr\% \le 10$), and ‘
- group II’ the higher alloy steels ($Cr\% \ge 16$).

Kung used nonlinear regression analysis of laboratory corrosion data to derive the following values of E_a (units cal/mole), α, β, γ and δ (all dimensionless), using the following values for the key parameters:

	'Group I'	'Group II'
α	3.20×10^5	1.04×10^7
β	0.574	0.290
γ	10.50	1.40
δ	1.234	1.370
E_a	15,818	19,230

With r expressed in mils.y^{-1},
R = 1.987 cal.K^{-1}.mol^{-1} for R,
T in Kelvin,
[H_2S] in mg/kg and
Cr in weight percent,

Kung quotes a correlation coefficient of 0.93 for the Group I equation, and 0.7 for Group II. He warns against applying these equations outside the ranges of exposure conditions employed during the laboratory study, i.e.,
[H_2S] < 500-5,000 mg.kg^{-1},
Cr <25 wt%, and
T < 482 °C (755K, 900˚F).

Using this approach, prediction of the corrosion rate of furnace wall tubing in reducing/sulfidising conditions operating at temperatures up to 482 ºC (900˚F) can be done, based only on the following information:

- surface metal temperature,
- H_2S concentration in the local combustion environment and
- Cr content of the tubing

The Kung model was derived using data from laboratory studies with mixed synthetic gases containing H_2S. When applying it to plant data, the local H_2S concentrations has to be measured or estimated in some way. No account is taken of the local CO concentration or the incident heat flux.

It is considered that the Kung model has proved useful in providing predictions of the corrosion rates in subcritical boilers, but has been less successful in more recent years when applied to supercritical boilers operating under low NO_x configurations [26]. For subcritical drum boilers, regardless of coal sulfur content, the maximum water wall wastage rates tend not to exceed values around 75 nm.h^{-1} (25 mil.y^{-1}), whereas for supercritical boilers the furnace wall wastage rates can be significantly higher.

It has been proposed that the highest corrosion rates observed in plant may be associated with the co-deposition of pyrite and unburnt carbon under reducing conditions. It was also considered that subsequent operation in an oxidizing environment can lead to extremely aggressive, under-deposit reducing conditions [29].

This process was clearly demonstrated and modelled using isothermal laboratory exposures of test coupons. The corrosion rate was dependent only upon:

- tube temperature

- O2 (%)
- CO (%) content of the flue gas

This model takes no account of the coal quality, other than assuming it is of relatively high sulfur content, this model, after applying a suitable factor, was claimed to predict maximum and average corrosion rates for low alloy (T2) in the same range as found in service. The equations are as shown below:

Max. Corr. Rate ($mil.y^{-1}$) = $1.81x10^4$ x $\exp(-10803/1.987T)x[(O_2)^{0.4}-2.1(CO)^{0.6}+7.9]$

Ave. Corr. Rate ($mil.y^{-1}$) = $1.21x10^4$ x $\exp(-10803/1.987T)x[(O_2)^{0.4}-2.1(CO)^{0.6}+7.9]$

The results of further work at the Hatfield Ferry pulverized coal fired Unit 2 boiler were presented by Bakker [25]. The ash deposits and corrosion scales on the tube surfaces contained 40-60% FeS deposits and 500-1500ppm Cl.

Detailed examination of the micrographs of the corroded boiler tubes suggests that the sulfides present on the tube surfaces were corrosion scales rather than deposited sulfides. The presence of significant levels of chlorides in the corrosion product layers indicated that these species played a significant role in the corrosion damage observed.

Similar accelerated corrosion rates were reported by Nava-Paz et al. in isothermal laboratory corrosion tests of a range of tubing alloys and corrosion resistant materials under deposits containing significant levels of unburnt carbon and pyrite [26].

Furnace wall fireside corrosion in the United Kingdom has long been linked with the chlorine contents of the coals being fired. Indeed, fireside corrosion rates of up to 600 $nm.h^{-1}$ (around 200 $mil.y^{-1}$) were reported in a 120 MW_{el} front fired, pulverized coal fired boiler as early as the 1970's [31]. This power plant had no low NO_x burners at that time, but had relatively compact furnaces that encouraged flame impingement, and suffered fireside corrosion from commissioning.

The corrosion rates steadily increased over time as the locally mined coal increased in chlorine content from ~0.4 to ~0.6%. The problem was not isolated to the boilers at this particular power station, with numerous UK boilers suffering damage rates in excess of 200 $nm.h^{-1}$ (~70 $mil.y^{-1}$) throughout the 1980's.

The presence of the chlorine species clearly destroys the protective effect of the oxide scale, but the precise mechanism is unclear. HCl, Cl_2, chlorine free radicals and molten alkali metal chlorides have all been identified as the dominant species [23][32].

2.3.3 Influence of Chlorine on Furnace Wall Corrosion

In the mid to late 1970s, efforts were directed toward establishing a link between the fuel chlorine content and the furnace wall fireside corrosion rates through analysis of corrosion rates experienced in the 120 MW_{el} front-fired boilers mentioned above [23]. The boilers were fuelled directly from an adjacent colliery over the period 1967-1977. This allowed for a correlation to be made between the coal chlorine content and the corrosion rate, since the single-source coal became progressively higher in chlorine as deeper seams at the colliery were exploited over the decade. A regression analysis of the data yielded a best fit equation for the maximum corrosion rate in $nm.h^{-1}$ of the form:

$$r_{max} = (m \times \%Cl) - C$$

This equation became known as the 'Lees Correlation' [24]. Extrapolation of this relationship to low chlorine concentrations identified a threshold value of approximately 0.2% chlorine, below which the chlorine appeared to have no influence on the furnace wall tubing corrosion rate.

As further data became available from boilers in other power stations, the values of m and C in the Lees Correlation were refined. Whilst the increasing wastage rate resulting from increasing coal chlorine content was essentially the same for all pulverized coal fired boiler designs, differences in absolute rates were observed between boiler designs. This was accommodated by deriving station-specific values of C.

The results of more recent pilot scale corrosion testing studies by Gibbs & Moores [33] provided information on the effects of chlorine on water wall fireside corrosion when firing three different chlorine content coals, at 0.42, 0.43, and 0.56% Cl in coal. They derived correlations of the same form as Lees, for both the average and maximum corrosion rates:

$$r_{ave} = (m_{ave} \times \%Cl) - C_{ave}$$
$$r_{\max} = (m_{\max} \times \%Cl) - C_{\max}$$

The authors recognized the limitations of this work, and considered that a more accurate correlation would involve the fuel Cl and S, together with the H_2S and CO_2 concentrations, the metal temperature and the heat flux.

A detailed review in the late 1990s of the experience of furnace wall fireside corrosion in UK boilers from the original CEGB data and from UK utility practice, confirmed that increasing chlorine content of the coal fired resulted in an increase in the rate of corrosion of furnace wall tubes [34]. Significantly this was only shown to hold true when all three of the following conditions applied:

- Operation of the furnace under persistent sub-stoichiometric conditions with CO concentrations at the walls in excess of 3.0%.
- A high level of unburned coal particles near the walls, which implies flame impingement conditions and high heat fluxes.
- The measured rate of corrosion or wastage of the tube was already in excess of 100 $nm.h^{-1}$ (34$mil.y^{-1}$).

These findings were consistent with the corrosion being worse in boilers having relatively compact furnace designs or front wall burners in close proximity to side walls. Such configurations would encourage contact between the furnace wall tubes and the actively combusting flame environment/envelope.

Significantly, this also implies that coals with increased chlorine contents can be introduced into boilers that do not satisfy the conditions listed above, without increasing the furnace wall corrosion rates.

An extensive program of short term corrosion probe exposures of almost 100 plain carbon steel furnace wall specimens was conducted by Davis, James & Pinder in a $1MW_{th}$ Combustion Test Facility [15]. In this program, specimens were exposed to the combustion products generated from five different UK coals, with chlorine contents in the range 0.03-0.56% and sulfur contents in the range 1.20-2.68%. In addition, one US coal containing 0.42% chlorine and 1.22% sulfur was also fired.

The test specimens were exposed to both oxidizing and reducing conditions. Analysis of the measured corrosion rates permitted the following overall predictive equation to be derived for average furnace wall metal loss under all combustion conditions (oxidizing and reducing), with an 'additional corrosion rate' term ACR to account for both heat flux and the chlorine content of the coal:

$$M = C \times \left[\left(t_o \times K_{p_o} \right)^{0.5} + \left(t_r \times K_{p_r} \right)^{0.5} \right] + \left[\frac{t_r \times ACR}{10^3} \right]$$

where M = metal loss (μm)
C = Constant
t = time (hours)

The expressions for the terms K_{po}, K_{pr} and ACR are discussed below.

The subscripts P and L relate to parabolic and linear rates, respectively, and the sub-subscripts o and r relate to oxidizing and reducing conditions, respectively. Reducing conditions were defined as a local combustion environment with O_2<0.5% and CO>2%.

The parabolic rate constant under oxidizing conditions, K_{po} ($cm^2.s^{-1}$), in the overall equation is a function of the absolute temperature T (K) and the activation energy Q ($KJ.mole^{-1}$) as follows:

$$K_{p_o} = C_{P_O} \times e^{-\left[\frac{Q_{P_O}}{RT}\right]}$$

where R is the Universal Gas Constant ($J.K^{-1}.mole^{-1}$).

The parabolic rate constant under reducing conditions, K_{pr} ($cm^2.s^{-1}$), in the overall equation is a function of both the absolute temperature T (K) and percentage of CO in the local combustion environment as follows:

$$K_{p_r} = C_{P_R} \times (\%CO)^n \times e^{-\left[\frac{Q_{P_R}}{RT}\right]}$$

An additional corrosion rate, associated with the chlorine in the coal, is expressed in the overall equation as ACR ($nm.h^{-1}$). This is a function of the chlorine content of the coal ($\%Cl$), the heat flux (HF in $kW.m^{-2}$), and the absolute temperature (K), as follows:

$$ACR = \left[(m \times \%Cl) \times (HF)^m \times e^{-\left[\frac{Q_{Cl}}{RT}\right]} \right] - P$$

The overall corrosion rate equation contains no terms to account for tubing alloying elements, and is only valid for plain carbon steel tubing. The equation was derived from experimental data collected at temperatures up to 450°C (842˚F), so caution should be exercised in extrapolating the equation beyond this temperature.

A very good fit was obtained between the predicted and measured values of metal loss for carbon steel samples which had seen constant conditions, both oxidizing and reducing, in the Combustion Test Facility. The slope of the best fit line was almost exactly unity, the intercept was negligible, and a correlation coefficient of almost 0.9 was obtained.

Further validation of the equation was provided by reference to historic furnace wall corrosion data from UK coal-fired plant, which were all found to fall within the scatter band defined by one standard deviation either side of the mean of the CTF data.

At constant temperature and CO concentration, therefore, the rate of metal loss is proportional to both the chlorine content of the coal, as in the Lees' model, and the heat flux raised to a power. This suggests that

under reducing conditions the measured corrosion rate is controlled by the coal chlorine content and the heat flux. This is in general agreement with plant experience [34].

In order to predict the average metal loss of carbon steel furnace wall tubing operating up to 450 ºC (842˚F) using this model, therefore, it is necessary to specify the following parameters:

- total number of hours in oxidizing and reducing conditions,
- metal surface metal temp (K),
- %CO in the local combustion environment during the reducing period,
- heat flux (kW.m-2) and
- chlorine content of the coal (% by weight).

Only a single value for the incident heat flux is required, as opposed to the more complex 'heat flux factor' in the earlier equation [23]. This is, however, still a difficult parameter to measure or to define accurately.

The Combustion Test Facility trials were carried out with pulverized fuels and burner configurations that were intended to reproduce, at smaller scale, the conditions expected in operating plant. The test specimens were exposed to all of the relevant variables, including a realistic heat flux and a continuous supply of combustion products (gases and ash). These conditions resulted in the formation of corrosion scales that were typical of those found in plant. In some cases, evidence of the formation of a chloride-rich band at the corrosion scale-metal interface was found.

Under reducing conditions, i.e. at CO concentrations in excess of 2%, the additional corrosion rate factor described above is considered active. In these circumstances, it is proposed that HCl from the combustion environment diffuses, under the influence of the heat flux, to the scale metal interface, forming an un-protective chloride-rich scale. This is only stable over a relatively narrow temperature range, the extent of which is dependent upon the chlorine or HCl partial pressure. No definitive stability range has been determined for a given coal chlorine content, rather it is anticipated that increasing the chlorine content increases the upper temperature stability limit. Once this temperature has been exceeded, the corrosion rates decrease to levels similar to those expected for low chlorine content coals at the relevant temperatures [35].

As the corrosion scale thickens, the temperature at the outer edge of the chloride rich phase increases, due to the presence of the heat flux. This reaches a temperature at which the chloride-rich phase becomes thermodynamically unstable and decomposes to iron and chlorine. The iron is oxidized in situ, whilst the chlorine migrates back to the scale-metal interface, where it promotes further corrosive attack. Under an increasing heat flux, the thickness of the chlorine rich phase decreases, reducing the distance for ion transport through the scale and increasing the corrosion rate. The results of metallographic examination of the corrosion scales showed a clear reduction in the thickness of the chlorine rich phase with increasing heat flux [15].

Although difficult to identify clearly, the chlorine rich phase frequently noted at the scale-metal interface is frequently referred to as $FeCl_2$. Spiegel and Grabke reported that under the low partial pressure conditions present at the scale-metal interface, that solid chlorides are stable [36]. They also described how recycling of the chlorine as described above, often referred to as "active oxidation", can occur under the influence of chloride containing deposits. This was observed in isothermal laboratory tests and in specimens from an investigation of a furnace tube failure which occurred in a German fluidized bed combustor burning coal with only $0.03^{w}/_{o}$ chlorine coal. The boiler deposits contained only $0.07^{w}/_{o}$ chlorine, but it was stated that this was sufficient to generate approximately 60vppm HCl in the combustion gases. In this case, the sulfur concentration in the flue gases was small, due to SO_2 absorption by in bed limestone injection.

The initial work reported by Davis, James & Pinder considered only plain carbon steel specimens. A further testing program on the Combustion Test Facility was conducted within the European COST522 program. This extended the original work to include test coupons with chromium contents in the range 0-12%. [37]. This work utilized deep mined and open cast UK coals having chlorine contents in the range 0.04-0.39% and sulfur contents in the range 1.72-2.45%.

Under oxidizing conditions, the measured corrosion rates decreased with increasing chromium content. The data were fitted to a logarithmic equation that was subsequently used to modify the oxidizing term of the original model.

Under reducing conditions, the measured wastage rate decreased in an approximately linear fashion with increasing chromium content, and the model was modified accordingly.

The mean metal loss rates under oxidizing and reducing conditions respectively were then expressed as:

$$M_o = [-A_o \times \ln(\%Cr) + 0.531] \times [(6 \times 10^5 \times (t_o \times K_{P_o})^{0.5}]$$

$$M_r = [-A_r \times (\%Cr) + 1] \times [(6 \times 10^5 \times (t_r \times K_{p_r})^{0.5}) + (t_r \times ACR / 10^3]$$

where the symbols and units are the same as before.

Substituting

$$M = (t \times K)^{0.5}$$

for each of the oxidizing and reducing terms in the original model, it was possible to produce a modified predictive equation incorporating an additional term to account for alloy Cr content:

$$M = 6 \times 10^5 \times [M_o + M_r] + \left[\frac{t_r \times ACR}{10^3} \right]$$

The required inputs are as before, but with the addition of %Cr in the tubing alloy material.

Back fitting the predicted mean metal loss data y (μm) as a function of measured mean metal loss data x (μm) yields an equation with a slope of approximately 1 and a small intercept offset as follows:

$$y = 1.0117x + 3.0367$$

The data showed a significant level of scatter with an R^2 value of 0.6357, i.e. although the trend is clear, this is generally not good enough for predictive purposes.

2.3.4 Effect of NO_x Emission Control Technology

Historically, the incidence of excessive rates of metal wastage of furnace wall tubes has been associated with flame impingement or poor combustion conditions. Since the 1980's increasingly stringent NO_x emissions limits have required the initial installation or retrofitting of low-NOx burners and subsequently of staged combustion systems.

Low NO_x burners provided a central area of fuel rich combustion wrapped in secondary/tertiary air in which the combustion is completed. This has the effect of delaying combustion, reducing the flame temperature and NO_x concentrations. Further reductions in NO_x were achieved through the use of over-fire air systems, in which some of the combustion air is removed from the burners and introduced at a higher point in the

furnace chamber. Increasing the proportion of combustion air introduced at the over-fire air ports, referred to as deeper staging, generally leads to a more reducing combustion environments and a larger flame envelope in the region between the burner belt and the over-fire air ports.

Experience of the impact of these NO_x control systems has been varied. In the UK, the fitting of low NO_x burners in general had a positive effect in greatly reducing the severe furnace wall fireside corrosion rates that were suffered during the 1980's [38]. This was attributed to the wrapping of the combustion zone in an air-rich envelope which prevented the formation of reducing environments at the furnace walls. Care was required in tuning the low NO_x burners after installation in order to ensure that the flames were not too long and did not impinge on the opposite furnace wall.

More recently in the US, where NO_x emissions limits are more stringent, deep staging with over-fire air systems has been required. For supercritical boilers especially, and to a lesser extent subcritical drum boilers, this has resulted in greatly increased furnace wall fireside corrosion rates. The problems have largely been attributed to operation with reducing conditions at the furnace walls. The formation of protective iron oxide scales on furnace wall tubes can be inhibited, and non-protective sulfide scales are produced, leading to accelerated wastage in the affected areas. Alternating reducing and oxidizing conditions, perhaps as a consequence of changing boiler loads, with co-deposition of un-burnt carbon and pyrite has also been blamed for the accelerated damage [27][29][30].

Gibbs & Moores [39] reported the results of a program of work to develop a simple equation relating the corrosion rate of the low alloy ferritic steel T-11 (1¼Cr½Mo) to the metal surface temperature, and the CO and H_2S concentrations. The corrosion rates were determined by exposing the test specimens to combustion gas mixtures generated in a small pulverized fuel fired combustion rig by burning two US coals, having different sulfur contents and very low chlorine contents, under low NOx burner conditions. The heat flux was not varied in any systematic way, but was held in the range 260-360 $kW.m^{-2}$ (82,420-114,120 $BTU.hr^{-1}.ft^{-2}$) whenever possible.

The dependence (for both coals) of the measured corrosion rate r ($nm.h^{-1}$) on combustion gas CO content (vol.%) over the range 3-9 % CO, was of the form:

$$r = m[CO] - C$$

The combined dependence (for both coals) of the corrosion rate r ($nm.h^{-1}$) on the combustion gas H_2S content (ppm vol.), was of the form:

$$r = m[H_2S] + C$$

The average corrosion rates measured for one of the coals at 3% and 6% CO were of the same order as predicted by the model from Davis et al, although the measured rate was somewhat higher than predicted at 9% CO [15]. The maximum rates measured were all higher than predicted. For the other coal, both the average and maximum measured corrosion rates were very similar to those predicted for the higher temperature and heat flux conditions.

Huijbregts et al [40] were involved in an extensive investigation of the accelerated furnace wall corrosion rates observed in a 680 MW_{el} pulverized coal-fired boiler in the Netherlands. The boiler fitted with low NO_x burners and a deeply staged two-stage combustion system. There was some evidence that the highest corrosion rates were within the cleaning circles of the soot blowers in the upper part of the burner belt and between the upper burners and the over-fire air ports.

By assuming a parabolic corrosion rate relating metal loss M to time t, of the general form

$$M = Kt^{0.5}$$

Hujibregts derived the following expression for K from corrosion exposure test data, i.e. the measured corrosion scale thicknesses on 13CrMo44 (T11) steel in a gas mixture intended to simulate the sulfidizing conditions in the boiler under investigation:

$$\log K = a_o + a_1 G + a_2 (1{,}000/T)$$

T is absolute temperature.

The 'gas factor' G incorporated partial pressure terms for sulfur, chlorine and oxygen and was defined as:

$$G = \log(pS_2) + 0.5\log(pCl_2) - 0.75\log(pO_2)$$

The expressions were determined from 40 hour laboratory exposures over the temperature range 350 - 450 ºC. The pS_2, pCl_2 and pO_2 values were dependent on the temperature, and were calculated thermodynamically for each gas composition.

Hujibregts was able to calculate the metal loss in a given time. Some microstructural evidence was presented to support the mechanistic validity of this simulation. Measured corrosion rates were plotted against calculated rates, although no correlation coefficient was stated.

2.3.5 Effect of Biomass Firing and Co-firing

Biomass fuels are variable in composition, and differ significantly from the coals for which the great majority of the pulverized fuel boilers were designed to burn. Biomass can contain variable quantities of chlorine and generally have very low sulphur contents. Although most biomass materials have relatively low ash contents, they tend to have significant levels of the alkali metals sodium and potassium and, in some cases, of heavy metals such as zinc and lead. When co-firing biomass with coal, the coal ash will tend dominate the behavior of the ash deposits unless very high percentage biomass firing is undertaken.

Very little published information is available on furnace wall corrosion when co-firing biomass in coal fired boilers, since the level of plant experience to date is small, and because most biomass co-firing has been at low co-firing ratios, where the risks of excessive ash deposition or corrosion are small.

Baxter and Koppejan [41] state that given sufficient sulfur in the combustion environment, then all available alkali metals will be converted to sulfates, which at the relatively low metal temperatures that apply in furnace walls, are relatively inert However, under reducing conditions, as found within the flame envelope and possibly at the furnace walls under flame impingement conditions, alkali metal chlorides are thermodynamically stable and not sulfates. This potentially gives rise to the possibility of depositing alkali chloride in the ash on the furnace wall tubes, something that would be considered very detrimental. To date, there is no evidence that this has been found in operating boilers.
Davis & Pinder reported the results of a program of 50 hour exposures of furnace wall specimens in a $1MW_{th}$ Combustion Test Facility firing pulverized coal blended with wood or cereal co-product (CCP) at both 10 and 20% thermal input [42]. When co-firing with the clean wood fuel regardless of thermal input, there was no discernible worsening of furnace wall corrosion, when compared to firing with coal alone.

When co-firing with CCP at either 10% or 20% thermal input, under reducing conditions, the already high furnace wall corrosion rates were comparable to those expected when firing coal alone. Under oxidizing conditions, however, the furnace wall corrosion rates were slightly increased from the expected low rates normally encountered. It was considered that the biomass alkali metal content was implicated in the enhanced fireside corrosion, but the fuel compositional range data were insufficient to permit a fully quantitative description of the aggressive components in the fuels. The fuel blend phosphorous, or

sulfur:chlorine ratios may be important factors in determining fuel corrosivity as this may impact on the chemistry of the furnace wall ash deposits.

2.3.6 Influence of Oxyfuel Firing

Oxyfuel firing involves the recirculation of the combustion flue gases to the furnace and the combustion of the coal in a CO_2/O_2 atmosphere rather than air. To date only relatively small demonstration oxy-fuel fired boilers with very conservative steam conditions are operational with these designed more to examine combustion issues than to study fireside corrosion problems. Several pilot scale combustion rigs have been made oxy-fuel capable and have been used to study corrosion as well as combustion issues. In addition laboratory scale isothermal studies using simulated conditions have also been conducted.

Kung et al have performed thermodynamic calculations to study changes in the ash formation and deposition processes when oxy-fuel firing, compared to those in conventional air-firing systems [43]. It was proposed that carbonate formation might introduce new, more damaging corrosion mechanisms if it were to occur with this new combustion system. The results of the calculations indicated:

- the carbonates remained unstable under oxy-fuel firing conditions, despite the enhanced CO_2 concentration in the combustion gases, and
- the ash formation remained essentially unchanged from that found when air-fuel firing.

In the absence of carbonate formation it was concluded that the same corrosion mechanisms active in air-fuel fired environments would remain active under oxy-fuel firing conditions.

Holcomb and Meir [44] have conducted isothermal laboratory trials simulating air and oxy-fuel conditions. Tests were conducted using coupons of T22, T91 and IN617 exposed at 450˚C (842˚F) to alkali sulfate containing model ash deposits. The simulated flue gases contained various water O_2 and SO_2 concentrations designed to simulate oxidizing and reducing conditions with and without flue gas desulfurization in the recycle loop. Under oxidizing conditions the results indicate that without flue gas desulfurization in the recycle loop, the wastage rates are increased significantly. Collaborative efforts are also to be undertaken in the Callide A 30MW demonstration project, in which it is intended to expose and analyze a number of furnace wall corrosion probes. These may take the form of passive plug type probes cooled by the furnace wall membrane, temperature controlled air cooled metallurgical probes or on-line electrochemical probes.

The results of laboratory scale, isothermal testing conducted by Robertson et al. have indicated that corrosion rates were typically no worse under oxy-fuel fired conditions than when air-fuel firing [45].

Fry et al. [46] presented work conducted using temperature controlled, electrochemical noise probes exposed in a 1.5 MW pilot scale furnace, firing two low sulfur US coals and a high sulfur Illinois coal, fired in air and oxy-fuel modes. The probe had carbon steel sensor elements that were exposed to predominantly reducing conditions with metal temperatures in the range 382-455˚C (720-851˚F). For all of the tests coals, the corrosion rates were found to decrease when changing from air to oxy-fuel firing.

Davis [47] reported the results of temperature-controlled corrosion probe work conducted in the E.ON pilot scale combustion test facility following its retrofitting to enable oxy-fuel fired operation. Tests were conducted using a number of bituminous coals with sulfur contents ranging from 0.6% to 3.4% and chlorine contents ranging from 0.02% to 0.45%, and they employed a range of oxygen enrichment/flue gas recycle regimes. The rig operated with a dirty recycle system, i.e. with no clean-up of the secondary, tertiary and over-fire gases, and only drying of the primary combustion gases. Furnace wall coupons, comprising 15Mo3, T23, T91, HR3C and IN671 materials, were subjected to short term exposures at temperatures representative of sub-critical drum and supercritical once through boilers.

The results indicated that there was no discernible change in wastage rates when comparing the expected rates in air and oxy-fuel fired systems, despite a significant increase in the concentrations of sulfur and chlorine species in the combustion gases.

The corrosion test exposures were relatively short, which precluded the study of any carburization of the specimen surfaces, a process which has been speculated could occur in the CO_2 rich combustion environments. There was, however, a clear indication of enhanced alkali sulfate deposition on the specimen surfaces that could, given extended operation, promote scale fluxing under the influence of molten pyrosulfate ash. The additional alkali sulfate deposition was attributed to increased SO_2 concentrations as a result of flue gas recycling, together with increased alkali release from the coal mineral matter under the influence of greater chlorine concentrations. This mechanism can be active at temperatures above 400˚C (752˚F) at which point pyrosulfates can exist in a molten form in the presence of sufficient SO_3 in the combustion gases [35]. This would require oxidizing conditions to produce the SO_2 and SO_3 and may be the reason for the enhanced corrosion reported by Holcomb and Meir as noted above.

Vattenfall operate an oxy-fuel pilot plant Schwartze Pumpe in Germany, which fires Lausitz lignite [21]. The intention is to demonstrate the oxy-fuel firing process and examine combustion, fouling and corrosion issues in economizers, water walls and superheaters, at 580, 650 and 750˚C or 1076, 1202 and 1382˚F. Operating in oxy-fuel fired mode with around 65% CO_2 in the gases resulted in the formation of around 7000 mg.m^3 SO_2 compared to 1600mg.m^3 air fired, and 27-29% H_2O, compared to around 9% air fired.

The deposited ash was very similar regardless of the operating mode and oxygen enrichment level. The low alloy steel coupons inserted to simulate furnace wall tubing suffered high wastage rates of 150-250 nm.h^{-1} (52-86 mil.y^{-1}), whilst alloy 1.4712 (X10CrSi6, 2.25%Si + 6%Cr) suffered a metal loss rate of only around 25 nm.h^{-1} (9mil.y^{-1}).

There were some indications of carburization and enhanced corrosion of the coupons exposed to simulated furnace wall conditions that were not present when operating in air-fuel fired mode.

2.3.7 Effect of Boiler Pressure and Tube Temperatures

For subcritical boilers, the furnace wall tube operating temperatures are determined by the operating pressure of the plant, and hence the water boiling temperature and the incident heat flux. The metal surface temperatures generally do not exceed around 450˚C (842˚F).

For once-through, supercritical boilers this is not the case and metal temperatures will progressively increase on traversing up the boiler from the furnace inlet and, as such, wall tube temperatures can exceed 450˚C (842˚F) towards the upper part of the furnace. The relatively high operating pressures and temperatures often necessitate the use of low alloy or creep strength enhanced ferritic steels in preference to carbon steel or weaker, traditional low alloy grades, in order to provide adequate tube life.

As noted above, in recent years there has been a tendency for supercritical boilers in the US to suffer severe fireside corrosion under the influence of reducing conditions brought about through the use of staged combustion systems. This was not accurately predicted by the models produced by Kung, and resulted in the proposed corrosion under pyrite rich deposits mechanism [8].

The predictive model relating wastage rates to fuel chlorine developed in the UK was found in many cases to hold true when extrapolated to the higher temperatures experienced in ultra-supercritical plant [37]. For 15Mo3 steel exposed to a 0.18% Cl coal burn at metal temperatures between 475-500ºC, and a 0.39% Cl coal between 525-550 ºC, the measured corrosion rates reached a peak and then fell back, implying a

declining influence of coal chlorine content on furnace wall corrosion rates at higher temperatures. Similar peaks in corrosion rates were observed for T23, E911 and HCM12 steels at similar temperatures to that of the 15Mo3 steel.

There is some uncertainty, therefore, about the validity of the predictive equations above 450°C in relation to the stability of the chlorine-rich phase at the scale/metal interface. Above certain temperatures, chlorine appears to take no further part in the wastage mechanism, and the predictive relationship breaks down. This results in a peak in wastage rates as a function of metal temperature and the temperature at which this peak occurs increases with increasing coal chlorine content. This is consistent with the perceived limited thermal stability range of the chloride rich layer, with the upper temperature limit being a function of the chlorine/HCl partial pressure in the local combustion gases.

2.4 Furnace Wall Tube Corrosion Prevention

2.4.1 Combustion Environment Solutions

In most practical situations, the prevention of furnace wall corrosion is more cost effective than the combating of excessive fireside corrosion damage. As noted above, it is generally accepted that damage occurs as a result of the furnace wall tubes operating in a reducing environment. The avoidance of a reducing environment local to the furnace walls is the key to preventing excessive fireside corrosion rates.

At the design stage of a boiler, the furnace should be sized to contain the expected flame envelope and avoid flame impingement and the deposition of un-burnt fuel. When operational, care must be taken in order to maintain milling and combustion equipment in good condition such that even when operating at full load, viz:

- the milling plant should deliver sufficiently fine coal to ensure good ignition and burnout,
- good fuel and air distributions should be maintained to all burners,
- the burners should be in good order and set up to provide good combustion conditions, and
- sufficient combustion air should be supplied to combust the coal efficiently, subject to primary NO_x control.

Where primary NO_x control measures, such as the use of over-fire air, are required, it may be impossible to maintain oxidizing conditions at the furnace walls, as a result of the delayed combustion and expanded flame envelope. In this instance, options such as the use of curtain air at the furnace wall have been tried at many power plants from the 1980's onwards. Care is required in installing or retrofitting curtain air systems. In some cases, these have proved unreliable or of little benefit. It can also be difficult to monitor the extent of the oxidizing conditions and corrosion protection provided [25][48].

Initially, installations of curtain air simply relied on cutting slots or holes in the furnace wall membranes at the appropriate locations, and allowing the negative pressure within the furnace to suck air into the furnace chamber. If the slots were too small they would not allow sufficient air into the furnace and could be easily blocked by ash deposits after very short operating periods. If the openings were too large the ingress of tramp air into the furnace could be excessive, leading to wider problems with draft control.

More recently curtain air systems employ fans to provide a supply of air to the slots in the furnace walls. Such a system is the subject of US patent application 08/730,581 filed by Kramer et al. in October 1996 [49]. In this design, 5 to 15% of the total combustion air is delivered via side wall curtain air slots, which introduce the air at low velocity and prevent it mixing with the bulk environment.

This type of curtain air system was installed in the Dutch 680MW_{el} Hemweg Unit 8 opposed wall fired boiler after fireside corrosion caused furnace wall tube failures after less than 4 years operation, although it was not reported how successful these were [40]. The corrosion was associated with reducing conditions at the furnace side walls. Such damage was not expected especially given that the plant routinely fired coals having only 1% S and 0.1% Cl.

Kihara et al [50] have also reported the successful installation of a curtain system in a Japanese boiler that was suffering furnace wall corrosion rates up to 0.75 mm. p.a. The effect of the curtain air was quite dramatic. An inspection carried out 18 months after installation indicated very low corrosion rates.

Consideration may be given to the use of fuel selection and blending to moderate the damage. Coals with lower sulfur or chlorine contents can be selected to replace damaging fuels, or they can be blended with the more aggressive fuels to reduce the concentrations of sulfur and chlorine introduced to the boiler.

Combustion additives may be considered to modify the corrosivity of the combustion environment. This is more frequently applied to plants firing low ash fuels such as mineral oils and biomass materials. For pulverized coal boilers, the additional costs associated with the use of fireside additives for corrosion control have usually been considered to be prohibitive.

2.4.2 Material Solutions

For furnace wall corrosion the design solutions employed to combat excessive fireside are dependent upon the rate and extent of the damage suffered.

If rates are only marginally above what is acceptable or economically viable, i.e. typically less than about 40 $nm.h^{-1}$ or around 14 $mil.y^{-1}$, the simplest solution is to install tubing having thicker walls [25]. For membrane walls these tubes can be slightly oversized in the affected area. For boilers having tangent tube construction where pitch and tube outside diameter are fixed, thicker walls are achieved through the use of profiled or faceted tubing that has normal wall thickness to the sides and greater wall thickness at the crown of the tube. Clearly, this approach does not modify or reduce the corrosion rates but simply provides an additional wall corrosion allowance in the appropriate areas. This approach can be useful, for example, to ensure that tubes operate without failure between planned maintenance overhauls. Similarly, it may be possible to use alternative ferritic alloys to reduce the corrosion rates to an acceptable level [28].

For areas with higher rates of corrosion, higher grade materials such as austenitic or nickel based alloys may be employed as composite tubes. Such tubes are required to have ferritic inner layers. Type 310 stainless steel co-extruded with plain carbon steel inner core has been successfully used for many years in UK boilers constructed using the tangent tube method. Flatley et al. reported Type 310 corrosion rates in a trial installation to be 55 $nm.h^{-1}$ or 20 $mil.y^{-1}$) compared to 180-250nm h^{-1} or 63-87 $mil.y^{-1}$ for adjacent plain carbon steel tubing [51]. From this it can be seen that even austenitic alloys can still exhibit considerable wastage under adverse conditions.

Kihara et al reported the successful installation of Type 310 co-extruded tubing in a Japanese boiler that had been suffering 0.75$mm.y^{-1}$ metal loss rate, which after 18 months operation had suffered no measurable damage [50].

More recently co-extruded tubes, with nickel based outer layers, have become available. Because of the reduced thermal expansion of these alloys relative to Type 310 austenitic stainless steel, these tubes have been produced with integral fins to enable membrane wall construction [52][53]. The tubes are marketed as co-extreme and have either IN625 or IN622 outer layers. They are reportedly able to offer the superior

corrosion resistance provided by wrought nickel based alloys with smother surface finishes and reduced residual stresses in comparison to weld overlays of the same composition.

Weld overlays have been employed since the mid-1990's within the US power industry to combat severe fireside corrosion rates, particularly in supercritical plants using over-fire air systems. These have frequently made use of Type 309 austenitic stainless steel and IN625 or IN622 nickel based alloys [53][54][55]. These installations initially proved very successful in combating furnace wall fireside corrosion. More recent experience, however, has shown that weld overlays can be susceptible to circumferential cracking damage, having an appearance similar to the alligator hide damage suffered by low alloy steel tubing. This damage has been attributed to segregation and selective corrosion coupled with a thermal fatigue element associated with thermal fluctuations due to slag shedding and load/firing changes.

IN622 has been favored in recent years in preference to IN625 as this alloy has a narrower freezing range leading to lower levels of segregation, and a reduced tendency to suffer interdendritic corrosion and the formation of circumferential cracking [6]. Other alloys that have been considered that exhibit less segregation include:

- alloy 33 (UNS R20033),
- alloy 50 (UNS N06650) and
- alloy 59 (UNS N06059).

Alloy 33 which has equal weight percent chromium, nickel and iron exhibited the best performance in laboratory exposures.

During the 1980's the use of sprayed corrosion resistant coatings was trialed and subsequently adopted in particular by the Central Electricity Generating Board in the UK. Numerous coatings compositions were either shop applied or applied in-situ within boilers during plant overhaul outages. The coating found to offer the best protection was based on a plasma sprayed 50% Cr-50% Ni composition.

Considerable care and attention with regard to establishing the correct spray parameters was required to produce consistent coatings with minimized oxide and porosity content. This was seen as crucial in order to avoid short cut paths for corrodents to reach the substrate tubing. Good quality systems and the regular production of test coupons for quality control were required in order to achieve satisfactory coating application and long term corrosion performance [56]. Whilst robot applied plasma spray coatings could be reasonably expected to achieve a consistent coating quality, hand spraying was found to provide very variable coatings of questionable long term integrity and performance. The use of thin thermally sprayed coatings was less successful in the US where thicker weld overlay coatings were generally preferred [55].

Alternative thermal spraying systems have been developed since the 1980's including the High Velocity Oxy-Fuel (HVOF) process. Using this system it is possible to apply very dense coatings with minimal oxide and porosity content. It is also more forgiving than plasma spraying as it is easier to produce coatings of consistently good quality. The system may have drawbacks, however, associated with lower deposition rates and greater residual stresses. Thinner coatings are generally deposited than for plasma sprayed coating. In addition, the HVOF coating process involves considerable noise, fume and thrust, making it more suitable for robot shop application than manual site application.

As with weld overlay coatings, there has been at least one report of circumferential cracking associated with 50Cr:50Ni sprayed coating where this had been applied in a Japanese boiler operating low NO_x systems and firing low sulfur and chlorine Australian coal [50].

2.4.3 Furnace Wall Corrosion Models

In a number of cases, the predictive equations reported above for sulfur and chlorine based furnace wall corrosion have been incorporated into combustion and boiler models using Computation Fluid Dynamics (CFD) codes and are currently being used with some success to predict furnace wall wastage rate variations with individual boilers.

Recent research by EPRI has made use of both pyrite deposition and chloride corrosion models with CFD models to predict wastage distributions within several power plant boilers burning coals containing a range of sulfur and chlorine concentrations [10][57].

The University of North Dakota has also applied corrosion models based on pyrite deposition and the sulfide/chloride content of the coal to a pulverized coal fired boiler fitted with separated over-fire air NO_x reduction technology. Some success was achieved with the prediction of both coal ash deposition and corrosion behaviors in the furnace [58].

2.4.4 Corrosion Monitoring

Off-load metal loss assessment of furnace wall tubing is perhaps the most commonly employed corrosion monitoring method. This involves carrying out non-destructive ultrasonic thickness checks at routine plant maintenance outages. Access to the tubing fireside is provided either via furnace scaffold or by making use of sky climbing equipment lowered from the upper furnace. Measurements are taken at regular intervals around the furnace section and at specific elevations. Traditional ultrasonic thickness measurements require the local cleaning of the tubing to bare metal by grinding or grit blasting, with the use of a liquid couplant for acoustic connection of the probe to the tube.

In recent years improved ultrasonic techniques such as Electromagnetic Acoustic Transducers (EMAT) have improved the accuracy of the technique and removed the need to provide a clean metal surface. EMAT probes can work through up to 7mm of ash deposit provided that the tube has a magnetite oxide layer on its surface to act as the couplant [59]. The technique is not suitable for areas of tubing suffering significant erosion, where the oxide has been removed.

The use of ultrasonic techniques over a series of maintenance outages can present a detailed picture of the average wastage rates throughout the boiler, identifying any areas that are suffering greater damage. Clearly, this can only provide estimates of the average wastage rates, and it is possible that the majority of the damage found might have occurred during relatively short periods of abnormal operation.

Temporary corrosion probes can be installed in furnace walls to monitor local corrosive conditions over relatively short periods of time. The probes require openings to be made in the furnace wall which could take the form of toggled tubes, or holes or slots cut in the membrane walls. These probes take a number of forms from passive screw in plug type probes, through to actively cooled probes using air, water or steam. Probes can use post-exposure techniques to measure metal losses can use on-line electrical resistance or electrochemical noise measurement techniques to infer real time or near rear time corrosion rates. [60][61][62].

A development of the temporarily installed electrical resistance probe is a permanently installed electrical resistance array system for use in membrane walled boilers. This system makes use of an array of electrodes welded to the cold side of the membranes and tubes on the furnace wall to be monitored. By scanning the resistance between adjacent electrodes at intervals it is possible to monitor the changes over time associated with the thinning of the wall tubes allowing the production of wastage maps. Whilst only a few such systems have been installed there has been reported good correlation between the on-line resistance array measurements and ultrasonic metal loss measurements made at routine boiler overhauls [63].

It is also reported that short term temperature fluctuations associated with sootblowing or slag falls can be monitored and that by comparing measurements of resistance in the vertical and horizontal directions it is possible to determine whether metal loss is associated with simple general corrosion or circumferential, thermal fatigue type cracking [64]. A further development of the technique enables measurement of the cold side tube and membrane temperatures which is reported to provide a good estimation of local heat flux.

2.5 Superheater/Reheater Corrosion

2.5.1 Technical Background

The primary stages of superheater and reheater sections in the convective pass of two pass boilers, or in the upper section of tower boilers do not, in general, suffer significant fireside corrosion damage. These tubes tend to experience parabolic wastage rates that decrease to very low rates over long periods of operation. In most cases, the tubes are formed from relatively low alloy, ferritic steels.

High temperature corrosion affects the higher temperature stages or elements in most boilers, and extending to the penultimate tube banks for plant operating with higher steam temperatures. Coal ash corrosion of these tubes manifests itself as distinct wastage flats on the hottest exposed faces of the tubes, or as a massive array of deep honeycomb pits. Geometrical or aerodynamic features such as support lugs, fillet weld beads and protruding tube butt welds can give rise to local deep isolated pits as a result of locally enhanced metal temperatures or thinner insulating ash deposits.

The worst corrosion occurs on aerodynamically exposed tubes: for example, the leading tubes of a superheater bank. Contra flow superheater banks, which combine the hottest flue gases with the hottest steam, are more vulnerable to fuel ash corrosion than those designs which have parallel flow.

The corrosion of the surfaces of the tubes is associated with the deposition of alkali metal sulfates, principally sodium, in the coal ash deposits in the superheaters and reheaters. The alkali metal compounds accumulate by condensation at the base of the porous ash deposits. These materials begin to become molten at tube surface metal temperatures of about 580 ºC, or 1076°F, and above, and form a thin layer of highly corrosive liquid next to the protective oxide scale. The molten sulfate layer contains free sulfur trioxide, which stabilizes the sulfate and attacks the scale by dissolving the normally protective oxide to form iron, chromium and nickel sulfates, ultimately forming compounds such as alkali iron trisulfate $(Na,K)_3Fe(SO_4)_3$.

The stability of the trisulfates decreases as the temperature increases, and the temperature gradient through the deposit causes a concentration gradient for the dissolved metal ions. These factors ensure that the dissolution is effectively a continuous process, with iron, chromium and nickel diffusing outward through the molten trisulfate layer. At the hotter outer surface, iron/chromium oxides are re-precipitated within the ash, but they are discontinuous and no longer form a protective layer. This dissolution process results in a linear corrosion rate that does not diminish with time, in contrast to the parabolic rate for protective oxidation found, for instance, in the cooler primary superheater and reheater stages.

The rate of this continuous transport process determines the rate of corrosion, which is therefore highly dependent upon the surface metal temperature and the heat flux. For a given metal surface temperature, therefore, higher corrosion rates are observed at higher gas temperatures.

The corrosion rate increases with increasing metal temperature to a peak value at around 650-750ºC, or 1202-1382°F, at which the molten trisulfate compounds become thermodynamically unstable and break down to form less damaging solid simple sulfates. This causes corrosion reaction rates to fall at higher

temperatures, eventually leading to normal high temperature sulfidation/oxidation. This results in the classical 'bell-shaped' curve commonly found when the corrosion rate is plotted against temperature.

The peak temperature is different for each alloy, since the temperature range in which the molten salt is stable depends on the interaction of the molten salt with the metallic components of the alloy [65]. The corrosion products generated by the alloy materials, therefore, have a significant effect on the melting temperatures of the salt.

2.5.2 Effects of the Combustion Environment

As for furnace wall corrosion, the role of chlorine in superheater corrosion has been studied many times. By the mid-1980s, operational experience in Britain had shown that there was a correlation between the chlorine content of the coal and the rate of corrosion of austenitic superheater and reheater tubes. It had been known for some time that chlorine strongly promotes the release of both sodium and potassium from the coal mineral matter. It was considered possible that chlorine might play a role in the corrosion mechanism, despite the fact that the higher temperature coal ash deposits do not contain chlorine. No such additional role for chlorine has ever been confirmed.

The curve fitting of a database of operational data and the results of carefully controlled probe trials data by the former Central Electricity Generating Board ('CEGB') in the UK in 1985 resulted in the development of a corrosion rate equation for austenitic superheater tube materials known as 'modified PE8', which took the form [66]:

$$r = A \times B \left(\frac{T_g}{G} \right)^m \left(\frac{T_m - C}{M} \right)^n (\%Cl - D)$$

Where
- r = corrosion rate in nanometres per hour, $nm.h^{-1}$
- T_g = flue gas temperature, ºC
- T_m = surface metal temperature, ºC
- Cl = coal chlorine content, %
- A = tube position factor (dimensionless)
- B = material factor (dimensionless)

C, G, M, D, m, n are constants.

The constant A accounts for the different propensities for corrosion attack within a tube bank, having a higher value for leading tubes than for non-leading. This reflects the general observation that leading tubes corrode at a faster rate than the more sheltered non-leading tubes.

The constant B accommodated the relative performances of the different austenitic steels, taken as a higher value for the 15-19%Cr steels (T316, T321, T347, Esshete 1250), and having a lower value for type 310 (23-27%Cr) steels.

The limits of the data set from which the equation was derived are:

$$605\ ºC < T_m < 680\ ºC; \quad 870\ ºC < T_g < 1200\ ºC; \quad 0.12\% < Cl < 0.58\%.$$

In order to predict the corrosion rate of austenitic superheater tubing operating up to 680 ºC, or 1256°F, using this model, it is necessary to know:

- weight % chlorine in coal,

- tube position
- tube material,
- flue gas temperature (ºC), and
- surface metal temperature (ºC)

The corrosion rate can be seen to be linearly related to the coal chlorine content, but the mechanistic reasons for this were not clear. In Britain, where plants were predominantly firing indigenous coals, this equation was found to provide a very good indicator of fuel corrosivity. As noted above, the fairly narrow sulfur content range for British coals meant that it was impossible and unnecessary, to include a fuel sulfur term in the predictive equation.

The tube position has been identified as a key factor in modelling reheater corrosion. Based on an evaluation of the results of 45,000 hour exposure of various tube materials in a coal-fired boiler, Blough *et al* [67] stated that the location in the boiler, in addition to the tube metal temperature and alloy content, are the key variables that affect the wastage rate. The authors stated that these parameters include the velocity and temperature of the flue gas, the heat flux, and the ash deposition rate.

In 1986, Shigeta *et al* [68] derived a predictive model for the corrosion rate of superheater/reheater tubing based on a corrosion index which was defined in terms of acid-soluble oxides of the alkali metals sodium and potassium in the corrosion deposits, viz:

$$Metal\_loss = f\left(\frac{Na_2O}{K_2O}\right)_{as} .f(CaO)_{as} .f(MgO)_{as} .f(SO_2).t.(-0.08+(Na_2O+K_2O)_{as})$$

This relationship appears useful in accommodating the effect of fuel sulfur on corrosion, most of the corrosion parameters were derived from laboratory scale, isothermal tests performed on one material, T347, at a single test temperature and using synthetic ashes.

2.5.3 Effects of the Tube Material and the Steam Temperature

Most of the conventional and candidate boiler tube alloys have been subjected to isothermal laboratory corrosion tests over several decades using simulated flue gases and ash deposits containing alkali metal sulfates and iron oxides [69][70].

A progressive increase in the measured corrosion rate with increasing temperature up to a maximum value at approximately 700˚C (1292˚F) has been reported in all cases. Wastage rates start low for steam temperatures of 540˚C (1004˚F). At these temperatures, the sulfate ash deposits are solid and not able to causing fluxing of the scales grown on the metal surface. As a result low alloy ferritic materials are suitable for operation under these conditions.

Increasing the metal temperatures to approximately 580-600˚C (1076-1112˚F), consistent with steam temperatures of 568˚C (1054˚F), brings operation into the range in which the sulfate ash deposits can become molten and can start to flux the corrosion scales. At this temperature higher alloy austenitic materials are required as these offer greater corrosion resistance. Few if any alloys are immune to corrosion above this temperature and wastage rates increase rapidly with increasing temperature.

As noted above, corrosion resistance for a given material again increases, and wastage rates decrease, at metal temperatures above approximately 700˚C (1292˚F) at the point where the molten sulfates become thermodynamically unstable and are replaced by simple solid sulfates. At the very highest proposed operating temperatures, therefore, relatively modest corrosion rates can be expected for the high creep

strength materials that would be utilized to construct the superheater stages. However, at some point within the boiler, the metal temperatures would need to transition through the peak wastage rate region, and this may be a variable, depending on boiler load, etc.

Boiler tubing alloys for use in the highest temperature section in any boiler have historically been selected based upon their creep strength. The most expensive, higher alloyed materials are employed only where deemed necessary at the design stage, or where experience demonstrates that the lower alloy materials do not offer sufficient tube operating life.

The demand for increasing power plant efficiency has driven the final steam temperatures of power plants from 540˚C (1004˚F) to ever higher values, with an upper limit of 760˚C (1400˚F) having been proposed for future plants. Similarly steam pressures will also rise from the typical sub-critical drum boiler plant operating at 165bar, to supercritical pressures of approximately 300bar.

These increases in operating temperature and pressure place considerable demands in terms of creep strength. At the lowest end of the pressure-temperature range, low alloy ferritic materials such as T22, T23 and T24 are sufficient. Martensitic, austenitic and nickel based alloys are required as steam conditions increase. The resistance to fireside corrosion resistance also improves with progressively increasing creep strength, largely as a result of increasing chromium and nickel contents within the alloys.

In 2001, Blum et al [71] reported fireside corrosion rate measurements for a number of boiler tube materials in identical test superheaters installed in the steam generator at a Danish power station, after 7,700 hours and 23,000 hours exposure. Four martensitic, and five high alloy austenitic materials were used. The flue gas temperature in the area of the superheater had an average value of 900°C, and the heat flux was approximately 50 kW/m2 (15,850BTU.hr-1.ft-2).

For all the martensitic materials tested (X20CrMoV121, HCM12, T91 and T92), the corrosion rates were modest. At metal temperatures up to 570 °C, the metal losses for the first three were all less than 100 µm after 23,000 hours exposure. For T92, the metal loss approached 100 µm after 23,000 hours, i.e, an average rate of 4.3nm h^{-1} (1.5mil.y^{-1}).

All the austenitic materials tested (1.4988, TP347HFG, TP310N, HR3C and NF709) also showed considerably lower rates, with corrosion losses of less than 50µm after 23,000 hours exposure, i.e. an average rate of 2.2nm h^{-1} (0.76mil.y^{-1}).

It was concluded that fireside corrosion for these materials could be better modelled by a cubic, rather than parabolic, dependence on time. If valid, the consequence of this is that the application of a parabolic dependence results in rather conservative estimates of the operating time of martensitic and austenitic superheater tubing.

It might however be the case that the high temperature fireside corrosion damage had a significant initiation period, perhaps extending to several thousand operating hours. Indeed, for the high chromium austenitic alloys in particular, it could be expected that the initial oxidation would form a protective chromia scale. Given extended operation the reserve of chromium in the underlying alloy becomes depleted and the chromia scale can no longer be maintained, at which point less protective duplex oxide scales comprising outer magnetite and inner spinel oxides are formed.

In 2003, Davis & Pinder [72] reported the results of 8,000-11,000 hour exposure of precision metrology probe samples of austenitic stainless steels, and more highly alloyed Fe-Ni-Cr materials (up to and including 50Ni50Cr, IN671), in the superheater and reheater stages of a coal-fired power station burning

predominantly UK coals of varying composition. Although no corrosion rate correlations were derived, the following observations were made:

- The measured corrosion rates decreased rapidly with increasing chromium content of the alloys studied.
- The measured corrosion rates increased rapidly with increasing flue gas temperature.
- Evidence for a 'bell-shaped' curve was found for TP347H and TP347HFG steels, with a peak in wastage rates appearing at approximately 670 ºC. No evidence of a bell-shaped curve was seen for Super304H, or for any of the other, more highly alloyed materials. It should be noted however that the exposure temperatures did not exceed 700°C.

Blough et al [67] exposed samples of 304, 347, 800H, NF709, HR3C, CR30A, and chromised T22, in the reheater section of a coal-fired boiler for 45,000 hours at temperatures ranging from 521 to 685 °C, covering the expected tube metal temperatures for an ultra-supercritical plant. The measured metal wastage rates were relatively high, and erosion, from fly ash-laden flue gas, appeared to have made a significant contribution to the tube metal wastage observed.

Baker and Smith [73] have summarized test loop data including a range of austenitic alloys, a high strength / creep resistant nickel based alloy IN740 and corrosion resistant coatings, which demonstrated that the IN740 material performed reasonably well, suffering approximately half the wastage rates of the highest alloy austenitic materials but less well than the corrosion resistant weld overlay materials.

Hack and Stanko [13] have conducted perhaps the most long-term and robust corrosion probe studies for many materials operating in conventional, supercritical and ultrasupercritical power plants. In combination with laboratory scales studies these tests have been used to demonstrate the ability of tubing alloys and coatings to withstand fireside corrosion when exposed to low and high sulfur coal firing. For low sulfur coals many alloys should be capable of successful deployment. However even some of the nickel based alloys are likely to require corrosion protection to enable them to operate under advanced supercritical conditions when firing higher sulfur coals.
Other plant manufacturers, utility companies and research institutions have been active in major international collaborative projects conducting either long term probe or test loop exposures of superheater materials. However, for many of these projects the results have not been openly published and the knowledge gained has remained confidential to the project partners.

2.5.4 Effects of Biomass Co-firing

The risks of increased rates of high temperature corrosion of superheater tubing due to chloride deposits is a possible technical issue associated with biomass co-firing [74]. This may require a change of materials, e.g. use of martensitic or austenitic steels in preference to ferritic steels or the application of corrosion resistant coatings. The de-rating of the plant may also be considered, although this can involve decreased efficiency and lost output.

The results of test work in pulverized coal fired boilers co-firing straw suggested that there may be no significant change in the corrosion mechanism with co-firing [75][76]. The metal losses were attributable to simple oxidation or molten alkali sulfate fluxing of the corrosion scales. The modest increase in the measured metal wastage rates of up to a maximum 1.5 times relative to coal firing was most likely associated with an enhanced volatile potassium level that accelerated the formation of alkali iron sulfates. The bulk of the potassium released from the straw ash was considered to have been captured by the alumina silicates from the coal ash, and was not available to form aggressive sulfate deposits. The chlorine remained in the flue gas and did not deposit on to superheater tube surfaces, and as such, reportedly played no significant part in the corrosion processes.

The Vestkraft Unit 1 at Esbjerg, Denmark, operated by ELSAM, comprises a natural circulation front wall fired boiler, having 4 burners in each of 3 levels. The two middle burners in the middle row were converted to fire straw with hard coal [77][78]. Some burner modifications were required in order to prevent the impingement of straw on the rear wall.

The experimental work at Esbjerg involved test materials, ranging from 2% chromium ferritic to 27% chromium austenitic alloys, exposed in the gas pass whilst firing 10% straw for periods of 500-1250 hours. For comparison, samples were also exposed for 250 hours whilst firing 100% coal. The test exposures occurred at metal temperatures in the range 570-620°C (1058-1148°F). The coal fired contained 0.2% chlorine and 0.25% potassium, whilst the straw contained 0.25% chlorine and 0.75% potassium [75].

Similar forms of attack occurred when firing coal alone and when co-firing with straw. The corrosion process was assumed to follow parabolic kinetics, due to the formation of protective corrosion scales. However, it was noted that if repeated spalling of the protective corrosion scale occurred, the corrosion would tend towards linear kinetics. Spalling may be associated with repeated start/stop cycles, due to the thermal expansion differences between the corrosion scale and tube alloy. The corrosion rate comparisons between the 100% coal tests and the 10% straw co-firing tests indicated no increase, or only a modest increase. It was reported that, at most, the corrosion rate increased by a factor of 1.5. In terms of tube material corrosion performance, increasing alloy content led to a reduction in corrosion rate when coal firing or co-firing straw.

The results of fly ash analysis indicated an increase in potassium when co-firing straw compared with firing coal. The majority of the potassium was found to be insoluble and most probably occurred as silicates. The chlorine content of the fly ash was negligible regardless of whether straw was co-fired or not, and it is implied that almost all of the chlorine was emitted as HCl in the flue gas. This was consistent with an increase in the measured flue gas chlorine concentration when co-firing straw.

The Studstrup Unit 1 boiler was originally commissioned in 1968. The boiler is front wall pulverized coal fired and the middle row burners have been converted to co-fire coal and straw. The unit can operate at up to 20% straw on a heat input basis at full boiler load and has operated for long periods with 10% and 20% straw firing rates since 1996 [79].

Trial sections of superheater tube and temperature-controlled corrosion probes have been exposed for approximately 3,000 hours [75]. A number of alloy materials were exposed, including:

- 2¼%Cr 1%Mo (10CrMo910, T22) ferritic steel,
- X20CrMoV121 martensitic stainless steel,
- basic austenitic stainless steels (X8CrNiMoNb1616, TP347), and
- high alloy materials such as Sanicro31, AC66, Sanicro28, FeCr alloy (containing 20%Cr 5%Al).

The tube test loops were installed in the last stage of the final superheater which operated at steam temperatures of up to 540°C (1004°F).

The co-firing of up to 20% straw on a heat input basis was achieved without significant chlorine-induced superheater corrosion, although the rates measured were higher than for coal firing, particularly at the higher metal temperatures. It was suggested that, with final steam temperatures of 540°C (1004°F), wastage rates would increase by a factor of 1.5 to 3 when co-firing 20% straw. These rates are similar to those experienced in plant burning medium corrosive coals [80].

Examination of samples removed from the corrosion probes exposed at relatively low superheater metal temperatures revealed the corrosion scale morphologies to be similar to that found in coal fired plant [81]. When co-firing 20% straw, at metal temperatures of 580°C (1076°C) or greater, large broad corrosion pits were found in addition to the normal thin oxide scales. The pitting was especially noticeable on the high alloy austenitic materials. An HR3C specimen, exposed at 586°C (1098°F) when co-firing 20% straw, suffered pitting to a depth of 150µm after 3,000 hours operation.

The proposed corrosion mechanism believed to have been active in Studstrup Unit 1, involved the reaction of the biomass-derived potassium chloride with SO_2 in the flue gas, forming potassium sulfate. The potassium sulfate subsequently deposited on the superheater tube surfaces. The areas subjected to the broad pitting attack were seen to retain extensive potassium sulfate ash distributed amongst the particulate alumino-silicate ash material. With metal temperatures of 580°C (1076°F) or greater, it is possible for complex molten sulfates, such as alkali iron trisulfates, to form, leading to fluxing of the protective corrosion scale.

The ash deposits in Studstrup were found to contain additional potassium alumina-silicates and potassium sulfate, when compared with 100% coal firing, with the majority of the potassium associated with alumino silicate coal ash mineral matter [82]. It was proposed that the bulk of the potassium from the biomass reacted with the alumino-silicate material in the flue gas, preventing KCl deposition on the superheaters. Chlorine from the fuel instead remained in the flue gases as Cl_2 or HCl and passed through the boiler in the gas phase. The corrosion of the superheater was dominated by simple gaseous oxidation, although there was possible evidence for alkali sulfate melt corrosion. It was considered that the corrosive effects in pulverized fuel plant are likely to be less than that in CFB plant, where lower flame temperatures occur.

It was proposed that the coal ash composition may have an effect on alkali metal capture, with those coals having low alumina-silicate levels being less efficient at capturing potassium. The corrosion tests conducted in Studstrup Unit 1 suggest that co-firing straw at up to 10% on a heat input basis, is achievable in plant with steam temperatures of 580°C with tolerable superheater corrosion rates [80].

Based on the experience gained from the semi-commercial trials conducted in Studstrup Unit 1 from 1996 to 1998, ELSAM took the decision to convert Studstrup Unit 4 to straw co-firing [81]. Since 2002, Unit 4 has undertaken commercial operation co-firing straw at 10% thermal input. Unit 4 was commissioned in 1985 and comprises an oppose wall-fired Benson boiler with 24 coal fired burners arranged in 4 rows of 6. Four burners in the top row were modified to fire coal and straw. Straw is fired at a rate of 20 tonnes per hour, equating to more than 100,000 tonnes per year.

The fate of the potassium in the straw was reported as:

- 10% potassium as straw ash particles (Quartz / Calcium silicate)
- 90% potassium converted to gaseous potassium, potassium hydroxide and potassium chloride.

Of the 90% released in volatile form:

- 80- 85% was associated with potassium alumino-silicate coal ash
- 5-10% reacted with SO_2 to form K_2SO_4 vapor which condensed on the surface of the boiler tubing.

There have been no significant slagging or fouling problems when co-firing straw in Unit 4 at Studstrup, and no increase in sootblowing requirement when compared with coal firing. A summary chart based on the data from Studstrup and elsewhere, which describes the wastage rate ranges when co-firing straw, can be seen in Figure 2-3.

Figure 2-3: Measured Corrosion Rates for Austenitic TP347HFG When Firing and Co-Firing Straw [81]

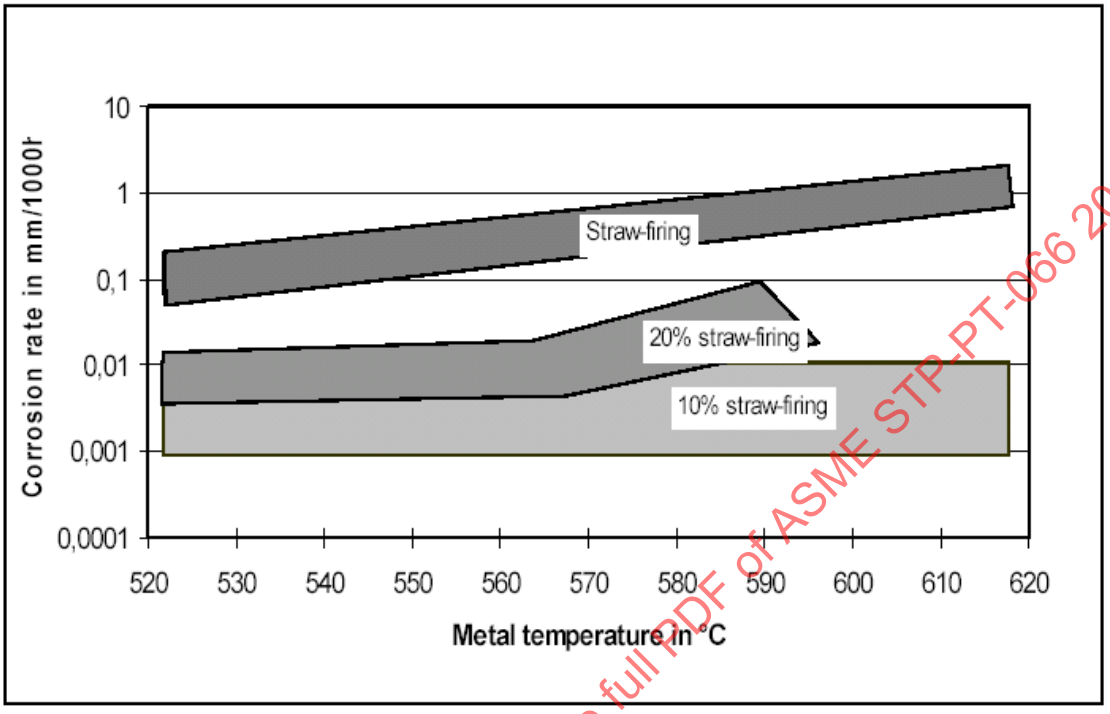

For 10%, 20% and 100% straw firing, metal wastage rates for TP347HFG superheater tubing can be seen. Note that a wastage rate of 25nm h^{-1}, (8.6mil.y^{-1}) would be considered tolerable in coal fired plant. The wastage associated with firing 20% straw can be up to 4 times greater, bordering on what would traditionally be considered very serious wastage rates. These rates would still be significantly lower than those expected for 100% straw firing, which could result in very serious to catastrophic corrosion rates at all temperatures shown.

Superheater corrosion rates have been measured using a short term, 50 hour, corrosion probe exposure in a United Kingdom 500 MW coal fired boiler whilst co-firing 5% Palm Kernel Expeller (PKE) on a heat input basis. The PKE had 4.3% ash, 0.17% sulphur and 0.18% chlorine. The PKE ash had 24.62% K_2O and 0.72% Na_2O. The PKE was co-fired with a South African coal with 12.9% ash, 0.57% sulfur and 0.02% chlorine. The coal ash had 1.42% K_2O and 0.29% Na_2O.

The PKE fuel analysis would suggest that it was relatively aggressive [84]. The corrosion probe was of the type commonly used in the E.ON pilot scale combustor and employed a series of 11 individual specimens, produced from low alloy T22 ferritic steel, and TP321 and HR3C austenitic stainless steels as installed in the boiler superheater and reheater stages. The probes were located close to the final superheater stage. The measured metal losses and derived wastage rates were compared with data obtained from previous pilot and full scale plant, short and medium term probe exposures, in which a range of coals were utilized. The probe data for the low alloy T22 ferritic steel specimens fell within the data scatter band expected when firing only coal, indicating that there was no discernible increase in wastage rates that could be attributed to co-firing PKE at 5% on a heat input basis.

Although no short term 100% coal data was available for comparison with the austenitic stainless steels, the rates measured when co-firing 5% PKE followed a similar trend to that found in pilot scale studies when

co-firing a benign wood fuel [18]. The measured wastage rates for the high alloy steels were found to be approximately an order of magnitude lower than the rates for the T22 material at similar temperatures, which were representative of the final superheaters in plant operating with a final steam temperature of 568°C.

The austenitic steel wastage rates were also at least an order of magnitude lower than those found when co-firing Cereal Co-Product (CCP) in the pilot scale combustion test facility. There was no indication of severe localized pitting of the stainless steel samples, a feature that was attributed to the CCP biomass in the previous pilot scale studies. Rather, simple oxidation had resulted in very slight general metal losses with no discernible difference between the TP321 and HR3C alloy wastage rates. The results of the short term testing indicated no discernible worsening of superheater or reheater fireside corrosion associated with co-firing PKE fuel at 5% when compared with firing 100% coal. Analysis of the ash deposit indicated this to be relatively benign, predominantly comprising alumino-silicate particulate material. The only sulfur was present as calcium sulfate. The ash contained negligible potassium and no detectable chlorine.

It is interesting to compare the corrosion data from the co-firing of biomass in pulverized coal boilers with that in circulating fluidized bed combustors. It has been demonstrated, principally in Scandinavia, that the co-firing of straw in circulating fluidized bed (CFB) plant can lead to higher fouling and corrosion rates, compared to those when firing coal. [78].

The Grenå CFB plant in Denmark has been operated both firing 100% coal and co-firing up to 60% straw on a heat input basis. The plant was commissioned in 1992. The boiler has 3 superheater stages within the flue gas pass and 2 additional final superheaters in the cyclone loop seal [85]. The plant operates at 92 bar with a final steam temperature of 505˚C (941˚F). At 80% load, the gas temperature exiting the cyclone was approximately 850°C (1562˚F) and there were no particular fouling problems. At 100% load, the gas temperatures increased to 900°C-1000°C (1652-1832˚F), at which point excessive fouling of the superheater section occurred. After 18 months operation at this load, excessive corrosion of the superheater elements was identified, requiring wholesale replacement of the superheating tubing [79]. It was found that co-firing 50% straw with coal under the high load conditions resulted in superheater corrosion rates in the range 5-25 times greater than that experienced when firing coal alone.

The plant was modified to include additional furnace tubing to reduce the furnace gas exit temperature, amongst other things, and lower sulfur coals and higher quality limestone were used. The fuel and limestone changes, the cooling of the flue gases prior to the superheater and an optimized sootblowing regime, together with increasing tube thicknesses have combined to increase superheater tube life to more than 7 years [85].

The low alloy test materials generally exhibited greater metal losses than the higher alloy steels. However, selective corrosion/internal attack of the high alloy materials has also been identified. This was associated with chloride penetration into the metal, where it predominantly reacted with, and removed the chromium from the alloy. This type of attack led to sub-surface porosity and exfoliation corrosion, particularly at high temperatures, where un-corroded metal grains close to the sample surface were lost as a result of grain boundary attack. Selective corrosion of this type was not found when firing only coal. When co-firing, no significant protective corrosion scale was formed, and the superheater corrosion was presumed to be following linear kinetics. Where present, the oxide corrosion scales were irregular, porous, cracked and partly exfoliated, offering no barrier to diffusion of corrodents or corroding metal elements.

It was found that changing the superheater materials from low alloy ferritic 2%Cr steel to the 12%Cr martensitic alloys resulted in a significant reduction in corrosion rates. Increasing the alloy content in the austenitic materials resulted in an increase in corrosion rates, frequently to values greater than that noted for low alloy ferritic materials.

The severe superheater corrosion rates were considered to be associated with the deposition of potassium chloride in the ash on the superheater tubes. The ash deposits in the Grenå plant contained large quantities of potassium chloride and calcium sulfate [76]. A large fraction of the potassium in the ash deposit was water soluble, suggesting that only a minor amount of the potassium was associated with alumino-silicate mineral matter. It was suggested that the lower flame temperatures in CFB plant compared with pulverized coal fired plants did not favor the interaction of the alkali metal salts with alumina-silicate ash particles.

It was suggested that the corrosion mechanism involved sulfation of the potassium chloride ash deposit at the metal surface to release chlorine gas [86]. Alternatively, the deposited potassium chloride may have reacted with haematite (Fe_2O_3), to form potassium ferrate ($K_2Fe_2O_4$), again releasing chlorine gas at the metal surface. The chlorine then selectively reacts with the chromium (and to a lesser extent the iron), forming chromium chloride and oxychloride. The chromium compounds are relatively volatile at superheater metal temperatures and diffuse away from the metal to areas of higher oxygen or sulfur partial pressure, where the chlorides decompose forming oxides or sulfides, releasing the chlorine to attack yet more metal.

No solid or liquid ash or flue gas components had penetrated the metal except for the chlorine, suggesting that gas phase corrosion by HCl or Cl_2 was responsible, despite a lower bulk chlorine concentration than that found in Studstrup Unit 1.

It has also been suggested that low melting point chloride mixtures may have played a role in fluxing of corrosion scales. With the compositional variability of straw, its slagging propensity and ability to form aggressive ash deposits vary from year to year. The more severe fouling and corrosion are associated with a dry summer causing high potassium and chlorine contents. It has been identified that rain during the maturing and harvest period has a big influence on potassium (0.8 – 2%) and chlorine (0.1 – 0.5% or greater) contents [79]. Dry years result in greater concentrations of potassium chloride in the ash deposits, necessitating a reduction in the proportion of straw burnt.

In order to maintain the biomass percentage, a proportion of the straw share has been replaced with other materials, such as sunflower shells, shea nut residue, grain screenings or wood dust. These materials generally have lower levels of potassium chloride, although shea pellets have caused some problems as a result of their relatively high potassium content.

The Alholmens Kraft CFB CHP plant in Finland fires 50% peat, 25% wood fuels (logging residues and bark) and 25% coal, and can operate from 100% biomass to 100% coal [87]. The final steam conditions are 165 bar and 545˚C (1013˚F), with reheat steam conditions of 38bar and 545˚C (1013˚F). The maximum chlorine content of any of the fuels was 0.02%, with sulfur ranging from 0.04 to 0.3%. The sulfur to chlorine ratio in all fuel combinations was always greater than 2, with a maximum value slightly in excess of 4. Sodium, potassium and chlorine have been identified in superheater ash deposits, although chlorine was reportedly absent from the ash deposits when at least 55% coal was co-fired.

Where chloride containing ash deposits were identified, a minimum threshold temperature of 450°C was quoted for the onset of chlorine induced superheater corrosion. This corresponds to a steam temperature in the range 400-415°C (752-779˚F), which was attained in the first stage superheater.

The superheater corrosion was combated when co-firing coal by sulfation of alkali chlorides, forming HCl in the gas which passes through the boiler. The proposed sulfation reaction took the form:-

$$2KCl + SO_2 + ½O_2 + H_2O \Rightarrow K_2SO_4 + 2HCl$$

It was suggested that the sulfur:chlorine ratio in the fuel was not suitable for assessment of the propensity for chlorine-induced superheater corrosion. Instead, it was proposed that the sulfur:chlorine ratio in the gas phase may be more useful in determining the risk of chloride attack, with values in excess of 1.5 resulting in at least a 60% conversion of KCl to HCl.

Kaolin ($Al_2O_3.2SiO_2$) was also added in varying quantities, with values of 50% of ash flow being found to reduce the chloride contents of ash deposits from levels in excess of 3% to less than 1% when firing predominantly bark. The alumino-silicates were reported to remove potassium from the potassium chloride forming potassium alumino-silicates, with the liberated HCl remaining in the gas phase. The proposed reaction took the form:

$$Al_2O_3.2SiO_2 + 2KCl + H_2O \Rightarrow K_2O.Al_2O_3.2SiO_2 + HCl$$

As such, it was proposed that the coal or peat co-firing provided protection to the superheaters through the introduction of sulfur and alumino-silicates into the system.

Straw co-firing tests with coal have also been conducted in the Midtkraft Multi Circulating Fluidized Bed plant in Denmark. Separate test tube loops with controlled steam flow were installed in the superheater that ran hotter than 520°C (968˚F). Corrosion probes were also placed in the gas pass prior to the superheater. Both straw and limestone were fed into the bed. The coal utilized contained 0.03% chlorine and around 0.9% sulfur, and approximately 12% ash [88].

Samples of ferritic, martensitic, and austenitic tube alloys were exposed at metal temperatures in the range 540-660°C (1004-1220˚F), with test durations of between 500 and 1000 hours. The tests involved firing 85% straw +15% coal and 45%straw + 30%wood chips + 25% coal. A further test was completed firing 100% poultry litter.

It was observed that the flue gas conditions were important in determining the type of alkali metal deposit formed. Under oxidizing conditions, alkali sulfates were reported to be stable and formed on the superheater surfaces, but under reducing conditions, the deposition of chlorides was favored.

The plant experienced severe selective chlorine-induced superheater corrosion when firing all of the fuel mixtures. It was anticipated that an X20CrMoV121 martensitic superheater tube would have an operating life of 5-10 years at a final steam temperature of 500°C (932˚F). The estimated tube life would be reduced to 3-7 years if the final steam temperatures were raised to 540°C (1004˚F), even when utilizing TP347H austenitic stainless steel as the most corrosion resistant tube material. Increasing the steam temperatures to above 565°C (1049˚F) would result in an anticipated tube life of less than 2 years, regardless of the material selected for the final superheaters.

The corrosion of martensitic and austenitic tube alloys at metal temperatures in the range 640-670°C (1184-1283˚F) was also examined in the Nassjo CFB [89]. The metal temperatures were selected to simulate steam temperatures of 600-620°C (1112-1148˚F). Air cooled corrosion probes were exposed whilst firing 100% forestry wastes and 70%$_{th}$ forestry wastes with 30%$_{th}$ coal. Changing from 100% biomass to co-firing resulted in a halving of fireside corrosion rates. The reduction in wastage rates was associated with a large reduction in the chlorine content of the ash deposits. When firing 100% forestry wastes, the austenitic stainless steels such as Eshette1250 and TP347HFG, offered the greatest corrosion resistance. The more expensive, higher alloy materials, such as Sanicro28, offered no greater corrosion resistance than the basic austenitic stainless steels. When co-firing wood with coal, on the other hand, the corrosion resistance improved with increasing alloy content, suggesting that the influence of corrosive attack by chloride containing ash deposits was reduced.

Turning to the pilot scale studies on corrosion associated with biomass co-firing, E.ON UK, with part funding provided by the Department of Trade and Industry, has undertaken a limited biomass co-firing corrosion trial using a $1MW_{th}$ Combustion Test Facility (CTF) [18]. A series of four, nominally 50-hour, and tests were conducted firing:

- Daw Mill Coal, which had 9% ash, 1.42% sulphur and 0.2% chlorine. The ash had 2.07 K_2O and 0.97 Na_2O.
- A clean waste wood fuel, with (0.4% ash, 0.03% sulphur and 0.03% chlorine. The ash had 3.85% K_2O and 2.42% Na_2O 2.42%.
- Cereal Co-Product (CCP) with 5.3% ash, 0.2% sulphur and 0.13% chlorine. The ash hade 35.8% K_2O and 1.26% Na_2O.

The co-firing ratio of the biomass materials was either 10 or 20% on a heat input basis.

The project was concerned with the measurement of the corrosive effects of co-firing biomass with coal in existing subcritical and possible future (ultra) supercritical boilers. Conventional and potential boiler tube alloys were exposed to superheater/reheater environments. Sixteen superheater/reheater steel alloy specimens were exposed during each rig run to a range of metal temperatures, with a range of heat fluxes and gaseous environments, representative of pulverized coal combustion under low NO_x conditions with biomass additions. The results of a number of previous tests with other coals provided baseline comparative data for superheater/reheater metal losses. The specimens were exposed for up to 50 hours to the combustion environment in the test rig on air-cooled, precision metrology, corrosion probes.

When co-firing 10% and 20% wood, there was no discernible worsening of either furnace wall or T22 ferritic alloy superheater/reheater corrosion when compared with firing 100% coal. The measured TP316 metal losses were substantially lower than those determined for the ferritic T22 specimens exposed at the same location, as would be expected for 100% coal firing.

The T22 ferritic superheater/reheater specimens also exhibited metal wastage rates that were a little increased compared with those measured without biomass additions. There was a marked increase in the corrosion rate of the austenitic TP316 superheater samples, where localized pitting attack resulted in peak rates similar to those measured for the T22 samples. HR3C material, the highest grade material tested, also suffered severe localized pitting attack, with metal wastage rates similar to that for the T22 and TP316 alloys.

The increased superheater corrosion rates measured in these tests, were attributed to attack by molten alkali metal sulphates, i.e. the normal mechanism in coal fired plant. Chloride was not found in the superheater corrosion scales or ash deposits, and was not implicated in the enhanced corrosion mechanism.

The data indicated that plant operating at relatively low final steam temperatures (~540°C, 1004˚F), employing only low chromium containing ferritic alloys, could safely operate whilst co-firing both 10% and 20% CCP or similar fuel, and expect only a modest increase in the corrosion rates. Plant operating at higher steam temperatures (≥ 560°C, 1040˚F), which contains austenitic alloys, are potentially vulnerable to increased superheater and reheater corrosive attack. This could lead to a marked reduction in expected tube operating lives.

It was proposed, based on the results of the tests, that the biomass materials with high alkali metal contents are particularly aggressive. The CCP fuel also had a significant phosphorus level, although the role that it played, if any, in the corrosion process was not clear.

Other pilot scale ash deposition studies, using a variety of biomass and coal blends of differing proportions, in various combustors, have identified both alkali metal sulfate and chlorides in the ash deposits. It was also found that the chloride contents of ash deposits decreased with increasing fuel sulfur content [90].

In general, a negligible chloride ash content was found when the fuel sulfur content was greater than twice the fuel alkali chloride content. This was attributed to the sulfation of the alkali metal chloride ((Na,K)Cl) to form alkali metal sulfate ($(Na/K)_2SO_4$), with the chloride being retained in the combustion gases as hydrogen chloride [76].

Whilst much of the published biomass co-firing work does not deal specifically with the corrosive effects of adding biomass to boilers firing coal, the risks of accelerated fireside corrosion is considered to be a technical barrier to further implementation of biomass co-firing [78][80][91]. The corrosion rates in plant are clearly sensitive to temperature and deposit chemistry, and this requires further investigation. It is considered that there are no irresolvable issues, but that there are poor combinations of fuel, boiler and operation [92].

There is general agreement in the published work that increased levels of alkali metal species in the vapor phase, associated with rapid release from biomass fuels, and their subsequent condensation on the boiler surfaces, can lead to enrichment, especially of potassium compounds at the metal/oxide/ash deposit interface. Those biomass fuels containing relatively high chlorine contents can release significant concentrations of chloride into the boiler flue gases, leading to chloride enrichment at the same location. The ash can be especially damaging if potassium chloride is deposited in ash on superheater/reheater tubing. This has resulted in significant corrosion related problems in some cases [79].

The co-firing of most bituminous coals with biomass can reduce the potential for deposition of potassium or sodium chlorides on superheater tube surfaces through sulfation of the alkali metals, depositing sulphate species, rather than chlorides. More specifically, the molar ratio of fuel sulfur to available alkalis and chloride in the system should exceed 5 to help minimized the potential for chlorine containing deposits and chloride-induced fireside corrosion.

The high flame temperatures associated with pulverized coal firing plant appear to promote the capture of the volatilized alkali metal species by the alumino-silicate material associated with the coal ash. This does not occur to the same extent at the lower flame temperatures associated with fluidized bed combustion systems.

Much of reported operational data is for plant operating with final steam temperatures of 540°C to 545°C (1004 to 1013˚F), at which the risks of additional molten sulfate attack are modest. The majority of coal fired plant in the United Kingdom operates with a final steam temperature of 568°C (1054˚F), and the increased steam temperature will result in an increase in the risk of enhanced superheater fireside corrosion resulting from molten alkali iron trisulfate attack. Some evidence for this has been found in pilot scale and plant corrosion probe trials. The finding of a 50µm deep pit in a HR3C specimen after a 50 hour exposure in the CTF co-firing CCP, and a 150µm deep pit after a 3000 hour exposure in Studstrup Unit 1, whilst co-firing straw, may be significant

Currently, there is little or no published work on the corrosion rates associated with the wider range of biomass materials, such as PKE, shea nuts and olive wastes which have been co-fired with coal in northern Europe, and which can have relatively high alkali metal and chloride contents, approaching those normally associated with herbaceous materials. Further work needs to be undertaken in order to determine the corrosion potential of these fuels, especially when fired at relatively high percentages, or if fired using dedicated burners, from which a deposit containing high levels of alkali metals or chlorides may be formed selectively in specific areas of the superheaters.

In summary, therefore, the effects of biomass co-firing on superheater/reheater fireside corrosion rates are fairly complex and may involve a number of factors, viz:

- The alkali metals in biomass fuels are very reactive and easily released during combustion.
- The deposition of alkali metal chloride species is detrimental and should be avoided where ever possible by fuel selection and blending, ensuring sufficient sulfur is available to react with all alkali metals in the fuel, or, using additives to capture the chlorides and/or the alkali metals.
- Where alkali chloride-containing ash deposits are formed it is possible that little or no benefit in terms of reduced wastage rates would be obtained through the use of high alloy stainless steels, and that 12% chromium martensitic, or 15% chromium austenitic stainless steels could offer the best corrosion resistance.
- The production of alkali sulphate-containing ash in preference to alkali chlorides is effective in reducing the rate of fluxing of the oxide scales, and of metal wastage.

2.5.5 Effect of Oxyfuel Firing

In oxyfuel firing systems, the recycling of combustion gases to temper the flame brings with it the potential for up to a five-fold increase in the concentrations of the sulfur and chlorine species in the combustion environment relative to those from the air firing of the same coal. There are concerns, therefore, about the risks of increased corrosive attack by these species. This has been recognized by the industry and has been investigated at demonstration, pilot and laboratory scale.

For instance, a number of superheater probes equipped with specimens of different alloy compositions have been exposed at metal temperatures of 580 and 650°C (1076 and 1202˚F) in the Schwarze Pumpe lignite-fired demonstration oxy-fuel fired plant [21]. After exposure for 1300 hours at metal temperatures of 580°C (1076˚F):

- the low alloy ferritic materials, i.e. 13CrMo44 and T23, suffered around 90µm metal loss, equivalent to a corrosion rate of 70nm.h^{-1}, (24mil.y^{-1}),
- the martensitic alloy X20CrMoV121 suffered around 55µm loss, equivalent to 40nm.h^{-1}, (14mil.y^{-1}) and
- the austenitic alloys, i.e. TP347HFG and 253MA suffered mean losses of less than around 12µm, equivalent to 10nm.h^{-1}, (3.4mil.y^{-1}).

The Sanicro 63 monolithic material with similar composition to IN625 weld overlay did not offer any reduction in wastage rates, when compared to the austenitic stainless steels.

Increasing the metal temperature to approximately 650˚C (1202˚F) resulted in the following losses over the same exposure time:

- around 90µm for T91, equivalent to a corrosion rate of 70nm.h^{-1}, (24mil.y^{-1}),
- around 10µm, or 8nm.h^{-1}, (2.7mil.y^{-1}) for Super304H and
- around 2µm or 2nm.h^{-1}, (0.7mil.y^{-1}) for type 310 stainless.

The Sanicro63 performed relatively badly having suffered a mean loss of 20µm or 5nm.h^{-1}, (5mil.y^{-1}), while the IN625 weld overlay performed no better than the Type 310 austenitic stainless steel.

There were no indications of carburisation of any of the superheater specimens.

A program of short-term, superheater/reheater fireside corrosion studies using air cooled corrosion probes in a 1MW pilot scale were carried out by Davis [35][47]. The results indicate that the response of the

austenitic and nickel based alloy coupons was quite variable dependent upon the particular fuel or firing method, and the heat flux/position within the convective section.

Only the specimens exposed when firing the low 0.62% sulfur and 0.02% chlorine content El Cerrejon coal showed no observable corrosion. For all of the other oxy-fuel fired tests with coals containing greater quantities of sulfur and chlorine, at least some of the austenitic and nickel based alloys suffered at least minor pitting damage, which in the worst cases, developed into more irregular general metal wastage. As is the case in actual boiler plant, the worst damage to the tubular specimens was noted at the 2 and 10 o'clock positions, 12 o'clock representing the side facing the oncoming combustion gases.

The pitting damage was frequently associated with slight internal oxidation and/or occasional grain boundary penetration. The corrosion scales formed within the pits were largely chromium oxides or sulfides, and it was not uncommon for fuel-derived elements such as potassium or sodium to be found within the pits. The scales overlying the pits were frequently defective and incorporated inert particulate ash together with significant quantities of alkali metal sulfates. In some cases, the defective external scales were barely distinguishable from the overlying ash deposit.

The superheater pitting and irregular general corrosion was attributable to the presence of greater quantities of alkali sulfate in the ash deposits compared to that obtained when air-fuel firing 100% coal. The attack is attributed to the same damage mechanism that is already responsible for corrosion in air-fuel, coal fired plant. The source of the additional sulfatic ash deposits, however, is not as clear, although the recycling of the flue gases without scrubbing increased the SO_2 content of the flue gas by a factor of approximately five when compared to air fuel firing. It is also generally accepted that the formation of aggressive molten alkali iron trisulfates is stabilized by increased SO_3 concentrations in the combustion gases.

The T22 low alloy specimens exhibited wastage rates similar to those previously obtained when air-fuel firing coal in this test facility, although the data for the higher sulfur and chlorine content coals tended to lie at the top of the scatter band for the air-fuel fired data.

For the austenitic specimens no discernible damage was observed when firing the El Cerrejon coal, and only limited damage was seen when firing the Daw mill coal. For the other higher sulfur and chlorine content coals, the austenitic specimens suffered readily measurable corrosion with rates that sometimes approached or exceeded the data range for the low alloy T22 specimens. There was no clear trend in wastage rates with the coal sulfur content, but there was a rough trend of increasing wastage rate with increasing fuel chlorine.

Holcomb et al. presented results of isothermal laboratory studies using T91, TP347 and IN617 exposed at 700°C (1292˚F) to conditions simulating oxy-fuel combustion, with and without flue gas desulfurisation in the recycle loop [92]. The specimens were immersed in an alkali metal sulfate simulated ash deposit together with iron, aluminum and silicon oxides. The results were compared with simulated air-fuel fired conditions. The measured weight change data indicated significant fluxing of the ash and corrosion scale for the T91 coupons, whilst the TP347 and IN617 both suffered significantly greater metal loss under the oxy-fuel conditions.

Further laboratory scale simulations conducted by Holcomb et al. have demonstrated that for a number of tube alloys exposed at 650-700°C (1202-1292˚F) to various forms of simulated oxy-fuel conditions, there was accelerated corrosion even at temperatures at which the sulfate ash deposits remained solid. The results indicated that the SO_3 partial pressure was the primary variable, with a threshold value between 10^{-4} and 10^{-3} atm required to promote severe attack.

Fry et al. [46] the reported results of on-line electrochemical noise corrosion probe exposures in the 1.5MWth L1500 pilot scale oxy-fuel pilot plant firing 3 coals with sulfur levels varying from 0.23 to 3.98%. The T22, T91 and TP347H alloys were exposed at temperatures of 488°C, up to 566, 593 and 705°C (910˚F, up to 1051, 1099 and 1301˚F) respectively. The pilot plant was cycled between air and oxy-fuel firing for corrosion tests conducted at different temperatures. In all cases the superheater wastage rates were seen to increase on changing from air to oxy-fuel firing, with the greatest increase for the high sulfur coal.

Kung [93] reported results of an isothermal laboratory study comparing the wastage rates of numerous tube alloys and weld filler materials exposed to simulated air and oxy-fuel combustion environments. The gas compositions and deposits used in the tests were designed to reproduce the conditions measured during a pilot scale combustor trial firing a range of four US coals with sulfur contents ranging from 0.26-4.31% and chlorine contents ranging from 0.001 to 0.283%. The results for the low sulfur PRB coal showed no consistent change in the wastage rates at 700°C (1292˚F) between the air and oxy-fuel simulated tests.

Maier et al [94] reported on a combination 3MW pilot facility and laboratory scale study examining the corrosion rates of a range of superheater martensitic, austenitic and nickel based tube alloys exposed to conditions representative of firing a 0.4%S Indonesian bituminous coal. The samples were exposed at temperatures of 580 and 650°C (1076 and 1202˚F). At 580°C (1076˚F) only the T92 material had excessive corrosion rates, whereas at 650°C (1202˚F) both the T92 and the lowest grade austenitic alloy (TP304) were both badly corroded. At both temperatures the TP310, 253MA and Alloy 617 alloys had acceptable corrosion rates.

Laboratory-scale studies conducted by Tuurna et al [95] used simulated ash deposits comprising mixtures of $CaSO_4$ and $CaCO_3$ designed primarily to determine whether alloy surface carburization had an impact on corrosion rates. Indeed the authors noted that under conditions of flue gas recycling where the concentrations of sulfur and chlorine-containing species would be elevated, and there would likely be an enhancement of wastage rates relative to air-fuel firing. Similar laboratory scale tests conducted in simulated gases showed no increase in corrosion rates at 580˚C (1076˚F) when changing from air-fuel to oxy-fuel compositions [96]. However, it should be noted that the tests were conducted without any of the known aggressive species such as sulfur, chlorine or alkali metals and, as such, the results are of questionable value.

A laboratory-scale study was conducted by Robertson et al. [97]. It was suggested that 3200ppmv (wet) SO_2 should be an upper limit for retrofit applications so as to avoid the need for major, expensive boiler upgrades and that at this concentration the superheater/reheater wastage rates were typically no worse than that found when air fuel firing. Isothermal laboratory scale studies were conducted using 1,000 hour exposures with routine application of simulated ash deposits and temperatures of 538, 593 and 649°C (1000, 1099 and 1200˚F). A range of alloys and coatings were tested. None of the sprayed coatings gave particularly good protection and virtually all allowed penetration of oxides and sulfides.

2.5.6 Prevention of Corrosion in Superheaters and Reheaters

The high-temperature corrosion resistance of alloys can be roughly grouped by alloy type. The low alloy ferritic materials have the lowest corrosion resistance of the available tubing alloys, and are employed for lower temperature applications. The high chromium martensitic alloys and austenitic alloys with chromium contents in the range 12-15% tend to have similar corrosion resistance offering an improvement over the ferritic alloys. All of the 300 series alloys, with 18%-20% chromium, offer better corrosion resistance than the lower alloy steels.

Further improvement in fireside corrosion resistance of the 300 series type of alloys has been achieved by special thermo-mechanical processing to produce a fine grained material e.g., 347HFG, Super304H,

generally suitable for low S coal and mild corrosive conditions. Improved fireside corrosion resistance in higher S coals and relatively aggressive environments is offered by the TP310 based steels, which have approximately 20-25% chromium.

Further significant improvements in corrosion resistance beyond that offered by the type 310 steels can only be obtained by using nickel based alloys. These materials are significantly more expensive than the austenitic alloys and can be difficult to work. As such, they are unlikely to be used except for advanced ultra-supercritical boilers, where very high creep strengths are also required.

These high alloy materials are most frequently used in very aggressive conditions in the form of claddings, weld overlays or sprayed coatings. In most situations, the useful protection provided by a corrosion resistant coating layer will be determined by its thickness. Thin (~0.5mm) sprayed coatings will offer the least protection and improvement in anticipated tube life, whilst thicker laser clad coatings (~1mm) will survive longer and the thickest weld overlays and co-extruded clad materials (~2mm) will offer the greatest protection.

Coating and claddings optimized for corrosion resistance are not typically optimized in terms of creep strength, mechanical properties or workability. Materials such as 50%Cr50%Ni (IN671) have very good corrosion resistance but cannot be formed into tubing and have very poor creep strength. These materials are normally utilized as a corrosion resistant material applied to a less corrosion resistant, but Code approved boiler tubing alloy. Although it has not found widespread use due to the cost of co-extruded tubing, trial installations of IN671 outer and Alloy 800 inner have been deployed successfully on a trial basis [98][99].

As with furnace wall corrosion, improvements in the combustion environment can help to reduce the corrosion rates in plant. Fuel selection can play an important role with fuels chosen or blended in order to reduce the concentrations of aggressive sulfur, chlorine or alkali metal concentrations. Similarly, combustion additives may be used to modify the corrosivity of the fuel. Magnesium based compounds can be introduced to combat oil ash corrosion, principally by raising the melting temperature of the deposited ash. This has been applied in coal-fired plant on a trial basis, with little evidence of success to date [100].

The boiler design can also play a role in avoiding the worst effects of fireside corrosion. The position of the high temperatures stages within the boiler may be chosen so as to limit heat flux levels and reduce corrosion rates. Similarly, parallel combustion gas and steam flow will encourage the relatively cool tubing to be exposed to the highest gas temperatures within a particular superheater or reheater tube bank. In contrast, counter flow arrangements expose the highest temperature part of a tube bank to the highest temperature flue gases risking greater corrosion rates. In some cases, additional evaporative surface can be added to a boiler in order to reduce gas temperatures.

2.6 Self-Learning Corrosion Models

The great majority of the available corrosion models, a number of which have been described above, are of the empirical, curve-fitting variety. There has been, however, significant activity more recently on the development of alternative mathematical approaches to modelling. These have included the use of genetic algorithms, neural networks, and computational fluid dynamics.

2.6.1 Genetic Algorithms

Genetic algorithms are search algorithms that apply the evolutionary operators of selection and mutation to an initial population of solutions to a problem. In most cases these are possible models that explain the data set. After the initial description of the problem in terms that the genetic algorithms can work with, the populations are allowed to run through hundreds of generations. At each generation, the most fitting

solutions to the problem are chosen, using a set of prescribed success criteria, to populate the next generation. Mutations can be applied so that possible refinements to the best fitting solutions can also be discovered.

Genetic programming uses similar techniques of selection and mutation, but applies them to tree structures that describe a program or mathematical expression. This procedure is more complicated than using simple genetic algorithms, but can provide an output that is easier to understand

Figure 2-4: An Example of a Genetic Programming Tree Structure Representing a Simple Equation

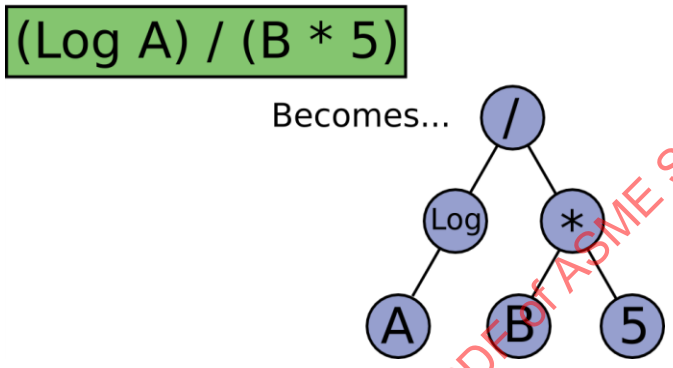

The example in Figure 2-4 shows how a simple equation can be expressed as a tree structure. For symbolic regression, an initial population of these trees is generated randomly, using mathematical expressions as the branch points of the trees, and problem-related variables and (optionally) random numbers as the leaves. Each of these tree-expressions is tested against a number of different data sets, taken from measured cases. The results of these tests are aggregated into a single "fitness" score which marks how well the expression describes the data set. The expressions with the highest fitness survive to the next generation, and are "bred", by grafting segments from one tree to another to form new child trees.

Figure 2-5: An Example of Two Parent Trees Being Bred to Create the Child Expression

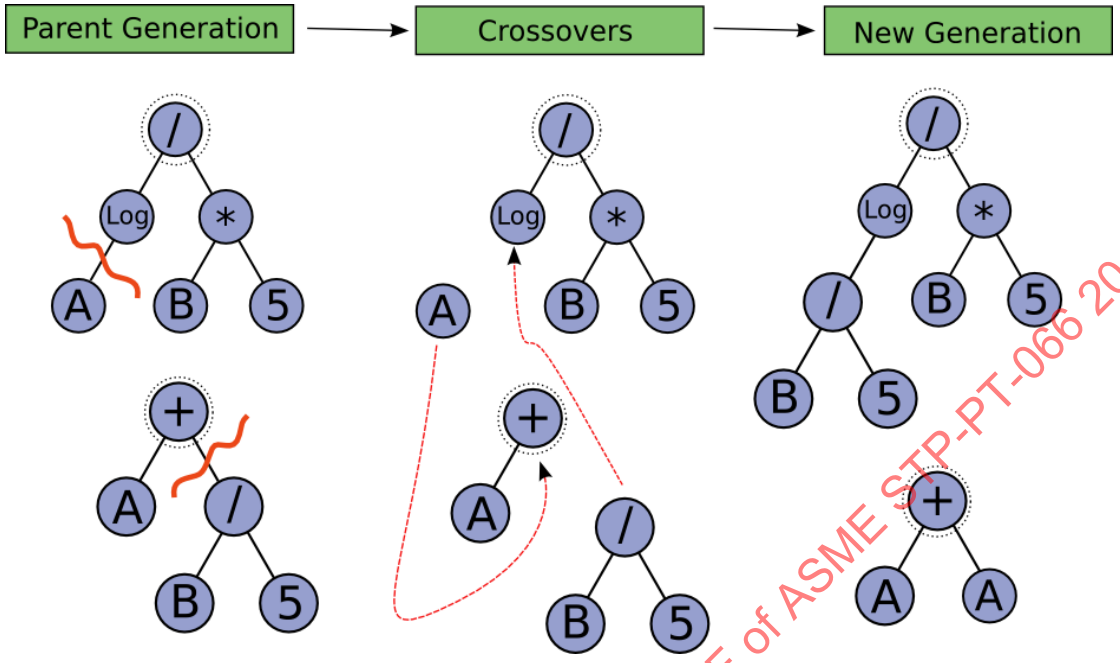

Two parent trees being bred are illustrated in Figure 2-5. Initially, random "graft" points, indicated by the wavy lines, are chosen. Then the tree parts below the graft points are exchanged, resulting in a new child generation. This process is repeated with each generation, the idea being that this 'natural selection' system grows towards an equation which can best fit the data.

The use of genetic algorithms works best where the relationship being modelled already has a mathematical description, and the technique can then be used to optimize the relationship. Practical experience in using this form of modelling approach would suggest, however, that the number of variables and the complexity of fireside corrosion processes means that this approach is unlikely to improve on the existing empirical models. An approach similar to GA, but which does not rely on a starting relationship, would have a greater chance of being able to model these fairly complex environments.

2.6.2 Neural Network Modelling

It has been argued that if the relationships between the inputs and outputs are not well understood, the conventional models depending on corrosion theories will fail. In contrast to the empirical curve-fitting modelling described in the previous sections, Makkonen [101] has described a neural network approach for the modelling of superheater corrosion.

To create a reliable prediction method for a large number of potential input variables, a large quantity of data has to be available for the network learning process. The use of the model for predictive purposes only should also be within the envelope of the data variables used for the learning process. Extrapolation outside these limits has been recognized to be a limitation of this form of modelling.

Makkonen included the following factors in his neural network model for superheater corrosion:

- fuel characteristics,
- bed material characteristics,
- gas temperatures in combustion zone and superheater area, and

- key boiler design parameters.

For the back propagation neural network developed in this work, a calculated corrosion rate y, related to the measured corrosion rate x, was defined as follows:

$$y = 0.9417x + 0.0072$$

No model equations are quoted, and a prediction is given, with no indication of how this conclusion was drawn.

Advanced 'neural fuzzy' networks have been developed which allow the predictions to be described in a logical manner [101]. These are supervised and trained in much the same way as multi-layered feed-forward (MLF) neural networks, i.e. the input variables are presented to the network along with the results/outcomes during the training stage. The difference is that instead of attaching weights to neurons to map the input/output relationships, a series of rules is constructed and refined. These rules are based on IF…AND…THEN logic. The rules, however, are fuzzy in nature, i.e. they utilize classes of both the input variables and outputs, none of which are precisely defined.

The MLF model has been found to be valuable for the modelling of stress corrosion cracking behavior in duplex stainless steels, and cyclic oxidation behavior in Ni-based superalloys. This approach was employed by Zhou et al [102], who used a neural network model to generate plots of the partial pressure of H_2S in the gas p versus temperature for a range of alloys and input parameters.

An example of the output for a standard 22%Cr duplex stainless steel is presented in Figure 2-6. The curves show the difference between a high risk and a low risk of cracking, with the maximum risk of cracking at a given H_2S level being at temperatures between 80 and 100°C (176 and 212˚F).

The model showed that at lower temperatures the susceptibility to cracking decreases as the solubility of hydrogen is lower and so less hydrogen is absorbed by the steel. This example demonstrates how a neural network model might be used as a predictive "pass" or "fail" criterion.

A more relevant example is given by the work reported by Simms and Fry [103]. They used a self-training neural network to develop a predictive model for furnace wall metal loss under fireside conditions. To train the model, a database consisting of 190 individual data points was used.

Figure 2-6: Change in Predicted Probability of "Pass" With Temperature and H2S, After Zhou et al

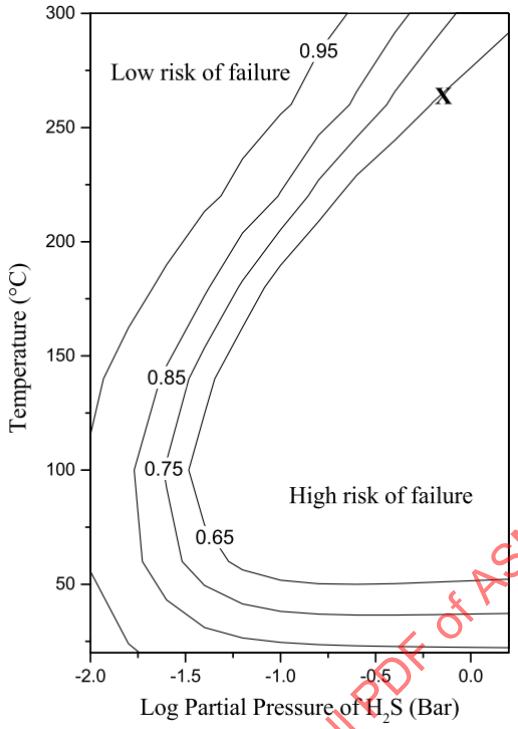

This comprised data generated from short term combustion rig trials covering a metal temperature range of 350 to 650 °C (662 to 1202˚F). The gaseous environment was monitored and the fuel analysis made available for the purposes of model training.

Figure 2-7: Predicted Metal Loss Compared With Actual Metal Loss Showing the Results from the Training Data and Those from the Test Data

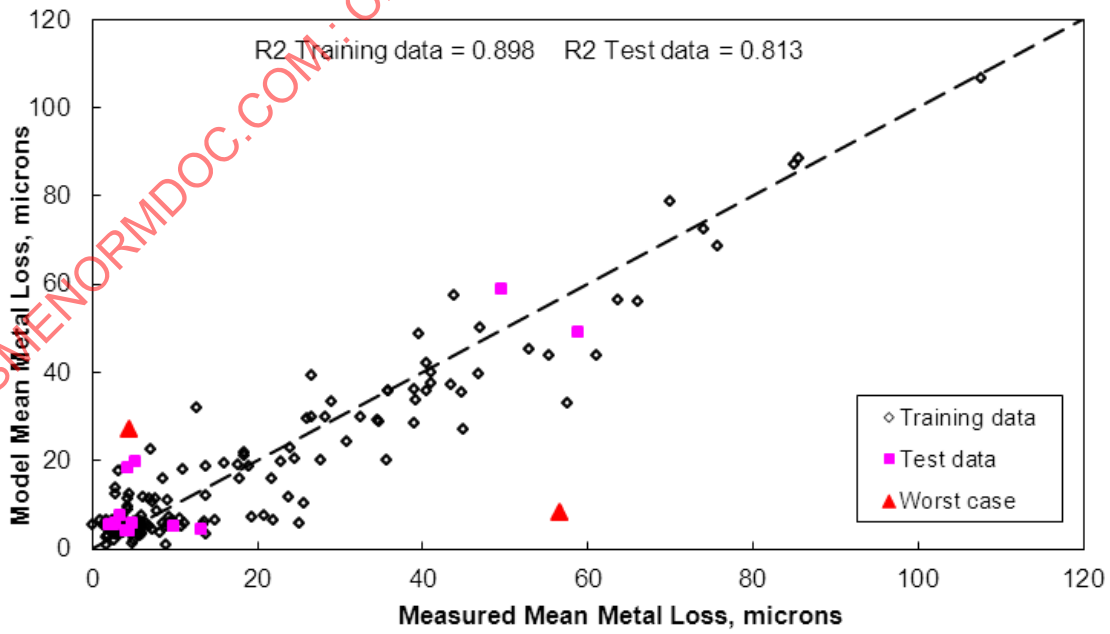

During the training, input parameters were introduced. The selection of the more dominant factors controlling the corrosion rates in boilers was supported by observations from literature [105][106][107][108][109][110][111][113][114]. The training of this final iteration of the low alloy furnace wall model was performed using 85% of the available data; the remaining 15% was used to test the neural network. The result of the training and testing are presented in Figure 2-7. The predictive capabilities of the model were demonstrated through the application of the model to a number of case studies. The first case relates to the assessment of the impact on the metal loss rate associated with a change in fuel. The plant operator would like to change from burning a Colombian coal, with low levels of sulfur and chlorine to one of three options, viz:

- co-firing with 20% cereal co-product (CCP);
- changing to a UK coal and co-firing with either 5% thermal miscanthus;
- changing to a UK coal with 20% short rotation coppice.

For a T23 furnace wall tube material, assuming a high maximum heat flux value of 1000kW.m^{-2} (317,000 BTU.hr^{-1}.ft^{-2}) across the tube, and using typical values for the fuel chemistry and resultant gaseous environment, the model can be used to provide corrosion rates as a function of metal temperature for each condition, as shown in Figure 2-8.

Figure 2-8: Predicted Corrosion Rate as a Function of Temperature and Fuel

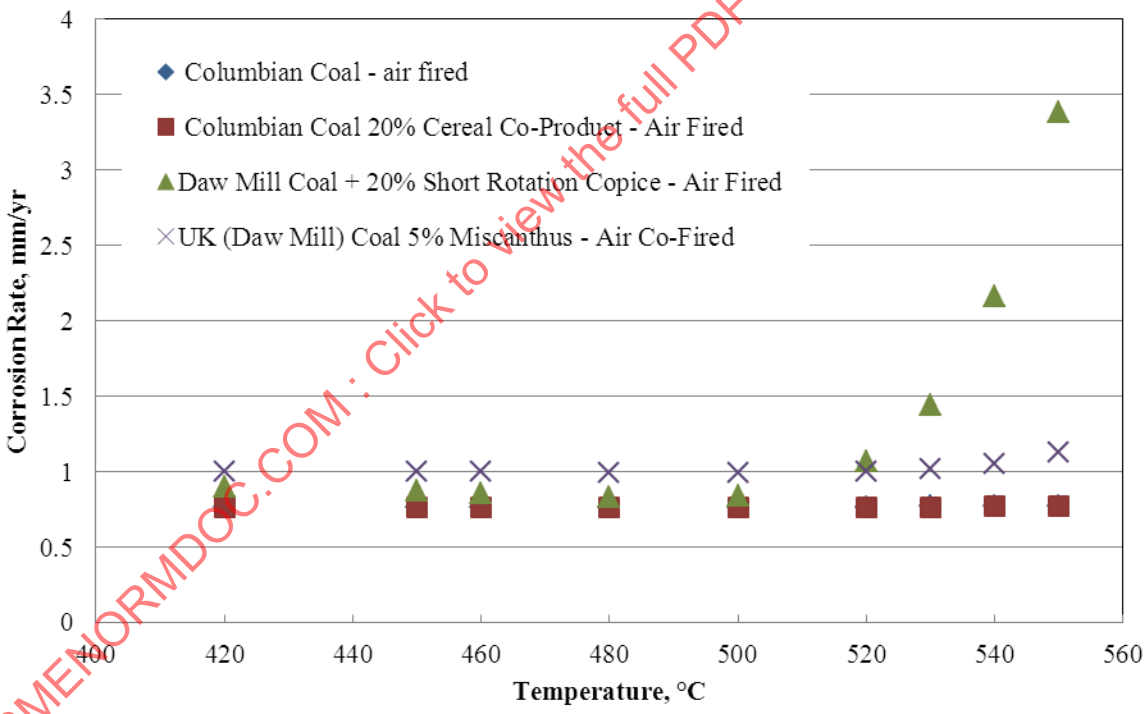

The result would suggest that there would be no detrimental effects on the corrosion rate of the tube by co-firing 20% CCP with the Colombian coal. Switching to the UK coal and co-firing with 5% miscanthus increases the corrosion rate slightly whilst co-firing with UK coal with the short rotation coppice biomass has similar rates of corrosion below 500°C (932˚F) but the model predicts these will accelerate at temperatures in excess of 500°C (932˚F).

This form of model can be used to predict the reduction in tube operating life that might be expected as a result of changing the fuel fired by the boiler. Alternatively this type of neural network model could be used to assess the metal wastage rates of different alloys, thereby allowing the designer to select the most appropriate alloy for the fuel to be burnt, as shown in the following example.

In this case, model is used to evaluate the corrosion resistance of three materials:

- a low alloy ferritic steel, T23, and
- two higher chromium containing steels, E911 and HCM12

The fuel mixture used is a UK Daw Mill coal co-fired with 20% short rotation coppice. The model has been used to provide a prediction of the corrosion rate as a function of temperature and alloy.

The results of the prediction are presented in Figure 2-9. They indicate that the predicted corrosion rates, at temperatures in excess of 480°C, increased with decreasing chromium content, as would be expected.

Figure 2-9: Predicted Corrosion Rate as a Function of Temperature and Alloy

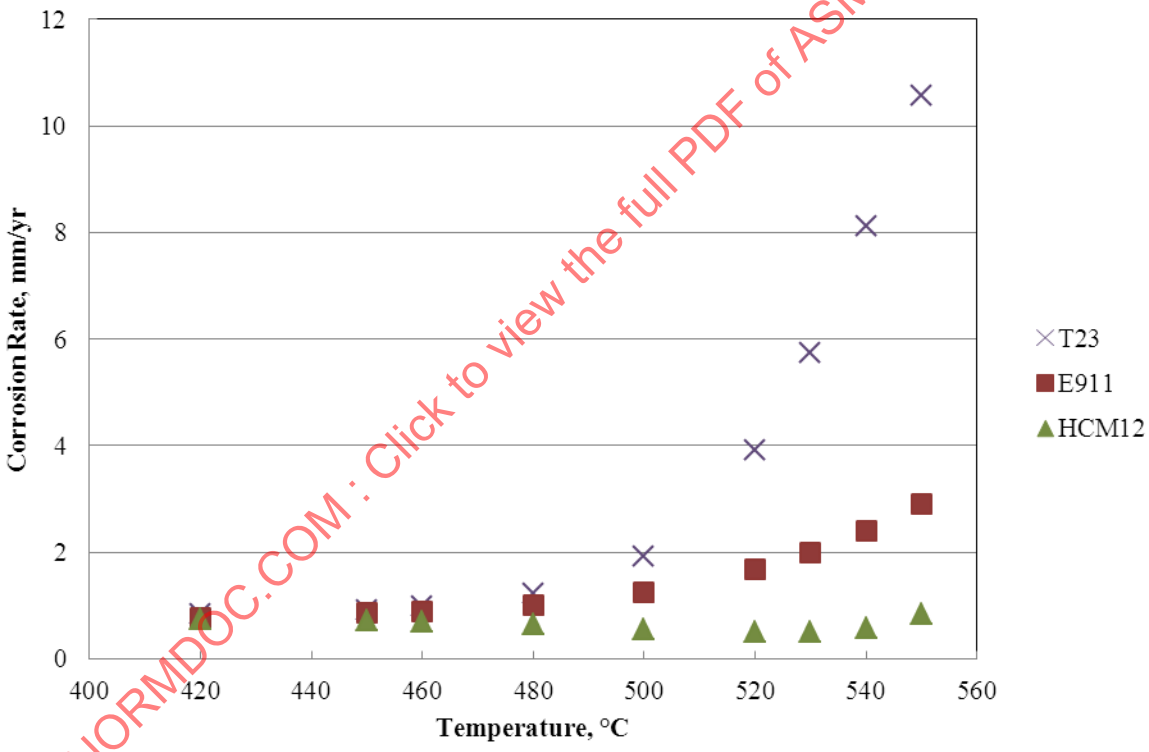

2.7 Corrosion Monitoring

The corrosion rates in superheaters and reheaters can be monitored at routine plant overhauls using ultrasonic techniques. EMAT probes can be used for the low alloy ferritic steels with minimal surface preparation, i.e. the removal of bulk ash deposits. The EMAT technique will not work for austenitic materials, and conventional ultrasonic thickness techniques are required. There is a requirement for cleaning and surface preparation to a bare metal surface. Care must be taken when grinding to avoid excessive damage.

Temporary corrosion probes, either using pre and post exposure thickness measurements or online, real or near real-time, probes based on electrical resistance or electrochemical noise techniques can also be employed. These techniques can be useful when attempting to understand and monitor changes in wastage rates when changing boiler fuel diets or operating conditions [113][114][115].

Hjörnhede evaluated a number of different on-line probes that made use of different resistance or electrochemical techniques and concluded that the majority were capable of measuring changes in corrosion rates but that they could not necessarily produce accurate metal loss rates. The probes were indicators of corrosion severity but needed calibration using other means [116].

2.8 Implications for Boiler Tube Design Codes

The superheater and reheater elements of large boilers are subject to creep degradation, and the tube materials and dimensions are selected in order to achieve a particular design life before requiring replacement. Frequently, a period of 100,000 hours for a given operating temperature and pressure is specified. Where fireside corrosion rates are low, i.e. less than 20nm.h^{-1}, (7mil.y^{-1}), this will have little or no impact and the design life is likely to be achieved. In such a case other damage mechanisms such as soot blower or dust erosion, overheating or thermal/mechanical fatigue may result in premature tube failure and the need for replacement.

Increasing fireside corrosion rates will progressively have a greater impact on tube operating life and may necessitate the use of higher grade alloys having greater corrosion resistance. Where high wastage rates are encountered, for example levels in excess of 200nm.h^{-1}, (70mil.y^{-1}), tube operating lives may be uneconomically short. In such an instance, the specifying of materials with high creep strengths may be false economy, as the benefits obtainable will not be realized.

For moderate corrosion rates simply increasing tube wall thickness in order to provide a greater corrosion allowance may provide an economic extension of expected tube operating life. Where this cannot be achieved consideration may be given to the use of higher alloyed materials that would have greater corrosion resistance. Alternatively, coextruded tubes having a corrosion resistant outer layer, or, weld overlays may be required.

In cases where the corrosion models predict unacceptably high wastage rates for a given fuel and tubing arrangement, even when using corrosion resistant materials, in order to achieve economic tube lives it may be necessary to consider more dramatic action. Operating with reduced steam conditions lower pressures and temperatures. Alternatively, changes to the fuel supply may be required, such as the selection, or blending of more benign coals in to the fuel basket.

Good boiler design practice may help to reduce the risks of excessive fireside corrosion rates. These may include the use of parallel flow rather than counter flow stages, such that the hottest operating tubes are exposed to cooler combustion gases and reduced heat fluxes. Similarly, the superheater and reheater tubing may be protected from radiant or high heat fluxes by positioning further from the radiant furnace section or by placing cooler operating tubing in front of the higher temperature stages.

2.9 References

[6] Paul, L., Clark, G., Eckhardt, M., Deacon, R., Dupont, J. and Marder, A., 2004, "Performance of Weld Overlay Materials in Simulated Coal Fired Combustion Environment", Paper No. 04523, NACE Corrosion 2004

[7] Van Weele, S., Blough, J. L., and DeVan,J. H. 1994, "Attack of Superheater Tube Alloys, Coatings and Claddings by Coal-Ash Corrosion", Paper No. 182, NACE Corrosion 1994

[8] Bakker, W. T and Kung,S.C. 2000, "Waterwall Corrosion in Coal-Fired Boilers A New Culprit: FeS", Paper No. 00246, NACE Corrosion 2000

[9] Seitz, W. and Blough, J., 2002, "Effect of Char and Sulfur Rich Deposits on Waterwall Corrosion", EPRI, Palo Alto, CA: 2002.1007097

[10] Bakker, W., Valentine, J., Davis, K., Blough, J., Danko, G. and Seitz, W., 2002, "The Effect of Coal Chlorine on Waterwall Wastage in Coal-Fired Boilers with Staged Low NOx Combustion Systems", EPRI, Palo Alto, CA; Ameren Corporation, St. Louis, MO; Dairyland Power Cooperative, La Crosse, WI:. 1004082.

[11] Coleman, K. E., Simms, N. J., Kilgallon, P.J. and Oakey, J. E., 2008, "Corrosion in Biomass Combustion Systems", Journal Materials Science Forum Vol.595-598, pp. 377-386,

[12] Blough, J. L., Stanko, G. J. and Krawchuk, M. T., 1999, "Superheater Corrosion in Ultra-Supercritical Power Plants: Long-Term Field Exposure at TVA's Gallatin Station", EPRI, Palo Alto, CA,: TR-111239

[13] Hack, H. and Stanko, G., 2006, "Experimental Evaluation of Fireside Corrosion Resistance of Advanced Materials for Ultra-Supercritical Coal-Fired Power Plants", 23rd An. Int. Pittsburgh Coal Conference, Pittsburgh, PA, USA,

[14] Krause, H. H., Nagarajan, V. and Wright, I. G., 2001, "Fireside Corrosion of High-Temperature Heat Exchanger Materials Exposed in Pulverized Coal-Fired Boilers", Paper No. 174, NACE Corrosion 1994

[15] Davis, C. J. James, P. J. and Pinder, L. W., 2001, "Fireside Corrosion in Pulverized-Coal-Fired Boilers: Effects of Coal Chlorine and Combustion Parameters", EPRI, Palo Alto, CA: 1001350

[16] Davis, C. J., James, P. J., Pinder, L. W. and Mehta, A. K. 2000, "Effects of Fuel Composition and Combustion Parameters on Furnace Wall Fireside Corrosion in PF-Fired Boilers", International Symposium on High Temperature Corrosion and Protection of Materials, 5, Les Embiez, France.

[17] Henderson, P.J., Davis, C. J. Montgomery, M. and Karlsson, A., 2005, "In-situ Fireside Corrosion Testing of Superheater Materials with Coal, Wood and Straw Fuels for Conventional and Advanced Steam Temperatures", VGB Powertech, 6/2005, pp53-59

[18] Davis, C. J. and Pinder, L. W., 2004, "Fireside Corrosion of Boiler Materials – Effect of Co-Firing Biomass with Coal", Report No. COAL R267, DTI/Pub URN 04/1795,

[19] Verhoff, F H. and Branchero J., 1974, "Predicting Dew Points of Flue gases", Chem. Eng. Prog. Vol. 78, pp71-71.

[20] Bahman ZareNezhad, 2009, "New correlation predicts flue gas sulfuric acid dewpoints", Oil & Gas Journal, Vol. 107,

[21] Gerhardt, A., Hjörnhede, A., Montgomery, M., Bjurman, M. and Henderson, P. 2011, "Corrosion in an Oxyfuel boiler – First results from Vattenfalls 30MWth Oxyfuel Pilot Plant in Schwarze Pumpe", IEAGHG Special Workshop on SO_2/SO_3/Hg/Corrosion Issue under Oxyfuel Combustion Conditions, London

[22] Hsiung Kiang, Y; 1981, "Predicting dew points of acid gases" Chemical Engineering,

[23] James, P. J., Robinson, M. T. and Gibb W. H. 1997, Possible Effects of the Chlorine Content of Coal on Fireside Corrosion in Pulverized Coal-Fired Boilers', Volume 2 'Effect of Fuel Chlorine on the Fireside Corrosion of Ferritic Furnace Wall and Superheater/Reheater Tubing – A UK Perspective', , EPRI report TR-108107,

[24] Lees D. J., 1977, Influence of Chlorine Content on Furnace Wall Corrosion Rates', , Central Electricity Generating Board internal report 1851/77/MT,

[25] Dooley, R. B. and McNaughton, W. P.; 2007, "Boiler and Heat Recovery Steam Generator Tube Failures: Theory and Practise, Volume 2: Water Touched Tubes", EPRI, Palo Alto, CA: 1012757

[26] Nava-Paz, J.C.; Plumley, A. L.; Chow, O. K.; Chen, W., 2002, "Waterwall Corrosion Mechanisms in Coal Combustion Environments", Materials at High Temperatures, Vol. 19(3), pp127-137,

[27] Bakker, W. T.; 1998, "Waterwall Wastage in Low NOx Boilers Root Causes and Remedies", EPRI, Palo Alto, CA: TR111155

[28] Kung, S. C., 1997, "Prediction of Corrosion Rate for Alloys Exposed to Reducing/Sulfidizing Combustion Gases", Materials Performance, Vol. 12

[29] Bakker, W. T. 1998, Effect of Iron Sulfide on Furnace Wall Corrosion', EPRI , Palo Alto, CA, TR-111152.

[30] Bakker, W. T.; 2003, "The Effect of Deposits on Waterwall Corrosion in Fossil Fueled Boilers", Materials at High Temperatures, Vol. 20 pp. 161-168.

[31] James, P. J. and Pinder, L.W.; 1997, "Effect of Coal Chlorine on the Fireside Corrosion of Boiler Furnace Wall", Materials at High Temperature, Vol. 14, pp187-196.

[32] Salmenoja, K., Hupa, M and Bamnab R., 1999, "Laboratory Studies on the Influence of Gaseous HCl on Fireside Corrosion of Superheaters", Journal of the Institute of Energy, Vol. 12,

[33] Gibbs, B. and Moores, G., 2001, "Effect of Chlorine on Waterwall Fireside Corrosion", EPRI report 1001352,

[34] Mehta, A. K., Davis, C. J., James, P. J. Pinder, L. W. and Wright, I. G., 1997, "Possible Effects of Coal Chlorine on Furnace Wall Fireside Corrosion in Utility Boilers", Proc. Int. Conf. on Corrosion, CONCORN '97, Mumbai, India,

[35] Davis, C.; 2011, "Pilot Scale Studies of the Fireside Corrosion Effects of Biomass Co-Firing and/or Oxy-fuel Coal Firing, Paper 11188, NACE Corrosion 2011, Houston, Texas,

[36] Spiegel, M. and Grabke, H. J.; 1998, "Chlorine induced corrosion of steels in fossil fuel power plants, NACE Corrosion 98, Paper 178.

[37] Davis, C. J. and Pinder, L. W., 2003, "COST 522: The Effect of Fuel Type on the Fireside Corrosion of Boiler Materials for Advanced Clean Coal Technologies: 1 Furnace Wall Corrosion", Powergen internal report PT/03/BB225/R.

[38] James, P. J. and Pinder, L. W., 1997, "Furnace Wall Fireside Corrosion: Taming the Beast Within", Third International Conference on Boiler Tube Failures in Fossil Plants, Nashville, TN, USA.

[39] Gibbs B and Moores, G., 2001, "Waterwall Fireside Corrosion Under Low-NOx Burner Conditions", EPRI report 1001351.

[40] Huijbregts, W. M. M., Janssen, J. B. and Rens, O. C. J. 1998, "Corrosion in Low NOx Firing Conditions", Power-Gen-'98, Milano.

[41] Baxter, L., and Koppejan, J.; 2005, "Biomass-Coal Co-Combustion: Opportunity for Affordable Renewable Energy", Fuel, Vol. 84, pp 1295-1302,

[42] Davis, C. J.; Pinder, L. W.; 2004, "Fireside Corrosion of Boiler Materials – Effect of Co-Firing Biomass with Coal," Report No. COAL R267, DTI/Pub URN 04/1795.

[43] Kung, S.C., Tanzosh, J.M. and McDonald, D. K.; 2008, "Fireside Corrosion Study Using B&W Clean Environment Development Facility for Oxy-Coal Combustion Systems", Advanced in Materials Technology for Fossil Power Plants 2007, Proc, 5th Int. Conf. ASM International, pp982-992.

[44] Holcomb, G. R. and Meir, G. H. 2012, "Fireside Corrosion", JCOAL / NETL Oxyfuel Workshop.

[45] Robertson, A., Gagliano, M., Seltzer, A. and Fout, T.; 2011, "Development of Boiler Materials for Oxy-Combustion Retrofits", Second Oxyfuel Combustion Conference, Yeppoon, Australia.

[46] Fry, A., Adams, B., Davis, K., Swensen, D., Munson, S. and Cox, W., 2011, "Fire-side Corrosion Rates of Heat Transfer Surface Materials for Air- and Oxy-coal Combustion", IEAGHG SO2/SO3/Hg /Corrosion Issue under Oxyfuel Combustion Conditions Workshop, London.

[47] Davis, C.; 2011, "Impact of Oxyfuel Operation on Corrosion in Coal Fired Boilers Based on Experience with E.ON's 1MWth Combustion Test Facility, IEAGHG Special Workshop on SO2/SO3/Hg/Corrosion Issue under Oxyfuel Combustion Conditions, London.

[48] Topolska, S and Labanowski, J, 2010, "Corrosion of Evaporator Tubes in Low Emission Steam Boilers", Archives of Materials Science and Engineering, Vol 42, pp 85-92.

[49] Breen, B. P., Gabrielson, J. E., Kramer, E. D, Lochart, K. S. and Urich, J. A.; "Corrosion Protection for Utility Boiler Side Walls", US patent application 08/730,581

[50] Kihara, S., Nakagawa, K. and Kajigaya, I.; 1997, "Waterwall Corrosion in Low-NOx Combustion Boilers", Proc. Int. Conf. on Corrosion, CONCORN '97, Mumbai, India.

[51] Flately, T., Latham, E.P., Morris, C. W.; 1980, "Co-Extruded Tubes Improve Resistance to Fuel Ash Corrosion in U.K. Utility Boilers "Paper 62, Corrosion 80, NACE, Houston.

[52] http://www.plymouth.com/products/plymouth-engineered-shapes/co-extreme-coextruded-boiler-tubing

[53] DuPont, J. N., Van Geertruyden, W., Caizza, A., Esposito, A.; 2010, "Corrosion Behavior of Alloy 600 and 622 Co-extruded and Weld Overlay Coatings", Paper 10201, Corrosion 2010 Conf. & Expo, NACE.

[54] Lai, G., Hulsizer, P.; 2000, "Corrosion & Erosion / Corrosion Protection by Modern Weld Overlays in Low NOx, Coal-Fired Boilers", Paper 00258, Corrosion 2000, NACE.

[55] "Long-Term Testing of Protective Coatings and Claddings at Allegheny Energy Supply Hatfield's Ferry #2 Boiler", EPRI, Palo Alto, CA, and Allegheny Energy Supply, Greensburg, PA: 2000. 1000186.

[56] Bennett, A.P.and Quigley, M.B.C; 1990, "The spraying of Boiler Tubing in Power Plants", Welding and Metal Fabrication, pp485-489.

[57] "Waterwall Wastage Mechanisms in Coal-Fired Boilers: The Effect of Coal Chemistry on Waterwall Wastage", EPRI, Palo Alto, CA: 2001. 1004021

[58] "Numerical Modeling of Waterwall Wastage on an Advanced Low NOx PC Fired Boiler", EPRI, Palo Alto, CA: 2004. 1004739

[59] "Corrosion Testing of power generation coal fired boiler tubes using EMAT probes and the MS Series", Sonatest Ltd., 2011

[60] Farrell, D. M. and Robbins B, 1998, "On-line monitoring of furnace wall and superheater corrosion in power generation boilers," VTER TECHNICAL PAPER, CSS 98, 39th Corrosion Science Symposium, University of Northumbria at Newcastle, U.K.,

[61] Eden, D. A., Breene, B.; 2003, "On-Line Electrochemical Corrosion Monitoring in Fireside Applications, Paper No. 03361, Corrosion 2003, NACE

[62] Covino, B. S., Bullard, S. J., Ziomek-Moroz, M., Holcomb, G. R., Eden, D. A.; 2006, "Fireside Corrosion Probes for Fossil Fuel Combustion", Paper No. 06472, Corrosion 2006, NACE.

[63] Farrell, D. M., Robbins B. J, Sikka, P. and Seaman M., 2004, "Online Monitoring and Control of Furnace Wall Corrosion in PF-Fired Boilers", Conference on High Temperature Plant and Life Extension, Cambridge.

[64] Robbins B. J, Farrell, D. M., Stallings J. and Cardoso S, 2010, "The Monitoring of Circumferential Fatigue Cracking of Furnace Tubes in Supercritical Boilers," HIDA 5 Conference.

[65] Blough J. L. and Seitz, W. W, "Fireside Corrosion Testing of Candidate Superheater Tube Alloys, Coatings, and Claddings – Phase III", Foster Wheeler Development Corp., www.fosterwheeler.fi

[66] Modern Power Station Practice: Volume B: Boilers and Ancillary Plant (Third Ed.)', section 2.2, Pergamon Press, 1991.

[67] Blough, J. L., Stanko, G. J. and Bakker, W. T, 2001, "Coal Ash Corrosion in a Reheater of an Ultra-supercritical Power Plant", 3rd Conference on Advances in Material Technology for Fossil Power Plants; Swansea; UK.

[68] Shigeta, J. I., Hamao, Y., Aoki, H. and Kajigaya, I. 1986, "Development of a Coal Ash Corrosivity Index for High Temperature Corrosion", ASME Paper 86-IJPGC-FACT-3.

[69] Nelson, W. and Cain, C. Jr., 1961, Corrosion of Superheaters and Reheaters of Pulverized Fuel-fired Boilers. J. Eng. Power, Trans. ASME, Oct. p468.

[70] Stringer, J., 1987, Metals Handbook, 9th Ed., Vol 13, Corrosion, ASM International, Metals Park, OH, p. 998.

[71] Blum, R., Chen, Q., Coussement, C., Gabrel, J., Testani, C. and Verelst, L., 2001, "Operational Tests of Superheater Materials at High Steam Temperatures in a Hard Coal-Fired Steam Generator", VGB PowerTech (10).

[72] Davis, C. J, and Pinder, L. W., 2003, 'COST 522: The Effect of Fuel Type on the Fireside Corrosion of Boiler Materials for Advanced Clean Coal Technologies: 2 Superheater/Reheater Corrosion', Powergen report PT/03/BB907/R.

[73] Baker, B. A., Smith, G. D.; 2004, "Corrosion Resistant of Alloy 740 as Superheater Tubing in Coal-Fired Ultra-Supercritical Boilers", Paper 04526, Corrosion 2004, NACE.

[74] Miles, T. R., Baxter, L. L., Bryers, R. W., Jenkins, B. M., Oden, L. L., 1995, "Alkali Deposits Found in Biomass Power Plants: A Preliminary Investigation of Their Extent and Nature", NREL/TP-433-8142, Vol. 1,

[75] Henriksen, N.; Larsen, O. H., 1997, "Corrosion in Ultrasupercritical Boilers For Straw Combustion", Proc. of the 2nd Int. Workshop on Corrosion in Advanced Power Plants, Tampa, Florida, Materials at High Temperatures Vol. 14, No.3.

[76] Frandsen, F. J., Nielsen, H. P., Jensen, P.A., Hansen, L. A., Livbjerg, H., Dam-Johansen, K., Hansen, P. F. B., Andersen, K. H., Sørensen, H. S., Larsen, O. H., Sander, B., Henriksen, N., Simonsen, P.; 1999, "Deposition and Corrosion in Straw and Coal-Straw Co-fired Utility Boilers, Danish Experiences", Impact of Mineral Impurities in Solid Fuel Combustion, Gupta et al editors, Kluwer Academic / Plenum Publishers, New York.

[77] Hein, K. R. G., 1994, "Combined Combustion of Coal, Biomass and Wastes" ,Co-Utilisation of Coal, Biomass and Waste, Clean Coal Technology Program 1992 – 1994, Section A4 Summary of Final Conference, Lisbon, Portugal.

[78] Gale, J.J., 1997, "A Review of Technology Status For Co-Utilisation of Coal and Biomass / Waste", DTI Cleaner Coal Technology Program Report No. COAL R119.

[79] van Loo, S.; Koppejan, J.;(editors) 2002, "Handbook of Biomass Combustion and Co-firing" Task 32 of the Implementation Agreement on Bioenergy, Published Twente University Press, Enschede.

[80] Overgaard, P., Kirkegaard, N., Junker, H., 2002, "Experience from Large Scale Commercial Co-firing of Biomass", 12th European Conference on Biomass for Energy, Industry and Climate Protection, Amsterdam, The Netherlands.

[81] Sander, B.; 2004, "Full-Scale Investigations on Co-Firing of Straw", Second World Conference & Exhibition on Biomass for Energy, Industry and Climate Protection", Biomass Co-firing – Current Trends & Future Challenges, IEA Workshop 4, Rome.

[82] Montgomery, M., Larsen, O. H., Biede, O.; 2003, "Corrosion and Materials Performance in Biomass Fired and Co-fired Power Plants", Corrosion 2003, Paper 03356, NACE

[83] Frandsen, F. J., 2005, "Utilizing Biomass and Waste for Power Production – a Decade of Contributing to the Understanding, Interpretation and Analysis of Deposits and Corrosion Products", Fuel, Vol. 84, pp1277-1294, Elsevier.

[84] Davis, C. J., 2005, "Effects of Co-Firing Palm Kernel Expeller (PKE) on the Superheater – Reheater Fireside Corrosion Rates", Power Technology Report PT/05/BB524/R.

[85] Wieck-Hansen, K., Sander, B., 2003, "10 Years' Experience with Co-firing Straw and Coal as Main Fuels together with Different Types of Biomasses in a CFB Boiler in Grenå/Denmark", VGB Power Tech 10, pp64-67

[86] Hansen, P. F. B., Andersen, K. H., Wieck-Hansen, K., Overgaard, P., Rasmussen, I,, Frandsen, F. J., Hansen, L. A., Dam-Johansen, K., 1998, "Co-firing straw in a 150MWe Utility Boiler: In-situ Measurements", Fuel Processing Technology, Vol. 54, pp 207-225.

[87] Vainikka, P., 2004, "Co-firing in Large Scale CFG-Experience Gained from Experiments with the World's Largest Biofuel Fired CFB of Alholmens Kraft, Finland", Second World Conference & Exhibition on Biomass for Energy, Industry and Climate Protection", Biomass Co-firing – Current Trends & Future Challenges, IEA Workshop, Rome.

[88] Lauridsen, T. L., Hyldgaard, N. J., Sørensen, K., Hulgaard, T.; "Multi Circulating Fluidized Bed with Advanced Steam Cycle for Coal / Biomass Combustion", Clean Coal Technology Program

1992-1994, Combined Combustion of Biomass / Sewage Sludge and Coals: Volume 2: Final Reports EC – Research Project: APAS – Contract COAL – CT92-000

[89] Henderson, P. J., Ljung, P., Eriksson, T., Westberg, S-B., Hildenwall, B., Åbyhammar, T., 2000, "Corrosion Testing of Superheater Steels for Biomass-Fired Boilers and the Effects of Co-Firing with Coal", Proc. Conf. Advanced Materials for 21st Centry Turbines and Power Plant, pp1094-1104, Institute of Materials Communications, London, UK.

[90] Robinson, A. L., Baxter, L. L., Sclippa, G., Junker, H., Widell, K. E., Dayton, D. C., Freeman, M., Walbert, G., Goldberg, P, 1997, "Fireside Considerations when Co-firing Biomass with Coal in PC Boilers", Engineering Foundation Conf. on the Impact of Mineral Impurities in Sold Fuel Combustion, Keauhou Beach Hotel, Kona, Hawaii.

[91] Brem, G. 2005, "Biomass Co-Firing, Technology, Barriers and Experiences in EU", Global Climate and Energy Program Advanced Coal Workshop, Provo, Utah.

[92] Holcomb, G. R., Tylczak, J., Meier, G. H., Jung, K., Mu, N. Yanar, N. M. and Petit, F. S. 2011, "Fireside Corrosion in Oxy-Fuel Combustion of Coal", 220th ECS Meeting, High Temperature Corrosion and Materials Chemistry 9 — A Symposium in Honor of Professor Robert A. Rapp, Boston, MA.

[93] Kung, S. C.; 2011, "Fireside Corrosion in Oxy and Air-Firing Combustion Environments", IEAGHG SO2/SO3/Hg /Corrosion Issue under Oxyfuel Combustion Conditions Workshop, London.

[94] Maier, J., Cumbo, D., Rossi, N., Tosi, E., Stein-Brzozowska, G., Miller, E., Scheffknecht, G., Viklund, P., Coraggio, G., Tognotti, L., 2011, "Corrosion of Candidate Superheater Materials During Oxyfuel Conditions", 2nd Oxyfuel Combustion Conference, Yeppon, Australia.

[95] Tuurna, S., Pohjanne, P., Auerkari, P.; 2011, "Performance of Superheater Materials in Simulated Oxyfuel Combustion", VTT Report VTT-R-02456-11.

[96] Pohjanne, P., Yli-Olli, S., Auerkari, P., Tuurna, S., Jauhiainen, P., Turunen, E., Varis, T., Ruusuvuori, K., MaKippaa, M., 2010, "Fireside Corrosion of Superheater Materials in Oxyfuel Combustion", Paper 10200, NACE Corrosion 2010, San Antonio.

[97] Robertson, A., Gagliano, M., Seltzer, A., Fout, T., 2011, "Development of Boiler Materials for Oxy-Combustion Retrofits", 2nd Oxyfuel Combustion Conference, Yeppon, Australia.

[98] Balting, U, et al, 1988, Fireside Corrosion and Ferritic / Austenitic Steels and High-Alloy Materials for Superheaters, Especially Reheaters of Coal-Fired Steam Generators", Werkstoffe und Korrosion, No.39, pp. 90-97.

[99] Meadowcroft, D. B., 1987, "High Temperature Corrosion of Alloys and Coatings in Oil- and Coal-Fired Boilers", Materials Science and Engineering, No.88, pp 313-320.

[100] Locklin, D. W.,et al, 1980, "Electric Utility Use of Fireside Additives", Battelle Columbus Laboratories, EPRI CS-1318,

[101] P Makkonen, 1998, "Neural Network for Prediction of Superheater Fireside Corrosion", Baltica IV Plant Maintenance for Managing Life & Performance, Vol. 1, Hietanen S. and Auerkari P. (Ed.), VTT Symposium 184, Technical Research Centre of Finland.

[102] Zhou, S., Coleman D. and Turnbull A, 2001, "Application of Neural Networks to predict Sulfide Stress Corrosion Cracking of Duplex Stainless Steels", NPL Report MATC (A)21.

[103] Simms, N.J and Fry, A. T., 2010, "Modelling Fireside Corrosion of Heat Exchangers in Co-Fired Pulverized Fuel Power Systems", Proceedings 9th Liege Conf,: Materials for Advanced Power Engineering, eds. J. Lecomte-Beckers, Q. Contrepois, T. Beck and B. Kuhn, pp1192-1201.

[104] Mehta, 2001, "Fireside Corrosion in Pulverized-Coal-fired Boilers, Effect of Coal Chlorine and Combustion Parameters", Final EPRI report 1001350

[105] Cios, K. L., Berke, L., Vary, A. and Sharma, S., 1996, "Soft computing methods in the design of superalloys", NASA Tech Memo 106888

[106] Rosen, E. M. and Silverman, D. C., 1992, "Corrosion prediction from polarisation scans using artificial neural network integrated with expert system", Corrosion, pp734-745.

[107] Cai, J., Cottis, R. A. and Lyon, S. B., 1999, "Phenomenological modelling of atmospheric corrosion using an artificial neural network", Corrosion Science, Vol. 41 pp. 2001-2030.

[108] Urquidi-Macdonald M. and Macdonald, D., 1994, 'Performance comparison between a statistical model, a deterministic model, and an artificial neural network model for prediction damage from pitting corrosion', J. Research of National Institute Standards and Technology, 99, pp495-504 (1994).

[109] H M G Smets and W F L Bogaerts, 'SCC Analysis of Austenitic Stainless Steels in Chloride-Bearing Water by Neural Network Techniques', Corrosion, pp618-623 (1992)

[110] M Urquidi-Macdonald and P Egan, "Validation and Extrapolation of Electrochemical Impedance Spectroscopy Data", Corrosion Reviews, 15, pp 169-194 (1997).

[111] S Zhou, D Coleman and A Turnbull, NPL Report MATC(A)21 (2001)

[112] T. Fry, S. Osgerby, 'Oxide Scale Growth and Spallation in Steam Environments – An Assessment of Different Modelling Approaches', Materials for Advanced Power Engineering 2006, pp. 1469-1478 (2006)

[113] 'Measurement and Compilation of Materials Degradation Data in the COST522 Program', N J Simms, S R Saunders, S Osgerby, J E Oakey, Life Cycle Issues in Advanced Energy Systems, 2003

[114] Mok, W. Y., Cox, W. M.; "High-Temperature Fireside Corrosion Monitoring in the Superheater Section of a Pulverized-Coal-Fired Boiler", EPRI Report No. TR-101799, December 1992

[115] Mabbutt, S., Simms, N., Oakey, J.; "High Temperature Corrosion Monitoring by Electrochemical Noise Techniques", Corrosion Engineering, Science and Technology, Vol 44, No.3, pp186 – 195, 2009

[116] Hjörnhede, A.; "Evaluation of Electrochemical Techniques for Measurement of Fireside Corrosion in Thermal Power Plants", Report Number M06-610, Värmeforsk Service AB, December 2007

3 EROSION - THE PARTICLE IMPACT EROSION WEAR OF BOILER TUBES

3.1 Introduction

The erosive and abrasive wear of the key components in the fuel handling and firing systems, within the convective section of the boiler and in the ash handling systems, are significant technical issues for the designers and operators of coal-fired power plants. In most countries, the particle impact erosion wear of boiler tubes and other components has historically been the first or second most important cause of the loss of availability of coal-fired boilers [1].

The severity of the problems is related principally to the ash content of the coal being fired. The ash contents of steam coals, as delivered, vary widely, from values less than 5% to more normal levels between 10 and 20%, to levels in excess of 50% for some of the low quality coals utilized for power generation principally in South Africa and India. For the users of the very high ash coals, the control of the abrasion and erosion of plant components is a key concern.

In the case of both abrasion and erosion the wear is due almost entirely to the presence of inorganic components of coals and ashes, which have hardness levels similar to or higher than those of the steels and the other materials of construction of the boiler components. In the great majority of coals, these are principally the quartz and pyrite particles. The carbonaceous matter and the clay minerals, which are major components of most coals, are relatively soft compared to steel, and cause little erosive or abrasive wear.

With fly ash and bottom materials, the situation is more complicated in that hard glassy materials formed by the fusion of the mineral components of the parent coal during the combustion process are commonly present as a major constituent. These materials can make a significant contribution to erosive and abrasive wear of boiler tubes and other components, in addition to the action of the residual quartz grains.

It is also important, in this context, to be clear about the differences between the abrasion and erosion processes, viz:

- **Abrasive wear** is caused by the sliding of hard particles over a surface or the pressing of the particles between two sliding metallic surfaces. In power plants, the main areas of concern are in coal handling, crushing and milling equipment, where abrasive wear of metal components in contact with the mineral constituents of the coal can affect the performance of the equipment, and can be a significant contributor to the maintenance costs. The abrasive wear of the components of ash crushing and handling equipment can also be a significant area of concern.
- **Erosive wear** is associated with the impact of hard particles, carried in a fluid at significant impact velocities, on metallic and other surfaces. The key areas of concern in coal-fired power plant are in the internal surfaces in coal mills, in the pulverized coal pipework, particularly at and near bends, and the internal components of burners. The erosive wear of heat exchange tubes and other surfaces in the convective section of the boiler is also of significant concern, as is the erosion of pneumatic ash conveying equipment. Excessive erosive wear rates due to the impact of pulverized coal or ash particles can have a significant effect on the performance of boiler tubes and other key items of equipment, and can result in premature component failures and increased plant maintenance costs.

As stated above, the erosion and abrasion damage due to the presence of hard coal and ash is a significant problem area in a number of locations in large pulverized coal-fired boilers, viz:

- coal handling system and bunkers,
- grinding elements and other internal surfaces of the coal mills,
- pulverized coal pipework and the burner internals,

- furnace bottom ash hopper slopes,
- heat exchange tubes and other components of the boiler convective section and airheater, and
- furnace bottom ash and fly ash handling systems.

The abrasion and erosion processes in each of these areas tend to have their own specific features, although the fundamental processes are similar.

In this document the emphasis is very much on the particle impact erosion of boiler heat exchange tubes, particularly in the boiler convective section, where the problems tend to be more serious.

In general terms, the majority of the reported boiler tube failures due to erosion are associated with the following:

- The particle impact erosion wear of superheater, reheater and economizer tubes, and particularly the leading tubes in both vertical and horizontal banks and the tube bends at the sides of the banks.
- The erosive wear of boiler tubes due to the action of the steam, air or water soot blowers and lances, in most cases due to the overuse or faulty operation of the on-line cleaning equipment.
- The erosive wear and mechanical damage of boiler tubes due to ash and slag falling on to boiler surfaces, particularly on the furnace bottom ash hopper slopes.

In this section of the document the emphasis is on the particle impact erosive wear of boiler tubes, principally in the convective section of the boiler, where the coal fly ash particles, generated in the furnace, are impacting directly on the boiler tubes at significant velocities.

In general terms, the impaction of coal fly ash particles on boiler tubes can be either captive, i.e. can result in the formation of, or addition to, the ash deposits that are normally present on the boiler tube surfaces, or can be non-captive and lead to erosive wear. In practical terms, erosion wear is normally associated with the primary superheater, the reheater banks and the economizer, and occurs at flue gas temperatures below about 1000°C, at which the ash particles are solid and have a much lower tendency to stick to the tube surfaces.

It is a fairly common observation in coal fired boilers, however, that both ash deposition and erosive wear can occur around a leading boiler tube in the superheater and reheater section of the boiler, at the same time. The crown of the tube facing in the direction of the flue gas flow, can have a fairly dense cone of coal ash fouling deposit material, deposited by direct impaction of particles carried in the flue gases. The sides of the tubes have little or no ash deposit and can be subject to significant ash particle erosion, and the downstream sides of the tubes can have a loosely-attached ash deposit layer deposited at lower flue gas velocities.

It has been the experience in the majority of cases, that the erosion wear rates are not sufficient to cause tube failure during the first few years of operation of a new pulverized coal boiler. It is more likely in most cases that these problems begin to emerge after continuous wear at modest rates over 5-15 years of operation. Since there is limited scope for the effective mitigation of endemic erosion problems in operating boilers, it is of primary importance that the arrangement of the convective tube banks and the selection of the flue gas velocities are such that the erosive wear rates are minimized at the design stage.

A good understanding of the fundamental aspects of the particle impact erosion process, and the ability to predict abrasive and erosive wear rates for particular coals and ashes is therefore of key importance to allow equipment suppliers to design specifically for the intended fuel diet. This can also be of practical assistance

to boiler plant operators in the planning of plant inspections and maintenance schedules for particular items of equipment.

3.2 Nature of Particle Impact Erosive Wear

The precise mechanism of material removal from a surface by particle impact erosion is complex, and is very dependent on the details of the properties of the target material, the angle of impact, the nature of the erodent, etc. There have been many attempts to model these processes mathematically, and it is not considered appropriate to present a detailed description of this subject in this section. A fairly brief practical description of the key features of the erosion process, as they apply to the metal loss from the convective section tubes in coal-fired boilers, is more appropriate in this context.

One of the key elements of the process is the transfer of kinetic energy from the particle to the target material during the impaction and rebound of the particle. In most cases, the loss of kinetic energy, and hence the energy transferred to the target material increases with increasing angle of impact.

Clearly, therefore, as the angle of incidence increases from zero, the energy transfer during impacts and the rate of erosion for all materials also increase. This trend continues up to perpendicular impact for brittle materials, for which the main process of material loss is surface fracture.

Ductile materials are able to deform under impacts without fracture, and erosive wear is at least partly the result of a cutting or gouging action, which reaches a maximum at a lower angle of impact. For most metallic materials, therefore, the rate of erosion by a cutting or gouging action exhibits a maximum at an angle of around 30-50º. At angles closer to 90°, there is extrusion of the material; around the impact point to form ridges, which are more prone to fracture.

The erosive wear rate is most commonly expressed in terms of the rate of mass loss from the target surface, expressed for instance in g cm^{-2} s^{-1}, per unit particle flux to the surface, also expressed in g cm^{-2} s^{-1}, or in terms of the mass of metal lost from the target per unit mass of erodent, commonly in units of mg kg^{-1}.

It has normally been found that the erosive wear (w), expressed, for instance, as the mass loss of target material per unit mass of erodent, is strongly dependent on the velocity of the particles on impact (v), and is usually found to vary according to the equation:

$$w = k\, v^n,$$

where:

k is a constant, and
n is the velocity exponent.

For most systems, the value of n, the velocity exponent, is typically between 2 and 3, i.e. it is generally found that wear rates increase sharply with increasing particle impact velocity.

The key properties of the erosive particles that have a major influence on their erosiveness include:

- The hardness and mechanical strength of the particles, i.e. the particle material has to have similar hardness to the target material to have significant erosive properties.
- The particle size distribution, i.e. larger particles tend to be more erosive than the same mass of smaller ones.
- The particle shape can have a significant effect, i.e. particles with sharp edges have a greater erosive effect, particularly in terms of their cutting action on ductile materials, than do rounded particles.

The properties of the target material also influence the rate of erosive wear. In general terms, it is considered that the wear resistance, i.e. the reciprocal of the wear rate, of most metallic materials increases with increasing hardness. It has been found, for instance, that there is a relationship between the measured erosion wear rate, expressed in units of metal loss in mg per kg of erodent, of a range of steel alloys, and the Vickers Hardness of the material, measured before the erosion experiment [2]. In these experiments, the erodent was quartz particles of 125-150μm in diameter, impacting on the steel targets at a velocity of 27.5 m s^{-1} and at an angle of 45°.

The data show a very good linear relationship between log erosion wear (mg kg^{-1}) and log Vickers Hardness (kg mm^{-2}). Based on these data and measurements reported by Patel [3], Raask suggested the following relationship between the erosive wear and the hardness of metals:

$$\log w_e = a_2 - (1 \pm 0.1) \log H_m,$$

where:

a_2 is the erosion coefficient, which is dependent on the nature of the erodent material, the impact velocity and the angle of impact, and
H_m is the Vickers Hardness of the steel target material, measured before the erosion experiment.

The erosion behavior of the carbides, such as silicon carbide and titanium carbide, which are hard, chemically and thermally inert materials that are increasingly employed for applications involving hostile environmental conditions, is considered to be somewhat different from that of most metals.

The carbides are brittle materials and descriptions of their erosive wear are often based on their hardness and fracture toughness properties. Evans et al. [4] and Gulden [5], for instance, developed a simple model of the erosion wear of brittle materials:

$$W_e = a\, E^{-1.33}\, H^{-0.25},$$

where:

W_e is the erosive wear in mg kg^{-1} of erodent,
a is the erosion wear coefficient,
E is the fracture toughness, and
H is the hardness.

In general terms, relative wear resistance measurements for a range of brittle materials have indicated that, for good erosion wear resistance, fracture toughness values in excess of 3 MN $m^{-1.5}$ and Vickers Hardness values in excess of 1,000 kg mm^{-2} are required.

3.3 Measurement of Erosive Wear Rates

There has been significant research and development work over many decades on a number of subject areas related to erosion processes, viz:

- particle impact erosion wear of coal ash particles on boiler components,
- assessment of the erosivity of coals and ashes,
- relative erosive wear resistance of materials and
- effect of process conditions such as the gas and particle velocities, the angle of impact, the temperature etc. on the measured erosive wear rate.

A number of organizations worldwide have built and operate erosion test rigs and have performed programs of test work on the erosion behavior of coals and ashes and the behavior of specific target materials under

relevant test conditions. These are of a number of different designs, and it is fair to say that no general consensus as to the best approach has been reached.

The principal technical approaches to the laboratory measurement of particle impact erosion include:

- ambient temperature air jet impactors, in which the erodent particles are accelerated towards the target material suspended in a jet of air at ambient temperature,
- pipe loop rigs, which are intended to simulate erosion behavior in pneumatic conveying systems,
- rotating arm impactors, and
- high temperature erosion rigs, based on rotating arm or air jet impactors.

These rigs are generally employed to measure the relative erosion properties of different particulate materials, such as pulverized coal or fly ash in a systematic fashion under laboratory conditions or to test the erosion resistance of specific materials of interest.

In most cases, the weight loss of the target material, due to erosive wear, is measured and the wear rate is expressed in unit of mg of wear per kg of erodent materials applied. Less commonly, the physical parameters of the erosion scar are measured.

This type of test work is most commonly done to provide data for design purposes, as part of the investigative work carried out in the case of problems on plant and as part of research and development projects. The work on test rigs of this sort and the collection of plant data over many years has formed the technical basis of our technical understanding of these processes.

3.4 Particle Impact Erosion Wear of Boiler Tubes

The technical literature on coal ash erosion has been blessed by the publication in 1988 of a very important monograph [6], entitled 'Erosion wear in coal utilization', which was written by Erich Raask, who was active as a consultant on his retirement after spending many years as a researcher on coal ash characteristics and behavior at the Central Electricity Generating Board laboratories in Leatherhead, England. This monograph provides a very comprehensive review of the literature on the particle impact erosion processes, and of the characteristics of fly ashes and ash deposits. Both the theoretical and practical aspects of the erosion processes that apply in coal plants are covered in this monograph, and there is extensive coverage of the characteristics and behavior of coals and coal ashes.

It is well known that fly ash erosion is a significant cause of boiler tube failure, and of availability loss in fossil-fuel-fired power plants, worldwide, depending principally on the ash content of coals being fired. Fly ash erosion of boiler tube surfaces causes metal wastage in two ways, viz:

- by direct material removal, and
- by removal of protective fireside oxide or corrosion product layers, which can result in an increase in the fireside oxidation/corrosion rate.

Corrosion product/oxide removal can be the dominant effect at metal surface temperatures above about 425 °C.

The important process variables which control the erosion wear process are relatively well understood, i.e.,

- particle velocity, which is related to the local gas velocity,
- particle loading of the local gas stream,
- angle of incidence of the particle on the metal target, and

- relative concentration of the more abrasive particles in the fly ash.

The abrasiveness of the ash particles depends on their hardness, their size, and their shape; and this is a function of the coal and the characteristics of the combustion system.

Fly ash erosion of boiler tubes is a fairly complex phenomenon, i.e. it is highly localized in nature, and the rate of erosion can be dependent on a number of boiler maintenance and operational factors. The average velocity and ash loading, and the ash characteristics are clearly important, but the ash particle flow can become concentrated in certain areas of the gas flow. Excessive levels of convective pass fouling, local turbulence and other effects can have the effect of bridging certain regions of the gas passes and increasing the local gas velocities in other areas, with significant impacts on the local tube erosion rates.

The angle of impact of the fly ash particles on the metal component is also important. For metal tubes, for instance, this may mean that the maximum erosion wear rate may be on the sides of the lead tubes rather than the crowns. This can also result in there being both ash deposition and erosion wear of the bare metal at the same tube, as described above.

As stated above, the local flue gas velocity, the ash particle flux and the erosiveness of the particles tend to be the most important parameters. During the design stage, boiler engineers generally place upper limits on the average velocities within the convective tube banks, depending on the ash contents of the coals to be fired and the erosion potential of the ashes. This is considered to be the first stage of the process of providing protection against excessive rates of erosive wear of the boiler components, before the more specific design features for protection of particular boiler components are considered.

3.5 Assessment of the Erosion Potential of Pulverized Coals and Ashes

A fairly wide variety of mineral species, principally oxides, sulfides, carbonates, phosphates and clay minerals have been identified in coals, however it is generally acknowledged that only those minerals that are harder than steel contribute significantly to the abrasive and erosive behavior of the coal particles. A list of the more abundant minerals in most coals, ranked according to their Mohs' and Vickers hardness values, is presented in Figure 3-1.

These data indicate that quartz and pyrite are the main components in coal that are responsible for abrasive and erosive wear. The clays, carbonates, sulphate, and phosphate minerals and the carbonaceous coal matrix are all significantly softer than steel, and therefore have little effect on the particle impact erosion wear of most boiler components.

This has been demonstrated by the results of a collaborative program of experimental work using a combination of laboratory erosion testing of samples of a range of pulverized fuels in an ambient temperature air jet particle impactors rig, and the detailed characterization of the fuels using the computer controlled Scanning Electron Microscope with EDX facilities [7].

Figure 3-1: Moh Hardness Values for the Major Mineral Species Found in Coals

Mineral Name	Chemical Formula	Hardness (Mohs' scale)	Vickers Hardness (kg mm^{-2})
Coal minerals			
Quartz	SiO_2	7.0	1100-1550
Pyrite	FeS_2	6.0-6.5	720-1840
Alkali feldspars	$KNaSi_3O_8$	6	730-
Mild steel	-	5.0-6.0	300
Siderite	$FeCO_3$	4.0-4.5	200-250
Dolomite	$CaMg(CO_3)_2$	3.5-4.0	420-580
Ankerite	$Ca(Mg,Fe)(CO_3)_2$	3.5-4.0	350-490
Calcite	$CaCO_3$	3.0	100-170
Muscovite	$KAl_3Si_3O_{10}(OH)_4$	2.5-3.0	40-80
Kaolinite	$Al_2Si_2O_5(OH)_4$	2.0-2.5	30-40
Illite	as for muscovite, but with other elements, e.g. Fe and Mg substituting for K	1.0-2.0	20-35
Pulverized fuel fly ash particles			
Solid glassy spheres with embedded mullite or quartz crystals		5	550-600
Non-spherical quartz particles		6-7	1100-1300
Spherical iron oxide particles		5-6	550-600

The results of this program of work have indicated the following:

- Only the "excluded" mineral matter needs to be considered when assessing the erosion potential of pulverized coals. The "excluded" minerals were defined as those with less than 90% of their borders adjoining to the carbonaceous coal matrix, when viewed under the electron microscope in cross-section.
- Only the larger mineral occurrences, greater than 25 μm in diameter, need to be considered, since the erosive wear caused by the smaller particles is relatively low.
- The quantity of large quartz, pyrite, feldspar or garnet particles in the pulverized coal is directly related to the quantity of the larger quartz, pyrite, feldspar or garnet particles in the raw coal.
- The particle angularity was not found to be an important parameter affecting the erosion process, for the suite of pulverized coal samples studied.
- The erosive wear caused by the different mineral species in a coal is an additive function of the quantity of each mineral present.

The data in Figure 3-2 indicate that the erosion wear rates for the full range of coals tested were in the range 0.5 to 5.5 mg of metal loss per kg of pulverized coal, as erodent, at an impact velocity of 40 m s^{-1}. The erosion rate was directly proportional to the fraction of the 'excluded' mineral particles greater than 25 μm in diameter and harder than steel, expressed as a percentage by volume.

Figure 3-2: The Measured Pulverized Fuel Erosion Rate Plotted Against the Hard Mineral Content of the Coals, Excluded Mineral Particles In Excess of 25 μm In Diameter. (After Wells et al. 2005)

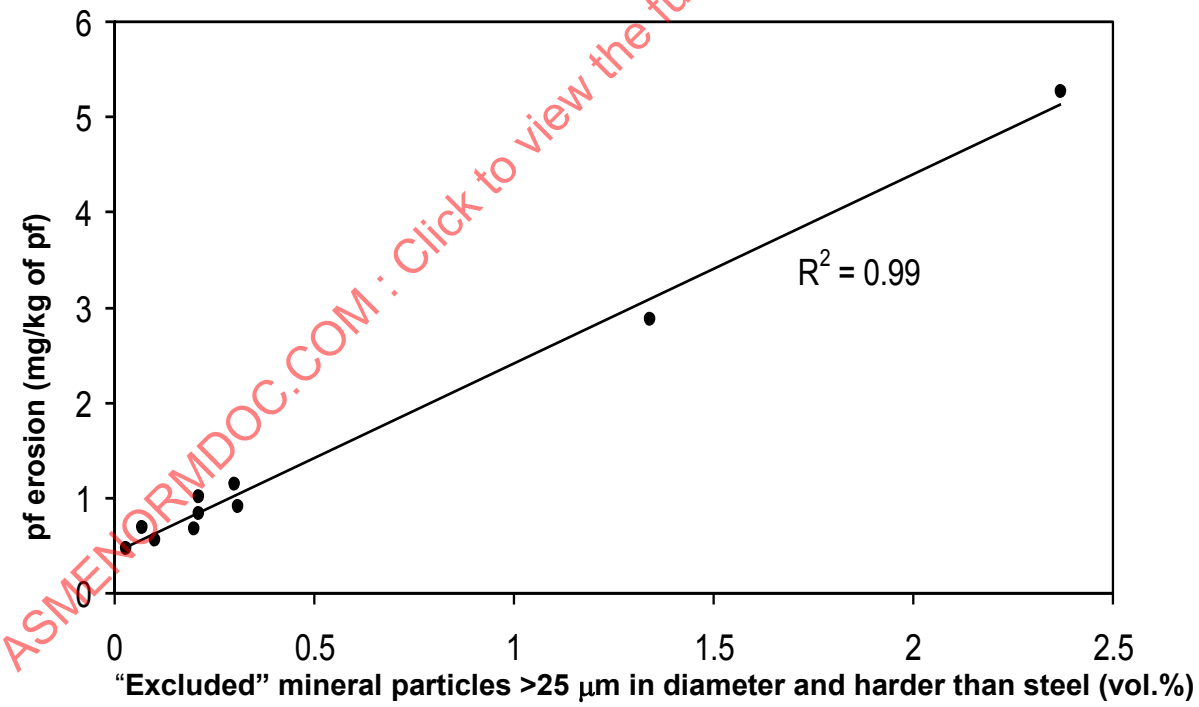

It is clear that the results of this work have provided a more complete description of the effect of the ash characteristics of pulverized on the particle impact erosion wear process than was available previously. The work involved the analysis and testing of a total of ten pulverized coal samples from five countries, with ash contents up to 55% on a dry basis.

When pulverized coal is burned, the inorganic and mineral components undergo a number of physical and chemical transformations to produce fly ash particles. The key mineral transformations for most coal ashes are listed in Figure 3-3.

Figure 3-3: The Major Mineral Transformations in A Pulverized Coal Flame

Mineral species	Major flame imprinted transformations
Quartz SiO_2	Partial melting, with some rounding of the edges of the partcles. There may be some chemical interaction with other minerals, principally the alkali metal and alkaline earth metal species.
Muscovite and Illitic clay minerals $KAl_3Si_3O_{10}(OH)_4$, with significant substitution of Ca, Mg , Fe and other metals for K	Melting to produce spherical ash particles of a wide range of particle sizes and internal porosities. There may be some chemical interaction with other minerals, principally the alkali metal and alkaline earth metal species.
Kaolinite $Al_2Si_2O_5(OH)_4$	Partial melting, depending on the flame temperatures. There may be some chemical interaction with other minerals, principally the alkali metal and alkaline earth metal species.
Pyrite FeS_2	Decomposition to the iron oxides and melting to generate largely spherical particles.
Calcite and dolomite $Ca(CO_3)_2$ and $CaMg(CO_3)_2$	Decomposition to the calcium and magnesium oxides. Major reduction in particle size distribution due to vigorous release of CO_2.
Siderite $FeCO_3$	Decomposition to iron oxides, with vigorous release of CO_2.

It is clear from the information on this table that, in most cases, the mineral species melt or partially melt at high temperatures in the flame to form predominantly spherical or rounded fly ash particles most of which have hardness values similar to, or higher than, those of mild steel. This is indicated in Figure 3-1, where the measured Vickers hardness values for a number of fly ash particle types are listed.

There are very few reports of direct comparisons of the erosion characteristics of pulverized coal fly ashes and their parent coals. The data in Figure 3-4 were generated during the same project as was reported by Wells et al [7], and which was described above. In this case, the data show the relative erosion rates for pulverized coals and the fly ashes prepared by combustion of two of the pulverized coals in a 1 MW_{th} combustion test rig. The results indicate that the measured erosion rates for these pulverized coals were 0.91 and 0.47 mg kg^{-1} respectively on a coal basis, and 8.49 and 5.44 on an ash basis.

There are two potential competing effects which will influence the relative erosion potential, viz:

- The melting of the coal minerals in the flame will tend to reduce the angularities and the aspect ratios of the harder particles, which would tend to reduce their erosiveness.
- The softer minerals, and particularly the clay mineral particles will be largely fused and transformed into harder glassy spherical particles. These particles tend to vary widely in internal porosity. A significant portion may be of high porosity and have thin walls. These will tend to contribute much less to the overall erosion rate.

For the fly ashes, the measured erosion rates were significantly higher, at 9.65 and 7.60 mg kg^{-1}, respectively. It is clear, therefore, that the erosion potentials of fly ash materials were significantly higher

than those of the corresponding pulverized coals, when expressed in units of mg of metal loss per kg of coal as erodent.

Figure 3-4: Relative Erosion Rate Data At An Impact Velocity of 40 m s^{-1}, for Two Bituminous Coals and Their Corresponding Fly Ashes, Generated In A 1 MW_{th} Combustion Test Rig. (After Wells et al. 2005)

Parameter	Coal A	Coal B
Moisture content of pulverized coal, (%)	3.9	2.9
Ash content of pulverized coal, (%, dry basis)	11.2	8.8
Erosion rate for pulverized coal, (mg kg^{-1} of coal)	0.91	0.47
Erosion rate for pulverized coal, (mg kg^{-1} of ash)	8.49	5.44
Erosion rate for pulverized coal ash, (mg kg^{-1})	9.65	7.60

The erosion potential of the fly ash was higher than that of the pulverized coal ash, when expressed in units of mg of metal loss per kg of pulverized coal ash, as erodent. This indicates that the flame imprinted characteristics of the fly ash particles result in an increase in the erosion potential compared to that of the mineral material in the parent coal, i.e. the second of the two competing effects listed above tends to have the most influence.

3.6 Predictive Modelling of the Erosion Wear Rates of Boiler Tubes

3.6.1 Erosion Models

Over the past few decades a number of researchers have been concerned with the predictive modelling of solid particle erosion at both normal and elevated temperatures. Initially, the interest was in the development of single particle erosion models, which treat the erosion process in terms of the interaction of individual erodent particles with the surface. These models are most appropriate for erosion due to dilute solid suspensions, in pneumatic conveying pipelines and elbows, heat exchanger banks or in turbine blade cascades, for instance. In these cases, the particle–particle interactions are considered to be negligible, and the erosion process involves the removal of surface material by the cumulative action of large numbers of individual erodent particles.

It should be recognized in this context that the evaluation of the velocity restitution coefficients for ash particles rebounding from an eroding surface and hence of the energy imparted to the surface, can often be problematic. This is principally because the target material surface becomes modified with time with increasing erosive wear, as the erosion scar develops. In this way, the local impact angle between an individual impacting ash particle and the eroded surface may deviate considerably from the average.

The ash particles themselves can also be irregular in shape, with some of the liberated quartz particles in coal boiler fly ashes, for instance, having relatively sharp corners. As the particles approach the target surface, their orientation is generally assumed to be random.

The erosive wear of most metals is predominantly ductile in nature, and the loss of material from the target can occur in two ways, viz:

- cutting wear, due to the impact of the particles with sharp corners at relatively low angles, and
- extrusion to form ridges, due to the impact of more rounded particles and of all particles at relatively high angles of impact.

These two mechanisms are not mutually exclusive, and the erosion wear of ductile materials can be considered as a combination of these two processes. The dominant process clearly depends on the angle of impact, and the properties of the particles and the target material, however this does make the mathematical modelling of the erosion wear process relatively complex.

The first significant and influential single particle analytical model of particle impact erosion was proposed by Finnie [8]. It was recognized that the wear of a surface due to solid particle erosion depends on the motion of the particles in the fluid, as well as the behavior of the surface when struck by the particles. The results of this work were very influential and set the basic approach for all of the subsequent single-particle models.

The principal assumption of the Finnie model is that a particle, approaching the surface of the target material at a relatively low impingement angle α, will remove material by a cutting action, in much the same way as a machine tool does. The erodent particle is assumed to be much harder than the surface, and does not break up on contact with the target. The surface material is assumed to deform plastically during the cutting process.

Finnie developed an equation of the form:

$$W = c\frac{MV^2}{\Psi_p K}\left[sin(2\alpha) - \frac{6}{K}\sin^2(\alpha)\ \right]\tan\alpha \le \frac{K}{6}$$

where W is the total volume of target material removed,
K is the ratio of vertical to horizontal (frictional) force,
Ψ is the ratio of the depth of contact to the depth of the cut.
c is a constant which allows for the fact that many particles will not be as effective as the idealized model particle;
M, is the total mass of abrasive particles,
V is the abrasive-particle velocity, and
p, the eroding surface 'flow stress'.

To obtain the mass of eroded material removed, W is multiplied by the density of the target material.

Single particle erosion models in general, and Finnie's erosion model in particular, clearly cannot be used to calculate absolute erosion rates from first principles. They are generally employed, together with estimates of the target material flow stress (or hardness), to derive a value for the particle effectiveness constant, c, to match the relevant test data. The derived values are then employed to model the effects of other process parameters on the erosion rate.

As stated above, when a particle strikes the surface of a ductile material at an angle nearer to 90°, the target material is extruded to the edge of the damage zone to form a system of ridges that will be vulnerable to subsequent impacts. The impacts of further particles cause further deformation, extrusion and work hardening, until fracture occurs and material is lost from the surface.

One of the more successful recent boiler tube erosion models was reported by Mbabazi et al. [9]. This model involves a combined erosion wear mechanism including both cutting wear and plastic deformation of the target surface to predict the erosion rate of boiler tubes as a function of the ash particle velocity, the impingement angle, the density of the target material and its tensile properties. The effect of the silica content of the ash on the erosion rate has also been investigated for various boiler grade steels at room and elevated temperature. A coal ash erosion index has been developed and employed to assess the erosion characteristics, principally of high ash South African coals.

The effect of the ash particle impact velocity and impact angle on the erosive wear of mild steel surfaces, using three different power station ash types, was measured as part of a program of experimental work, using an air jet impactors erosion test rig. The experimental data were used to calibrate a model for the prediction of erosion rates.

As described above, the model incorporates the properties of the ash particles and the target metal surface, as well as the characteristics of the ash particle motion in the form of the impingement velocity and the impingement angle. When tested using the three different types of power plant ash, the experimentally-calibrated erosion model yielded results that generally differed by less than 15% from the values that had been measured experimentally.

In very general terms, therefore, it is clear that the development of predictive models of the erosion rates of the surfaces of convective pass boiler tubes by fly ash particles from first principles has proved to be difficult. It has been recognized that, at the metal temperatures that apply in boilers, the corrosion rates of the metal surfaces will be significant and the rates of metal loss are likely to be significantly higher than those predicted by erosion models alone. This has led from the 1980s onwards to the development of physical descriptions and mathematical models of the erosion-oxidation and erosion- corrosion processes.

3.6.2 Erosion-Corrosion Models

As discussed above, at the elevated gas and metal temperatures that apply in the convective sections of coal-fired boilers, there is also the possibility of significant oxidation or corrosion of the metal surface by the hot flue gases, which contain the acid gas species SO_2, SO_3 and HCl at modest but significant concentrations in addition to oxygen. This can have a significant impact on the rate of metal loss. This depends on the corrosion/oxidation kinetics of the system, i.e. the metal surface temperature and the tube material, the particle flux and velocities, the nature of the surface and the erodent particles. The kinetics of the overall erosion-corrosion process also depends on the growth rate and properties of the oxide/corrosion product layer, and in particular whether it is eroded faster or slower than the parent metal.

The following basic scenarios can be identified:

- In situations where the corrosion rate is low and the oxide/corrosion product scale is very thin, the metal loss is clearly dominated by the rate of the erosion process. The principal impact of the presence of an oxide film is on the nature of the eroding surface, i.e. whether or not the corrosion product layer is eroded more quickly than the metal. The metal loss rate is relatively insensitive to increases in temperature, and depends mainly on the particle velocities and on the properties of the base metal and the erodent particles. This regime will apply in the main with all materials at low temperatures and with corrosion-resistant materials at higher temperatures. The modelling of this type of behavior will be based on the existing erosion models, suitably modified to take into account the effects of the presence of the thin oxide layer.
- As the temperature increases and the corrosion/oxidation rate increases, the erosion rate is increasingly affected by the formation and removal of the oxide scale, i.e. there is oxide-modified erosion. In this case, the processes are relatively complex and the metal loss rate is dependent on

the properties of the composite oxide/substrate, the ease with which the scale is removed and the oxidation kinetics.

- When the oxide forms sufficiently quickly and is thick enough that the impact of particles does not expose the base metal, only oxide is removed during impacts and the process is oxidation dominated. The erosion process continuously reduces the oxide thickness and this has the effect of increasing the oxidation rate, i.e. there is erosion-enhanced oxidation

The conditions under which these scenarios apply depend, therefore, on a number of factors, which include the temperature and gas composition, the particle size, velocity and flux of the erodent, the composition of the alloy, etc.

In a key experimental and theoretical paper of direct relevance to boiler applications, Xie and Walsh [10] reported the results of a study of the erosion of carbon steel by ash and unburned char particles from coal combustion in the convection section of an industrial boiler. The ash and carbon particles were accelerated toward the surface of the test coupons by the action of a nitrogen/oxygen jet. The key experimental variables were:

- particle velocities,
- surface temperatures over the range 450-650K and
- oxygen content of the jet.

The average erosion rate was determined by measurement of the maximum depths of the surface profiles of the erosion scars.

They found that the rate of metal loss by erosion was lowest at low temperatures, regardless of the oxygen concentration. The measured erosion rate was also low under strongly oxidizing conditions, i.e. at high temperatures and high oxygen concentrations. The measured erosion rate was highest at high temperature in the presence of very low oxygen concentration.

The authors presented a model of the simultaneous particle impact erosion and oxidation of carbon steel, which provides the basis for evaluation of the erosion rate coefficients and the estimates of erosion rates at lower gas velocities, in the absence of the accelerating jet. In this model, the following assumptions apply:

- The metal was assumed to undergo ductile erosion, at a rate increasing with increasing temperature.
- The surface oxide scale was assumed to be strongly attached to the metal, and to undergo brittle erosion at a rate independent of temperature.
- The oxide and metal were assumed to be removed in proportions depending upon their relative resistance to erosion and the thickness of the scale.

Over most of the range of temperature investigated, the oxide scale was more resistant to erosion than the carbon steel substrate. The presence of the oxide had little influence on the erosion rate at low temperatures, where the erosion rate of the metal was also low. The oxide layer contributed most to erosion resistance at high temperatures and at high oxygen concentrations, i.e. conditions which resulted in an increase in the metal oxidation rate coefficient and the thickness of the oxide scale. When the scale thickness decreased, the erosion rate tended to increase as the particle impacts began to penetrate the oxide and remove metal as well.

The following parameters were adjusted to fit the model to the measurements:

- erosivity of the particles toward the metal,

- erosivity of the particles toward the oxide,
- effective order of the metal oxidation process with respect to the oxygen concentration, and
- average area of scale removed by a single impact.

Using the values for the key process parameters which provided the best fit for the accelerated erosion measurements, the dependence of the erosion rate on the particle velocity was calculated for a typical set of coal combustion and boiler convection section conditions. The results indicated that the onset of the transition from oxide-to metal-controlled erosion, where the rate of tube wastage begins to increase rapidly, was predicted to occur at velocities around 16 m s^{-1} for collision at an angle of 90° and at velocities around 25 m s^{-1} for collision at angles near 30°.

In an important paper published in the mid-1990s, Wright et al. [11] described the development of models of the erosion-oxidation process. They indicated that there had been progress toward developing a capability for predicting the service life of metals subjected to high-temperature erosion-oxidation conditions. In general, the view was that the pace of the advances in the modelling work has been slow, and that this is a result of the number of variables that require consideration, and the limited knowledge of the interactions between erosion and oxidation in many of the erosion-oxidation processes that are of practical importance.

The approach to the modelling of these processes, which is presented in the paper has been shown to be capable of describing relatively simple erosion-oxidation interactions, and is intended to form the basis for the incorporation of more realistic scenarios, as required. They present a description of the erosion-oxidation processes which indicates that the rate of material loss under such conditions is likely to be significantly greater than for erosion alone. Most of the material loss, when there is an oxide layer of significant thickness, will be due to the exfoliation and shedding of the oxide scale rather than by the cutting or abrasion of the parent metal surface. The erodent particle kinetic energy required to cause this form of material loss is likely, in most cases, to be lower than that required for metal loss by erosion alone.

An innovative approach to the description of the erosion-oxidation of an alloy in a high-temperature oxidizing environment is presented. This approach involves the combination of the major parameters that determine the oxidation behavior of the alloy and the "erosion potential" of the environment in a way that preserves the observed nature of the mode of metal loss. The oxidation component is treated deterministically, while the erosive component is treated statistically because of the random nature of erosive particle impacts.

The oxidation process is described using a simple power law expression of the form:

$$S = kt^n$$

where: S is the oxide scale thickness
t is time, and
k and n are parameters dependent on the nature of the oxidation process.

The statistical approach is described in detail in a previous publication by Markworth [12]. It is assumed that particle impact erosive wear produces a characteristic footprint on the oxidizing surface. The nature of this footprint can be selected and described in a number of ways depending on the plant experience or experimental observations. The simple example presented in the paper involves the assumption that each erosion event results in the removal of all of the oxide scale within a given radius of the site of the particle impact. More complex footprints can be applied, for specific applications.

The combination of the oxidation and erosion processes to provide a description of the kinetics of the coupled erosion-oxidation process is achieved by the application of Poisson processes.

The authors were of the view that this approach provides a workable framework for the incorporation of erosion and oxidation parameters in a manner that is flexible and can be consistent with observed experience of the erosion-oxidation processes.

Das [13] reports the results of work on the development of models to describe the mechanisms of coal fly ash erosion of boiler components, covering the following key effects, viz:

- effect of cutting wear,
- effect of plastic deformation wear and
- effect of temperature

on the rates of fly ash particle impact erosion wear.

The modelling methodology employed for this work was very much influenced by the work of Wright et al. [11], i.e. they employed a simple power law relationship to describe the oxidation rates of nickel, iron and chromium oxide scales. The concept of the erosion footprint, as described briefly above, was also employed. It was considered that this methodology provides a quantitative predictive framework for the study of the effect of the fly ash characteristics, and in particular the silica content in the ash particles on the erosion potential.

The effects of particle impact velocity, angle of impingement and variation of surface temperature of the substrate were studied as a function of silica content in the ash. The model has been employed to predict the erosion rates at room and elevated temperature for various grades of steels under different particle impact conditions. The model predictions have been found to be in good agreement with the previously published data.

3.7 Boiler Design Methods and Design Features to Minimized Erosion

The first requirement for boiler design methods to minimize the problems associated with particle impact erosion is for a methodology which can characterize the erosion potential of coals and ashes, based on the kind of information that is normally available during the proposal stage of a boiler project, i.e.

- A design method which can provide a ranking of the erosion potential of a coal, based on the basic data provided in the fuel specification.
- Laboratory methods for the characterization and testing of small samples of coal or of fly ash, when available.

More advanced coal and ash characterization methods are available and may be required for research work or for investigations of specific incidences of erosion or erosion-corrosion processes. These methods are, however, outside the scope of this document.

Clearly, to a first approximation, the erosion potentials of a coal and the associated fly ashes will be related to the ash content of the coal, and the erosion rate will generally be a linear function of the pulverized coal or fly ash flux to the target material. On average, this will be a directly related to the ash content of the coal, although there will be localized flue gas flow effects which can have significant effects on the local gas velocities and particle fluxes.

There have also been many reports that the quartz content of the pulverized coal and of the fly ash can have a major influence on the erosion process. The quartz particles in fly ashes tend to have relatively high particle densities. They may not be completely fused in the flame and can have relatively sharp edges. These properties are also dependent on the combustion conditions.

The quartz contents of fly ashes vary widely between coals, and are not very easy to quantify accurately without using fairly sophisticated particle characterization techniques.

The quartz content of a coal ash can, however, be inferred roughly by assuming that the clay minerals have a SiO_2:Al_2O_3 mass ratio of 1.5, and that all of the alumina content is in the form of clay mineral material. This means that the balance of the SiO_2 in the ash is in the form of quartz.

Historically, the most commonly used fly ash erosion index within the industry [14] recognizes that the erosive wear on boiler pressure parts is primarily due to the fly ash particle size fraction greater than 45 µm in diameter.

The relative coarseness of fly ash materials can be graded into three categories:

- fine fly ash with 15% of the fly ash greater than 45 µm,
- coarse fly ash having 30% >45µm and
- exceptionally coarse fly ash having 50% >45 µm fraction

The fly ash erosion index is:

$$I_a = 0.44\ x_1\ (SiO_2 - 1.5\ Al_2O_3) + 0.18\ (SiO_2 - 1.5\ Al_2O_3) + 0.35\ x_1 + 0.14$$

where x_1 is the fly ash fraction > 45µm

The associated fly ash erosion potential classification is as follows:

<0.2	marginally erosive
0.2-0.4	moderately erosive
0.3-0.4	highly erosive
>0.4	exceptionally erosive

The Index is based on the calculation of the silica content of the fly ash from the ash composition, using the assumption that the average mass ratio of SiO_2:Al_2O_3 is around 1.5, as described above. This means that the silica content of the ash can be expressed as $SiO_2 - 1.5\ Al_2O_3$, where SiO_2 and Al_2O_3 are the total weight percentages of these species in the coal ash.

Also contained within this index is an assumption that 50% or so of the quartz in the parent coal survives the flame as liberated particles, without fully melting or coalescing with the alumino-silicate and other ash particles.

In the absence of specific information about the size distribution of the fly ashes, a very simple erosion index based solely on the total quartz content of the coal can be applied, with the quartz content of the ash estimated using the simple calculation described above.

The fly ash erosion potential classification applied in this case, would be:

< 2% quartz in coal	low
2-3% quartz in coal	medium
3-5% quartz in coal	high
>5% quartz in coal	severe

This type of index is employed fairly widely within the industry to provide a relatively crude assessment or ranking of the erosion potential of the coal ash based on data available in most fuel specifications. This type of ranking can be used to define the allowable average flue gas velocities, and the heat exchange tube cross pitches throughout the heat transfer banks, in the boiler convective pass to avoid excessive erosion.

In general terms, during the boiler design process, the average flue gas velocities for the convective pass tube banks are selected to maintain the erosion wear rates of the boiler tubes to acceptable levels, i.e. less than 20 nm h^{-1} or so, which is equivalent to a metal loss of around 2 mm over 100,000 hours of operation. In most cases, except for very low ash, benign coals, the average flue gas velocities will be less than 20 m s^{-1}. For the majority of bituminous steam coals with normal ash levels and moderate erosion index values, average flue gas velocities less than around 15 m s^{-1} are more commonly applied. For coals with higher ash contents and more erosive ashes, average flue gas velocities less than around 10 m s^{-1} may be required to avoid excessive erosion rates.

As stated above, it is commonly the case, however, that the incidence of particle erosion wear damage is highly localized. The non-uniform air and flue gas flow patterns and the non-uniform fuel and ash particle distributions that apply in most boilers result in localized regions of high flue gas velocities and high particle fluxes. It is also commonly the case that the distortion of the tube banks and other boiler components with time, and the formation of ash fouling deposits on the surfaces of the convective bank tubes, can lead to restricted flow in some regions, and localized regions of relatively high gas velocities and hence higher erosion wear rates.

Excessive levels of ash fouling, with significant ash bridging across the convective pass gas channels, can result in very high flue gas velocities through the channels that remain open, and very high localized erosion wear problems. The most obvious response to problems of this type is to get the ash deposition problems under better control, by fuel switching or other operational means or by improving the on-line cleaning systems.

The lead and other tubes in convective tube banks are also subject to erosive wear due to action of the soot blowers. These devices normally employ high velocity jets of steam, air or water to break up and dislodge the ash deposits that tend to accumulate on boiler surfaces. There is a tendency for the soot blower jets to entrain significant levels of flue gas and ash particles which are accelerated towards the boiler surfaces at high velocity.

The suppliers of this type of on-line cleaning equipment are well aware of these issues, and have long experience of avoiding potential erosion problems of this type. The design and the location of the soot blower systems are intended to maximize their cleaning efficiency without excessive erosive wear of the soot blowers themselves or of the boiler components.

In most cases, the instances of excessive erosion due to soot blower usage are associated with the overuse of the on-line cleaning systems, particularly when there are severe ash deposition problems, or with poor soot blower operation and maintenance.

The relatively wide variability of the flue gas velocities and fly ash particle fluxes that apply in most boilers means that local erosion rates can vary dramatically and the protection of some regions of the convective pass using baffles, vanes and other devices to redirect the flue gas flow, and reduce the high localized velocities and particle fluxes, can be very effective.

An illustration of some of these design features that are commonly applied by experienced boilermakers is presented in Figure 3-5: A Sketch of the Part of the Convective Section of the Boiler and Illustrations of a Number of Erosion Protection Features. The following design details are featured:

- The installation of sacrificial erosion shields to provide protection of the lead vertical and horizontal tubes in a convective bank,
- The use of sacrificial erosion shields to protect the installed convective section soot blowers,
- The use of sacrificial barrier plates or inclined perforated plates to divert the flue gas flow or to protect the tube bends.

These design features are commonly custom-designed to protect particularly vulnerable areas in the convective banks. It is obviously necessary when diverting the flue gas flow to avoid causing further erosion problems downstream of the baffles and shields. This may require the use of diagnostic techniques to characterize the flow of the flue gas and particles in what can be quite complex geometries.

3.8 Diagnostic Methods

In this context, the use of a number of physical and computer modelling techniques is becoming more widespread within the industry, to investigate specific boiler features, viz:

The use of cold air flow measurements in selected regions within the convective section of the boiler;

- use of physical air or water flow modelling of the boiler geometry at smaller scale, or
- use of computerized fluid dynamic (CFD) modelling.

These techniques are employed to characterize the regions of high flue gas velocities and to help identify the best locations and orientations of the proposed baffles, shields and vanes.

A recent application of this approach in India, where fly ash erosion is a major cause of boiler tube failures, was reported by Dhamangaonkar et al. [15]. The main cause of the failures is the localized increase in the velocity of flue gases and fly ash particles, and of the particle flux levels.

The objective of the work was to investigate the use of flow modification in conjunction with a cold air velocity test before and after modification. The methodology employed in this work was based on the EPRI Guideline document [16], which has been published recently, and which provides a step-by-step procedure for cold air velocity testing (CAVT) in large coal-fired utility boilers.

Figure 3-5: A Sketch of the Part of the Convective Section of the Boiler and Illustrations of a Number of Erosion Protection Features

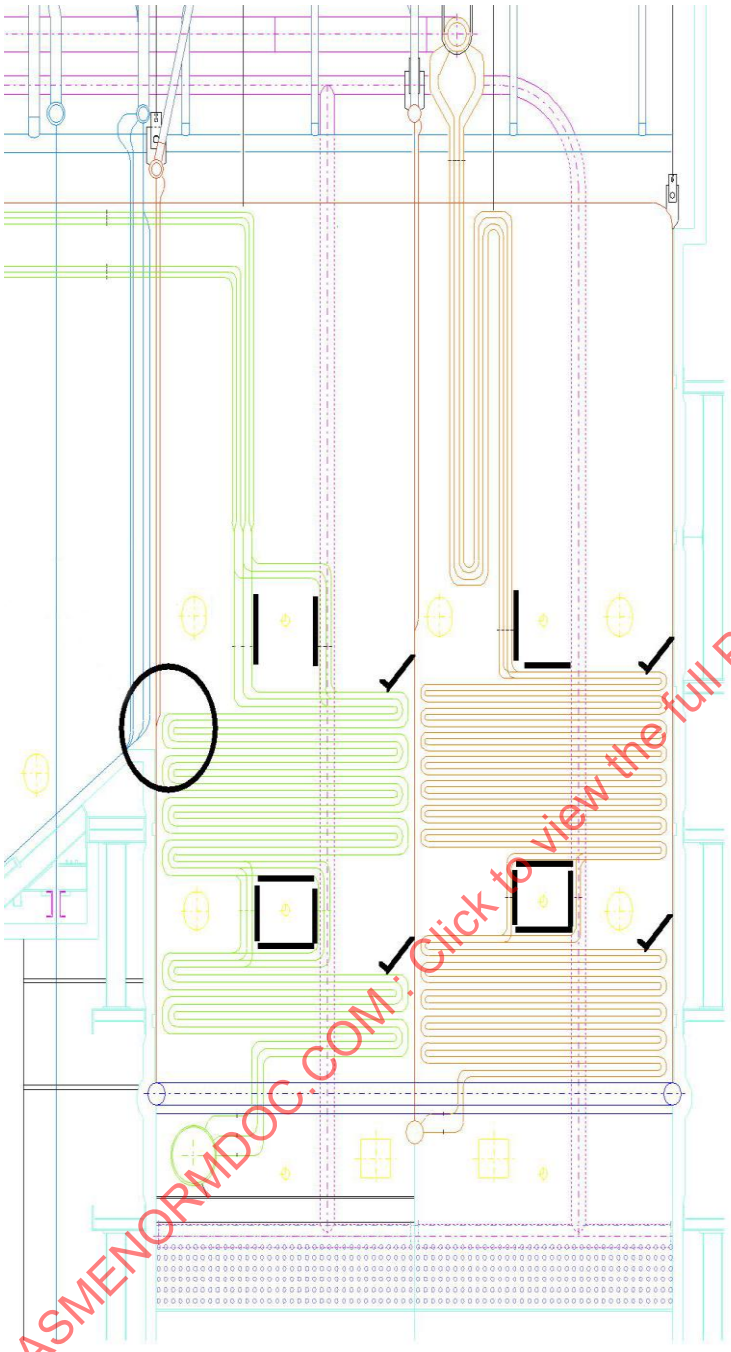

(a)

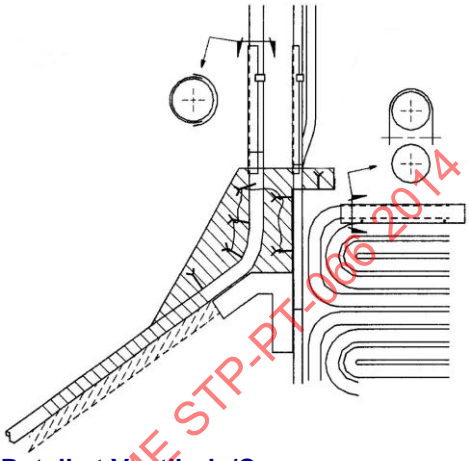

(b)

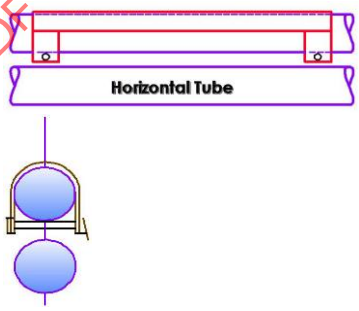

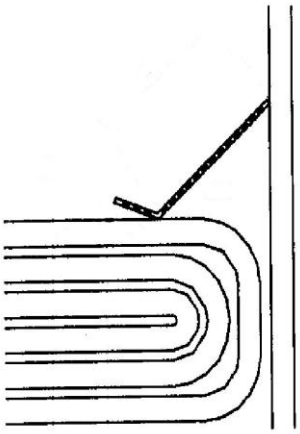

(c)

(a) Erosion shields on lead vertical and horizontal tubes
(b) Soot blower shields
(c) Barrier plates and inclined perforated plates to protect tube bends

In the work reported by Dhamangaonkar et al. [15], the cold air velocity techniques (CAVT) were employed to determine the local velocity profiles across various pressure parts in the convective section of a 210 MW_e boiler in India, principally to identify regions of excessive velocity. The results can be employed to assist with the design and location of diffusion and distribution screens, may provide utilities with the most optimum solution to the problem.

The authors also tried to predict the measured Cold Air Velocity levels using CFD methods. The geometry of the flue gas path of the boiler was modelled using Pro-E, meshed using GAMBIT and imported in FLUENT for analysis. The results obtained were then compared with the experimental data from the CAVT work to validate the model.

For the purposes of comparison, the points where the CAVT were performed were replicated in the CFD model. It was considered that the results of the CFD simulation were in relatively good agreement with the experimental results of CAVT, with error levels of the order of ±23 %.

There has been significant interest within the industry in recent years in the utilization of computational fluid dynamic (CFD) modelling for the study of flue gas and fly ash particle flow and ash particle impact erosion processes. In a recent paper, Ghandi et al [17] reported the results of the use of FLUENT, in conjunction with an erosion model to provide estimates of the erosion rates in selected locations within a large, 330 MW_e coal-fired utility boiler.

The flue gas flow throughout the boiler furnace and convective pass were characterized in terms of the flue gas velocities and temperatures, and individual fly ash particle tracking was applied. The boiler convective pass was modelled as a series of identical parallel plates rather than as tube bundles.

The particle sizes distributions, trajectories and velocities were employed to provide estimates of the erosion wear rates, making use of the erosion model developed by Mbabazi (2004), which is described briefly in Section 3.6 above. The effects of the particle velocities, the particle trajectories, the flue gas temperature distribution, the particle impact angle and the silica content of the ash were studied in detail.

The authors indicated that the predictions of the rate of erosion wear at selected locations were found to agree reasonably well with published data and plant observations, with fly ash particle impact velocities over the range 15-32 m s^{-1}.

3.9 Conclusions and Summary

In this section of the document, an attempt is made to provide a summary of the key technical issues associated with the ash particle impact erosion wear of the heat exchange tubes in the convective sections of large pulverized coal utility boilers. In most countries, this has been one of the most important causes of the loss of availability of coal-fired boilers. In countries such as South Africa and India, where coals with very high ash contents are fired, the impact of the high ash levels is the single most important technical problem encountered by the designers and operators of coal boilers and the associated equipment.

The intention is to provide boiler design engineers and other industry professionals with an introduction to more important technical aspects of the subject, and to provide some key references from the technical literature for further study.

A basic definition of erosive wear is provided, and the key areas of damage in coal-fired boilers and the principal causes of boiler tube failures have been identified. The basic nature of the erosion process and the dependence on the nature of the particles and the target surface, on the particle flux, and on the velocity and angle of impact are described.

In addition to site investigations of specific instances of wear, the key experimental approaches to the study of erosion are described briefly. Some guidance as to the available means of the assessment of the erosion potential of coals and ashes, using both standard and more advanced characterization methods is provided. The results of some recent results obtained using a combination of experimental test work in an air jet erosion rig, and advanced scanning electron microscope (SEM) characterization of the erodent particles, are discussed. The ash-forming processes that occur in coal flames and their effect on the relevant properties of the parent coal and the resultant fly ashes are described.

A very brief and selective summary of the fairly extensive technical literature on the predictive modelling of particle impact erosion and erosion-oxidation/corrosion processes is provided. It is fair to say that these modelling techniques are not yet capable of providing accurate estimates of erosive wear from first principles. The physical models and simplifying assumptions are still fairly crude and there is a need for significant 'tuning' of empirically derived parameters to take into account the fuel, site and location specific factors. The combination of CFD modelling with erosion or erosion-corrosion modelling does potentially provide a fairly powerful means of studying and possibly modelling these processes, and providing practically useful advice to design engineers and operators on the modification of the local flue gas flow patterns to minimized erosive attack.

Some basic aids to boiler designers based on relatively simple assessments of the erosion potential of coals and ashes, and on the approach to the control of erosion based on limitation of the average flue velocities across a tube bank and the protection of particularly vulnerable areas by the use of shields and baffles are provided. More advanced methods using cold air velocity measurements in boilers and CFD modelling of the flue gas flow patterns are also described.

3.10 References

[1] Dooley, B. and Chang P. S., 2000, "The current state of boiler tube failures in fossil plants." Power Plant Chemistry Vol. 2, 197-203.

[2] Raask E., 1979, "Impact Erosion Wear caused by Pulverized Coal and Ash." Conf. on Erosion by Solid and Liquid Impaction. Paper 41, Univ. Cambridge.

[3] Patel, D., 1968, "Erosion Process as influenced by Surface Hardness". M.Sc. Thesis, Washington State University.

[4] Evans, A. G., Gulden, M. E. and Rosenblatt, M., 1978, Impact Damage in Brittle Materials in the Elastic-plastic Regime. Proc. Roy. Soc. London, Ser. A, 361, 343.

[5] Gulden M. E., 1979, "Solid Particle Erosion of High Technology Ceramics", Erosion: Prevention and Useful Application. Ed. W F Adler, p. 101, ASME STP 664.

[6] Raask E,. 1988, "Erosion Wear in Coal Utilization." Hemisphere.

[7] Wells, J. J., Wigley, F., Foster, D. J., Livingston, W. R., Gibb, W. H., and Williamson J., 2005, "The Nature of Mineral Matter in a Coal and the Effects on Erosive and Abrasive Behavior. Fuel Process Tech. 86, 535-550.

[8] Finnie I., 1960, "Erosion of Surfaces by Solid Particles." Wear Vol. 142 pp. 87-103.

[9] Mbabazi J. G., Sheer T. J. and Shandu R., 2004, "A Model to Predict Erosion on Mild Steel Surfaces Impacted by Boiler Fly Ash Particles", Wear, Vol. 257, pp. 612-624.

[10] Xie J. and Walsh P. M., 1995, "Erosion-corrosion of Carbon Steel by Products of Coal Combustion, Wear, Vol. 186-187, pp. 2560265.

[11] Wright I. G, Sethi, V. K. and Markworth A. J., 2011, "A Generalised Description of the Simultaneous Processes of Scale Growth by High Temperature Oxidation and Removal by Erosive Impact. Proc. of the World Congress on Engineering Vol III London, U.K.

[12] Markworth A. J., 1992, "A Stochastic Model for the Simultaneous Occurrence of Oxidation and Erosion." Mat. Sci. Eng. A150 pp. 37-41.

[13] Das S. K., 2011, "Application of a Stochastic Modelling Framework to Characterise the Influence of Different Oxide Scales on the Solid Particle Erosion Behavior of Boiler Grade Steel." Sadhana Vol. 36, pp. 425-440.

[14] Raask E., 1985, "Mineral Impurities in Coal Combustion," Hemisphere.

[15] Dhamangaonkar P. R., Kajale S. R., Nandgaonkar M. R., Abhishek Deshmukh, Aditya Deshmukh, and Swaroop Thakur, 2011, "Use of Cold Air Velocity Test (CAVT) to Locate Erosion Prone Zones in Pulverized Coal-fired Utility Boiler. Proc.of the World Congress on Engineering Vol III, London, U.K.

[16] EPRI, 2011, "Guidelines for Control and Prevention of Fly Ash Erosion" EPRI Report No. 1023085.

[17] Ghandi M. B., Vuthaluru R., Vuthaluru H., French D. and Shah K., 2012, CFD-based Prediction of Erosion in a Large Wall-fired Boiler. Appl. Thermal Eng. Vol. 42, pp. 90-100.

4 OXIDATION - THE STEAM-SIDE OXIDATION OF BOILER TUBES

4.1 Introduction

It has long been appreciated that thin oxide scales form on the steam-touched surfaces of boiler tubes, and that typically these scales exhibit good adherence, relatively slow growth rates, and uniformity of thickness. These attributes are the basis of the use of thickness measurements of these scales for the 'oxide dating' technique [1]. The measured oxide thickness values, combined with knowledge of the oxide growth kinetics, are used to infer the average temperature, over the time taken to grow the oxide at a given location. From these data, and in conjunction with fireside corrosion rates and established material creep-rupture properties, the remaining creep life of the tube can be inferred.

Although both fireside and steam-side corrosion result in the loss of thickness of the tube wall, the loss on the steam-side has historically been significantly less than on the fireside. The progressive increase in the final steam temperatures in power boilers over the past few years has resulted in an expected, exponential increase in the rate of growth of steam-side scales. As the steam temperature approaches 602°C (1115°F), the thicknesses of steam-side scales become a significant consideration.

In addition to tube wall section thinning, increased oxide thickness contributes to decreased thermal conductivity, which in turn leads to higher metal temperatures, and faster-growing oxide scales. The implications for tube life of increasing metal temperatures are a reduction in the available creep strength combined with an increased rate of reduction in load-bearing section.

Another important issue associated with the increased rate of growth of steam-side oxide scales is the tendency for exfoliation or delamination of all or parts of the scale thickness. Delamination on the lower chromium steels, without loss of scale, can result in an increase in the rate of oxide growth, thicker scales, and increased temperature gradients. Delamination without loss of scale on the ferritic-martensitic steels can lead to the formation of large blisters in the scale, which may contribute to localized decreases in thermal conductivity through the tube wall, resulting in localized overheating.

Periodic loss of separated scales by exfoliation, often during rapid thermal transients in boiler operation, can lead to the development of deposits, often at U-bends in superheater tubes that may, in turn, restrict steam flow and initiate overheating. The transport of flakes of exfoliated scale in the steam also can lead to erosion of the steam turbine and of valves and steam drain lines [2].

With increasing steam temperatures metal loss from steam-side oxidation can become sufficiently rapid that its potential to reduce the load-bearing capability of higher-temperature heat exchanger tubes in steam boilers must be considered. It is important for boiler designers and operators to understand and to be able to quantify the key factors involved in steam-side oxidation.

The aims of this section of the document are:

- To describe the current understanding of the steam-side oxidation processes on the alloy classes used in steam boilers.
- To demonstrate how the loss of tube metal thickness is related to, and can be measured from, the morphology of the oxide scales produced.
- To compile the available experimentally-determined scale thickness and morphological data considered applicable to determining the loss of tube metal thickness due to steam-side oxidation.
- To describe the basic features of a model intended to analyze the experimental data and provide the best available predictions of scale thickness variation with boiler operating parameters.

- To present the output of this model, to enable the determination of the tube metal thickness loss from steam oxidation for given alloys and boiler operating conditions and to provide examples for each class of alloys considered.

4.2 Basic Concepts of High-Temperature Oxidation in Steam

The reaction of metals with steam is an oxidation process that results in the development of scales made up of the same individual oxide phases that are formed by oxidation of the same alloy in air. The oxidants in steam are O^{2-} and OH^-, compared to only O^{2-} in air, and this leads to differences in the compositions and morphologies of the resulting scales. Similarly, there are differences between the scale morphologies formed in steam and those in air-water vapor mixtures that are used sometimes in laboratory simulations [3].

These differences can have a significant influence on the composition, properties and growth kinetics of scales produced, and a large body of laboratory research has been devoted in recent years to exploring these factors [4]. Good progress has been made in understanding the effects of the major variables. The resulting trends and insight gained from this body of research are described in the following sections.

The basis for understanding the high-temperature oxidation behavior of alloys in gaseous environments has been fully described in numerous standard texts [5][6][7][8][9]. A short summary of the salient issues, after Wright [4], is presented in this section.

4.2.1 Oxide Stabilities

The high-temperature oxidation behavior of alloys in an oxidizing gaseous environment, starting with exposure of a clean alloy surface to the oxidizing gas, initiates with reactions to form all of the oxide compounds that thermodynamic considerations indicate are stable under the prevailing conditions. A convenient compilation of thermochemical data relevant to high-temperature oxidation has been presented by, for instance, Kubaschewski and Alcock [10]. The thermodynamic stability of the oxide is expressed in terms of the oxygen partial pressure at which it dissociates, which is derived from the basic oxidation reaction.

4.2.2 Oxidation in Oxygen

A simple example of a high-temperature oxidation reaction involves metal (M) and oxygen reacting to form the oxide M_aO_b

$$aM_{(s)} + b/2O_{2(g)} = M_aO_{b(s)} \quad (4.1)$$

under conditions where the effective oxygen partial pressure of the gas (pO_2) is greater than that required for the oxide to be stable or, for the reverse reaction, below which it dissociates, [$(pO_2)_{dissoc.}$].

The value of the prevailing oxygen partial pressure (pO_2) in the gas depends on the total gas pressure (P) via:

$$pO_2 = (\text{moles } O_2/\text{total moles in gas})P \quad (4.2)$$

and the oxide is expected to form if $pO_2 > (pO_2)_{dissoc.}$

The value of $(pO_2)_{dissoc}$ is obtained from the equilibrium constant for the reaction shown in equation (4.1) ($k_{4\text{-}1}$) via:

$$Log_{10}k = Log_{10}\left[p(O_2)^{\frac{b}{2}}_{dissoc}\right] = \frac{-\Delta G^0}{(2.303RT)} \quad (4.3)$$

where: $\Delta G^0_{4\text{-}1}$ is the Gibbs free energy for the reaction;
R is the Universal Gas Constant; and
T is the reaction temperature (K).

Values of $\Delta G^0_{4\text{-}1}$ are available from standard tables, e.g.as in Kubaschewski [10].

4.2.3 Oxidation in steam

In pure steam, it is assumed that the oxygen required to drive the oxidation process is generated by dissociation of the steam via:

$$H_2O_{(g)} = H_{2(g)} + \tfrac{1}{2}O_{2(g)} \tag{4.4}$$

and the effective oxygen partial pressure in the steam, $(pO_2)_{st}$, is obtained from:

$$k = \frac{[(pO_2)_{st}{}^{0.5}(pH_2)]}{(pH_2O)} \tag{4.5}$$

where $k_{4\text{-}4}$ is the equilibrium constant for dissociation of steam, and is related to the free energy of the dissociation reaction, $(\Delta G^0_{4\text{-}4})$, via:

$$\mathrm{Log}_{10}k = \frac{-\Delta G^0}{(2.303RT)} \tag{4.6}$$

And:

$$(pO_2)_{st} = (\frac{k}{2})^{2/3}P^{2/3} \tag{4.7}$$

Thus, equations (4.6) and (4.7) provide the basis for calculating the equilibrium dissociation oxygen partial pressure for steam over a range of temperatures and pressures.

The equilibrium values of $(pO_2)_{st}$ calculated for temperatures in the range 550 to 700°C (1022 to 1292°F), over a range of total pressures representing typical applications:

- reheater (20 bar/290 psi);
- superheater/subcritical steam (165 bar/2,395 psi);
- superheater/supercritical steam (241 bar/3,500 psi); and
- superheater/ultra-supercritical steam (345 bar/5,000 psi),

are listed in Figure 4.1.

The values for 1 atm/1 bar illustrate that the oxygen levels available from steam under conditions often used in laboratory testing are notably higher than at typical plant pressures, and consequently may have some effect on both oxidation kinetics and scale morphology. These differences may account for some of the discrepancies between laboratory and field observations of scale growth.

While for a given temperature the effective oxygen partial pressure in the steam increases, and its oxygen content decreases, with increasing total steam pressure, both sets of values increase with increasing temperature. This trend has implications for changes in oxide growth rates with increasing temperature, and issues such as chromium volatilization under advanced steam conditions [11].

Figure 4-1: Partial Pressures of Oxygen from the Dissociation of Steam

Temperature (°C)	Total Pressure (bar)	$Log_{10}(pO_2)_{st}$ (atm)	O_2 content (ppb)
550	1	-8.75	2
	20	-7.88	0.7
	165	-7.28	0.3
	241	-7.17	0.3
	345	-7.07	0.3
600	1	-8.16	7
	20	-7.29	3
	165	-6.68	1
	241	-6.57	1
	345	-6.47	1
650	1	-7.62	24
	20	-6.75	9
	165	-6.15	4
	241	-6.04	4
	345	-5.94	3
700	1	-7.17	72
	20	-6.27	27
	165	-5.67	13
	241	-5.56	12
	345	-5.46	10

4.2.4 Application to Fe-Cr-Based Alloys

For Fe-Cr-based alloys, in the absence other alloying elements, there are five possible oxides that can form in steam, i.e.

Fe_2O_3, Fe_3O_4, FeO, Fe-Cr spinel, and Cr_2O_3.

Oxides of other elements present in the alloys as strengthening additions or impurities, notably Mn and Si, also will form but for simplicity their roles are not considered here. FeO (wüstite) is stable only above approximately 550°C/1022°F, and in practice the exact value of this temperature changes slightly with alloy Cr content. On cooling back through this temperature, any FeO in the scale will transform to Fe_3O_4 and finely-divided Fe [12].

The Fe-Cr spinel has a variable composition, represented as $FeFe_{2-x}Cr_xO_4$, in which increasing the Cr level leads to reduced ionic transport, hence reduced rate of scale growth.

The relative stabilities of these oxides are presented in Figure 4-2. It can be seen that the oxide stability values can be seen to increase with decreasing $(pO_2)_{dissoc.}$. These curves also suggest the order in which layers of these oxides are expected to be located in a mature oxide scale under equilibrium conditions, with the most thermodynamically-stable oxide, in this case Cr_2O_3, chromia, next to the alloy.

These data also indicate that the values of $(pO_2)_{dissoc.}$ for all the oxides are much lower than $(pO_2)_{st}$ at 241 bar, indicating that all the oxides are expected to be stable and to form in steam. Similarly, all the oxides would be expected to form in air at 1 atm., where $\log_{10}pO_2$ is approximately 0.7 atm.

Figure 4-2: The Stability of the Oxides of Interest as a Function of the Oxygen Partial Pressure (pO2) and Temperature

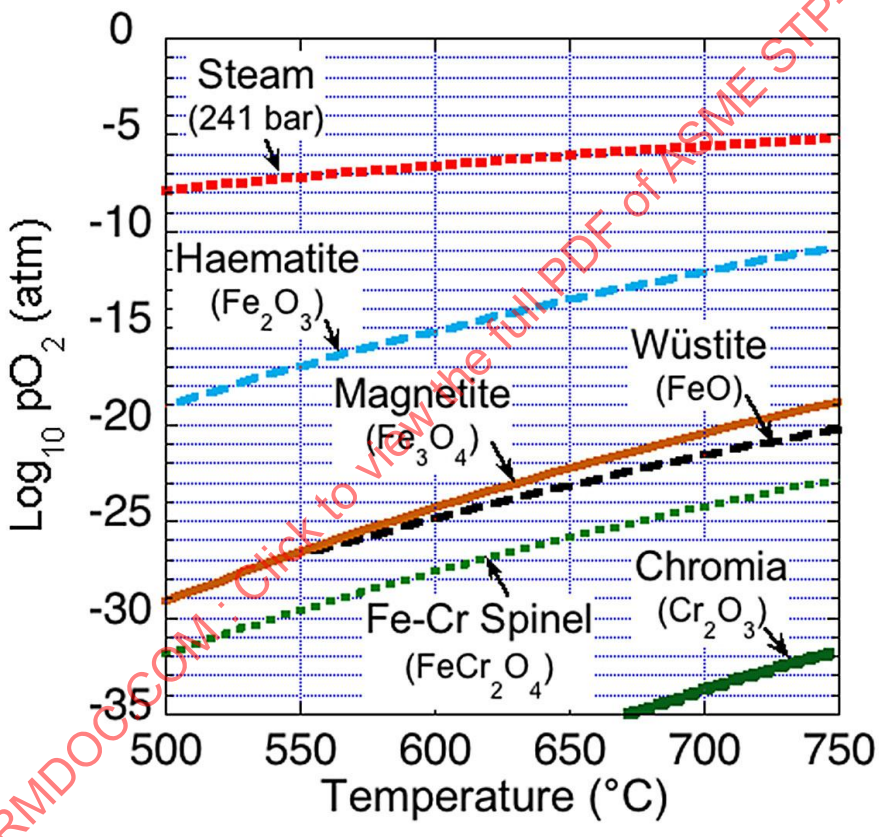

The relative quantities of each oxide formed initially on the alloy surface depend on the concentration of the elements in the alloy and of the oxidizing species in the gas. The rates at which the oxides grow depend on their ionic lattice structure.

This means that the alloy composition, i.e. the Cr content, plays an important part in determining the oxidation behavior. In particular, the incorporation of Cr in the Fe_3O_4 lattice to form a Fe-Cr spinel reduces the diffusion rate of metal ions significantly, with increasing Cr levels exerting larger effects. Consequently, relatively small changes in the Cr content of the alloy will significantly influence the rate of overall scale growth, as well as the scale morphology.

4.2.5 Development of an Oxide Scale

The schematic diagrams presented in Figure 4-3 and Figure 4-4 below, are intended to show that, although the same series of oxides make up the scale formed on a given alloy in air (oxygen) and steam, the morphologies of those scales can be different in ways that affect not only their rate of growth, but also their overall properties.

While the fully-developed scales formed in air, oxygen, or steam on simple Fe-Cr alloys have a similar, double-layered structure, it is suggested in Figure 4-2 that those formed in air grow almost exclusively outward from the metal surface. In Figure 4-3 it is suggested that in steam there is both outward and inward growth, resulting in the boundary between the inner and outer scale layers being coincident with the original alloy surface.

When the inward-growing inner oxide layer formed in steam remains adherent to the alloy, measurement of the thickness of remaining inner layer can be considered to provide an acceptable value for the thickness of metal lost due to the oxidation process. This is the case even where the outward-growing outer layer of scale may be lost due to exfoliation,

The sequence of events shown in Figure 4-3 represents the development of a scale in an oxidizing gas on a multivalent metal M that forms two oxides: M_3O_4 and M_2O_3. The oxidizing species are assumed to be oxygen ions (O^{2-}) from the ambient gas that adsorb on the metal surface. The initial oxidation reaction may be extremely rapid as nuclei of both oxides are formed, as indicated in Figure 4-3a.

As soon as a complete layer of oxide nuclei is formed, this acts as a barrier to further oxygen ingress and the oxidation rate falls. Oxide formation depends on the diffusion of reactants across this barrier, as illustrated in Figure 4-3b. It is suggested that the most stable oxide (M_3O_4) undercuts the M_2O_3 nuclei and forms a layer next to the alloy surface [13]. As a result, the scale becomes organized into two layers. The effective oxygen partial pressure (pO_2) adjacent to the alloy is set by the equilibrium between the alloy and the innermost oxide (M_3O_4).

Continuity between the inner layer (M_3O_4) and the alloy is maintained by the oxide lattice collapsing on to the alloy as cations (M^{2+}, M^{3+}) are transported away from the alloy-oxide interface. The extent to which the completed scale provides protection depends on the rate at which the reacting species can diffuse through it. This is determined by the ionic structure of the oxide and its crystallographic features that affect the type and number of diffusion paths. The morphology developed by the scale is determined by the relative rates of growth of the different oxides, which also depends on the rate at which the reacting species can diffuse through the scale.

In order for an external scale to confer protection to the alloy it must be solid, form a continuous layer along the surface, and remain adherent to that surface.

Figure 4-3: A Simplified Schematic Diagram Indicating That Scale Growth in an Oxidizing Gas Results in the Location of the Oxide-Metal Interface Near the Original Metal Surface [13]

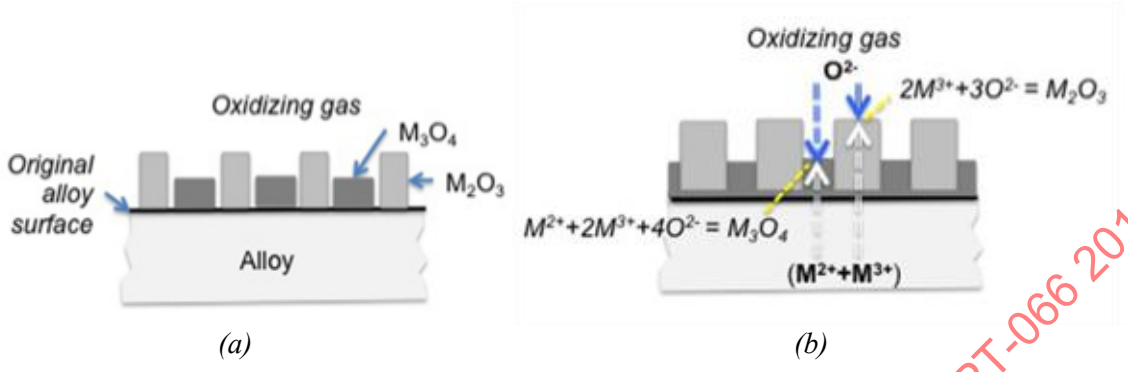

(a) Nuclei of all possible oxides are formed (M_3O_4 most stable; M_2O_3 least stable).
(b) Oxide nuclei grow laterally until they impinge and the most stable oxide undercuts the least stable oxide.

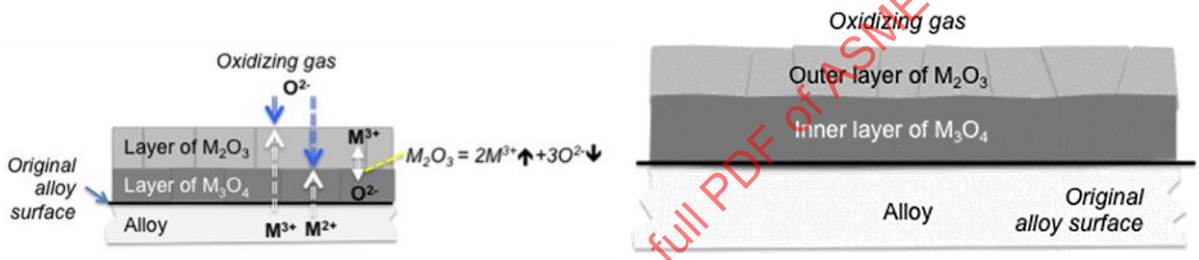

(c) The inner and outer oxide layers become continuous. Further growth is dependent on diffusion, i.e. growth of the outer layer on a supply of M3+ from the alloy transporting through the inner and outer layers, and the inner layer needs M2+ from the alloy and oxygen from the environment through the outer layer. Also, dissociation of the M2O3 at the inner-outer oxide interface is a further source of M3+ ions that diffuse outward, and oxygen ions that feed the growth of the spinel layer.

(d) The mature scale structure consists of two uniform layers, an inner of M3O4 and an outer layer of M2O3. Continued oxide growth by outward transport of M2+ and M3+ ions results in the location of the original metal surface close to the base of the scale.

In steam, the oxidizing species considered to be present from dissociation, see equation 4, are oxygen ions (O^{2-}) and hydroxyl ions (OH^-). These species are assumed to be produced from steam adsorbed on the oxide surface via:

$$H2O(g, ads) = O2- + 2H+ \quad (4.8)$$

or

$$H2O(g, ads) = 2H+ + OH- \quad (4.9)$$

There is little guidance from mechanistic understanding on which of these species may be favored, since O^{2-} and OH^- have similar ionic size. The protons (H^+) that are also released during dissociation are much smaller [14]. Protons may influence the oxidation process by modifying the transport behavior of the oxides [15][16][17].

It is suggested that the initial stages of oxidation in steam are similar to those in air/oxidizing gases, as illustrated in Figure 4-4(a). However, when the outer layer of oxide nuclei becomes complete, subsequent oxidation reactions are modified because the effective pO_2 at the alloy-oxide interface is no longer controlled by the equilibrium between the alloy and M_3O_4 but is modified because of the ability of oxygen-

carrying species (possibly O^{2-} or OH^-) to transport from the steam-oxide interface through the outer layer. The direction of growth of the inner (M_3O_4) oxide layer is inwards, towards the alloy, and the interface between the inner and outer oxide layers remains at the original metal surface.

Figure 4-4: A Simplified Schematic Diagram to Illustrate That Oxide Growth in Steam Results in the Original Alloy Surface Being Located at the Interface Between the Main Inner and Outer Oxide Layers.

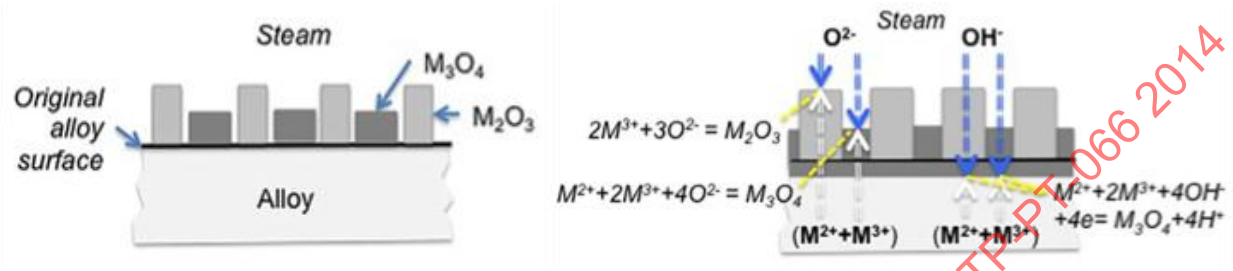

(a) Nuclei of all possible oxides are formed and grow laterally until they impinge.

(b) The ability of an oxidizing species, assumed to be OH^- from steam, to transport through the oxides increases the rate of growth of the inner layer.

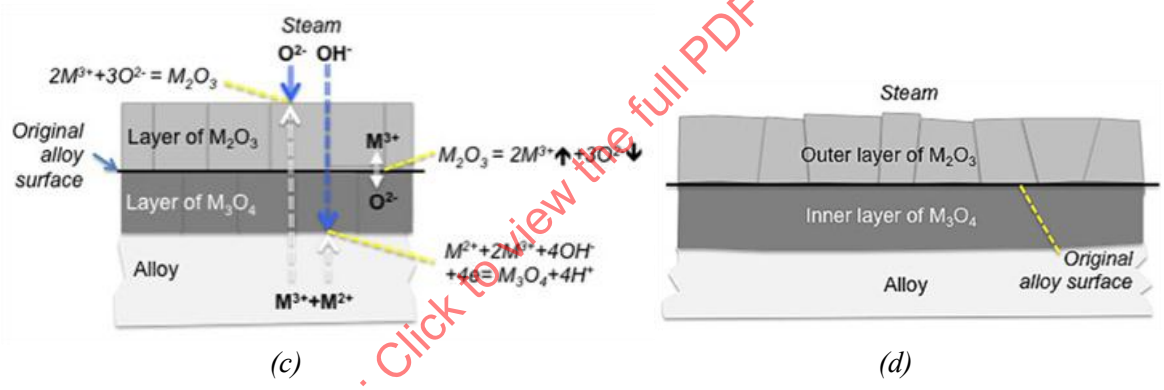

(c) Both layers become continuous. The outer layer continues to grow due to M^{3+} from the alloy transporting through the inner and outer layers, as well as from dissociation of the M_2O_3 at the inner-outer interface. The inner layer grows by reaction of M^{2+} and M^{3+} from the alloy and OH^- transporting from the environment through the outer and inner layers, as well as from oxygen derived from dissociation of the M_2O_3.

(d) The completed (equilibrium) scale structure consists of two uniform layers of oxide, an inner layer of M_3O_4 and an outer layer of M_2O_3. The location of the original metal surface is close to the interface between the two oxide layers as a result of the additional supply of oxygen to the inner layer from the steam (compared to air or oxygen).

4.2.6 Oxidation Kinetics

The high-temperature oxidation of alloys in steam, or in air or oxygen is considered to involve a number of stages:

Stage 1: Transient Oxidation

The direct access of the environment to the alloy surface at the beginning of exposure results in rapid formation of all possible oxides, as in Figure 4-3(a). This stage typically is of short duration, and the kinetics are not very amenable to mathematical description.

Stage 2: Steady-State Oxidation
The scale is continuous and adherent, and thickens with time at a predictable parabolic rate. The rate of scale growth is related to temperature by an Arrhenius relationship.

Stage 3: Modified Steady-State Oxidation
The scale exfoliation initiates, and loss of fragments of scale modifies the scale thickness and results in localized increases in oxidation kinetics which, nevertheless continue to follow a parabolic rate law.

Stage 4: Breakaway Oxidation
The loss of the protective component of the scale and depletion of the Cr level in the underlying alloy results in the formation of non-protective scales, and eventually rapid parabolic kinetics, where a continuous layer of a more rapidly-growing oxide is formed, or even linear kinetics, where the oxide formed is not adherent, predominate until the end of the service life.

Since the duration of Stage 1 oxidation usually is very short, calculation of the kinetics of scale growth typically is based on relationships derived for the growth of protective oxide scales in Stage 2, where the overall process is controlled by diffusion of ions through a continuous, external layer of scale. In Stage 3 the rate of scale growth follows a series of parabolic rate laws, the extent of successive increases in rate depending on the thickness of scale lost, the surface area involved, and the frequency of occurrence. In practice the oxidation rate in Stage 3 is commonly treated as being linear.

The standard practice for reporting oxidation kinetics data is via rate constants based on Stage 2 considerations. Typically, these rate constants are derived from:

$$\text{Scale thickness (dox) [or mass gain per unit area (W/A)]} = (2\ k_{ox}\ t)1/n \quad (4.10)$$

where:
k_{ox} is the rate constant, and
t is time;
for parabolic oxidation, $k_{ox} = k_p$, and the exponent $n = 2$.

The parabolic rate constant (the parameter most often reported) is given by:

$$kp = Ae\text{-}Q/RT \quad (4.11)$$

where:
Q is the activation energy for the rate-controlling process;
T is the metal temperature (absolute);
A is the Arrhenius constant, and
R is the Universal Gas Constant.

Since some of the thickness of the oxide present after oxidation testing was due to growth during Stage 1, the actual thickness of oxide on specimens exhibiting identical values of k_p may not be the same. In practice, however, ignoring Stage 1 does not appear to have had practical consequences so far. Measuring the oxide thickness attributable to Stage 1 is not a trivial task and requires detailed measurement over time to determine the full influence of the oxidation processes operating during Stage 1. This type of information is not reported in the literature. As a result, the actual scale thickness data reported in the literature have been compiled and used without reference to any reported rate constants derived from them.

4.2.7 Effects of Steam Pressure on Oxidation Kinetics

The expected effect of steam pressure (P) on the oxidation behavior of alloys can be derived from consideration of the oxygen pressure-dependence of the diffusion processes involved in scale formation, as given by Kofstad [6]:

$$D_m = D_m^0 (pO_2)^{\frac{b}{2a(\alpha+1)}} \tag{4.12}$$

Where: D_m and D_m^0 are the self-diffusion coefficients of the metal in the oxide at the (pO_2) of interest, and 1 bar O_2, respectively, and α is the effective charge on the metal vacancies in the oxide M_aO_b.

The corresponding parabolic rate constant will exhibit the same oxygen pressure dependence. Hence, the oxygen pressure-dependencies of the parabolic oxidation rates for the growth of Fe_2O_3 (haematite), Fe_3O_4, and FeO are expected to be: 0.19; 0.22-0.17; and 0.17, respectively.

Since in steam the effective oxygen pressure from equilibrium dissociation of steam is proportional to $P^{2/3}$ [18], the parabolic rate constants for Fe_2O_3, Fe_3O_4, and FeO would be expected to be proportional to P^x, where $x = 2/3[b/2a(\alpha+1)]$. Using the oxygen pressure-dependencies indicated above, for magnetite the expected value of x would be 0.15 to 0.11, and the expected effects of steam pressure on the values of k_p and oxide thickness are shown in Figure 4-5.

Experimental efforts to measure the influence of steam pressure on the rate of oxidation have not produced very consistent or conclusive results [19][20]. Nevertheless, some service-derived and laboratory-generated data indicate that increasing steam pressure can result in an increase in scale thickness under certain conditions, and the observed pressure dependences typically were of the same order as that predicted from oxidation theory.

Overall, the current understanding of the oxidation behavior of the alloys of interest suggests that a noticeable increase in oxidation rate would be expected by increasing total steam pressure.

Figure 4-5: Expected Effect on Oxidation Kinetics of Increasing Steam Pressure

ΔP_{steam} bar	k_p factor increase (magnetite)	Scale thickness increase, % (magnetite)
1 to 34	1.5-1.7	22-30
34 to 241	1.2-1.3	12-16

4.3 Oxide Scale Morphologies

The relationship between the metal thickness lost and the oxide scale grown during steam-side oxidation, and how it varies with alloy type cannot be fully understood without a good appreciation of the development of oxide scales in steam.

Despite the different chemical compositions and crystal structures of ferritic and austenitic steels, when exposed to steam, these alloys form layers of the same oxides. Important differences arise because alloy composition determines the relative amounts of each oxide present and this, in turn influences the relative diffusion rates through the scale, the scale growth rates, and the mechanisms by which the scale structure changes with time, temperature, and pressure.

To assess the quantity of metal consumed by the oxidation process from scale thickness measurements, it is important to be familiar with the structures of the typical scales formed on the various classes of alloys of interest after specified conditions of service. This is to ensure that the appropriate features and especially location of the original alloy surface can be identified and measured.

4.3.1 Oxide Scale Morphologies on Ferritic Steels

The morphologies of the oxides scales formed on ferritic steels in steam initially comprise a single inner layer of Fe-Cr spinel with a single outer layer of relatively pure magnetite. This is illustrated in Figure 4-6 for alloy T22, nominally Fe-2.25Cr-1Mo. The magnetite layer is characterized by a columnar grain structure with some porosity, particularly at the grain boundary triple points. The spinel layer has an equi-axed grain structure with finer, irregular porosity, sometimes in rows parallel to the alloy surface. The spinel is iso-structural with the magnetite [18], and consists of Fe_3O_4 + Cr with levels of Cr commensurate with the Cr content of the parent alloy.

The presence of haematite is also expected along the magnetite-steam interface, though this oxide sometimes may be absent [21]. The haematite does not usually form as a regular layer, but may be observed as bands of discrete precipitates close to the steam interface in the magnetite grain boundaries and grain bodies. This is illustrated in Figure 4-6b. The extent of haematite decoration of this type is considered to be a function of the defect fraction in the magnetite outer surface [22].

Figure 4-6: Typical Duplex Scale Formed on the 1-2% Cr Ferritic Steels

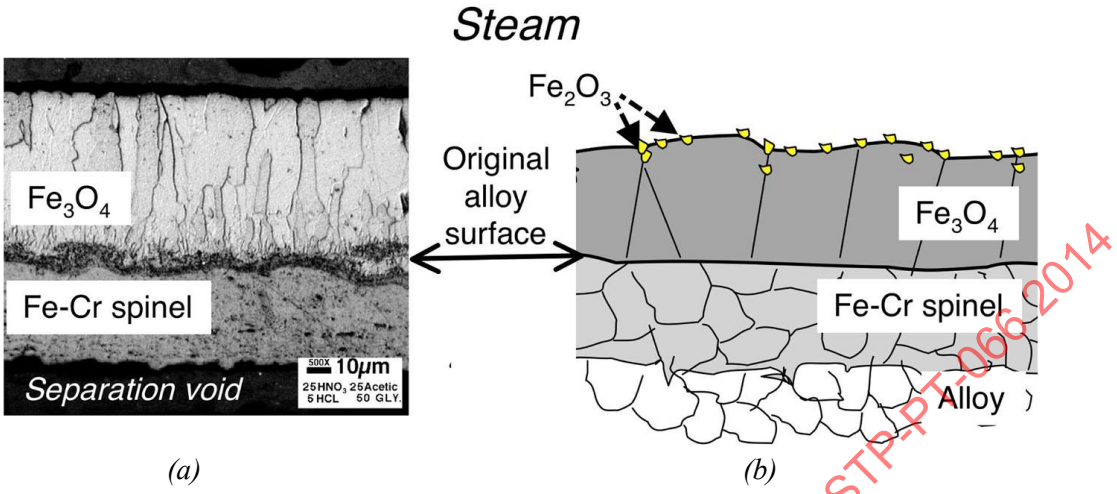

(a) An optical image of an etched cross section of T22 after 127kh service in steam at 547°C (1017°F)
(b) A simplified schematic representation of the same scale morphology.

This basic morphology is found on all standard ferritic steels with 1-9% Cr, and also applies to the ferritic-martensitic alloy T91, nominally Fe-9Cr-1Mo-V. The alloy Cr content affects the Fe-Cr spinel layer composition and, in turn, the relative layer thicknesses. This duplex morphology may persist for the whole service lifetime of T91 and the 1-9%Cr standard ferritic steels. These simple, essentially double-layered scale structures are adherent to the alloy surface even at very large thicknesses, so that they exhibit consistent, predictable growth kinetics.

While the total scale thickness may vary around the circumference of a tube, the oxide layers on ferritic steels are commonly found to be of uniform thickness. It is widely held that the ratio of the thicknesses of the inner and outer layers is constant at about 1:1, however, detailed measurements have shown that the relative thickness of the inner layer tends to increase with increasing time, temperature, and alloy Cr content.[23] Nevertheless, the accuracy with which the thickness of the inner layer of these uniform scales, and hence the depth of metal lost to oxidation can be measured is excellent, since the interface between the main spinel and magnetite layers is well defined and flat, and is usually visible even in un-etched cross sections.

For the higher-Cr ferritic and ferritic-martensitic steels, oxide nodules can be formed at higher temperatures. While the interface between the inner and outer oxides in these nodules is usually relatively flat, the inner oxide may extend far into the base metal. This can make accurate measurement of the average thickness of the inner layer more difficult. In these cases, the approach used for measuring scale thicknesses on the similarly undulating scales formed on austenitic steels may be applied.

The inner (spinel) layer can be transformed into a multi-laminated structure with a repeating series of double layers of relatively large-grained magnetite and fine-grained Fe-Cr spinel. This type of scale structure formed on alloy T22 is illustrated in Figure 4-7a. The actual scale cross section shown has been heavily etched to reveal the multi- laminated structure of the inner layer. A simplified schematic diagram intended to explain this structure is shown in Figure 4-7b.

Figure 4-7: A Typical Scale with a Multi-Laminated Inner Layer on Ferritic Steels

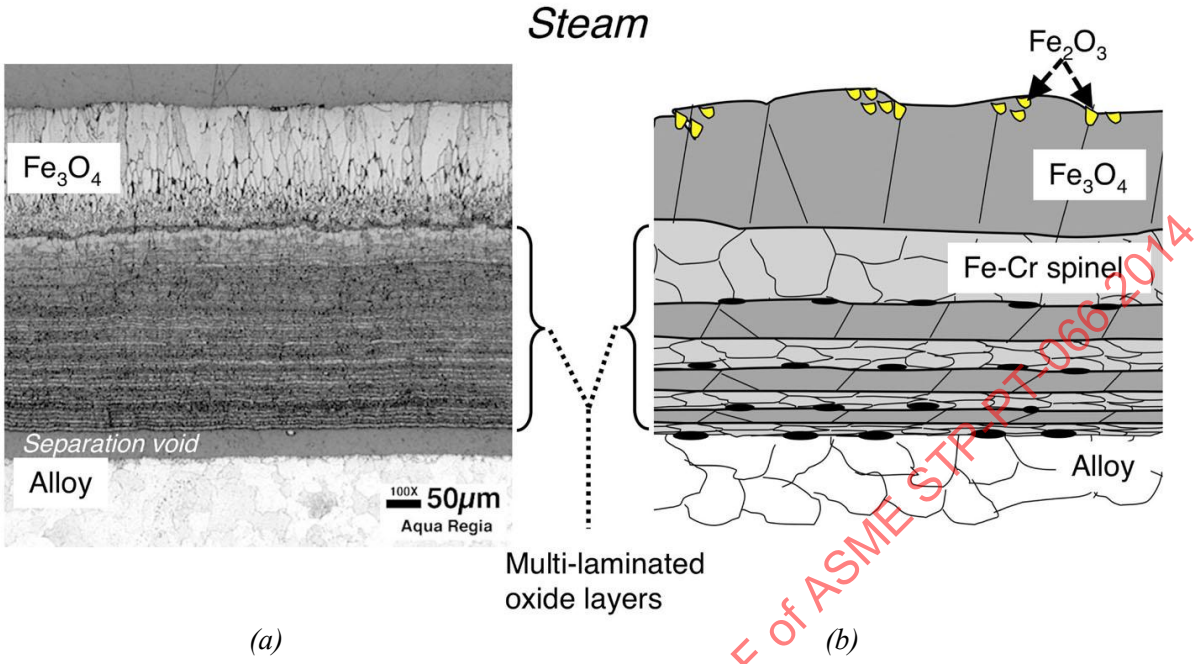

(a) An optical image of a heavily etched cross section of T22 after 127kh service in steam at 570°C (1058°F)
(b) A simplified schematic representation of the same scale morphology

It has been suggested that the transformation from duplex to multi-laminated scales may be linked to some critical scale thickness, i.e. that the occurrence of multi-laminated scales would be expected after long times at lower temperatures, and at shorter times at higher temperatures. In the UK, the appearance of multi-laminated scales has been correlated with tubes nearing the end of their service life, when they are experiencing increasing temperatures and creep [22]. It is considered that laminations initiate at the alloy-spinel interface. Manning and Meadowcroft [24] have suggested that the main driving force is a periodic disruption of the scale when unable to withstand the strains imposed by creep of the alloy substrate.

When multi-laminated inner layers are present in the scale, exfoliation of successive pairs of magnetite and spinel layers can occur [23][25]. While the growth rate of these multi-laminated, exfoliating scales may be faster than for non-laminated scales, there is no systematic documentation of any differences. In scales where the original inner layer has transformed into a multi-laminated structure, the interface between the outer magnetite and inner layers is easily recognized.

For the simple duplex scale structure shown in Figure 4-7, the location of the original alloy-oxide interface is commonly taken to be the junction between the Cr-free magnetite and the Fe-Cr spinel. For oxide structures containing multi-laminated inner layers this is less clear. Exfoliation from these scales involves the outer magnetite layer and perhaps a few of the laminates from the inner layer [23][24][26]. Regrowth of scale in the exfoliated areas largely involves the development of a new outer magnetite layer, which contacts a different spinel laminate than the original magnetite layer did before exfoliation. In such cases, the remaining inner layer is thinner than the thickness of alloy consumed. A practical approach for compensating for this discrepancy, when evaluating boiler tubes, involves the use of the measured total scale thickness to represent the metal loss [22].

The scale thickness measurements collected in this work for the standard ferritic steels include data for both simple duplex and multi-laminated types of scales. Since the original studies did not indicate which type

of scale structure was involved, no distinction in subsequent use of the data is possible. The oxide growth algorithms derived are less conservative, therefore, than would have been the case if data only for duplex scales had been used.

4.3.2 Oxide Scale Morphologies on T91

Multi-laminated scales are rarely reported for the ferritic-martensitic steel T91, which typically forms scales with a simple duplex structure similar to that shown in Figure 4-6b. The inner, spinel layer can, however, have a banded appearance that, in optical microscopy, is reminiscent of the multi-laminated inner layer described above and shown in Figure 4-6b.

In fact, the banded appearance of the oxide scales on T91 consists of continuous waves of Cr-rich spinel parallel to the alloy surface. This is illustrated in the backscattered electron image in Figure 4-8a. In this image, the Cr-rich portions of the spinel appear as dark bands, and as bright bands in the Cr X-ray fluorescence image of the same area in Figure 4-8b. This structure results from the way in which the Cr from the alloy is incorporated into the oxide. The difference between the banded structures in the inner layers formed on T22 in Figure 4-7a and T91 in Figure 4-8a resides on the bands having different Cr levels and different structures, coarse and fine-grained, on T22, whereas on T91 they contain different levels of Cr in fine-grained magnetite without any crystallographic differences.

A definite, semi-continuous layer of haematite along the scale-steam interface is shown in Figure 4-8a. In BSE images, haematite appears darker than magnetite, while the reverse is true for optical images. These observations have been confirmed by detailed examination of fracture cross sections and transmission electron microprobe specimens of the relevant layers [27]. The haematite layer shown in Figure 4-8a is thicker than normally found in the scales formed on alloy T22. This is a result of the presence of the Cr-rich bands in the inner layer on T91, which reduces the rate of Fe^{2+} and Fe^{3+} transport from the alloy and allows the outer region of the magnetite layer to be further oxidized to haematite. The interface between the major inner and outer scale layers on T91 is easily distinguished, and is taken to be the location of the original metal surface.

Figure 4-8: A Scanning Electron Micrographs of a Cross Section of the Oxide Scale Formed On T91 in Steam After 63kh at 1050°F (566°C)

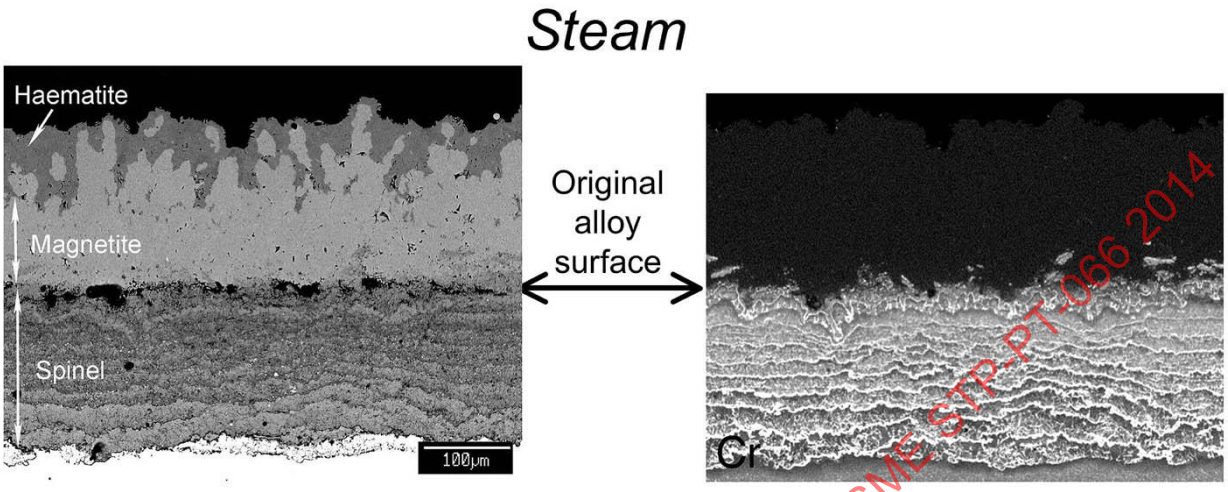

(a) A BSE image showing the layered structure of the inner layer, and the location of Fe2O3 (darker-appearing precipitates) in the outer layer;

(b) A Cr X-ray image in which the bright-appearing layered features in the main inner layer are Cr-rich

4.3.3 Oxide Scale Morphologies on Austenitic Steels

The scales formed in steam on the 300-series austenitic steels have similarities to those formed on the ferritic steels in that they consist of the same oxides, but differ because of modifications resulting from the increased Cr content of the Fe-Cr spinel. A major consideration that determines the oxidation behavior of these austenitic steels in steam is the level of Cr actually available at the alloy surface in the initial stages of oxidation. For coarse-grained austenitic steels with 17-19 wt.% Cr and 9-12 wt.% Ni, the availability of Cr at the alloy surface is often insufficient to allow rapid formation of a continuous, protective Cr-rich scale upon initial exposure to steam [26]. Instead, the scale formed consists initially of patches of protective, single-layered, Cr-enriched oxide near emergent alloy grain boundaries, with nodules of faster-growing of Fe-rich oxides formed mostly over alloy grain bodies. The nodules have a duplex structure comprising an inner layer of Fe-Cr spinel and an outer layer of magnetite containing precipitates of haematite at the magnetite-steam interface. With time this structure spreads over the entire alloy surface, resulting in scales such as that illustrated in 4-9a. The main features of this type of scale are illustrated schematically in 4-9b.

The major difference compared to ferritic steels is that slower rates of transport of the oxidizing species due to the higher Cr levels in the Fe-Cr spinel layers on austenitic steels lead to a slower oxide growth rate, hence much thinner scales. Depending on detailed alloy composition and grain size, the protective nature of the Fe-Cr spinel may increase with time, leading to extensive transformation of the initially-formed magnetite layer to haematite and the formation of interfacial voids [26].

More protective oxidation behavior can be achieved by two main routes, viz:

- by increasing the alloy Cr and Ni contents of austenitic steels [18] or,
- by cold working the alloy and/or reducing the alloy grain size [27].

Recent laboratory results for higher-Cr austenitic steels have suggested that increasing the Cr content has a much greater impact on steam-side oxidation behavior than increasing the Ni content [28].

Figure 4-9: The Typical Scale Formed in Steam on the 300-Series Stainless Steels

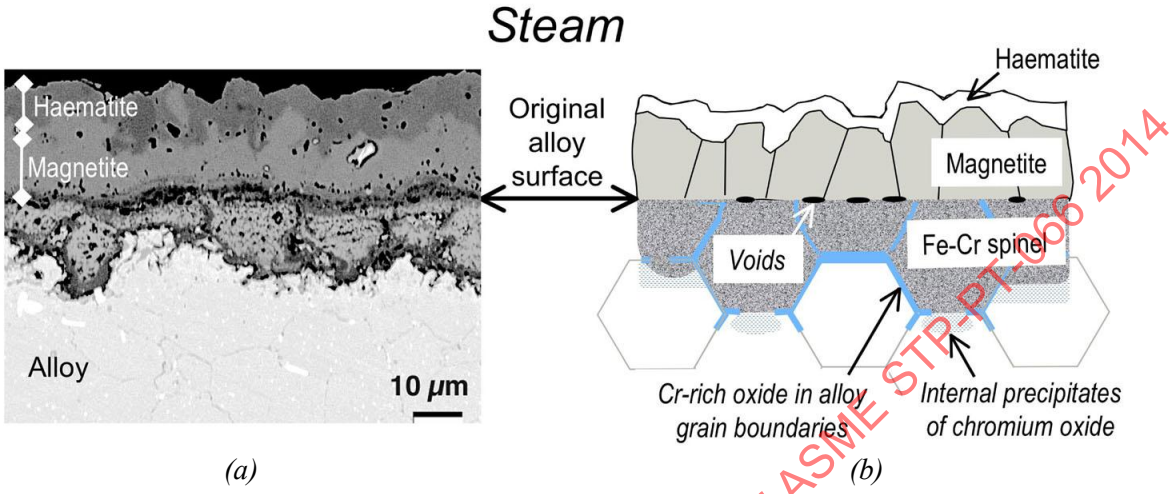

(a) BSE image of a cross section of TP347H after 4kh service in steam at 1085°F and 3,775 psi (585°C and 260 bar), and

(b) A simplified schematic representation of the same scale morphology

Cold working has the effect of facilitating increased Cr transport to the alloy surface via an increase in the number of diffusion paths, i.e. an increased density of dislocations after cold working, equivalent to having more grain boundaries.

Exfoliation from austenitic steels usually involves loss of the whole thickness of the outer layer (magnetite + haematite), whereas the inner spinel layer typically remains intact and adherent, as illustrated in Figure 4-10. As expected, exfoliated flakes usually consist of magnetite with varying levels of haematite. The general experience is that after exfoliation initiates on austenitic steels, loss of the outer layer from a large fraction of the circumference of the tube quickly follows [29].

As can be seen by comparing the scale morphologies shown in Figure 4-9a and Figure 4-10, the interface between the adherent Fe-Cr spinel layer and the exfoliating magnetite (plus haematite) layer is well defined. The thickness of the inner/non-exfoliating outer layer is therefore considered to be an acceptable measurement of the thickness of alloy lost due to oxidation in steam.

Figure 4-10: Optical Cross-Section of a Typical Area of a Superheater Tube From Which the Outer Layer of Scale Has Exfoliated, i.e. TP304H After 22kh Service in Steam At 1000°F and 2,400 psi (538°C and 165 bar)

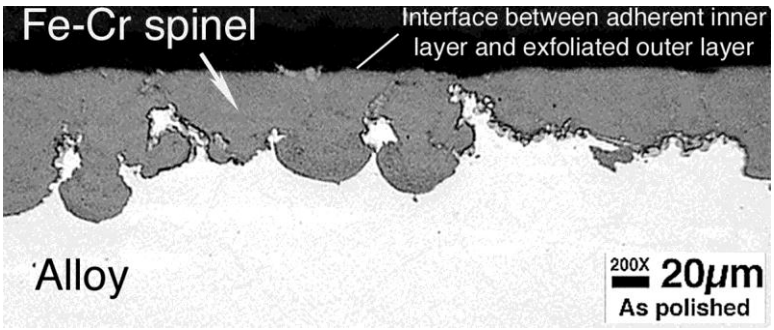

One issue with such measurements is the non-uniformity of the thickness of the Fe-Cr spinel layers on these alloys, which often consist of large nodular penetrations into the alloy. In practice this issue is normally handled by making numerous measurements to account for the frequency of nodules and the range of depths. The usual preponderance of deeper-penetrating spinel growths typically ensures that the overall measurement of thickness of metal lost is conservative.

4.4 Data Selection for Modeling

There is a large body of published data on the growth of oxide scales in steam [27]. The majority of reports relate to information from laboratory testing, which is widely-used for building understanding of steam oxidation phenomena and for characterizing and ranking the performance of existing and future materials and coatings.

These kinetic data may be reported in different ways in terms of;

- specific mass change, either as mass gain, or as mass loss from descaled specimens,
- total scale thickness,
- average thickness of the inner scale layer, or
- measured metal loss.

The oxidation kinetics measured by each technique for an alloy on which relatively uniform scales are grown are generally quite self-consistent. However, the overall oxidation rates are not consistent among these different measurement approaches [30][31]. One major source of this discrepancy is the need for an assumed density of the scale when converting mass gain-based kinetics into scale thicknesses. The densities of growing oxide scales are very difficult to estimate, since they depend not only on the proportions of the different oxides, but also on the porosity of the scale. Both of these parameters can change significantly with increasing scale thickness, and this renders the task of making direct comparisons among thickness-based and mass gain-based kinetic data very difficult.

A major advantage of laboratory-scale tests is that they are well controlled and provide the opportunity to relate differences in oxidation behavior to specific changes in exposure conditions. This type of work has driven progress in the understanding of the mechanisms governing the oxidation processes.

In contrast, the oxidation conditions that steam tubes experience in service are complex and variable. A number of the key parameters are difficult and expensive to reproduce in laboratory testing. The absence of agreed standards for this type of laboratory testing and the resulting differences among the results from

different laboratories have led to difficulties in the inter-correlation of results among laboratories and with service-derived data.

The importance of controlling laboratory procedures is illustrated by the results of a 'round robin' exercise carried out under the auspices of the COST522 collaborative program in Europe [32]. Specimens from the same batch of P92 alloy were exposed at 1112 and 1202°F (600 and 650°C) for 1,000 hours, at nine different institutes each using their own procedures, to give a total matrix of 11 different exposure procedures. The results of this inter-comparison produced a variation in the scale thickness values reported by the different laboratories, from 2.5 to 4 mils at 1112°F, and 1.6 to 9.5 mils at 1202°F (60 to 100 μm at 600°C, and 40 to 240 μm at 650°C).

The laboratory testing procedures included the use of both once-through and recirculating exposure systems, and the use of water vapor in a carrier gas, typically argon, in varying concentrations, and 100% pure steam. The preponderance of laboratory steam oxidation testing is at ambient pressure. There is, however, growing activity internationally to conduct exposures at elevated pressures to produce more realistic operating conditions. Studies focused on understanding the effects of different experimental variables have been performed [33][34] to enable such future standardization of steam oxidation testing, but as yet no recognized standards are applied. One problem is that including more features in the laboratory exposures, such as heat flux, pressure, cycling etc. will increase the complexity of the test work, making it more expensive and difficult to control.

The differences between scale growth kinetics from laboratory tests and exposures in operating boilers are not well understood, and it is clear that laboratory tests have not yet fully reproduced the scale morphologies seen in service-exposed tubes. Nevertheless, the understanding, trends, and effects of specific variables derived from laboratory studies have been fully incorporated into the descriptions in this document of scale morphologies and their development. For the purposes of the current work, only oxide thickness data from scales grown on alloys exposed to steam under actual boiler operating conditions have been used. The thickness of the inner oxide layer is considered to represent the thickness of alloy surface consumed by the oxidation process [21]. This is the same basis that commonly is used to report steam oxidation kinetics by the utility industry worldwide.

4.5 Compilation of Oxidation Kinetic Data

The classes of ferritic and austenitic steels considered include those in current and historical use for boiler tubes, as well as the new or modified alloys that are being introduced in new boilers or are being considered for future plants with advanced steam conditions, when these are available. In general terms, the similarity of the morphologies of the oxide scales formed on most of the ferritic, martensitic-ferritic, and austenitic steels in steam allow the same measurements procedures to be used.

On high-strength Ni-based alloys, although the main scales typically are of uniform thickness, a subscale formed by the internal oxidation of minor additions of alloying elements often is present, and may penetrate to considerable depths along alloy grain boundaries that intersect the alloy surface, sometimes deeper than the thickness of the main oxide layer. In these cases, the value used for the depth of alloy consumed by steam oxidation was taken as the maximum depth of subscale penetration measured on each sample considered.

As with all such measurements, the conservatism of the measurements made is improved by ensuring that the scale thickness around the total tube circumference is sampled, and by maximizing the number of specimens sampled. The data considered in this document were generated by a number of different research groups, and care was taken to follow these principles when selecting the data for inclusion in the study. For

alloys that form an inner oxide layer of uneven thickness, as is the case for most austenitic steels and for high-Cr ferritic steels at the higher temperatures, the value used in this database for the inner layer thickness was the maximum measured on each sample considered. A compilation of the original data used is shown in Appendix A.

In some cases large differences in the oxidation kinetics in steam for nominally the same alloy can be related to relatively small differences in the content of alloying additions within the accepted specification. For this reason the actual compositions of the alloys used to generate the data reported are listed in Appendix C (where available) along with the nominal or specified alloy composition, so that the applicability of the data to the needs of the user can be assessed.

4.6 Modeled Kinetic Curves

As described above, steam-side oxidation is a complex phenomenon with a number of factors that influence the performance of alloys in specific conditions of operation. These include the alloy chemistry, the surface condition, the exposure temperature and time, the steam pressure and the heat flux. When attempting to model the oxidation kinetics it is possible to adopt a curve-fitting approach to the analysis of experimental data, which on the whole works well and can generate equations for the kinetics.

Experience has shown that whilst these relationships can describe the data from one laboratory or utility, they are unlikely to describe data coming from other sources. It is desirable, therefore, to have a more general relationship that uses data from different sources to generate a more generic model.

One approach that lends itself to modeling such complex situations is the use of artificial neural networks. This approach previously has been used with laboratory-based short-term steam oxidation data [36].

Using the same approach to data generated from plant measurements for a range of temperatures, pressures, alloys and times, a new artificial neural network algorithm was generated to predict the inner layer thickness of oxide scales formed in steam as a function of selected input parameters.

Using data collated from the literature, a neural network model was constructed. Since plant data typically relate to relatively long exposure times, the training data for the network was lacking in short-term information. Additional laboratory-generated steam oxidation data for exposure times up to 5,000 hours were used to supplement the plant data to provide the required shorter-term data. These data are listed in Appendix B.

A commercial software package was used in conjunction with the input data to train the neural network. In the initial stages of training all of the input parameters available were used to train the neural network. These included the full alloy chemistry, time, pressure and the metal and steam temperatures. The network was trained with the aim of predicting the inner oxide layer thickness. Additional networks were also developed to predict the total oxide thickness, since these are useful for comparison purposes.

One feature of the training process is that the architecture of the neural network can be manipulated. This can be achieved, for instance, by manipulation of the neurons and, in particular, controlling their number. In this case, the number of neurons used in the network was varied until a compromise between the best fit to the data using the fewest possible neurons was achieved. The use of too many neurons in the model tends to result in the over-training of the network, inhibiting the model's ability to extrapolate outside the dataset used in the training process.

It is also possible to identify the most influential input parameters in terms of their contribution to the final predicted value. The number of input parameters can be changed, and the impact on the final prediction and robustness of the model can be evaluated.

The number of input parameters was refined and reduced to the most influential parameters. Based on the data used in this work the most important parameters were found to be: alloy chemistry in terms of the Cr, Mo, Fe, Si, S contents, the metal temperature, the exposure time, and the system pressure. The Ni content of the alloy has been included to extend the range of the model to higher alloyed materials.

The following parameters were used in the construction of the final model:

- Metal temperature, °C
- System pressure, bar
- Exposure time, h
- Alloy Cr content wt.%
- Alloy Mo content, wt.%
- Alloy Fe content, wt.%
- Alloy Si content, wt.%
- Alloy S content, wt.%
- Alloy Ni content, wt.%

In this case, the final model consisted of five neurons, and produced an R^2 fit to the measured data of 0.910. The predicted inner oxide layer thickness is compared with the actual measured inner oxide layer thickness from the literature data, in Figure 4-11. The maximum outlying data points are marked by a green circle, and have been identified as data for alloys T22 and VM12. These points are most likely to be from the laboratory tests.

Figure 4-11: A Comparison of the Final Model Prediction of Inner Oxide Thickness Plotted Against the Measured Values

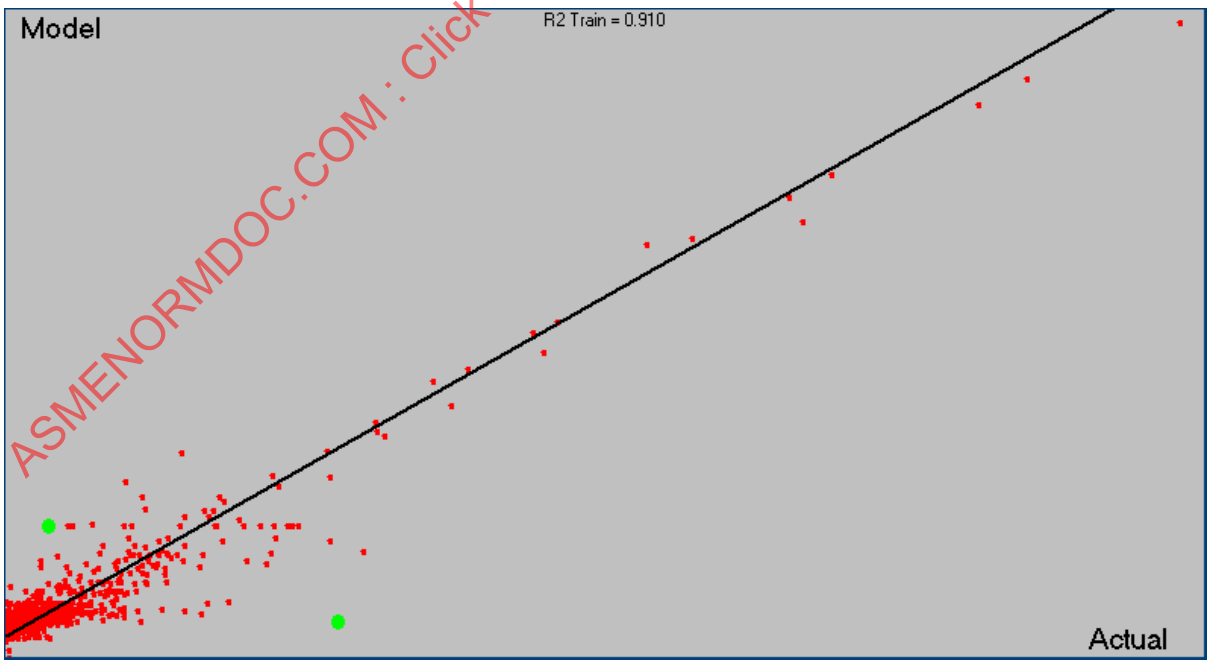

The results of the predictions compared to the measured values are presented as a line plot in Figure 4-12. This shows the ability of the model to follow, to a good approximation, the trends in the measured data.

The region in the center of the plot highlighted by the black square shows the prediction to be flat compared with a rising inner oxide layer thickness of the measured data. This inability to predict the rise is misleading and reflects the occurrence of multiple data points for the same exposure time, illustrating the scatter in the oxide thickness values reported, as illustrated in Figure 4-13.

The source of this scatter could be from ash coverage and tube geometry, scale exfoliation, changes in alloy surface preparation or from differences in alloy composition, or water chemistry. When confronted with scatter the model will adapt, and the basis of the training will use a mean value.

The final form of the algorithm derived from the trained neural network is quite complex and so is not reproduced within this document. All artificial neural networks suffer from limitations when extrapolating beyond the training limits, which is a further reason why the algorithm is not presented.

Figure 4-12: A Comparison of the Model Prediction (Red Line) of Inner Oxide Thickness and the Measured (Black Line) Value for Inner Oxide Thickness for the Neural Network Model Developed

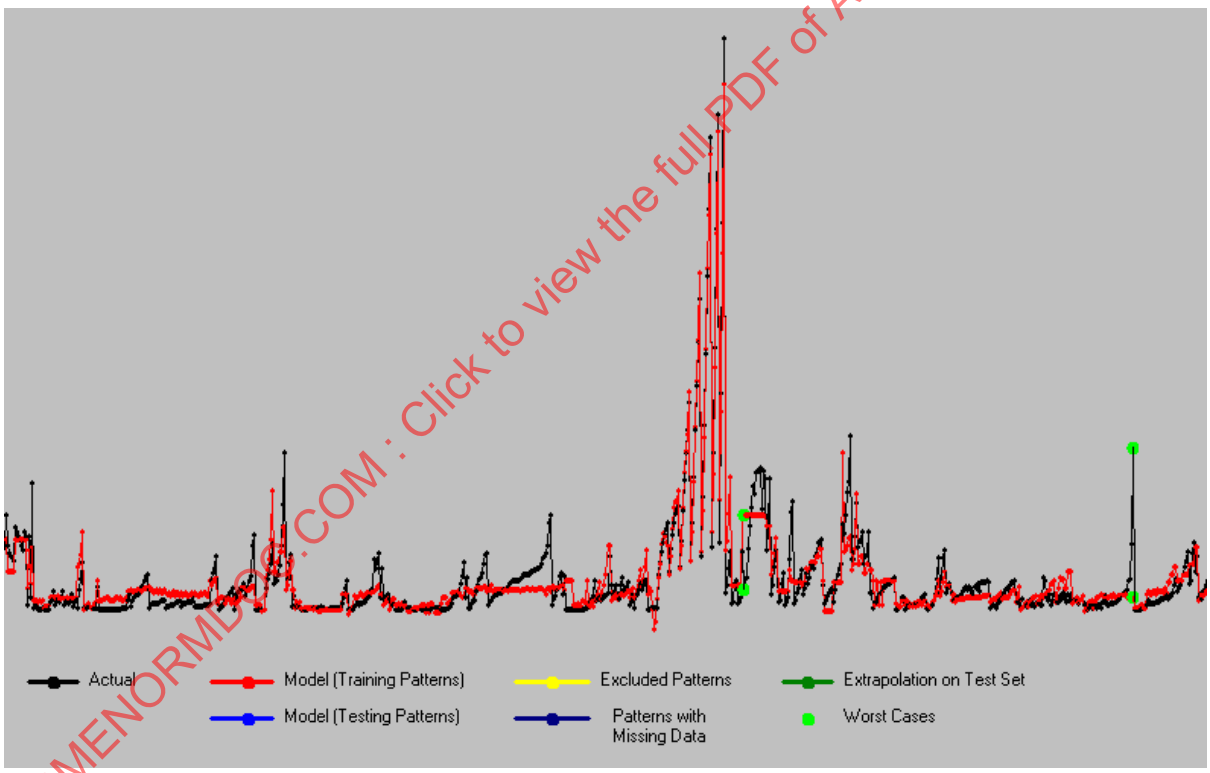

Figure 4-13: The Scatter in the Total Oxide Thickness Measurements from the Laboratory Test Data for P92

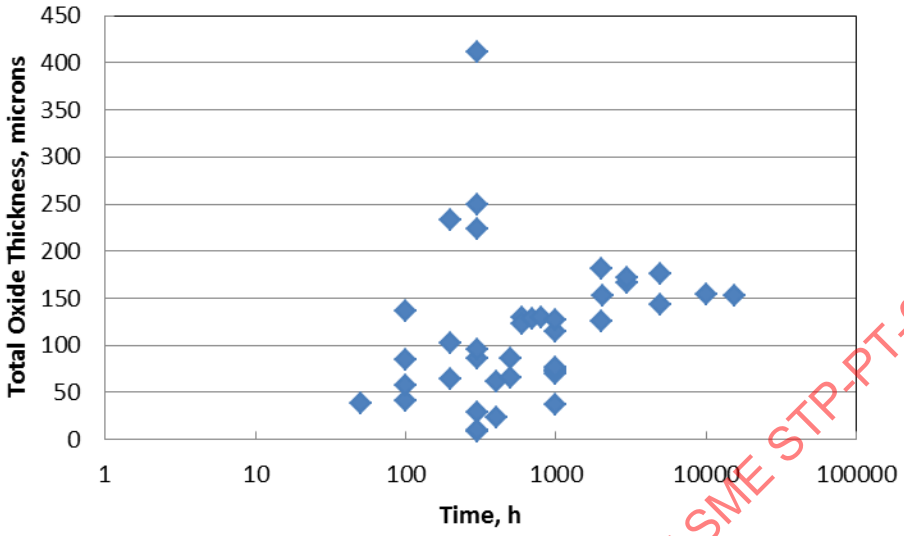

4.7 Use of the Model to Calculate Tube Metal Losses

4.7.1 Examples of Model Predictions

Examples of the use of the model to predict relationships for oxide growth on alloy T22 as a function of time and total pressure, from 50 to 160 bar, representing reheater and superheater conditions, are shown for metal temperatures of 1022°F (550°C) and 1112°F (600°C) in Figure 4-14 and Figure 4-15, respectively. The level of agreement between the predicted oxide thickness values presented as curves with the values measured in service, presented as data points, for oxides formed in 146 bar steam as a function of time for temperatures ranging 1022 to 1202°C (550 to 650°C), is presented in Figure 4-16.

While there is generally good agreement with the plant data at 2,786 psi and 1022°F (192 bar and 550°C), as indicated in Figure 4-16, as the temperature increases the model tends to under-predict the oxide thickness, although there is significant scatter in the plant data.

The model also was used to generate plots showing the relative oxidation rates for a range of alloys, i.e. T22, T23, T91, T92 and T122, in terms of the predicted values for the inner oxide layer as a function of steam pressure at 1022 and 1112°F (550 and 600°C). These data are plotted in Figure 4-17 and Figure 4-18 and show the general trends that would be expected, i.e. decreasing levels of oxidation with increasing Cr content; increasing oxidation as a function of temperature; and increasing oxidation as a function of steam pressure. These data also suggest that the effect of pressure is more pronounced for some materials than others, although there is only very limited evidence of this.

Figure 4-14: Comparison of the Predicted Inner Oxide Thickness of Alloy T22 at 1022°F (550°C) for a Range of Pressures

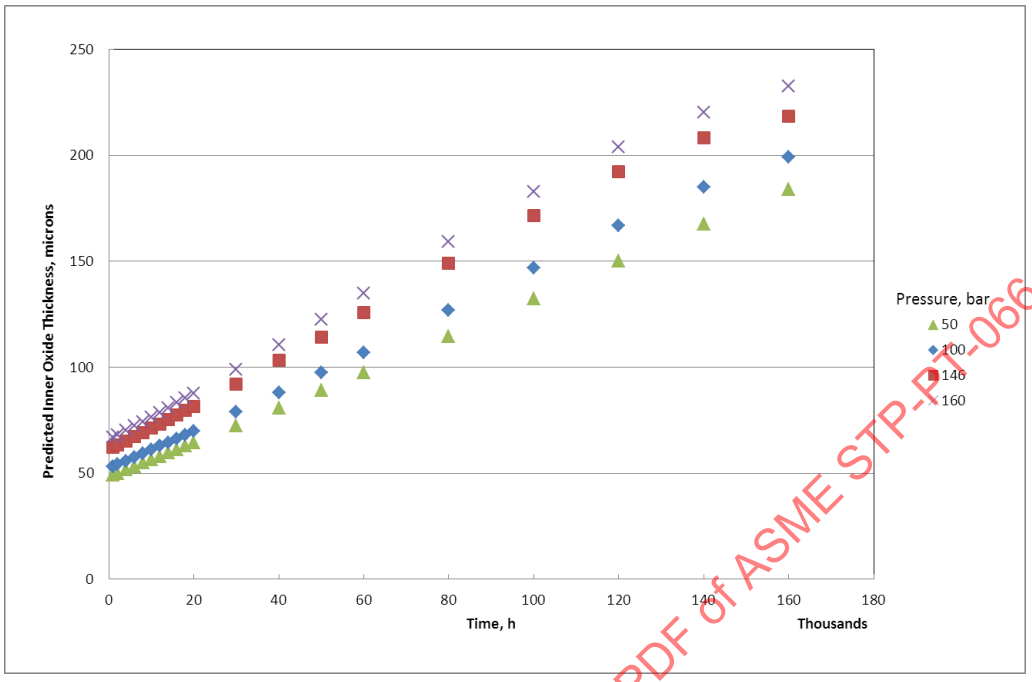

Figure 4-15: Comparison of the Predicted Inner Oxide Thickness of Alloy T22 at 1112°F (600°C) for a Range of Pressures

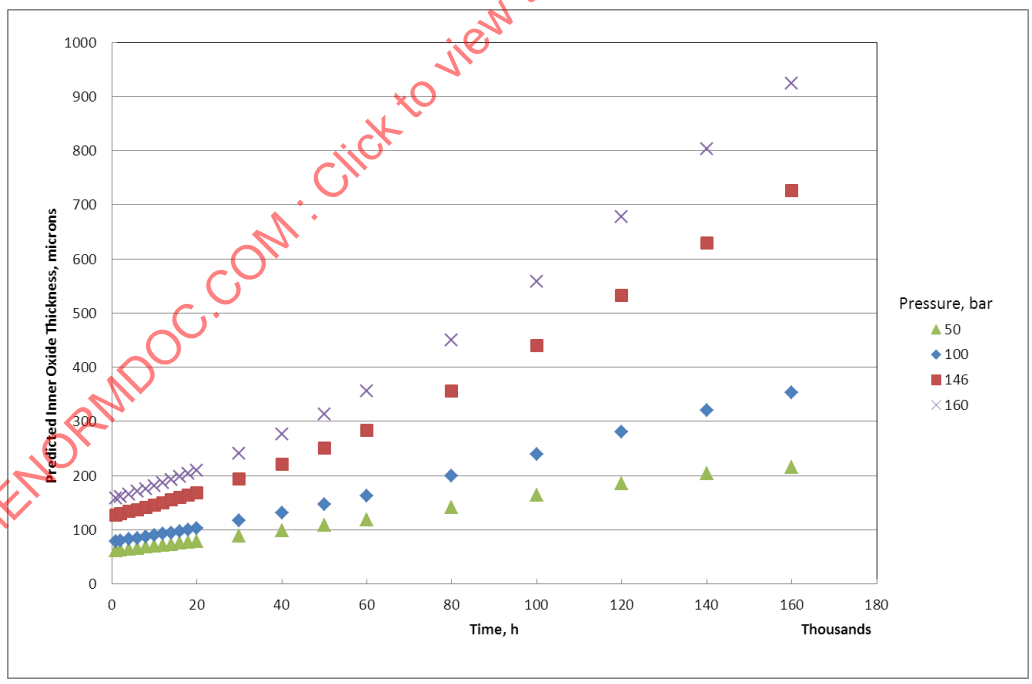

Figure 4-16: Comparison of the Predicted Values of Inner Oxide Thickness for Alloy T22 at 2,120 psi (146 bar) Over a Range of Temperatures; Also Shown Are Plant Data From the Literature

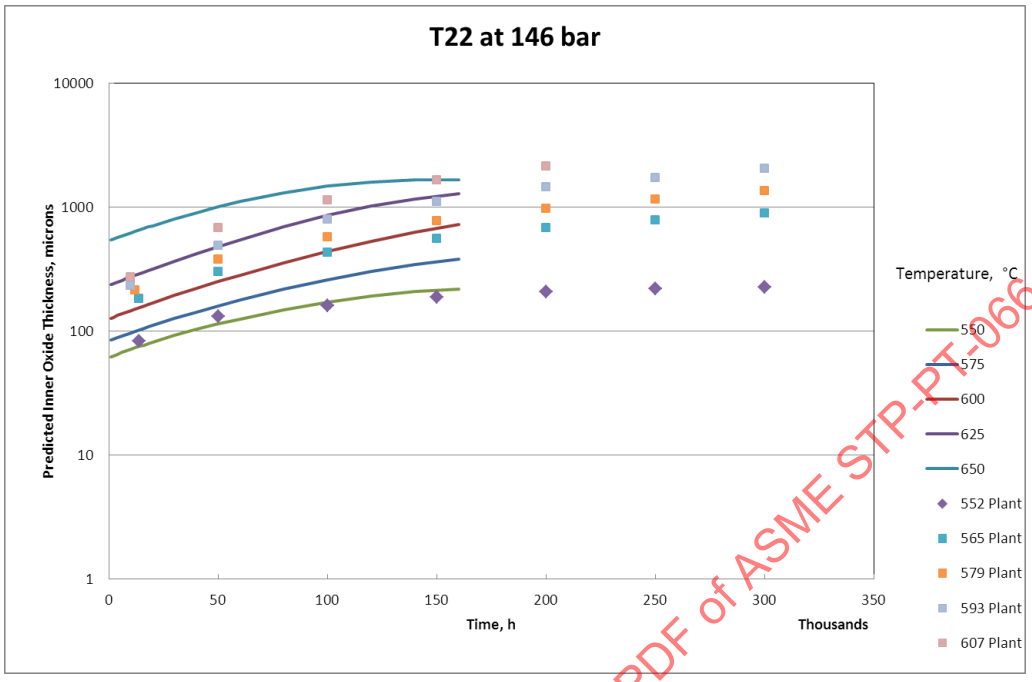

Figure 4-17: Comparison of the Predicted Values of Inner Oxide Thickness for Alloys T22, T23, T91, T91 and T122 at 725, 1,450, and 2,120 psi at 1022°F (50, 100, and 146 bar at 550°C)

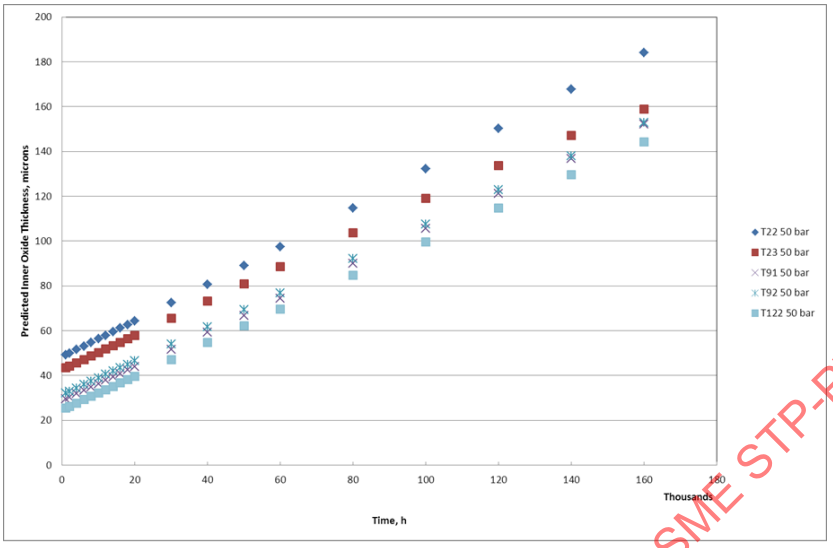

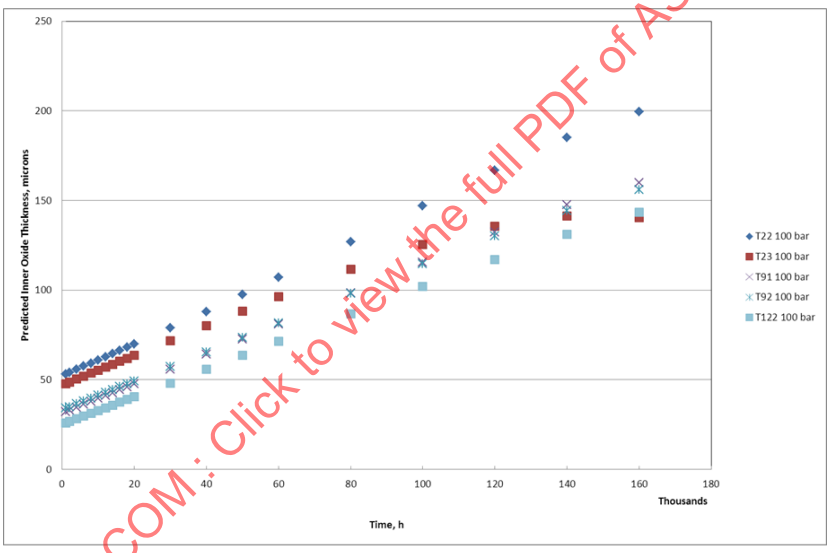

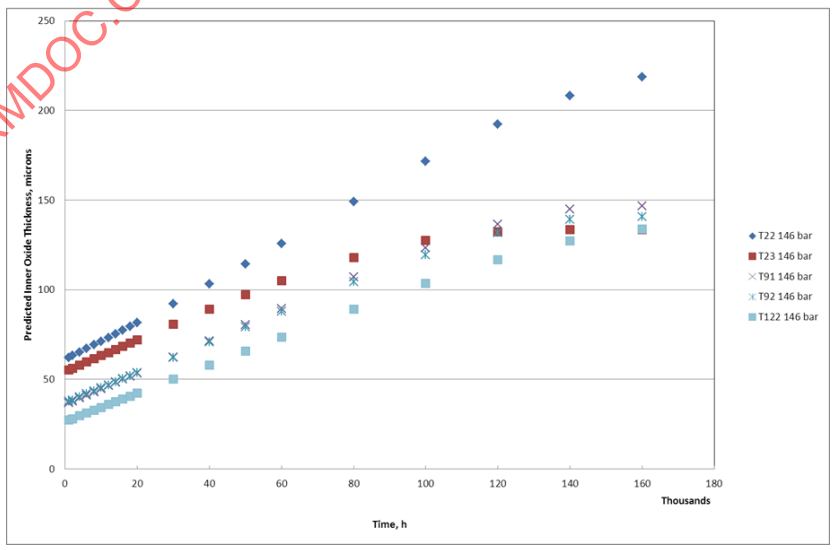

Figure 4-18: Comparison of the Predicted Values of Inner Oxide Thickness for Alloys T22, T23, T91, T91 and T122 at 725, 1,450, and 2,120 psi for 1112°F (50, 100 and 146 bar for 600°C)

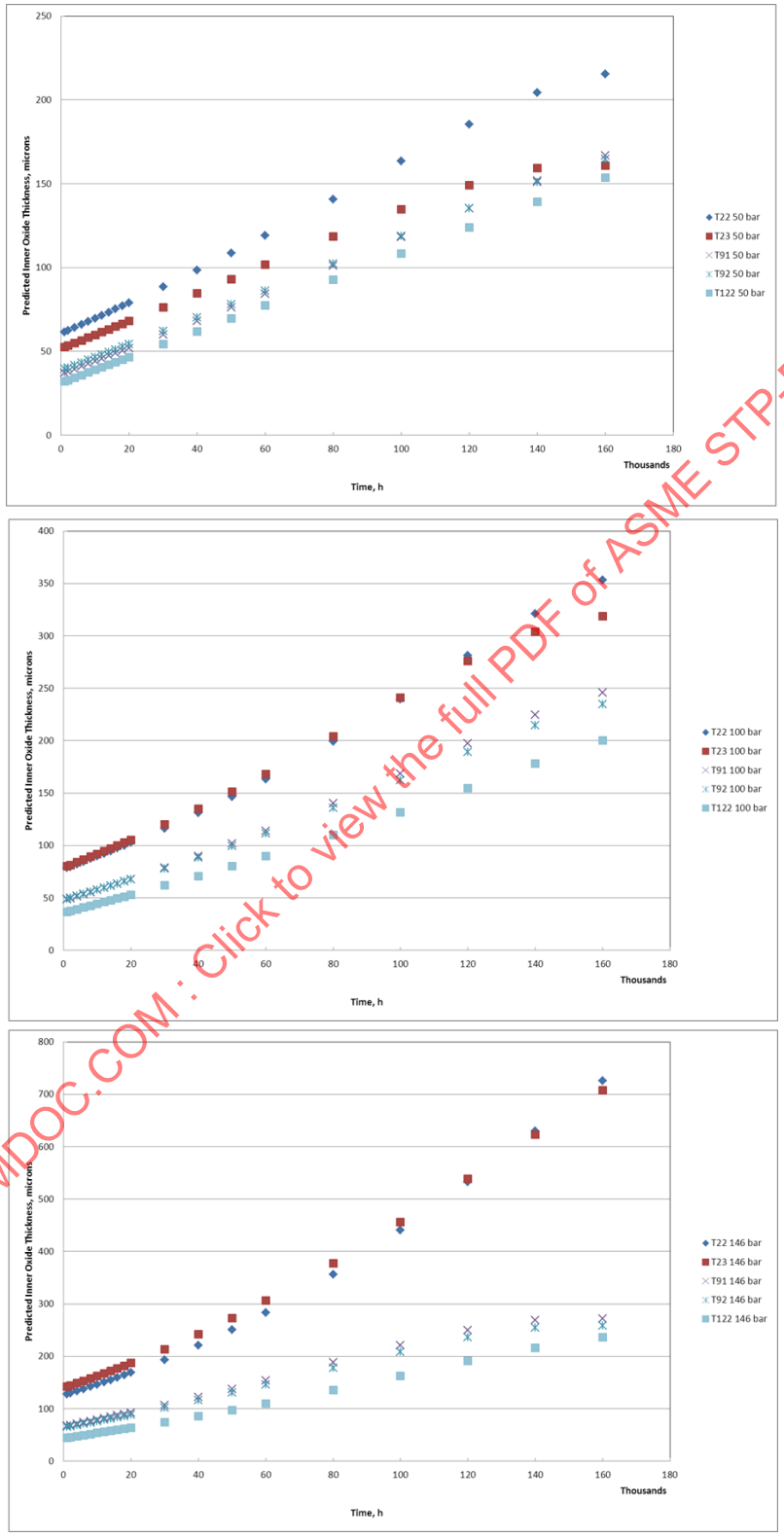

4.7.2 Comparison of the model predictions with plant data

Where sufficient data were available, predictions made by the model were compared directly with measured plant data. Examples are shown in Figure 4-19 to Figure 4-25.

The level of agreement between the limited plant data for the key alloys and the modeled data was found to be variable, as is summarized below. In general terms, the degree of fit between the model predictions and the plant data reflected the availability of suitable data during the training of the model for any particular alloy.

Alloy	Prediction
T22	Reasonable
T23	Good
T91	Good
T92	Good
E911	Low
HCM9M	High (over conservative)
HCM12	Slightly high (over conservative)
T122	Slightly high (over conservative)
1714CuMo	Good
X3CrNiMoBN 17-13-3	Good/low at longer durations

Figure 4-19: A Comparison of the Predicted Values of Inner Oxide Thickness (Curves) for Alloy T23 at 192 Bar Over a Range of Temperatures. Also Shown, As Individual Points, Are Plant Data from the Literature [37]

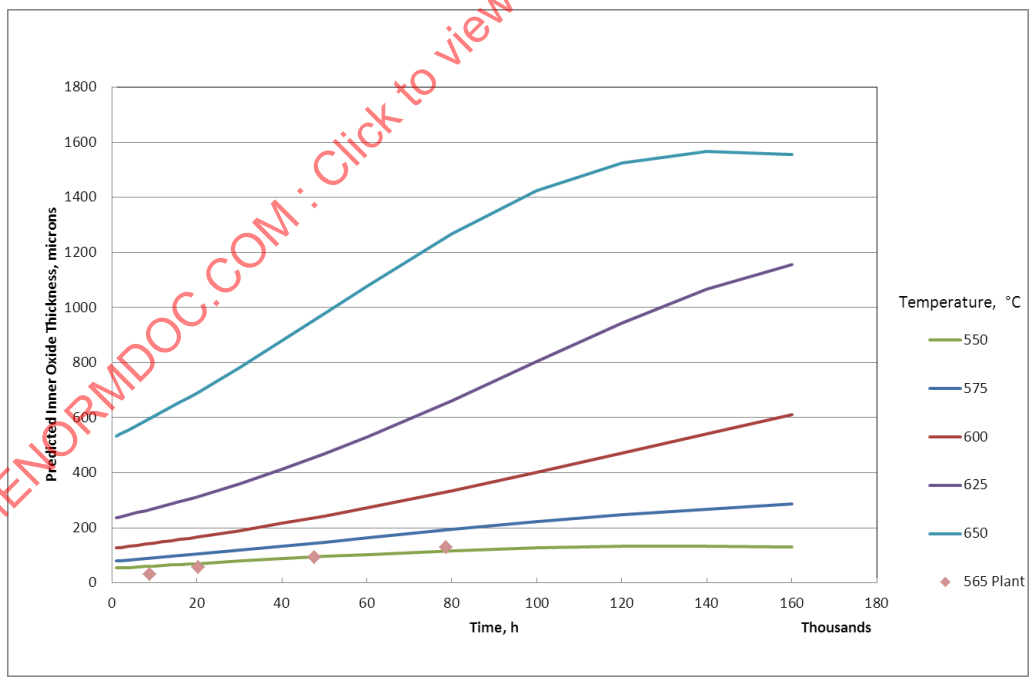

Figure 4-20: A Comparison of the Predicted Values of Inner Oxide Thickness (Curves) for T91 at 3,630 psi (250 bar) Over a Range of Temperatures. Also shown, As Individual Points, Are Plant Data from the Literature [38]

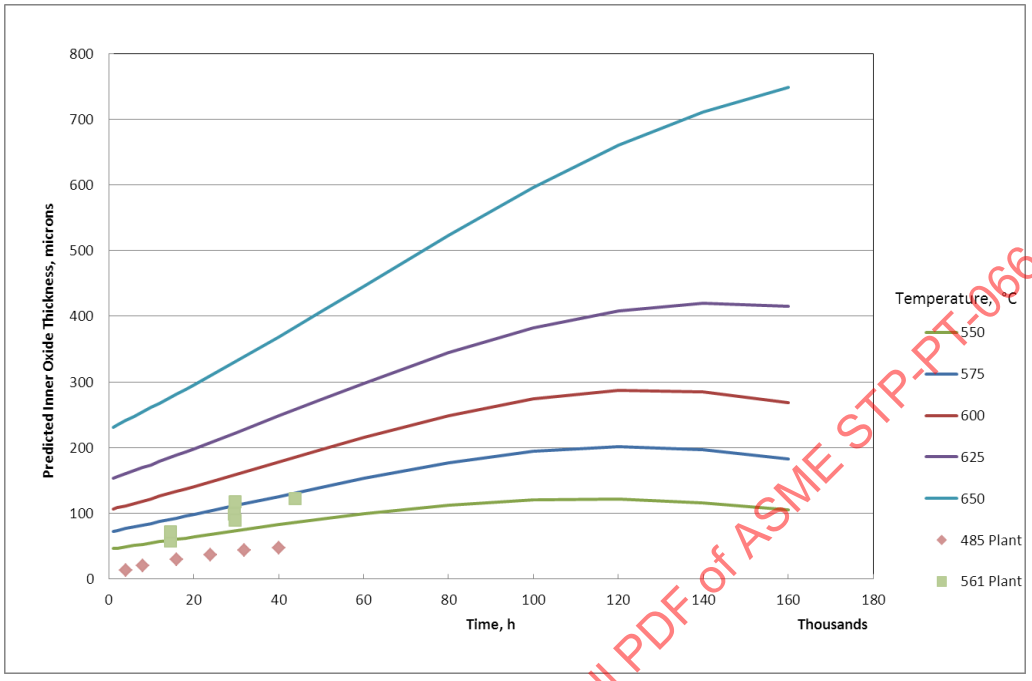

Figure 4-21: A Comparison of the Predicted Values of Inner Oxide Thickness (Curves) for T92 2,800 psi (192 Bar) Over a Range of Temperatures. Also Shown, As Individual Points, Are Plant Data from the Literature [39]

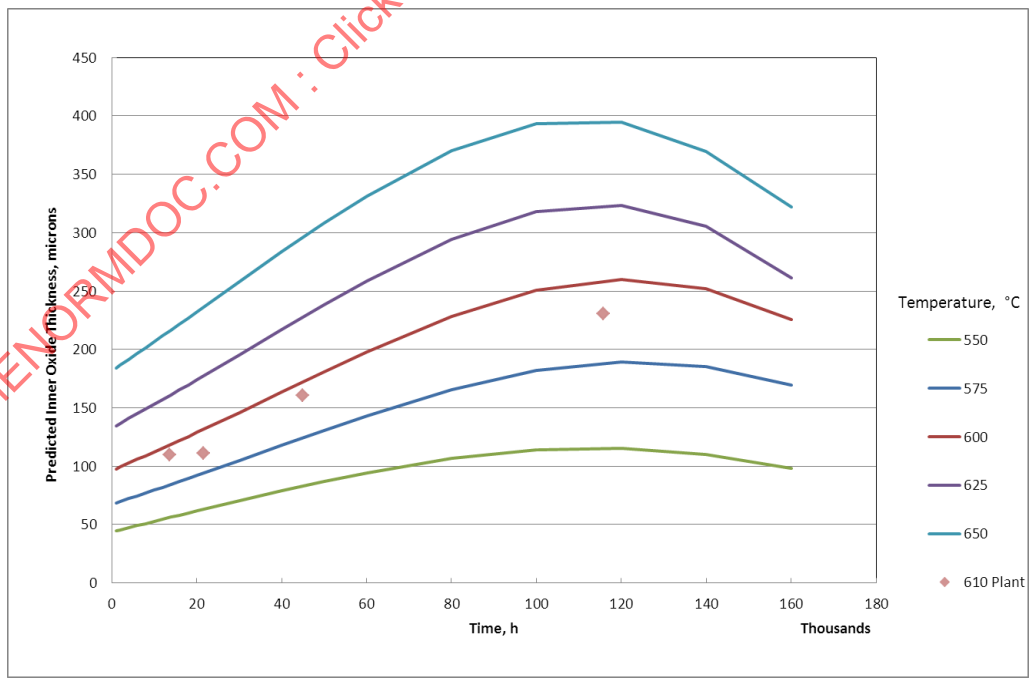

Figure 4-22: A Comparison of the Predicted Values of Inner Oxide Thickness (Curves) For E911 at 2,700 psi (186 Bar) Over a Range of Temperatures. Also Shown, As Individual Points, Are Plant Data from the Literature [40]

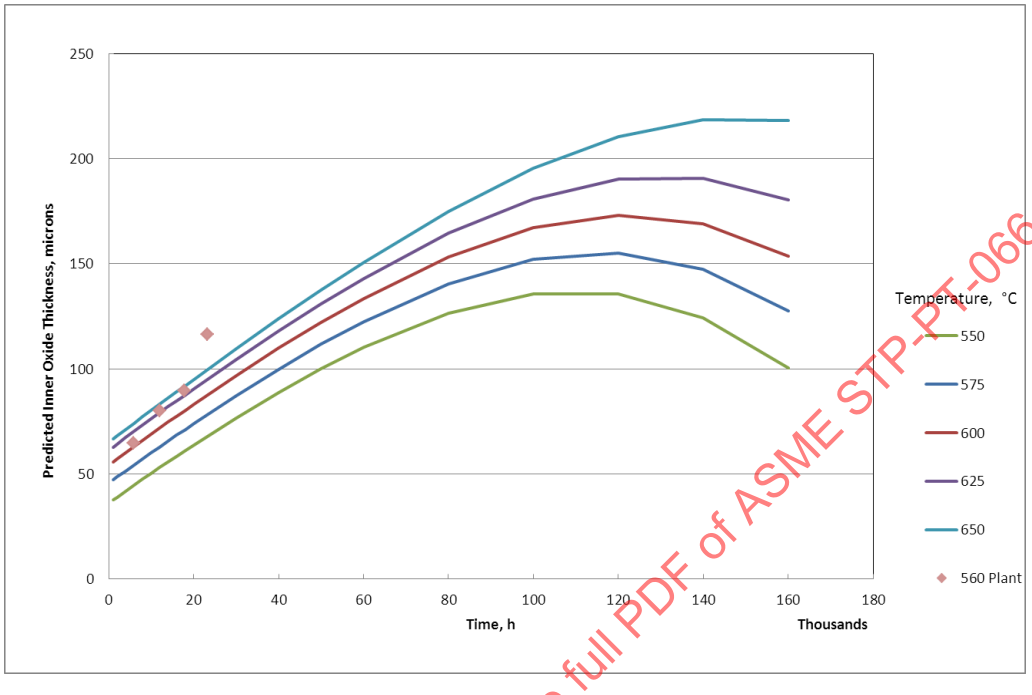

Figure 4-23: A Comparison of the Predicted Values of Inner Oxide Thickness (Curves) for HCM9M at 2,785 psi (192 Bar) Over a Range of Temperatures. Also Shown, As Individual Points, Are Plant Data from the Literature [37]

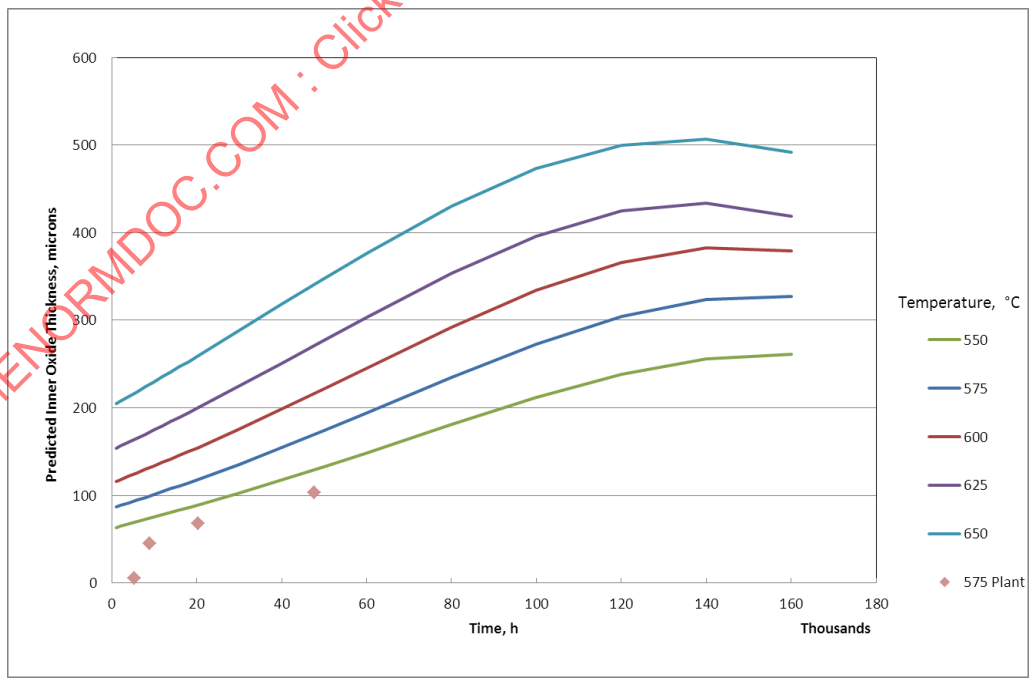

Figure 4-24: A Comparison of the Predicted Values of Inner Oxide Thickness (Curves) for HCM12 at 2,785 psi (192 Bar) Over a Range of Temperatures. Also Shown, As Individual Points, Are Plant Data from the Literature [37]

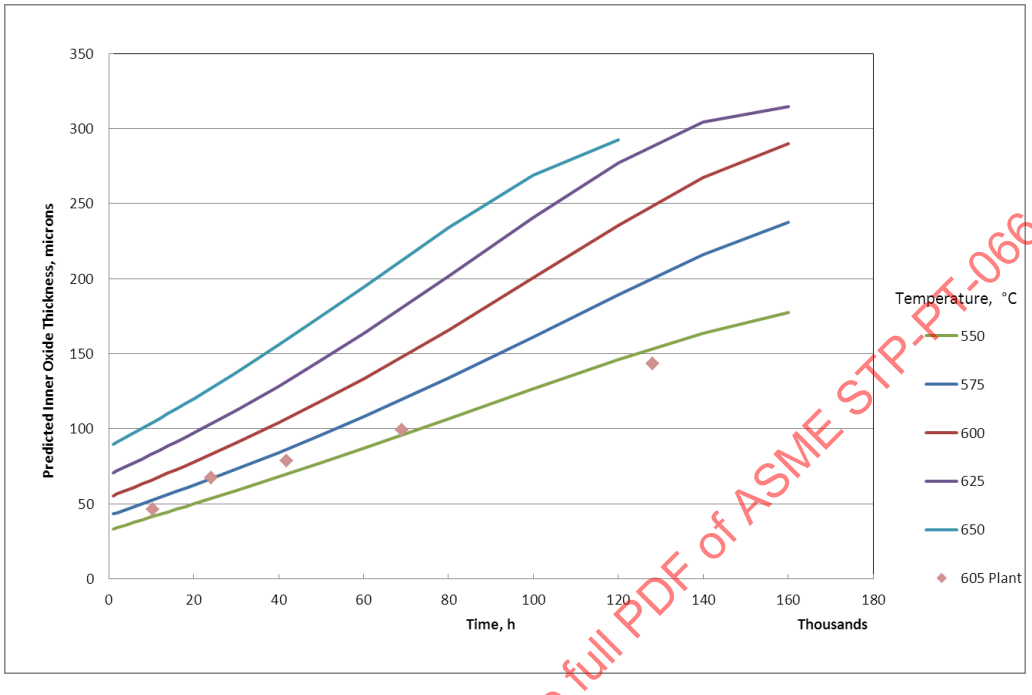

Figure 4-25: A Comparison of the Predicted Values of Inner Oxide Thickness (Curves) for T122 at 2,785 psi (192 Bar) Over a Range of Temperatures. Also Shown, As Individual Points, Are Plant Data from the Literature [37]

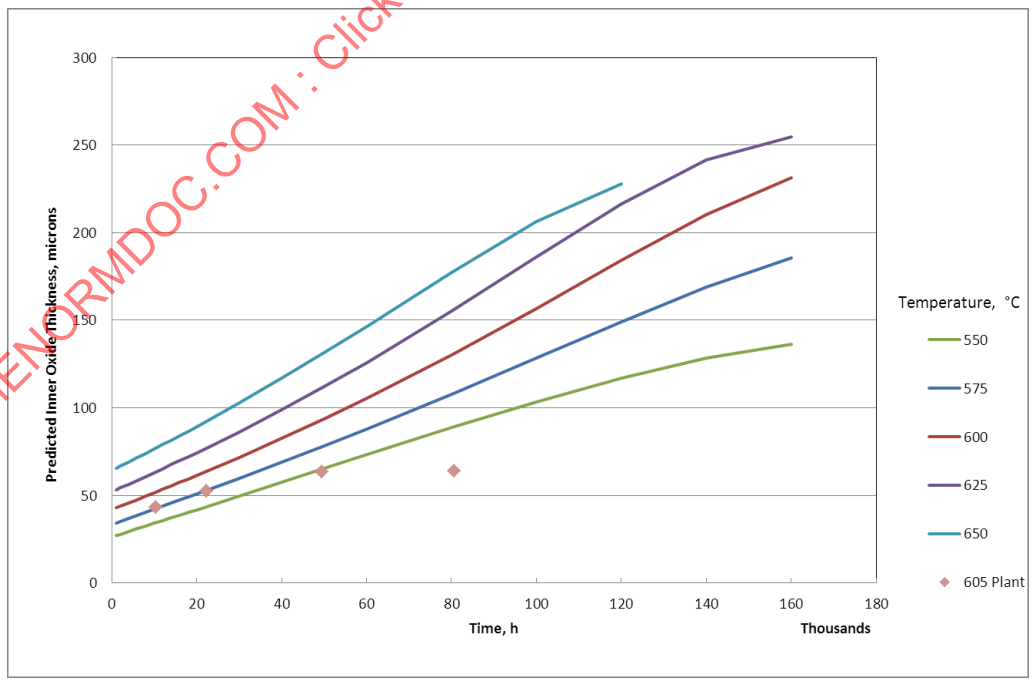

Figure 4-26: A Comparison of the Predicted Values of Inner Oxide Thickness (Curves) for 1714CuMo at 4,496 psi (310 bar) Over a Range of Temperatures. Also Shown, As Individual Points, Are Plant Data from the Literature [41]

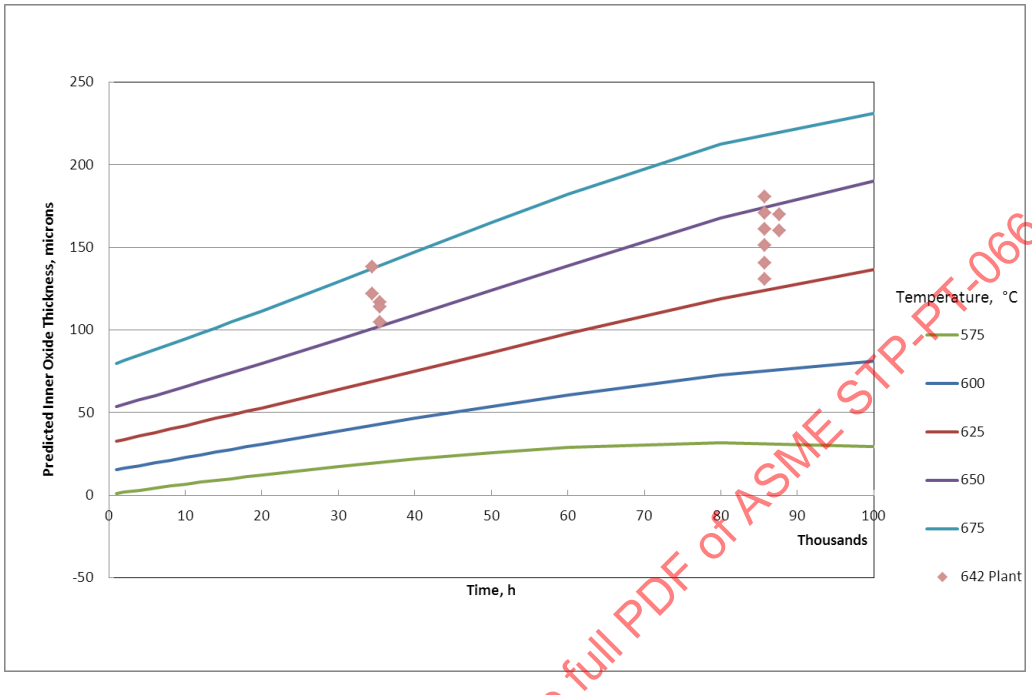

Figure 4-27: A Comparison of the Predicted Values of Inner Oxide Thickness (Curves) for X3CrNiMoBN 17-13-3 at 2,700 psi (186 Bar) Over a Range of Temperatures. Also Shown, As Individual Points, Are Plant Data from the Literature [40]

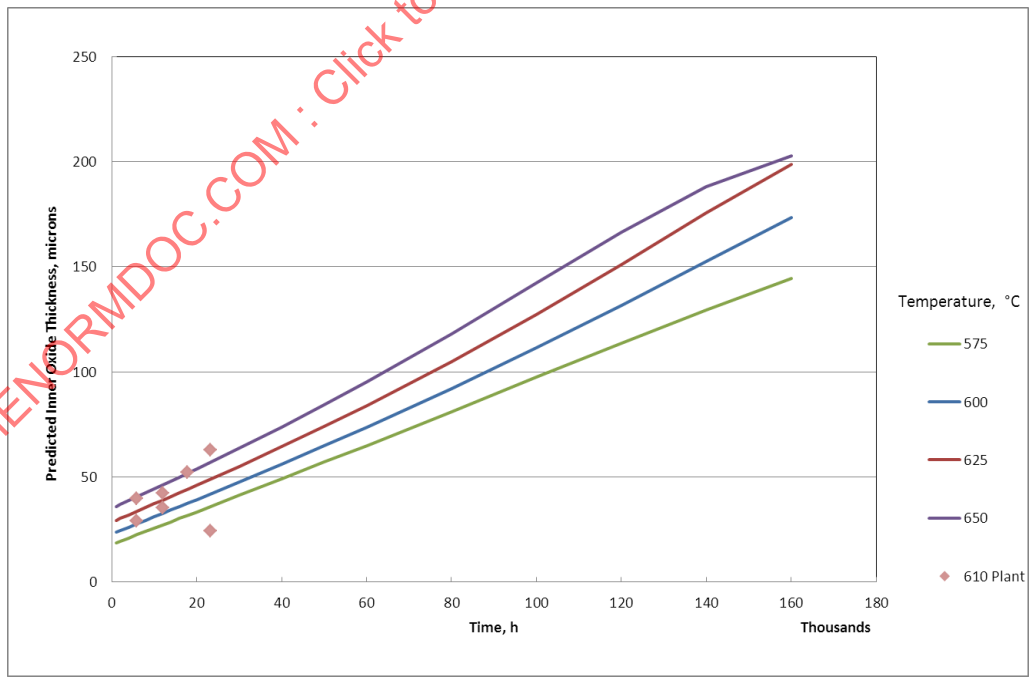

4.8 Reference Data for Metal Thickness Loss

4.8.1 Oxidation Curves

Because the final version of the neural network model is not easily expressed as a simple algorithm, oxidation kinetic curves were generated to provide reference data for the alloys of interest. These plots are intended to be used to look up values for metal thickness loss, i.e. inner oxide thickness, associated with specific service conditions of time, temperature, and steam pressure, and are presented in Appendix D. For predictions for long exposure times the uncertainty associated with the predicted value increases. In some instances, the model is no longer valid and the predicted values begin to fall. Generally, predictions to 100,000 hours can be considered to be within the applicable range of the predictive capability of the model.

4.8.2 Contour Plots

An alternative use of the model is in the construction of contour plots, an example of which is shown in Figure 4-28. This plot shows the predicted inner oxide thickness for alloy T22 at 1022°F (550°C) as a function of time and pressure. Plots such as this for all the alloys considered are presented in Appendix E, since they may be easier for designers to use than the standard oxidation curves when searching for data to specify materials and operating limits.

Figure 4-28: Contour Plot Example for Alloy T22 at 1022°F (550°C) Showing the Predicted Inner Oxide Thickness as a Function of Time and Pressure

4.9 References

[1] Metcalfe, E., Taylor, M. R. and Broomfield, J.P., 1984, "Oxide dating for service failure investigation - an error assessment of the technique," *Corrosion Science*, Vol. 24, pp.871-884.

[2] Shingledecker, J.P., 2013, "U.S. Industry Experience & EPRI Perspective on Steam-Side Exfoliation," Second EPRI-NPL Workshop on Scale Exfoliation From Steam-Touched Surfaces, Proc. Workshop held at Bushy House, National Physical Laboratory, Teddington, London, EPRI, Palo Alto, Calif., Report No. 1026663.

[3] Saunders, S.R.J., M. Monteiro, F. Rizzo, "The oxidation behavior of metals and alloys at high temperatures in atmospheres containing water vapor: A review," Progress in Materials Science, 53, 775-837 (2008).

[4] Wright, I.G., and R.B. Dooley, 2010, "A Review of the Oxidation behavior of Structural Alloys in Steam," International Materials Reviews, Vol.55, 129-167.

[5] Kubaschewski, O., and B.E. Hopkins, 1962, "Oxidation Of Metals And Alloys", Butterworths, London.

[6] Kofstad, P., 1988, "High-Temperature Corrosion", Chapter 6, Elsevier Applied Science Publishers, Ltd., London.

[7] Birks, N., Meier, G. H. and Pettit, F. S., 2006, "Introduction to the High-Temperature Oxidation of Metals", Cambridge University Press, 2nd Edition.

[8] Young, D.J., 2008, "High-Temperature Oxidation And Corrosion Of Metals", Elsevier.

[9] Pinder, L. W., Dawson, K. and Tatlock, G. J., 2010, "High Temperature Corrosion of Low-Alloy Steels," Shreir's Corrosion--Fourth Edition, Volume 1: Basic Concepts, High-Temperature Corrosion, R.A. Cottis, M.J. Graham, R. Lindsay, S.B. Lyon, J.A. Richardson, J.D. Scantlebury, and F.H. Stott, Eds., Part IV: High-Temperature Corrosion Environments, pp. 558-582 Elsevier Ltd.

[10] Kubaschewski, O., and Alcock, C. B., 1979, Metallurgical Thermochemistry, 5th Edition, Pergamon Press

[11] Holcomb, G.R., 2011, "Steam oxidation in steam boiler and turbine environments," Chapter 11 in Power Plant Life Management And Performance Improvement, J.E. Oakey, Ed., Woodhead Publishing Limited, Oxford, UK (2011).

[12] Fry, A.T., Osgerby, S. and Wright, M., 2002, "Oxidation of Alloys in Steam Environments: A Review", NPL Report MATC(A) 90.

[13] Wood, G.C., 1970, "High-temperature oxidation of alloys," Oxid. Metals, 2 (1), 11-57 (1970).

[14] Shannon, R. D., 1976, "Revised effective ionic radii and systematic studies of interatomic distances in halides and chalcogenides," Acta Cryst. A, Vol. 32A, pp. 751–767.

[15] Fujii, C. T., and Meussner, R. A., 1964, "The mechanism of the high-temperature oxidation of iron-chromium alloys in water vapor," J. Electrochem. Soc., Vol. 111, pp. 1215–1221.

[16] Tomlinson, L., and. Cory, N. J. 1989, "Hydrogen emission during the steam oxidation of ferritic steels: kinetics and mechanism," Corros. Sci., Vol. 29, pp. 939–965.

[17] Bamba, G., Wouters, Y., Galerie, A., Borchardt, G., Shimada, S. Heintz, O. and Chevalier, S., 2007, "Inverse growth transport in thermal chromia scales on Fe–15Cr steels in oxygen and in water vapor and its effect on scale adhesion," Sci. Mater., Vol. 57, pp. 671–674.

[18] Wright, I.G., 2009, "Oxidation of Candidate Alloys in Steam at 17 bar," Final Report on Phase 1 Efforts in Support of the U.S. Consortium Program on Boiler Materials for Ultra-Supercritical Coal Power Plants, ORNL/TM-2009/232,

[19] Paterson, S.R., Moser, R. and Rettig, T. R., 1992, "The Oxidation Behavior of Boiler Tubes," Proc. EPRI-VGB Int. Conf. on Interaction of Iron-Based Materials with Water and Steam, R. B. Dooley and A. Bursik, Eds., Heidelberg, Germany, June 3-5, 1992; EPRI Report No. TR-102101.

[20] Montgomery, M. and Karlsson, A., 1995, "Survey of Oxidation in Steamside Conditions," VGB Kraftswerkstekmik, Vol. 75, pp. 235-240.

[21] Wright, I.G., and R.B. Dooley, 2011, "Morphologies of oxide growth and exfoliation in superheater and reheater tubing of steam boilers," Materials at High Temperatures, Vol. 28, pp. 40-57.

[22] James, P.J., 2012, "Scale growth and exfoliation from steam-touched tubes: UK utility experience, management, Approaches, and needs," presented at the 2nd EPRI-NPL Workshop on Scale Exfoliation From Steam-Touched Surfaces, Bushy House, National Physical Laboratory, Teddington, London.

[23] Wright, I.G. and Dooley, R.B., 2013, "Steam-side Morphologies associated with Scale Exfoliation from Ferritic Steel T22", Materials at High Temperatures, Vol. 30, pp. 168-182.

[24] Manning, M.I., and D.B. Meadowcroft, 1980, "Effects of Tube Creep Strains on Laminated Scale Formation in Ferritic Pressure Tubing", Central Electricity Research Laboratories Report No. RD/L/R 2012.

[25] Armitt, J., Holmes, R., Manning, M. I., Meadowcroft, D.B. and Metcalfe, E., 1978, "The Spalling of Steam-Grown Oxide from Superheater and Reheater Tube Steels," EPRI Report No. FP-686, Feb. 1978.

[26] Mayer, P., and. Manolescu, A. V., 1983, "The role of structural and compositional factors in corrosion of ferritic steels in steam," High-Temperature Corrosion, R.A. Rapp, Ed., Intl. Corrosion Conf. Series NACE-6, NACE, pp. 368-379, Houston, Texas.

[27] Wright, I.G., 2009, "Oxidation of Candidate Alloys in Steam at 17 bar," Final Report on Phase 1 Efforts in Support of the U.S. Consortium Program on Boiler Materials for Ultra-Supercritical Coal Power Plants, ORNL/TM-2009/232.

[28] Wright, I.G., and R.B. Dooley, 2010, "A review of the oxidation behavior of structural alloys in steam," International Materials Reviews, Vol.55, pp. 129-167 (2010).

[29] Sarver, J. M., 2013, private communication with I.G. Wright.

[30] Dooley, R.B., and Paterson, S. J., 2003, "Oxide Growth and Exfoliation in Steam: Plant Experience," paper presented at the EPRI-NPL Workshop on Scale Growth and Exfoliation in Steam Plant, National Physical Laboratory, Teddington, England.

[31] Lepingle, V., Louis, G. and Allué, D., 2008, "Comparison between current methods for measurement of high-temperature corrosion of boiler steels in steam environments," Materials Science Forum, Vol. 595-598, pp. 323-332.

[32] Osgerby, S.J., and Quadakkers, W.J., 2005, "The influence of laboratory test procedures on scale growth kinetics and microstructure during steam oxidation testing," Materials at High Temperatures, Vol. 22 pp. 27-33.

[33] Ennis, P.J., and Quadakkers, W. J., 2002, "The Steam Oxidation Resistance of 9-12% Chromium Steels", Materials for Advanced Power Generation, Eds. J Lecomte-Beckers, M Carton, F Schubert and P J Ennis, Energy Technology, Vol. 2,1 Part II, pp. 1131-1142.

[34] Fry, A.T., and Piedra, E. M., 2011, "Review of factors affecting steam oxidation testing," Materials at High Temperatures, Vol.28, pp. 290-296.

[35] Osgerby, S. and Fry, A. T., 2005, "Good Practice Guide No 74: Laboratory Test Procedures for Exposures to High Temperature Steam Atmospheres," National Physical Laboratory, Teddington, England.

[36] Osgerby, S. and Fry, A. T., 2007, "The use of neural networks in understanding and predicting oxidation and corrosion behavior in advanced energy conversion systems," Materials at High Temperatures, Vol. 24, pp. 259-263 (2007).

[37] Masuyama, F., 2007, "Overview of the field test experience and creep failure tests in Japan," Institute of Metals New Materials Seminar, IOM3, London,

[38] Montgomery, M., S.A. Jensen, F. Rasmussen, and T. Vilhelmsen, "Fireside corrosion and steamside oxidation of 9-12%Cr martensitic steels exposed for long-term testing," Corrosion Engineering, Science and Technology, 44 (3), 196-210 (2009).

[39] Muraki, T., M. Ohgami, N. Komai, K. Matsufuji, M. Katat, F. Masuyama, N. Naoi, and Fujita, T., 2004, "Creep stability of high-strength 9%Cr Cr-W ferritic heat-resistant tube GR.92 after 15 years in service," Experience with Creep-Strength Enhanced Ferritic Steels and New and Emerging

Computational Methods, Y-Y. Wang, M. Gold, B.N. Rao, and J. Tang, Eds., PVP-Vol. 476, pp. 39-44 ASME, New York.

[40] Uerlings, R., Bruch, U. and Meyer, H., 2008, "Investigations of the operational behavior of boiler materials and their welded joints at temperatures up to 650°C," VGB Power Tech., Vol. 3, pp. 1-7.

[41] Masuyama, F., and Boyles, P. R., 2006, "Effect of service exposure on materials properties of austenitic boiler steels," Examination of mechanical properties and corrosion of high-temperature alloys after long-term service under advanced power plant boiler conditions-the Eddystone studies," Bulletin 517, pp. 211 to 219, Welding Research Council, Inc.

[42] Eberle, F., and C.H. Anderson, "Scaling behavior of superheater tube alloys in ASME high-temperature steam research tests at 1100-1500°F," J. Engineering Power, 84, 223 (1962).

[43] Haarmann, K., W. Schwenk, J. Venkateswarlu, and M. Zschau, "Hochtemperatur-korrosionsbeständigkeit des warmfesten Stahles X10CrMoVNb91 (P91/T91) im Vergleich zu höher- und niedrig-legierten warmfesten ferritischen Chromstählen in Wasserdampf," VGB Kraftwerkstechnik, 73, 837-840 (1993)

[44] Sumida, T., T. Ikuno, N. Otsuka, and T. Saburi, "High-Temperature Oxidation Behavior of 2.25%Cr-1%Mo Steel Boiler Tubes in Long-Term Exposure to Superheated Steam," Matls. Trans. JIM, 36 (11), 1372-1378 (1995).

[45] Komai, N., F. Masuyama, S. Yamamoto, and M. Igarashi, "10-year experience with T23 (2.25Cr-1.6W) and T122 (12Cr-0.4Mo-2W) in a power boiler," paper presented at the EPRI-NPL Workshop on Scale Growth and Exfoliation in Steam Plant, National Physical Laboratory, Teddington, England (2003).

[46] Nishimura, N., N. Komai, Y. Hirayama, and F. Masuyama, "Japanese experience with steam oxidation on advanced heat-resistant steel tubes in power boilers," Materials at High Temperatures, 22 (1/2), 3-10 (2005).

[47] Blum, R., Q. Chen, C. Coussement, J. Gabrel, C. Testani, and L. Verelst, "Operational tests of superheater materials at high steam temperatures in a hard coal-fired steam generator," VGB-PowerTech, 18 (10), 86-91 (2001).

[48] Knödler, R., S. Straub, and B. Scarlin, "Oxidation of steels and coatings during exposure in a bypass of a steam power plant at 605-637°C: correction and investigations of the morphology of the layers," VGB-PowerTech, 88 (9), 112-118 (2008).

[49] Komai, N., M. Igarashi, Y. Minami, H. Mimyura, F. Masuyama, M. Prager, and P.R. Boyles, "Field test results of newly-developed austenitic steels in the Eddystone Unit No. 1 boiler," pp. 1-1 to 1-18 in "Examination of mechanical properties and corrosion of high-temperature alloys after long-term service under advanced power plant boiler conditions-the Eddystone studies," Bulletin 517, Welding Research Council, Inc., Dec 2006. Also in Proc. Eighth Intl. Conf. on Creep and Fatigue at Elevated Temperatures, San Antonio, Texas, July 22-26, 2007.

[50] Kan, T., Y. Sawaragi, Y. Yamadera, and H. Okada, "Properties and experiences of a new austenitic stainless steel Super304H (0.1C-18Cr-9Ni-3Cu-Nb-N) for boiler tube application," pp. 441-450 in Materials for Advanced Power Engineering 1998, J. Lecomte-Beckers, F, Schubert, and P.J. Ennis, Eds., Forschungszentrum Jülich (1998).

[51] Matsuo, H., Y. Nishiyama, Y. Yamadera, "Steam oxidation properties of fine-grained steels," pp. 441-450 in Proc. Fourth Int. Conf. on Advances in Materials for Fossil Power Plants, R. Viswanathan, D. Gandy, and K. Coleman, Eds., ASM International (2005).

[52] Chen, Q., A. Helmrich, and G-N. Stamatelopoulos, "Esbjerg Unit 3—Investigation of advanced materials at steam temperatures up to 720°C," presented at VGB Workshop on Material and Quality Assurance, Copenhagen, May 13-15, 2009.

[53] Minami, Y., and T. Fukui, "Properties and experience of high Cr austenitic stainless steel for boiler tubes," pp. 5-1 to 5-9 in "Examination of mechanical properties and corrosion of high-temperature alloys after long-term service under advanced power plant boiler conditions-the Eddystone studies," Bulletin 517, Welding Research Council, Inc., Dec 2006.

[54] Montgomery, M., O. Biede, and O.H. Larsen, Corrosion Investigations at Masedø CHP Plant (Part VII), Report Dec. 2002.

[55] Montgomery, M., S.A. Jensen, A. Hansson, O. Biede, and T. Vilhelmsen, High-Temperature Corrosion Testing at Maribo Sakskøbing and Avedøre Straw-Firing Plants, manuscript associated with poster no. SS 2-P-7984 presented at European Corrosion Congress, Nice, France. Sep. 6-10, 2009. Also, private communication between M. Montgomery and I.G. Wright concerning results from PSO Projects 6510 and 6511, 2009/2.

[56] Hansson, A.N., L. Korcakova, J. Hald, and M. Montgomery, "Long-term steam oxidation of TP347HFG in power plants," Materials at High Temperatures, 22 (3-4), 263-268 (2005).

[57] Fry, A.T., "Key experimental parameters in steam oxidation testing and their impact on interpretation of experimental results," Energy Materials: Materials Science and Engineering for Energy Systems, 2 (4), 214-221 (2007).

[58] Mogire, E.O., R.L. Higginson, A.T. Fry, and R.C. Thomson, "Microstructural characterization of oxide scales formed on steels P91 and P92," Materials at High Temperatures, 28 (40), 361-368 (2011)

[59] Fry, A.T., "The Role of Alloy Composition on the Steam Oxidation Resistance of 9-12%Cr steels", Materials Science Forum, 522-523, 129-137 (2006).

[60] Osgerby, S.J., and A.T. Fry, 'Steam oxidation resistance of selected austenitic steels," Materials Science Forum, 461-464, 1023-1030 (2004).

[61] Gorman, D.M., R.L Higginson, H Du, G McColvin, and A.T Fry, "Microstructural analysis of steam oxidation of IN617 for use in ultra-supercritical steam plants," Materials at High Temperatures, 29 (2), 81-88 (2012).

APPENDIX A – THE ORIGINAL OXIDE SCALE THICKNESS DATA

Alloy	Reference	Notes	Exposure		Results	
			T °C	P_{st} bar	Exposure h	Total thickness µm
CrMoV	Eberle 1962 [42]		593	145	4,380	178
			593	145	8,742	254
			593	145	8,742	229
2.25Cr-1Mo	Eberle 1962 [42]		592	145	4,380	127
			592	145	8,742	178
			592	145	8,742	191
			647	145	4,380	406
			647	145	4,380	432
			648	145	8,742	508
			648	145	8,742	660
T22	Paterson 1992 [19]		482	146	9,280	3
			482	146	50,000	5
			482	146	100,000	6
			482	146	150,000	7
			482	146	200,000	8
			482	146	250,000	8
			482	146	300,000	9
			538	146	17,900	156
			538	146	50,000	205
			538	146	100,000	254
			538	146	150,000	293
			538	146	200,000	328
			538	146	250,000	349
			538	146	300,000	375
			552	146	13,900	166
			552	146	50,000	264
			552	146	100,000	322
			552	146	150,000	378
			552	146	200,000	418
			552	146	250,000	438
			552	146	300,000	451
			566	146	13,900	184
			566	146	50,000	301
			566	146	100,000	428
			566	146	150,000	561
			566	146	200,000	678
			566	146	250,000	782
			566	146	300,000	899
			579	146	11,940	215

Alloy	Reference	Notes	Exposure		Results	
			T °C	P_{st} bar	Exposure h	Total thickness µm
			579	146	50,000	377
			579	146	100,000	575
			579	146	150,000	780
			579	146	200,000	973
			579	146	250,000	1,161
			579	146	300,000	1,348
			593	146	9,950	234
			593	146	50,000	492
			593	146	100,000	797
			593	146	150,000	1,110
			593	146	200,000	1,444
			593	146	250,000	1,737
			593	146	300,000	2,048
			607	146	9,950	273
			607	146	50,000	682
			607	146	100,000	1,133
			607	146	150,000	1,647
			607	146	200,000	2,147
			621	146	8,490	293
			621	146	50,000	938
			621	146	100,000	1,676
			621	146	150,000	2,472
2.25Cr-1Mo	Haarmann 1993 [43]		550		100	22
			550		100,000	316
			600		100	58
			600		100,000	548
T22	Masuyama 2007 [37]		555	192	8,911	75
			555	192	20,390	111
			555	192	47,640	181
			555	192	78,640	254
T22	Wright 2013 [23]	RH, 69/1	544	40	200,000	125
		inner layer only	544	40	200,000	45
			544	40	200,000	66
			544	40	200,000	71
			544	40	200,000	132
			544	40	200,000	183
			544	40	200,000	222
			544	40	200,000	268
			544	40	200,000	250
			544	40	200,000	297
			544	40	200,000	302
			544	40	200,000	300
			544	40	200,000	308
			544	40	200,000	220

Alloy	Reference	Notes	Exposure		Results	
			T °C	P_{st} bar	Exposure h	Total thickness µm
			544	40	200,000	301
			544	40	200,000	283
		RH, 89/1	585	40	200,000	130
		inner layer only	585	40	200,000	171
			585	40	200,000	284
STBA24	Sumida 1995 [44]	inner layer only	587	SH	100,000	309
			550	SH	170,000	72
T23	Komai 2003 [45]; Masuyama 2007 [37]		555	192	8,911	65
			555	192	20,390	110
			555	192	47,640	185
			555	192	78,640	259
3Cr-1Mo	Eberle 1962 [42]		592	145	4,380	203
			592	145	8,742	203
			592	145	8,742	254
			647	145	4,380	406
			648	145	8,742	457
			648	145	8,742	584
5Cr-0.5Mo	Eberle 1962 [42]		592	145	4,380	152
			592	145	8,742	254
			592	145	8,742	279
			647	145	4,380	432
			648	145	8,742	533
			648	145	8,742	533
5Cr-0.5Mo-Si	Eberle 1962 [42]		592	145	4,380	178
			592	145	8,742	203
			592	145	8,742	203
			647	145	4,380	381
			648	145	8,742	406
			648	145	8,742	508
			648	145	8,742	559
5Cr-0.5Mo-Ti	Eberle 1962 [42]		592	145	4,380	127
			592	145	8,742	165
			592	145	8,742	178
			592	145	8,742	229
			647	145	4,380	381
			647	145	4,380	457
			648	145	8,742	508
			648	145	8,742	533
			648	145	8,742	584
			648	145	8,742	610

Alloy	Reference	Notes	Exposure		Results	
			T °C	P_{st} bar	Exposure h	Total thickness µm
9Cr-1Mo	Eberle 1962 [42]		592	145	4,380	102
			592	145	8,742	152
			592	145	8,742	178
			647	145	4,380	254
			648	145	8,742	330
			648	145	8,742	330
T91	Montgomery 1995 [20]	inner layer only	475	SH	4,000	13
			475	SH	8,000	20
			475	SH	16,000	30
			475	SH	24,000	36
			475	SH	32,000	43
			475	SH	40,000	47
			550	SH	4,000	32
			550	SH	8,000	45
			550	SH	16,000	63
			550	SH	24,000	77
			550	SH	32,000	90
			550	SH	40,000	101
T91	Nishimura 2005 [46]	inner layer only	650	SH	15,500	186
T91	Masuyama 2007 [37]		555	192	8,911	65
			555	192	20,390	92
			555	192	47,640	160
T91	Montgomery 1995 [20]	inner layer only	475	SH	4,000	13.0
		inner layer only	555-568	250	1,451	72 max
			555-568	250	2,963	99 av
			555-568	250	2,963	98 max
			555-568	250	2,982	90 av
			555-568	250	2,982	118 max
			555-568	250	4,394	122 av
			555-568	250	4,394	145 max
			555-568	250	5,915	144 av
			555-568	250	5,915	154 max
E911	Uerlings 2008 [40]		550	186	5,890	129
			550	186	12,000	160
			550	186	17,770	179
			550	186	23,215	232

Alloy	Reference	Notes	Exposure		Results	
			T °C	P_{st} bar	Exposure h	Total thickness µm
T92	Blum 2001 [47]	Vestkraft unit 3;	600	250	56	167
		inner layer only	600	250	7,660	204
			600	250	13,777	254
			600	250	21,318	279
			600	250	22,981	376
T92	Muraki 2004 [39]	inner layer only	600	193	13,600	110
			600	193	21,562	111
			600	193	45,000	160
			600	193	115,688	230
T92	Montgomery 2009 [38]	Avedore unit 1;	555-568	250	29,920	136 av
		inner layer only	555-568	250	29,920	149 max
			555-568	250	43,830	149 av
			555-568	250	43,840	168 max
		Amager unit 3;	555-568	250	15,110	99 av
		inner layer only	555-568	250	15,110	115 max
			555-568	250	31,010	119 av
			555-568	250	31,010	169 max
9Cr-2Mo	Masuyama 2007 [37]		565	192	54	10
			565	192	8,998	90
			565	192	20,387	136
			565	192	47,742	206
NF616	Uerlings 2008 [40]		550	186	5,890	218
			550	186	12,000	178
			550	186	17,770	208
			550	186	23,215	248
HCM9M	Masuyama 2007 [37]		565	42	8,696	86
			565	42	20,000	134
			565	42	47,443	207
			565	42	79,284	241
FB2	Knödler 2008 [48]	RWE Westfalen	608	186	10,500	90
		inner layer only	608	186	21,700	125
			637	186	10,500	125
			637	186	21,700	300
X20CrMoV12-1	Montgomery 2009 [38]	Avedore unit 1;	555-568	250	14,510	23 av

Alloy	Reference	Notes	Exposure		Results	
			T °C	P_{st} bar	Exposure h	Total thickness µm
		inner layer only	555-568	250	14,510	30 max
			555-568	250	29,820	29 av
			555-568	250	29,820	36 max
			555-568	250	44,040	55 av
			555-568	250	44,040	66 max
X20CrMoV12-1	Montgomery 2009 [38]	Amager unit 3;	555-568	250	16,000	41 av
		inner layer only	555-568	250	16,000	49 max
			555-568	250	16,000	53 av
			555-568	250	16,000	63 max
			555-568	250	31,010	76 av
			555-568	250	31,010	94 max
			555-568	250	31,010	107 av
			555-568	250	31,010	125 max
			555-568	250	46,920	56 av
			555-568	250	46,920	63 max
			555-568	250	50,800	122 av
			555-568	250	50,800	147 max
			555-568	250	84,400	85 av
			555-568	250	84,400	115 max
HCM12	Komai 2003 [45]; Masuyama 2007 [37]		595	192	10,358	93
			595	192	24,169	135
			595	192	41,816	158
			595	192	69,054	199
			595	192	128,130	287
HCM12	Montgomery 2009 [38]	Avedore unit, Amager unit 3	555-568	250	16,110	57 av
		inner layer only	555-568	250	16,110	68 max
			555-568	250	31,010	63 av
			555-568	250	31,010	77 max
			555-568	250	46,920	98 av
			555-568	250	46,920	140 max
			555-568	250	84,400	228 av

Alloy	Reference	Notes	Exposure		Results	
			T °C	P_{st} bar	Exposure h	Total thickness µm
			555-568	250	84,400	341 max
T122(a)	Komai 2003 [45]; Masuyama 2007 [37]		565	42	135	8
			565	42	8,696	66
			565	42	20,000	67
			565	42	47,443	90
			565	42	79,284	114
T122(b)	Komai 2003 [45]; Masuyama 2007 [37]		595	192	10,358	86
			595	192	22,251	105
			595	192	49,488	127
			595	192	80,563	128
Esshete 1250	Uerlings 2008 [40]		575	186	5,890	65
			575	186	12,000	53
			575	186	17,770	80
			575	186	23,215	95
17-14CuMo	Eberle 1962 [42]	inner layer	649	145	4,380	0
			649	145	8,742	94
			649	145	8,742	140
			649	145	13,138	38
			649	145	13,138	53
			732	145	4,380	0
			732	145	8,742	8
			732	145	8,742	127
			732	145	8,742	13
			732	145	8,742	28
			732	145	13,138	112
17-14CuMo	Komai, 2006 [49]	inner layer only	625	351	75,075	135 av
			625	351	75,075	207 max
17-14CuMo	Masuyama 2006 [41]	inner layer only	632	310	34,411	138
			632	310	34,411	122
			632	310	35,477	117
			632	310	35,477	114
			632	310	35,477	105
			632	310	85,770	180
			632	310	85,770	171
			632	310	85,770	161
			632	310	85,770	151
			632	310	85,770	141
			632	310	85,770	131
			632	310	87,622	170

Alloy	Reference	Notes	Exposure		Results	
			T °C	P_{st} bar	Exposure h	Total thickness µm
			632	310	87,622	160
X3CrNiMoBN 17-13-3	Uerlings 2008 [40]		550	186	5,890	58
			550	186	12,000	71
			550	186	23,215	49
			600	186	5,890	79
			600	186	12,000	84
			600	186	17,770	104
			600	186	23,215	125
TP304	Eberle 1962 [42]	inner layer	646	145	8,742	117
			646	145	8,742	58
			648	145	13,138	36
			648	145	13,138	23
			733	145	8,742	46
			732	145	13,138	66
			813	145	13,138	71
Super304H	Kan 1998 [50]	inner layer only	571	190	8,918	22
			571	190	22,399	23
			571	190	57,404	28
Super304H	Matsuo 2005 [51]	inner layer only	571	105	9,200	22
			571	105	20,508	25
			571	105	47,914	30
			571	105	79,102	32
Super304H	Komai 2007 [49]	inner layer only	625	351	75,075	37 av
			625	351	75,075	118 max
Super304H	Uerlings 2008 [40]		575	186	5,890	109
			575	186	12,000	70
			575	186	17,770	80
			575	186	23,215	109
			600	186	5,890	51
			600	186	12,000	46
			600	186	17,770	110
			600	186	23,215	140
			630	186	5,890	85
			630	186	12,000	80
			630	186	17,770	100
			630	186	23,215	120
Super304H	Chen 2009 [52]		548	275	30,000	12
			585	275	30,000	19
			603	275	30,000	33
TP316	Eberle 1962 [42]	Inner layer	649	145	8,742	84

Alloy	Reference	Notes	Exposure		Results	
			T °C	P_{st} bar	Exposure h	Total thickness µm
			649	145	8,742	104
			649	145	8,742	102
			649	145	8,742	102
			649	145	13,138	91
			649	145	13,138	79
			649	145	13,138	79
			732	145	4,380	43
			732	145	8,742	79
			732	145	8,742	64
			732	145	8,742	10
			732	145	8,742	48
			732	145	13,138	71
			732	145	13,138	89
			732	145	13,138	62
			816	145	8,742	69
			816	145	8,742	25
			816	145	8,742	76
			816	145	8,742	38
			816	145	13,138	43
			816	145	13,138	13
			816	145	13,138	48
			816	145	13,138	36
TP321	Eberle 1962 [42]	inner layer	646	145	4,380	25
			646	145	8,742	91
			646	145	8,742	48
			646	145	8,742	28
			646	145	8,742	25
			648	145	13,138	43
			648	145	13,138	48
			732	145	4,380	20
			732	145	4,380	76
			733	145	8,742	18
			733	145	8,742	15
			733	145	8,742	20
			733	145	8,742	28
			732	145	13,138	28
			732	145	13,138	8
			732	145	13,138	127
			732	145	13,138	5
			732	145	13,138	43
			813	145	8,742	107
			813	145	8,742	10
			813	145	8,742	94
			813	145	8,742	46
			813	145	8,742	127

Alloy	Reference	Notes	Exposure		Results	
			T °C	P_{st} bar	Exposure h	Total thickness µm
TP321H	Kan 1998 [50]	inner layer only	571	190	8,918	35
			571	190	22,180	67
			571	190	57,404	112
TP321H	Matsuo 2005 [51]	inner layer only	571	105	9,200	37
			571	105	20,508	70
			571	105	47,914	114
			571	105	79,102	128
TP321H	Minami 2006 [53]		700	351	300	76
			700	351	1,000	93
			700	351	2,000	114
TP347	Eberle 1962 [42]	Inner layer	646	145	4,380	3
			646	145	8,742	10
			646	145	13,138	8
			732	145	4,380	8
			732	145	4,380	33
			733	145	8,742	3
			733	145	8,742	46
			733	145	13,138	135
			733	145	13,138	3
TP347H	Montgomery 2002 [54]	inner layer only	500	92	5,228	19
			536	92	5,228	27
			540	92	5,228	24
			542	92	5,228	31
			545	92	5,228	35
			551	92	5,228	40
			557	92	5,228	47
			564	92	5,228	49
			567	92	5,228	45
			571	92	5,228	52
			574	92	5,228	48
			575	92	5,228	36
			575	92	5,228	32
			576	92	5,228	52
			578	92	5,228	48
			581	92	5,228	56
			584	92	5,228	39
			586	92	5,228	60
			593	92	5,228	59
			598	92	5,228	61
			607	92	5,228	60
			609	92	5,228	64
			618	92	5,228	60
TP347H	Montgomery 2009/2 [55]	inner layer only	505	92	4,535	6
			505	92	9,284	8
			505	92	10,380	11

Alloy	Reference	Notes	Exposure		Results	
			T °C	P_{st} bar	Exposure h	Total thickness µm
			505	92	10,390	9
			505	92	11,079	6
			505	92	20,172	14
			505	92	26,218	22
			505	92	30,753	21
TP347H	Montgomery 2009/2 [55]	inner layer only	543	92	4,535	27
			543	92	9,283	37
			543	92	10,390	45
			543	92	10,390	49
			543	92	11,079	43
			543	92	20,172	53
			543	92	26,218	62
			543	92	30,753	60
			543	92	31,246	64
TP347(CG)	Chen 2009 [52]		621	275	7,720	74
			621	275	23,000	40
TP347HFG	Kan 1998 [50]	inner layer only	571	190	9,137	18
			571	190	22,180	17
			571	190	56,975	18
TP347HFG	Hansson 2005 [56]	inner layer only	511	256	7,720	9
			536	256	7,720	24
			541	256	7,720	7
			591	256	7,720	16
			595	256	7,720	9
			499	256	22,985	14
			545	256	22,985	21
			563	256	22,985	10
			602	256	22,985	14
			604	256	22,985	7
			619	256	22,985	13
			515	256	29,588	15
			541	256	29,588	14
			590	256	29,588	12
			603	256	29,588	10
			506	256	57,544	69
			534	256	57,544	64
			541	256	57,544	26
			566	256	57,544	22
			567	256	57,544	33
			615	256	57,544	10
			620	256	57,544	22
			648	256	57,544	32
TP347HFG	Matsuo 2005 [51]	inner layer only	571	105	9,200	20
			571	105	20,508	18

Alloy	Reference	Notes	Exposure		Results	
			T °C	P_{st} bar	Exposure h	Total thickness µm
			571	105	47,914	18
			571	105	79,102	32
TP347HFG	Komai 2007 [49]	inner layer only	625	351	75,075	25 av
			625	351	75,075	37 max
TP347HFG	Masuyama 2006 [41]	inner layer only	632	310	35,477	27
			632	310	35,477	18
			632	310	85,770	34
			632	310	86,565	21
			632	310	87,622	34
TP347HFG	Uerlings 2008 [40]		575	186	5,890	30
			575	186	12,000	42
			575	186	17,770	40
			575	186	23,215	40
			600	186	5,890	31
			600	186	12,000	40
			600	186	17,770	47
			600	186	23,215	62
TP347HFG	Chen 2009 [52]		514	275	7,720	22
			538	275	7,720	24
			546	275	7,720	5
			598	275	7,720	11
			598	275	7,720	20
			620	275	7,720	9
			500	275	23,000	14
			563	275	23,000	20
			603	275	23,000	11
			603	275	23,000	19
			620	275	23,000	20
			628	275	23,000	10
TP347HFG chromized	Masuyama 2006 [41]	inner layer only	632	310	35,477	3
			632	310	86,565	5
			632	310	87,622	5
NF709	Komai 2007 [49]	inner layer only	625	351	75,075	28 av
			625	351	75,075	89 max
NF709	Uerlings 2008 [40]		630	186	5,890	49
			630	186	12,000	37
			630	186	17,770	60
			630	186	23,215	71
NF709	Chen 2009 [52]		563	275	7,720	24
			632	275	7,720	14
			632	275	23,000	10
			632	275	23,000	15

Alloy	Reference	Notes	Exposure		Results	
			T °C	P_{st} bar	Exposure h	Total thickness µm
TP310	Eberle 1962 [42]	Inner layer	649	145	8,742	33
			649	145	8,742	5
			649	145	8,742	48
			649	145	8,742	46
			649	145	13,138	5
			649	145	13,138	5
			732	145	8,742	10
			732	145	8,742	5
			732	145	8,742	3
			732	145	13,138	8
			732	145	13,138	81
			732	145	13,138	18
			732	145	13,138	25
HR3C	Komai 2007 [49]	inner layer only	625	351	75,075	9 av
			625	351	75,075	31 max
HR3C	Chen 2009 [52]		618	275	7,720	24
			618	275	23,000	17
			627	275	7,720	21
			627	275	23,000	17
Incoloy 800	Eberle 1962 [42]	inner layer	649	145	8,742	10
			649	145	8,742	10
			649	145	8,742	58
			649	145	13,138	13
			649	145	13,138	102
			732	145	8,742	20
			732	145	8,742	51
			732	145	8,742	5
			732	145	8,742	23
			732	145	13,138	10
			732	145	13,138	13
			732	145	13,138	20
Inconel 600	Eberle 1962 [42]	inner layer	649	145	8,742	20
			649	145	8,742	28
			649	145	13,138	3
			649	145	13,138	76
			649	145	13,138	51
			732	145	8,742	25
			732	145	8,742	41
			732	145	8,742	23
			732	145	8,742	25
			732	145	13,138	5
			732	145	13,138	51

Alloy	Reference	Notes	Exposure		Results	
			T °C	P_{st} bar	Exposure h	Total thickness µm
			732	145	13,138	3
			732	145	13,138	53
Inconel 617	Uerlings 2008 [40]		630	186	5,890	1
			630	186	12,000	5
			630	186	17,770	10
			630	186	23,215	3
22Cr-15Ni -Nb-N	Minami 2006 [53]		700	351	300	12
			700	351	1,000	13
			700	351	3,000	13
AC66	Uerlings 2008 [40]		600	186	5,890	3
			600	186	12,000	3
			600	186	17,770	6
			600	186	23,215	9
			630	186	5,890	3
			630	186	12,000	3
			630	186	17,770	5
			630	186	23,215	4

APPENDIX B – THE LABORATORY SCALE THICKNESS DATA USED TO SUPPLEMENT PLANT DATA FOR TRAINING THE MODEL

Alloy	Reference	Exposure			Results
		T °C	P_{st} bar	Exposure h	Total thickness µm
T22	Fry 2007 [57]	550	1	100	25
		550	1	300	37
		550	1	1000	53
		550	50	100	30
		550	50	300	38
		550	50	1000	115
		550	50	1000	126
T23	Fry 2007 [57]	550	1	100	22
		550	1	300	35
		550	1	1000	53
		550	50	100	42
		550	50	300	34
		550	50	1000	113
		550	50	1000	161
		600	1	500	30
		600	1	500	40
		600	1	500	76
		600	1	500	96
		600	1	500	137
		600	1	500	171
		650	1	1000	425
		650	1	3000	470
		650	50	1000	220
9Cr1Mo(1)	Fry 2007 [57]	550	1	100	24
		550	1	300	36
		550	1	1000	47
		550	50	100	38
		550	50	300	45
		550	50	1000	81
9Cr1Mo(2)	Fry 2007 [57]	550	1	100	20
		550	1	300	34
		550	1	1000	38
		550	50	100	38
		550	50	300	48
		550	50	1000	81
9Cr1Mo(3)	Fry 2007 [57]	550	1	100	16
		550	1	300	34
		550	1	1000	47
		550	50	100	34

Alloy	Reference	Exposure			Results
		T °C	P_{st} bar	Exposure h	Total thickness µm
		550	50	300	31
		550	50	1000	67
P91	Mogire 2011 [58]	650	1	100	53
		650	1	300	61
		650	1	500	27
		650	1	1000	60
		650	1	2000	76
		650	1	3650	66
		700	1	1000	150
		700	1	2000	114
		700	1	3000	206
P92	Fry 2006 [59]; 2007 [57]	550	50	516	39
	Mogire 2011 [58]	550	50	516	41
		600	1	100	85
		600	1	300	136
		600	1	500	58
		600	1	1000	233
		600	1	2000	102
		600	1	2000	64
		600	1	3000	412
		600	1	5000	224
		600	1	5000	86
		600	1	10000	95
		600	50	100	29
		600	50	300	9
		600	50	300	10
		600	50	1000	249
		650	1	50	62
		650	1	100	24
		650	1	100	65
		650	1	100	86
		650	1	100	129
		650	1	200	123
		650	1	200	128
		650	1	200	129
		650	1	300	37
		650	1	300	69
		650	1	300	72
		650	1	300	74
		650	1	300	77
		650	1	300	115
		650	1	300	127
		650	1	300	181
		650	1	400	126

Alloy	Reference	Exposure			Results
		T °C	P_{st} bar	Exposure h	Total thickness µm
		650	1	400	152
		650	1	500	166
		650	1	500	172
		650	1	600	143
		650	1	600	176
		650	1	696	154
		650	1	800	152
		650	1	1000	153
		650	1	1000	154
		650	1	1000	168
		650	1	1000	182
		650	1	1000	201
		650	1	1000	23
		650	1	1000	150
		650	1	2000	47
		650	1	2000	102
		650	1	2057	150
		650	1	3000	188
		650	1	3000	277
		650	1	5000	376
		650	1	5000	160
		650	1	10000	42
		650	1	15622	65
		650	25	100	58
		650	25	502	138
		650	50	100	78
		650	50	353	134
		650	50	353	138
		650	50	483	159
		650	50	1000	105
		650	50	1000	201
		650	50	2010	239
		700	1	3650	248
T92	Fry 2007 [57]	650	1	50	57
		650	1	150	76
		650	1	300	8
		650	1	300	38
		650	1	300	98
		650	1	600	124
		650	1	1000	104
		650	1	1000	110
		650	1	1000	111
		650	1	1000	115
		650	1	1000	134
		650	1	3000	142
		650	50	1000	72